

LD 9500
> 100000
TR 3020

3000

TR3020

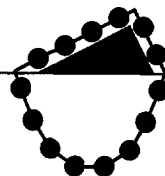
Strengthening of Reinforced Concrete Members in Bending by Externally Bonded Steel Plates

Design for Beam Shear and Plate Anchorage



Delft University of Technology

Stevin Laboratory



Strengthening of Reinforced Concrete Members in Bending by Externally Bonded Steel Plates

Design for Beam Shear and Plate Anchorage



PROEFSCHRIFT

Ter verkrijging van de graad van doctor
aan de Technische Universiteit Delft,
op gezag van de Rector Magnificus Prof.dr.ir. J. Blaauwendraad,
in het openbaar te verdedigen ten overstaan van een commissie,
door het College van Dekanen aangewezen,
op maandag 27 oktober 1997 te 16.00 uur

door

Willem JANSZE

civil ingenieur
geboren te Voorhout

Dit proefschrift is goedgekeurd door de promotor:

Prof.dr.ir.J.C. Walraven

Samenstelling promotiecommissie:

Rector Magnificus, voorzitter	Technische Universiteit Delft
Prof.dr.ir. J.C. Walraven, promotor	Technische Universiteit Delft
Prof. Dr.-Ing. M. Wicke	Leopold Franzens Universität Innsbruck
Prof.dr.ir. D. van Gemert	Katholieke Universiteit Leuven
Prof.dr.ir. Y.M. de Haan	Technische Universiteit Delft
Prof.Dipl.-Ing. J.N.J.A. Vambersky	Technische Universiteit Delft
Prof.ir. J.W.B Stark	Technische Universiteit Delft
Dr.ir. J.G. Rots	Technische Universiteit Delft / TNO

Published and distributed by:

Delft University Press
Mekelweg 4
2628 CD Delft
The Netherlands
Telephone: +31 15 278 3254
Fax: +31 15 278 1661
E-mail: DUP@DUP.TUDelft.NL

CIP-DATA KONINKLIJKE BIBLIOTHEEK, DEN HAAG

Jansze, W.

Strengthening of Reinforced Concrete Members in Bending by Externally Bonded Steel Plates / W. Jansze. - Delft : Delft University Press. - Illustrations.

Thesis Delft University of Technology. - With ref. - With summary in Dutch.

ISBN 90-407-1528-9

NUGI 841

Subject headings: concrete structures / plate bonding / plate-end shear

Copyright © 1997 by W. Jansze

All rights reserved. No part of the material protected by this copyright notice may be reproduced or utilised in any form or by any means, electronic or mechanical, including photocopying, recording or by any information storage and retrieval system, without permission from the publisher.

Aan mijn vader en moeder



PREFACE

The work for this Ph.D. thesis was carried out at the Stevin Laboratory of the Concrete Structures Group of the Delft University of Technology, The Netherlands. The research project was carried out from March 1993 until April 1997 and was financed by the "Commission Beek". The sponsorship by Spanstaal of the epoxy resin is gratefully acknowledged.

I am very grateful to my promotor Prof. Walraven for giving me the opportunity to conduct my Ph.D. study. I want to thank him for giving good direction to my project and for giving valuable comments during the past four years. I want to express my sincere appreciation to my daily supervisor Joop den Uijl, with whom I discussed most of my problems, findings and progress. I thank him as well for helping me with my project and for assisting me with writing the papers and this thesis. Prof. van Gemert and Kris Brosens are gratefully recognised for the technical discussions on the plate bonding technique. Also, I want to thank Björn Täljsten for the interesting conversations we had during our FIP conference and trip in South Africa.

Especially, I am indebted to Albert Bosman, who fabulously assisted me during the experimental work by working out technical drawings, designing and building the set-up, and enthusiastically carrying out the tests. He was able to produce a lot of ideas. Also I thank my roommate Tobias Wermann for the stimulating daily talks, and the computer trick lessons. A special word of thank is addressed to Arnold van der Marel for taking care of the financial affairs, to Erik Horeweg and Ton Blom for the constant concrete quality, and to Theo Steijn for the prompt delivery of some final drawings. My (former) colleagues and foreign guests of the Concrete Structures Group I would like to thank for the relaxing lunch and coffee breaks, and activities that we did together. The valuable comments on all my English texts by Margerita de Miranda are highly appreciated. My present employer Van Hattum en Blankevoort is recognised for giving me the time and opportunity to prepare the final manuscript of this thesis.

Delft, August 25, 1997
Wim Jansze

SAMENVATTING

Deze samenvatting geeft in het kort een overzicht van het proefschrift. De studie omvat onderzoek naar de dwarskrachtcapaciteit van constructieonderdelen versterkt op buiging met opgelijmde stalen platen en onderzoek naar de verankeringscapaciteit van de plaat.

Inleiding

Zowel de bruikbaarheidsgrenstoestand als de uiterste grenstoestand van een bestaande betonconstructie kunnen onvoldoende gewaarborgd zijn om aan de eisen van de gebruiker te voldoen. Een attractieve methode is dan het versterken van de bestaande betonconstructie door middel van het oplijmen van stalen platen. Onderzoek op dit gebied startte reeds in de jaren zeventig. Vandaag de dag is de techniek van het versterken van bestaande betonconstructies door middel van opgelijmde platen geaccepteerd als een efficiënte manier om de bruikbaarheids- en/of uiterste grenstoestand te verbeteren. In de vele praktijkprojecten is deze eenvoudige versterkingstechniek vooral toegepast om de momentcapaciteit te vergroten: de stalen platen worden aan de trekzijde van het ondergewapende constructieonderdeel gelijmd, en zodoende van additionele langswapening voorzien. Daarnaast wordt in de literatuur ook gerapporteerd over het vergroten van de dwarskrachtcapaciteit door het oplijmen van platen in de vorm van beugels.

Doel van het onderzoek

Het onderzoek is gericht op het ontwikkelen van een ontwerpmethode voor de dwarskrachtcapaciteit van de met opgelijmde stalen platen versterkte ligger en voor de verankeringscapaciteit van de opgelijmde plaat. Daarnaast is het onderzoek gericht op het beschrijven van de interactie tussen de momentcapaciteit en de dwarskrachtcapaciteit, in combinatie met het voortijdig bezwijken van een versterkte constructie.

Stand van zaken (hoofdstukken 2, 3)

De literatuurstudie liet zien dat de dwarskrachtcapaciteit van constructieonderdelen nauwelijks onderzocht was. De aandacht was wel gericht op het toepassen van opgelijmde platen voor het versterken van de dwarskracht. De rol van de dwarskracht indien betonconstructies alleen op buiging versterkt worden is echter onduidelijk. Dit probleem werd pas onderkend door Oehlers [1992] in zijn studie naar de interactie tussen afschuiving en buiging. Ondanks zijn onderzoek konden echter geen harde conclusies getrokken worden met betrekking tot de dwarskrachtcapaciteit van versterkte liggers. Wel concludeerde Oehlers dat de

verankering van de opgelijmde platen afhankelijk was van het ontstaan van dwarskrachtscheuren.

Tot op heden is op het gebied van de techniek van uitwendig gelijmde wapening nauwelijks gepubliceerd over eindige-elementen analyses, en dan met name niet-lineaire simulaties. In vergelijking met analytische studies, stelt een numeriek model ons in staat om meer inzicht te verkrijgen in het vervormingsgedrag en de herverdeling van spanningen tijdens bezwijken. Dit onderzoek was daarom uitgevoerd met experimenten en simulaties, om meer informatie te verkrijgen over het afschuifdraagvermogen van versterkte liggers en de verankering van de opgelijmde platen, omdat de indruk bestond dat deze twee bezwijkmechanismen niet te scheiden zijn.

Experimentele studie (hoofdstukken 4, 5, 6)

Om inzicht te verkrijgen in het bezwijkgedrag van gewapende betonnen constructieonderdelen die versterkt zijn met uitwendig gelijmde stalen platen, werd een onderzoeksprogramma opgezet. Experimenten werden uitgevoerd op liggereinden, met betrekking tot het verankeringsgedrag alsmede het afschuifdraagvermogen.

In de proeven met betrekking tot het verankeringsgedrag van de opgelijmde platen werd de invloed van drie variabelen onderzocht, namelijk de niet-geplate lengte, het toevoegen van een bout en de invloed van een herhaalde belasting. De niet-geplate lengte is gedefinieerd als de afstand tussen het einde van de plaat en het hart van de oplegging. Een grotere niet-geplate lengte liet zien dat het maximale draagvermogen afnam. Aan het einde van de plaat ontstond een typische eindeplaatscheur, die zich verder ontwikkelde tot een dwarskrachtscheur. Echter, als gevolg van de inwendig aanwezige beugelwapening stopte deze scheurgroei, zodat de uitwendig gelijmde plaat van het beton scheurde ter hoogte van de inwendige langswapening. Bij het toevoegen van een bout in de verankeringszone van de plaat kon het maximale draagvermogen verhoogd worden. Tegelijkertijd werd waargenomen dat het bezwijkmechanisme veranderde van bros afscheuren van de plaat naar een meer ductiel bezwijken van de beton-epoxy grenslaag. Twee effecten speelden hierbij een rol. Aan de ene kant was door het aanbrengen van de bout de ongewapende dekkingszone gewapend, zodat het afscheuren van de gelijmde plaat gestopt werd. Aan de andere kant werd door het aanbrengen van de bout, met een voorspanning, een normaaldrukspanning op de verankeringszone uitgeoefend. Hierdoor werd in combinatie met de schuifspanningen de capaciteit van de beton-epoxy grenslaag verhoogd tot plastisch vervormen van de grenslaag zelf optrad. Experimenten met herhaalde belastingsproeven lieten geen negatief effect op de verankeringscapaciteit zien. Anderzijds beïnvloedde het wel de groei van de dwarskrachtscheur aan het einde van de plaat.

In de proeven naar de dwarskrachtcapaciteit werden de invloeden van de geometrie van de stalen plaat en de geometrie van het betonnen liggereind

onderzocht. Twee typen afschuiving werden waargenomen, namelijk afschuifbuigbreuk en einde-plaatafschuifbreuk. Afschuifbuigbreuk werd waargenomen wanneer de liggereinden volledig beplaat waren, dat wil zeggen, met de uitwendige plaat tot voorbij de oplegging gelijkmd. Bezwijken ontstond doordat een buigscheur zich ontwikkelde tot een afschuifbuigscheur. Anderzijds, einde-plaatafschuifbreuk werd waargenomen wanneer de betonnen liggerdelen gedeeltelijk beplaat waren, dat wil zeggen, waarbij de uitwendig gelijkmd plaat op een zekere afstand voor de oplegging werd beëindigd. Tijdens de proef werd waargenomen dat nadat een einde-plaatscheur ontstond, deze zich ontwikkelde tot een einde-plaat afschuifscheur. Deze einde-plaatafschuifscheur groeide in de richtingen van het belastingsaangrijpingspunt en de oplegging. Tegelijkertijd ging de eerder ontstane einde-plaatscheur dicht, zodat spanningen ten gevolge van het haken van de toeslag zich konden ontwikkelen voor intern evenwicht. De niet-geplate lengte beïnvloedde duidelijk de maximale einde-plaat bezwijkbelasting. Net als bij de verankeringscapaciteit, liet een grotere niet-geplate lengte een afname van het maximale afschuifdraagvermogen zien. Het uitwendige wapeningspercentage dat verkregen werd door de oppervlakte van de stalen plaat te veranderen, beïnvloedde nauwelijks het maximale afschuifdraagvermogen. Bredere en hogere afmetingen van het beton leidden tot vergroting van het afschuifdraagvermogen door een vergrote bijdrage van het ongescheurde beton.

Numerieke studie (hoofdstukken 7, 8)

Om zowel einde-plaatafschuiving als het afscheuren van de plaat te analyseren is het uitgesmeerde-discrete scheuren model ontwikkeld. Dit eindige-elementenmodel maakte het mogelijk om de verschillende bezwijkmechanismen van constructieonderdelen die in buiging versterkt zijn met volledig of gedeeltelijk uitwendig gelijkmd stalen platen te analyseren. Bovendien, door de keuze van uitgesmeerde scheuren in combinatie met discrete scheuren, beide met trek-softening, bleek het model zeer nauwkeurig te zijn. De simulaties bevestigden de experimentele observaties dat met name de niet-geplate lengte de einde-plaatafschuifbelasting beïnvloedde. Het mechanisme van einde-plaatafschuiving werd grondig geanalyseerd. Deze analyse liet zien dat de einde-plaatscheur hoge aanhechtspanningen tussen het beton en de interne wapening opwekte, waardoor een verandering van het verticaal verdeelde schuifspanningsverloop optrad, met als gevolg dat de schuifspanning in een horizontale en verticale doorsnede voorbij het einde van de plaat toenam. Dit leidde ertoe dat de einde-plaatscheur zich ontwikkelde in een einde-plaatafschuifscheur. Tevens lieten de numerieke simulaties zien dat het reguliere einde-plaatafschuif-bezwijkmechanisme identiek is aan het afschuifbuig-bezwijkmechanisme, met dien verstande dat de locatie van de afschuifscheur gedwongen wordt op te treden aan het einde van de plaat, waardoor het zogenoemde einde-plaatafschuiving mechanisme optreedt.

Interpretatie van de resultaten (hoofdstukken 9, 10, 11)

De experimenten en de numerieke simulaties tonen duidelijk aan dat einde-plaatafschuiving een dominante rol speelt in de dwarskrachtcapaciteit van een liggereind, maar ook in de verankeringscapaciteit van de opgelijmde plaat. Om de einde-plaatafschuifbelasting te bepalen, is een einde-plaatafschuifmodel ontwikkeld, gebaseerd op de experimenten en de simulaties. Voor constructies met uitwendig gelijmde wapening is de fictieve afschuifarm geïntroduceerd, welke wordt geactiveerd door de niet-geplate lengte van het versterkte liggereind. Een formule is ontwikkeld om de fictieve afschuifarm te berekenen, via de niet-geplate lengte, de wapeningsratio van het niet-versterkte deel van de ligger en de nuttige hoogte van de inwendige wapening. Met de formule van de fictieve afschuifarm in combinatie met de formule van de CEB-FIP MC90 voor de afschuifbuigcapaciteit kan de einde-plaatafschuifcapaciteit worden berekend (zie hoofdstuk 9.5).

Met grote nauwkeurigheid voorspelt het einde-plaatafschuifmodel de gemiddelde experimentele bezwijkbelasting en kan dus tot een betrouwbare ontwerpregel voor een gedeeltelijk versterkte ligger worden omgevormd. Bovendien is aangetoond dat einde-plaatafschuiving niet alleen de afschuifcapaciteit bepaalt, maar in geval van beugels ook de verankeringscapaciteit beïnvloedt. Een vergelijking met experimentele resultaten uit de literatuur over het afscheuren van de plaat laat zien dat het einde-plaatafschuifmodel gebruikt mag worden als ondergrensbenadering voor de maximale belasting waarbij de plaat afscheurt. Met behulp van ophangwapening in de vorm van bouten die aan het einde van de plaat geïnstalleerd zijn en verankerd zijn in de betondrukzone, kan men correct detailleren op einde-plaatafschuiving en afscheuren van de plaat.

Nu uitdrukkingen beschikbaar zijn om de afschuifbuigcapaciteit en einde-plaatafschuifcapaciteit te bepalen, kan de interactie met buiging gevisualiseerd worden door middel van afschuifdalen. In vergelijking met de afschuifbuigcapaciteit en de momentcapaciteit, leidt het versterken met een verkeerd ontwerp van de uitwendig gelijmde stalen plaat tot dominantie van einde-plaatafschuiving. Met name lage waarden van de afschuifarm-tot-nuttige hoogte verhouding en grote niet-geplate lengten van een gedeeltelijk versterkt constructieonderdeel leiden qua buiging en afschuifbuigbreuk tot een lager maximaal draagvermogen.

Conclusies: toepassing voor de praktijk

Dit proefschrift geeft een ontwerpmethode voor de einde-plaatafschuifcapaciteit, gebaseerd op de fictieve afschuifarm in combinatie met de afschuifbuigcapaciteit berekend volgens de CEB-FIP MC90. Bovendien wordt een ontwerpmethode aangereikt om te detailleren voor einde-plaatafschuiving door middel van het toevoegen van ophangwapening.

TABLE OF CONTENTS

Preface	vii
Samenvatting	ix
Table of Contents	xiii
1 INTRODUCTION	1
1.1 Strengthening with Externally Bonded Plates	1
1.1.1 Techniques for Strengthening	1
1.1.2 Execution of Plate Bonding Work	2
1.1.3 The Principle of Plate Bonding Technique	3
1.2 Background Information	4
1.3 Research Objective	6
1.4 Research Approach	6
1.5 Outline of the Thesis	7
 <i>Part I - State-of-the-Art</i>	
2 STRENGTHENED REINFORCED CONCRETE STRUCTURES - STRUCTURAL BEHAVIOUR	9
2.1 Ultimate Limit State	9
2.1.1 General	9
2.1.2 Flexure	9
2.1.3 Shear	11
2.1.4 Plate Separation	14
2.2 Serviceability Limit State	16
2.2.1 General	16
2.2.2 Structural Stiffness	16
2.2.3 Cracking Behaviour	17
2.2.4 Long-Term Behaviour of Bond	18
2.2.5 Fire Conditions	19
2.3 Detailing Provisions for Bonded-on Steel Plate	19
2.3.1 General	19
2.3.2 Peak Stresses at Plate End	19
2.3.3 Interaction Between Concrete and Steel Plate	22
2.3.4 Maximum Plate Force and Anchorage Length	24
2.4 Fatigue Limit State	25
2.4.1 General	25
2.4.1 Structural Response of Strengthened Member	26
2.4.2 Anchorage Resistance of Externally Bonded Plate	27
2.5 Conclusions	28

3 CONVENTIONALLY REINFORCED CONCRETE STRUCTURES - SHEAR BEHAVIOUR	29
3.1 Mechanisms of Shear Failure	29
3.1.1 Shear Span-to-Depth Ratio a/d	29
3.1.2 Shear Failure Behaviour for $a/d > 2.5$	30
3.1.3 Shear Failure Behaviour for $1.0 < a/d < 2.5$	31
3.2 Kani's Flexural Shear Valley	31
3.3 Formulations for the Shear Resistance	32
3.3.1 Expressions on Flexural Shear: Rafta and MC90	32
3.3.2 Evaluation of Mean Maximum Nominal Shear Stress	33
3.3.3 Comparison between Rafta and MC90	34
3.4 Shear Resistance of Members with Web Reinforcement	34
3.4.1 Truss Analogy	34
3.4.2 Truss and Arch Contribution	34
3.4.3 Elements Requiring Design Shear Reinforcement According EC2	35

Part II - Experimental Study

4 FRAMEWORK OF EXPERIMENTAL STUDY	37
4.1 Aim of Experimental Program	37
4.2 Reference Tests on Unplated and Plated Beams	37
4.2.1 Estimation of Flexural and Shear capacity	37
4.2.2 Experimental Set-up	40
4.2.3 Failure Behaviour	41
4.2.4 Development of Plate Stresses	43
4.2.5 Conclusion	43
4.3 Test Set-up and Testing Procedure	44
4.3.1 Experimental Modelling	44
4.3.2 Test Set-up	46
4.3.3 Measurements	46
4.3.4 Test Control	47
4.4 Specimen Preparation	47
4.4.1 Materials	47
4.4.2 Specimen Storage	48
4.4.3 Strengthening Procedure	48
4.5 Overview of Test Series	49
4.5.1 Design of Test Series	49
4.5.2 Experiments on Plate Anchorage	49
4.5.3 Experiments on Beam Shear	50
5 EXPERIMENTAL OBSERVATIONS ON PLATE ANCHORAGE	51
5.1 Introduction to the Plate Anchorage Tests	51
5.2 Influence of the Unplated Length	52
5.2.1 Contents of Test Series A-L	52
5.2.2 Failure Behaviour	53
5.2.3 Maximum Loads in Relation to the Unplated Length	55
5.2.4 Anchorage Stresses	56
5.2.5 Conclusions	58

5.3	Influence of the Addition of a Bolt	59
5.3.1	Contents of Test Series A-B	59
5.3.2	Failure Behaviour	60
5.3.3	Anchorage Capacity	64
5.3.4	Conclusions	64
5.4	Influence of Repeated Loading	65
5.4.1	Contents of Test Series A-RL	65
5.4.2	Failure Behaviour	65
5.4.3	Conclusions	66
5.5	Conclusions	66

6 EXPERIMENTAL OBSERVATIONS ON BEAM SHEAR 67

6.1	Introduction to the Beam Shear tests	67
6.2	Influence of Unplated Length and Plate Cross Section	68
6.2.1	Contents of Test Series S-P	68
6.2.2	Failure Behaviour	68
6.2.3	Maximum Loads in Relation to Unplated Length	72
6.2.4	Maximum Loads in Relation to External Reinforcement Ratio	72
6.2.5	Initiation of Plate-End Crack	73
6.2.6	Aggregate Interlock	74
6.2.7	Conclusions	76
6.3	Influence of Width of Concrete Cross Section	77
6.3.1	Contents of Test Series S-W	77
6.3.2	Failure Behaviour	77
6.3.3	Maximum Load in Relation to External Reinforcement Ratio	78
6.3.4	Conclusions	78
6.4	Influence of Height of Concrete Cross Section	79
6.4.1	Contents of Test Series S-H	79
6.4.2	Failure Behaviour	79
6.4.3	Maximum Loads in Relation to External Reinforcement Ratio	80
6.4.4	Conclusions	80
6.5	Conclusions	80

Part III - Numerical Study

7	DEVELOPMENT OF SMEARED-DISCRETE CRACK MODEL	81
7.1	Aim of Numerical Simulations	81
7.2	Macro Material Models	82
7.2.1	Concrete	82
7.2.2	Ribbed Bar Reinforcement	84
7.2.3	Steel Plate Reinforcement	85
7.2.4	Epoxy Resin	86
7.3	Finite Element Modelling	87
7.3.1	Design of Continuum Finite Element Model	87
7.3.2	Solution Techniques	89
7.3.3	Model Uncertainties	89

7.4	Development and Calibration of Finite Element Model	92
7.4.1	Design of Stages for Development of Model	92
7.4.2	Stage 1: Simulations on Flexural Cracking	92
7.4.3	Stage 2: Simulations on Plate-End Shear Cracking	93
7.4.4	Stage 3: Simulations on Plate Separation Cracking	96
7.5	Conclusions	98
8	SIMULATIONS WITH SMEARED-DISCRETE CRACK MODEL	99
8.1	Introduction on Numerical Simulations	99
8.2	Simulation of Types of Failure	99
8.2.1	General	99
8.2.2	Flexure	99
8.2.3	Flexural Shear	100
8.2.4	Plate-End Shear	101
8.2.5	Plate Separation by Shear Peeling	101
8.2.6	Plate Separation by Shear Flexural Peeling	102
8.2.7	Conclusion	102
8.3	Mechanism of Plate-End Shear	102
8.3.1	Stresses in Strengthened Members before Cracking	102
8.3.2	Stresses in Strengthened Members at Plate-End Shear	105
8.3.3	Conclusions	107
8.4	Influence of Unplated Length	107
8.4.1	Contents of Simulation Series	107
8.4.2	Simulations on Unplated Length	108
8.4.3	Maximum Loads	109
8.4.4	Conclusions	110
8.5	Influence of External Reinforcement Ratio	110
8.5.1	Contents of Simulation Series	110
8.5.2	Simulations on External Reinforcement Ratio	110
8.5.3	Maximum Loads	111
8.5.4	Conclusions	111
8.6	Influence of Shear Span Length	112
8.6.1	Contents of Simulation Series	112
8.6.2	Simulations on Shear Span Length	112
8.6.3	Maximum Loads	114
8.6.4	Conclusions	114
8.7	Conclusions	114

Part IV - Interpretation of Results

9	PLATE-END SHEAR MODEL	115
9.1	Introduction on the Plate-End Shear Model	115
9.2	Summarising: Quantification of Variables	115
9.3	Derivation of Plate-End Shear Model	117
9.3.1	Fictitious Shear Span	117
9.3.2	Modelling Analogy with Critical Crack Section	118

9.3.3	Validation and Application of Plate-End Shear Model	123
9.3.4	Summarising: Expressions for Plate-end Shear	124
9.4	Validation of Plate-end Shear Model with Literature	125
9.4.1	Beam Shear Tests	125
9.4.2	Steel Plate Separation Tests	126
9.4.3	FRP Plate Separation Tests	127
9.4.4	Evaluation of Plate-End Shear Model: Additional Parameters	128
9.5	Design Method for Plate-End Shear	130
9.6	Conclusions	132
10	DETAILING PROVISIONS FOR PLATE-END SHEAR	133
10.1	Introduction to the Detailing Provisions	133
10.2	Truss Analogy for Internal Force Distribution	133
10.2.1	General	133
10.2.2	Configuration of Truss Model	134
10.2.3	Stiffness of the Truss Members	135
10.2.4	Analyses with Truss Model	136
10.2.5	Suspension Reinforcement by Bolts at Plate End	138
10.3	Design Method for Bolts for Plate-End Shear	139
10.4	Conclusions	142
11	APPLICATION: SHEAR FLEXURE INTERACTION	143
11.1	Introduction to the Shear Flexure Interaction Graph	143
11.2	Expressions for Shear Flexure Interaction	144
10.2.1	Flexural Capacity	144
10.2.2	Shear Capacity	144
11.3	Case Studies on Shear Flexure Interaction	145
10.3.1	Assumptions for Case Studies	145
10.3.2	Variation of Unplated Length for Strengthening Ratio 1.0	146
10.3.3	Variation of Unplated Length and Strengthening Ratio	150
10.3.4	Discussion: Initial Stresses and Unloading	153
11.4	Conclusions	153
12	RETROSPECTIVE VIEW, SUMMARY AND OUTLOOK	155
References		161
List of Publications		169
Notations		170
Appendices	A Literature Data on Maximum Shear Stress	173
	B Concrete Material Properties	177
	C Crack Development and Load-Deflection Diagram	181
	D Literature Data on Maximum Peeling Loads	201
Curriculum Vitae		206

1. INTRODUCTION

The introduction discusses strengthening of existing concrete structures and focuses on the plate bonding technique. §1.1 describes the need for strengthening and explains the principle of plate bonding. §1.2 discusses background information and lacks of knowledge concerning this strengthening method. Subsequently, §1.3 formulates the research objective and §1.4 clarifies the research approach. Finally, §1.5 gives a concise outline of this thesis.

1.1 Strengthening with Externally Bonded Plates

1.1.1 Techniques for Strengthening

Nowadays, maintenance of existing structures is of great importance. In Germany, according to Jungwirth [1995]¹⁴, analyses on the cause for repair of structures show that about 40% is due to design errors, about 40% is caused by construction errors and about 20% is the result of time-dependent material behaviour. The deficiency is usually the result of insufficient reinforcement, excessive deflections, structural damage (such as vehicular impact or fire damage), reinforcement corrosion or poor concrete quality, or insufficient bearing capacity as a result of change of use. Also, as already mentioned, the construction phase could ask for strengthening due to a poor detailing during the design phase. Also, there is a lot of interest in extending the lifespan of concrete structures by upgrading or strengthening techniques.

For the strengthening of existing concrete structures a number of techniques have been developed to satisfy the demand for an increased maximum load bearing capacity or to fulfil the serviceability requirements. Some common techniques are:

- introducing extra supports;
- adding extra bar reinforcement by subsequently removing and casting concrete;
- applying (additional) internal or external prestressing;
- replacing non-structural toppings by structural toppings;
- bonding external steel plates.

On the strengthening of reinforced concrete structures by means of bonding steel plates a first report was given at the RILEM symposium 1967 (l'Hermite & Bresson¹, Lerchental¹⁹, Kajfasz¹⁹ and Fleming & King¹⁹). Then, the plate bonding technique found its way into practice relatively quickly after numerous publications as Fig. 1.1 indicates. In the Netherlands, the plate bonding technique was only just introduced in 1983. Since, the number of projects in which bonded-on steel plates were applied, has been growing Fig. 1.2. There is a growing market demand for plate bonding.

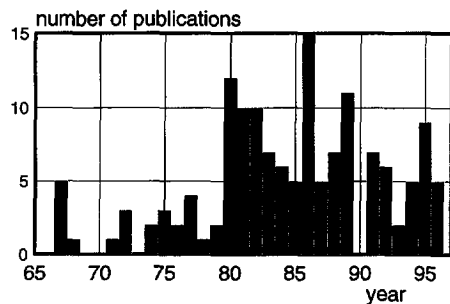


Fig. 1.1 Number of publications on plate bonding technique with steel plates

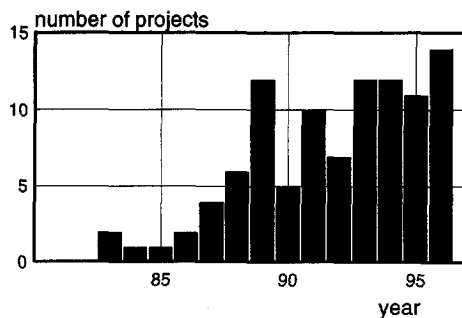


Fig. 1.2 Number of plate bonding projects in the Netherlands (Spanstaal [1996]³)

1.1.2 Execution of the Plate Bonding Work

The plate bonding work is simple and could be carried out relatively quickly. Before strengthening, the condition of the existing structure must be ascertained. The plate bonding work starts with preparation of the concrete surface of the existing structure by grit blasting, to remove the weak and greasy top layer. Subsequently, the clean and primed steel plates are placed on a wooden installation beam and the freshly mixed epoxy is poured on the innerside of the plate in a roof-shaped configuration, see Fig. 1.3. Then, the wooden supporting beam is mechanically pressed to the existing concrete structure, see Fig. 1.4. Immediately, the beam and steel plate are fixed in place by temporary scaffolding. Also, when the scaffolding is applied, pressure is put on the epoxy layer and the excessive epoxy is pushed aside and drips away, see Fig. 1.5. A epoxy layer of about 1 to 2 mm is preferable. After a minimum hardening time of the epoxy of about 24 hours, the supporting scaffolding

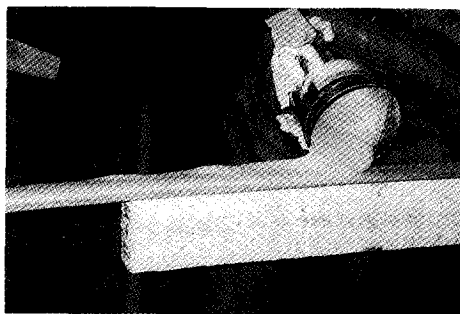


Fig. 1.3 Pouring of two-component epoxy resin on innerside of steel plate



Fig. 1.4 Mechanically applying the steel plate with epoxy to concrete surface

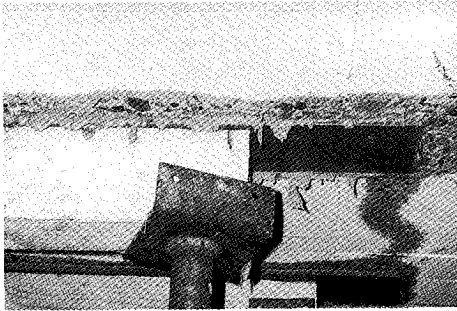


Fig. 1.5 Mounting of temporary supports and removal of excessive epoxy



Fig. 1.6 Removal of temporary supports; floor strengthened with steel plates

is removed and the existing concrete structure is strengthened externally, see Fig. 1.6. Additional protection of the steel plate against corrosion is needed. Major practical advantages of this technique are the relative simplicity and speed of execution of the plate bonding work at the construction site. One must be aware that, to obtain a composite action between the steel plate and the concrete, the quality of execution of the plate bonding work is very important.

1.1.3 The Principle of Plate Bonding Technique

Strengthening by plate bonding is mainly applied in order to increase the flexural capacity: steel plates are bonded to the tension side of a reinforced concrete structure, thus supplying additional longitudinal reinforcement. Fig. 1.7 displays a concrete member strengthened in flexure with a bonded-on plate. It visualises the internal forces which provide internal equilibrium at the ultimate limit state. As this figure shows, other favourable aspects of this technique are the larger internal lever arm of the bonded-on plate compared to bars and the small change in structural size of the strengthened member by the thin plate, in the order of a few millimetres.

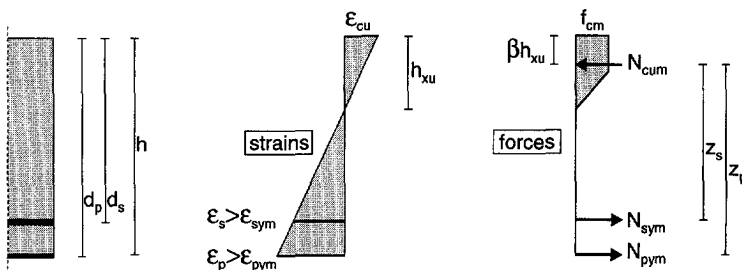


Fig. 1.7 Internal forces in ULS of beam strengthened in flexure with plate

1.2 Background Information

To enable the formulation of the research objective and the research approach, before the state-of-the art is discussed in Chapters 2 and 3, major issues and lacks of knowledge concerning strengthening with externally bonded plates are discussed.

Although in Europe, including the Netherlands, many structural members have been strengthened, design rules for the engineering practice are still scarce. First steps towards codes were taken in the Swedish Codes 47.33 [1995]¹³ and in the German Betonkalender [1996]¹³, in which an extensive part is dedicated to the design of bonded-on plated members. Models are available to estimate the maximum load bearing capacity of plated members, but are hardly useful for an engineer without knowledge and experience in this field. Particularly, problems that arise from the fact that the external plate is mostly stopped with a short distance from the support due to execution conditions, are difficult to deal with. On this point, the Standing Committee on Structural Safety of ISCE [1989]¹³ recommended "*If, after careful structural appraisal of the problem, it is decided to use the method, specialist advice should be obtained on the selection of the plate and the resin types and thicknesses, standards of surface preparation, and other details. Mechanical fixings must be provided as a construction expedient and to prevent the plates becoming a hazard, should they become detached by failure of the resin bond because of fire, degradation or other cause*". At the same time, this confirms that the structural engineer remains reluctantly as far as the use of epoxies for structural applications is concerned.

For thirty years strengthening with externally bonded plates has been investigated experimentally and analytically with the aim to understand phenomena with respect to safety, serviceability and detailing provisions.

As far as safety is concerned, a correct design of the strengthened member shows a ductile response by yielding of the internal bars and the external plate. However, if incorrect plate geometries were used, experiments showed a very brittle failure response of the strengthened members (Swamy & Jones et al. [1982, 1987, 1988]⁶ and Van Gemert [1980]⁴). Plate separation caused failure and was initiated by the formation of a peeling crack at the plate end, which progressively developed at the level of the internal reinforcement. Accordingly, much of the researchers effort has been put into the problem of plate separation, with particular analytical interest in the normal- and shear stress distribution at the plate end (Roberts [1988, 1989abc]⁷).

With regard to serviceability, both concrete cracking and long-term bond were studied. As far as bond of epoxies is concerned, tests showed a very satisfactory behaviour of the long-term bond between the plate and the concrete (Calder [1979]² and Swamy & Hobbs [1995c]⁶).

The interest in detailing provisions concentrated mainly on the bond stress-slip relation between the steel plate and the concrete (Rostásy [1980]⁵, Pichler

[1993]¹¹ and Holzenkämpfer [1994]⁵). The latter two authors managed to describe this interaction correctly. Accordingly, the anchorage length of the bonded-on plate can easily be calculated. With respect to detailing of the anchorage zone, additional mechanical anchorage by bolts showed a more ductile plate separation.

Nowadays, despite extensive experimental research, most safety considerations are still lacking knowledge as far as the mechanisms of failure are concerned. Former analytical analyses only addressed to anchorage problems. However, by these theoretical descriptions, hardly any insight has been gained with regard to the failure behaviour. Too much attention was paid to the local behaviour of the bonded-on plates. By reviewing literature, it turned out that the unplated part of the strengthened member played a dominant role in the majority of the described experiments. Crack patterns demonstrated that the unplated part clearly influenced beam shear, but also plate anchorage (Fig. 1.8). Hence, in this study shear of members strengthened in flexure is a main topic.

Concerning shear failure, experiments have been reported in which shear failure occurred (Sharif & Hussain et al. [1994a, 1995a]¹⁰ and Oehlers [1992]⁸). However, still very few clear experimental data exists on this subject. Oehlers [1992]⁸ obtained considerable scatter in his maximum shear loads, so that firm conclusions could not be drawn. Furthermore, in almost all other reported tests, internal stirrups or externally bonded shear plates were applied in addition to flexural strengthening and, therefore, the mechanism of shear failure could often not be investigated. Despite, in some reports on experiments, remarks were made that shear played an important but undefined role (Hussain et al. [1995a]¹⁰). Accordingly, the influence of the bonded-on steel plates on the shear resistance is yet unclear, if members without or with insufficient shear reinforcement are strengthened in flexure.

Concerning plate separation, only few data is available on the influence of the unplated length of a bonded-on plate. In contrast to what can be expected from analytical analyses, Oehlers [1990, 1992]⁸ reported on experimental results which inexplicably showed no influence of the unplated length of the steel plate on the ultimate load bearing capacity of the strengthened member.

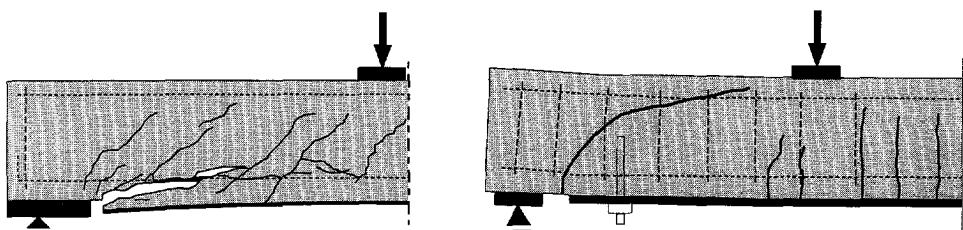


Fig. 1.8 Typical modes of failure of members with externally bonded steel plates: plate separation (Oehlers [1989]⁸) and shear failure (Sharif et al. [1994a]¹⁰)

1.3 Research Objective

The main objective of the research study is to develop a method to design for beam shear and plate anchorage, for structures strengthened in flexure with externally bonded steel plates. Based on observations, an analytical model has to be derived that ultimately could be used to describe the interaction between flexure, shear and premature failure of externally plated members. Therefore, this thesis investigates the mechanisms of shear failure and plate separation in detail. To that end, influences of the geometry of the bonded-on steel plate and the concrete member are investigated. In particular, the unplated length of the shear span, the plate anchorage configurations, the external reinforcement ratio, the shear span-to-depth ratio of the strengthened member, and the concrete cross-section are analysed.

1.4 Research Approach

The approach used in this study is quite different from studies carried out by other researchers. It does not focus on the stress concentrations at the plate end, but it focuses on the shear capacity of the partially strengthened beam. A priori, it was the author's opinion that the shear resistance of the unplated part governed the maximum load bearing capacity, as well as for beam shear as for plate anchorage.

The research approach followed in this study consists of a literature survey, experiments and numerical simulations, see Fig. 1.9. A state-of-the-art literature survey is carried out to collect information on the plate bonding technique and on the shear resistance of conventionally reinforced concrete members. Subsequently, by experimental and numerical analyses on beam shear and plate anchorage, an understanding of phenomena has been developed. Finally, the knowledge gained has been used to develop a method to design for beam shear and plate anchorage.

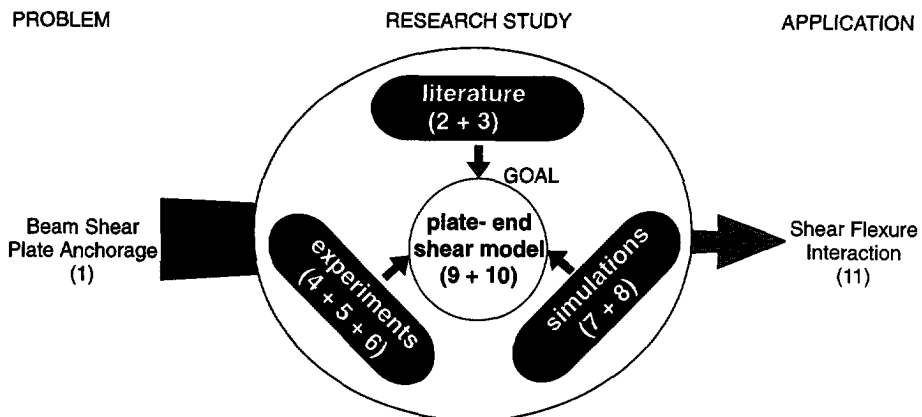


Fig. 1.9 Schematical representation of research approach, (-) indicates Chapter number

Concerning experiments, a lot of tests have thoroughly been described in the literature. However, with respect to beam shear, only brief information and results were found. Also, generally spoken, it is very important for the researcher to gain experimental experience and evidence.

Concerning numerical simulations, until now only little has been published on the use of finite-element analyses in the field of the plate bonding technique. In other fields, the combination of experiments and simulations has proved to be very valuable. By performing simulations with a finite-element model, much more insight is gained on the failure behaviour and stress redistribution during failure. The numerical model can be validated by experiments and, in addition, a parameter study can be carried out in a short period where geometries can be easily changed.

1.5 Outline of the Thesis

Subsequent to this introductory chapter, this thesis is subdivided into four parts.

Part I presents the *State-of-the-art*. Chapter 2 outlines the current knowledge on the structural behaviour of members strengthened with externally bonded plates. Respectively, the ultimate limit state, serviceability limit state, detailing provisions and fatigue limit state are discussed. Chapter 3 discusses the shear behaviour of conventionally reinforced concrete structures. It describes the various mechanisms of shear failure in relation to the shear span-to-depth ratio. Also, it elucidates Kani's shear valley and provides formulations on flexural shear.

Part II provides information on the *Experimental Study*. Chapter 4 describes the test set-up and the experimental procedure. Also, it gives an overview of the test series. Chapter 5 investigates plate anchorage. Particularly, it discusses the influence of the unplated part and the addition of a bolt on the anchorage capacity. Also, experiments with repeated loading conditions are dealt with. Chapter 6 analyses beam shear of members strengthened in flexure with an externally bonded steel plate. In detail, it investigates the influence of the unplated length and the geometry of the plate. Also, the geometry of the strengthened member is dealt with by varying the concrete cross section.

Part III overviews the *Numerical Study*. Chapter 7 describes the initial simulations which were carried out to develop a proper numerical model. It calibrates some typical tests, and concludes with the selected model based on a combined smeared-discrete crack concept. Chapter 8 describes simulations with this developed smeared-discrete crack model. It analyses stresses in the reinforcement and epoxy layer, and clarifies the governing failure mechanism. Furthermore, it dedicates a large part to the additional numerical studies on the unplated length, the external reinforcement ratio and the length of the shear span.

Part IV concludes the parts with the *Interpretation of Results*. Chapter 9 describes

the derivation of the plate-end shear model. This model is based on a fictitious shear span. Then, it validates the derived analytical model with experimental results from literature concerning beam shear and plate anchorage. It concludes with the modification of the plate-end shear model into a design method for plate-end shear. Chapter 10 analyses detailing provisions with the truss analogy. It shows that bolts as suspension reinforcement are necessary to take plate-end shear into account, if structural members are strengthened in flexure with externally bonded steel plates. It concludes with a design method for bolts if they are to be installed. Chapter 11 deals with an application of the plate-end shear model, namely shear flexure interaction. It analyses the interaction of plate-end shear with flexural shear and flexure. It varies the unplated length and strengthening ratio for comparison.

Finally, this thesis summarises with a retrospective view on the research study, and it briefly outlooks the development of the plate bonding technique.

References concerning the primary and secondary literature used in this study have been grouped with regard to the various research institutes. In the text this is marked by a number in superscript that represents the institute. It must be noted that references are not necessarily quoted in this thesis.

2. STRENGTHENED REINFORCED CONCRETE STRUCTURES - STRUCTURAL BEHAVIOUR

Strengthening of existing concrete structures by externally bonded steel plates is extensively described in literature. A large part of these publications describe results of experiments, some go into analytical analyses and others deal with practical applications. This chapter presents a state-of-the-art overview of this plate bonding technique. The literature references are subdivided according to the Eurocode 2 (EC2). §2.1 starts with the ultimate limit state, §2.2 discusses the serviceability limit state. Then, §2.3 overviews the detailing provisions and §2.4 ends with the fatigue limit state of members strengthened with externally bonded steel plates. Finally, §2.5 concludes this chapter on the state-of-the-art.

2.1 Ultimate Limit State

2.1.1 General

EC2 defines the ultimate limit state as that state beyond which the structure no longer satisfies the design performance requirements. It includes the loss of equilibrium or failure by excessive deformation, rupture, or loss of stability of the structure. This paragraph considers the ultimate limit states in flexure, beam shear and plate anchorage with great emphasis on experimental observations.

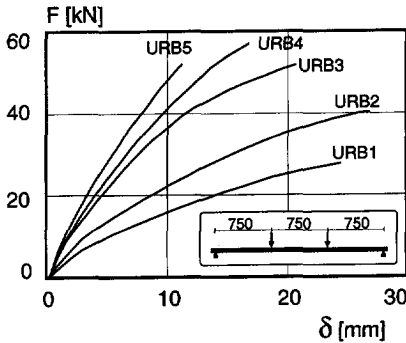
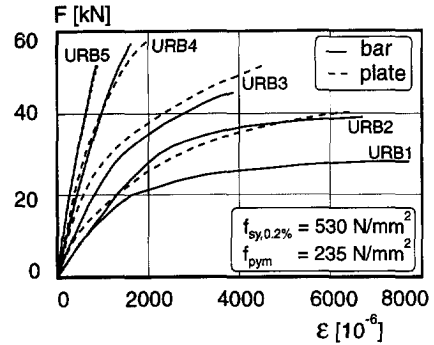
2.1.2 Flexure

Flexural failure occurs if beams are correctly designed. Failure is initiated by yielding of the internal bar reinforcement and the bonded-on plate, subsequently followed by crushing of the concrete compression zone.

An instructive investigation on the composite flexural behaviour was conducted by Jones, Swamy & Ang [1982]⁶. Initially under-reinforced beams ($\rho_s = 1.05\%$) were strengthened with bonded-on steel plates of various thicknesses stopped at a distance of 50 mm from the supports, see Table 2.1. Fig. 2.1 shows the load-deflection characteristics of the tested beams. Beams URB1 to URB3 reached the full flexural capacity. This is illustrated by Fig. 2.2. It indicates that the steel plate and the two 10 mm diameter bars yielded. A significant increase of 142% and 196% compared to the unplated beam was obtained. Beams URB4 and URB5 failed at respectively 88% and 62% of the theoretical maximum flexural moment capacity, because separation of the bonded-on plate prevented the strengthened member to attain the full flexural capacity.

Table 2.1 Details of tests on flexural capacity (Jones, Swamy & Ang [1982]⁶)

tested beam	plate [mm ²]	ρ_{sp} [%]	F_{max} [kN]	failure mode
URB1	unplated	1.05	28.1	steel yielding
URB2	1.5×80	1.85	40.0	steel yielding
URB3	3×80	2.65	55.0	steel yielding
URB4	5×80	3.75	57.5	plate separation
URB5	10×80	6.38	53.1	plate separation

Fig. 2.1 Load-deflection relations of plated beams (Jones, Swamy & Ang [1982]⁶)Fig. 2.2 Tensile strains in bars and steel plate (Jones, Swamy & Ang [1982]⁶)

The design of plates bonded externally on RC structures is usually based on conventional procedures: the external plate is treated as conventional bar reinforcement assuming perfect bond between the concrete and the external plate. By virtue of the greater lever arm, the bonded-on plate is more effective than the internal reinforcement. Still, in some practical applications the flexural capacity is only partly increased, because during the execution of plating the structure is not supported. Consequently, the strengthened section provides enhanced capacity for the live and imposed loads. Then, the structural analysis involves summation of stresses that are present before and after strengthening. Enhanced capacity for the dead load is partly obtained as a result of the time-dependent creep, and during redistribution of loads in the ultimate limit state.

For the design of the flexural capacity of an externally strengthened member, Van Gemert et al. [1986a]⁴ presented graphs to calculate the cross-sectional area of the steel plate, see Fig. 2.3. In this graph M_o/M denotes the degree of unloading, and M_p/M the degree of strengthening. The method developed by Van Gemert was based on the assumption of elastic behaviour. Brosens & Van Gemert [1997b]⁴ extended this design method with the non-linear properties of steel and concrete to control the ultimate limit state and serviceability limit state. In addition, bonded-on CFRP reinforcement was also considered. In the ultimate limit state design, the internal bars may yield which results in higher stresses in the external reinforcement. The stress distribution over the cross section of the concrete member at the instant of gluing plays an important role in these design graphs, see Fig. 2.4. One must be

aware that the stress distribution differs before and after strengthening, but the strains remain linear. After unloading, the tensile stress in the bars are reduced from $\sigma_{s,M}$ to $\sigma_{s,0}$. After plate bonding the stress in the bars increases to $\sigma_{s,Mp}$ and the stress in the external plate corresponds to σ_p . Hence, the stress distribution is not linear. For more information the reader is referred to the cited references.

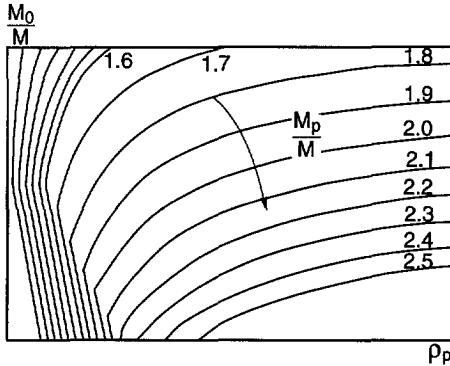


Fig. 2.3 Design graph for determining the amount of external reinforcement (Van Gemert et al. [1986a]⁴)

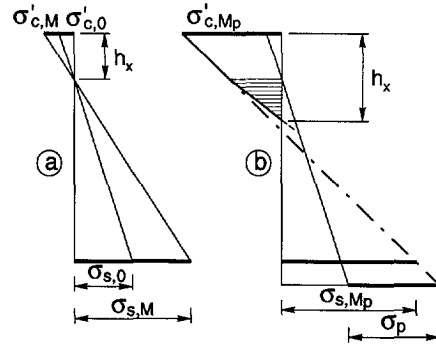


Fig. 2.4 Stress distribution before and after strengthening (Van Gemert et al. [1986a]⁴)

As in daily practice, the unstrengthened members are loaded and, therefore, cracked prior to bonding. Swamy, Jones & Charif [1989]⁶ and Hussain et al [1995a]¹⁰ reported amongst others on tested beams which were initially loaded in flexure and subsequently strengthened in unloaded position. Despite the cracking damage on beforehand, the flexural behaviour of these beams was hardly influenced by the load history. Also, the maximum plate separation load was not negatively influenced.

2.1.3 Shear

While most studies focus on the deformational and failure behaviour of plate separation and anchorage, only a few deal with shear. Moreover, these go into the possibility of strengthening in shear by bonding shear plates at the web sides.

Shear Failure Modes

While reviewing the available literature, two types of shear failure are distinguished, namely *flexural shear failure* and *diagonal tension failure*.

l'Hermite [1977]¹ discussed the idea to reinforce plain concrete by gluing external reinforcement. He concluded that if no stirrups were provided, the most probable failure mechanism would be flexural shear failure as clearly reported in l'Hermite and Bresson [1967a]¹, see Fig. 2.5. This type of failure was, amongst others, also observed by Täljsten [1994]⁹ when an incorrect shear plate design was made. If internal or correctly designed externally bonded stirrups were provided, shear cracks were arrested and more distributed shear cracks were visible in a large part of the shear span (Van Gemert [1990]⁴ and Täljsten [1994]⁹).

A completely different failure mode was explicitly observed by Sharif et al. [1994a]¹⁰ and Hussain et al. [1995a]¹⁰, although stirrups were provided in the tested member. A flexural crack initiated beyond the plate end, which propagated vertically and then diagonally with increased loading. As a result of this diagonal tension crack failure occurred in the shear span, Fig. 2.6. It was mentioned that "*premature failure was due to tearing of the concrete in the shear span at loads less than that calculated based on the ACI code shear strength formula*". The term diagonal tension introduced by Sharif & Hussain et al. may be confused with the diagonal tension failure of conventional RC members. In this thesis therefore the new term *plate-end shear* is introduced to avoid indistinctnesses. At the same time, this term clearly indicates the origin and location of the shear crack.

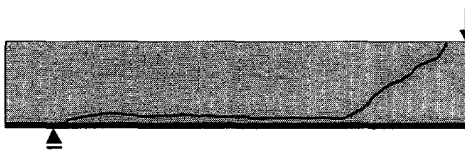


Fig. 2.5 Shear failure by a flexural shear crack in unreinforced beam C5 plated in flexure (l'Hermite and Bresson [1967a]¹)

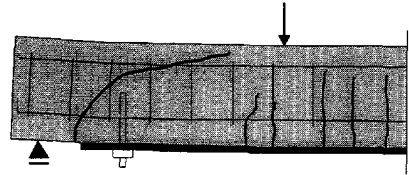


Fig. 2.6 Shear failure by a plate-end shear crack in RC beam P2B plated in flexure and additionally bolted for anchorage (Sharif et al. [1994a]¹⁰)

Plate-End Shear

Actually, Oehlers [1992]⁸ is the only reference found in which shear failure of strengthened members without stirrup reinforcement was discussed. He studied peeling due to shear forces and the interaction between shear peeling and flexural peeling. To that end, the distance from the centre of the support to the end of the plate was varied to change the moment-to-shear-force ratio at the plate end. Oehlers reported that "*When the research program was first developed, it was felt that the length of the plate as a proportion of the shear span may affect the shear strength of the beam as the diagonal crack would be forced to occur over the unplated region.*" However, after the experiments he concluded that "*the extent of plating ($a-L$)/ a did not affect the shear strength V_{cum}* ", as the scattered results in Fig. 2.7 show. With regard to this unplated length, Jones & Swamy et al. [1988]⁶ indicated that the length from the support to the end of the plate definitely influences the anchorage capacity of the plate. Accordingly, as Oehlers also concluded that "*the load at which peeling occurred is a function of the shear strength of a beam without stirrups*" and that "*the formation of the diagonal shear crack causes shear peeling*," it must be inevitable that the scattered results of Fig. 2.18 must hide an influence of the unplated length.

From the above mentioned references it is obvious that the influence of the unplated part on the beam shear capacity is still not clarified.

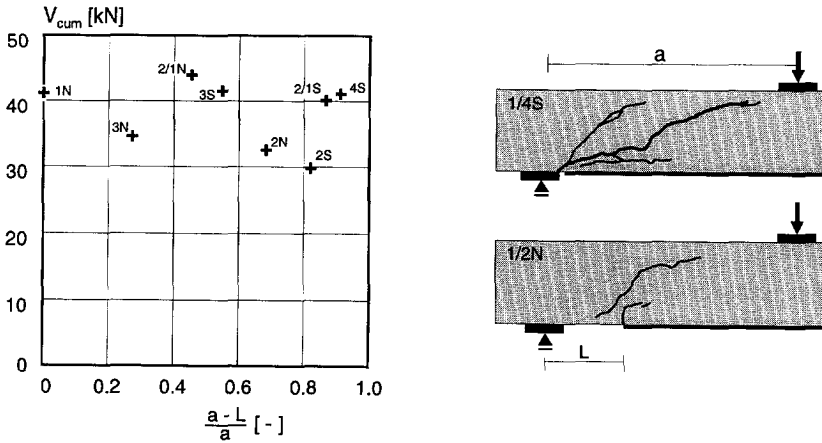


Fig. 2.7 Extent of plating in relation to shear strength (Oehlers [1992]^o)

Strengthening in Shear

Besides flexural strengthening, strengthening for shear with bonded-on steel plates was also investigated. Generally, it was concluded that the shear capacity of concrete beams could be increased by plates glued to their sides. Täljsten [1994]^o clearly illustrated this. Beams ($A_c = 180 \times 500 \text{ mm}^2$, $\rho_s = 2.00\%$) were strengthened in shear by means of $2.9 \times 80 \text{ mm}^2$ steel plates. Various shear plate designs were provided, Fig. 2.8 sketches the failure modes of the plated beams. Beam F2A failed in flexure due to the large amount of shear reinforcement, the other beams did fail in shear. The maximum load of beam F2B with inclined plates was equal to the bearing capacity of beam F3 with vertical plates. However, as a result of the shear plate design the location of the governing shear crack differed. A comparison between beams F3 and F4 indicated that the cracks in F4 went around the steel plates due to the short plate length: the failure load was approximately 80% of that of beam F3.

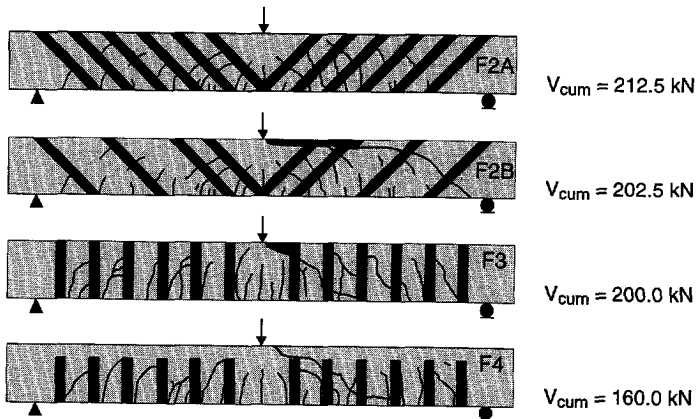


Fig. 2.8 Failure of beams strengthened in shear with steel plates (Täljsten [1994]^o)

2.1.4 Plate Separation

Failure Modes of Plate Separation

A new failure mode is introduced if additional reinforcement is glued on the (unreinforced) concrete cover, namely *plate separation*. Separation of the steel plate occurs before the flexural capacity is attained. A lot of effort has been put into solving the problem of this premature and brittle type of failure.

Oehlers [1989, 1990 and 1992]⁸ clearly discussed the various failure modes of plate separation, see Fig. 2.9. As a plate was only bonded in the constant moment region, increasing curvature induced *flexural peeling* and separation occurred gradually. The formation of diagonal shear cracks induced *shear peeling* as a plate terminates at a distance short of the support in a region of high shear forces and a low bending moment. This type of peeling occurred rapidly and is therefore known as very brittle. If a shear span was partially plated, a combined *shear flexural peeling* occurred. All peeling modes occurred at the level of the internal reinforcement. *Interface failure* by glue-bond failure is mainly caused by poor workmanship. However, it also occurs when bolts are additionally applied in the anchorage zone at the end of the steel plate (Pichler [1993]¹¹). Consequently, the concrete-epoxy-bond interface yields due to the high normal stresses introduced by the (pre-stressed) bolt as described in the next section. Ladner & Weder [1981]⁹ observed that even in the zone of constant bending moment, where the steel plate undergoes severe plastic deformations, separation could occur as well. Due to the large deformations, the bond between the plate and the concrete was completely destroyed. An effect of peeling, as described, was the occurrence of *reverse peeling* cracks: cracks propagated into the reverse direction at the concrete-epoxy interface.

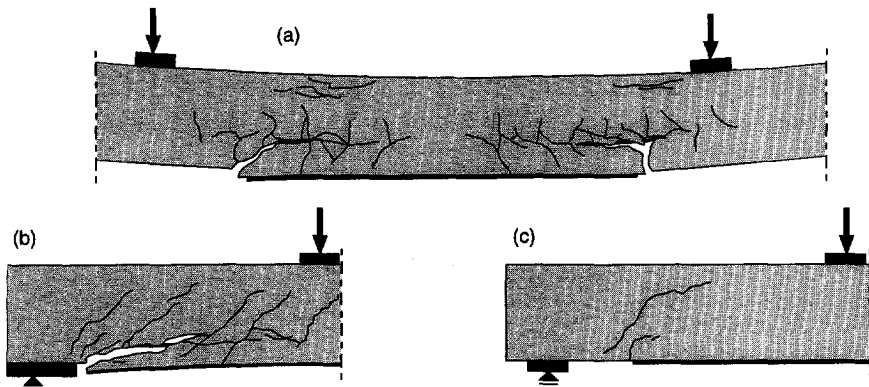


Fig. 2.9 Peeling modes of beam with externally bonded plate; (a) flexural peeling (b) shear peeling (c) shear flexural peeling (Oehlers [1989, 1990 and 1992]⁸)

In reply to a discussion by Oehlers on Roberts & Haji-Kazemi [1989b]⁷, Roberts questioned whether or not the various modes of failure should be associated with failure of the external plate and, therefore, be categorised in such detail. As an example he quoted the case of an under-reinforced beam which exhibited concrete

crushing, but where the cause of failure was yielding of the reinforcement. Accordingly, the various modes of plate separation appeared to have been initiated by conventional shear or flexural failure beyond the end of the bonded-on plate. Thus, these modes may be quantifiable with conventional calculations.

With respect to this, Holzenkämpfer [1994]⁵ showed three video shots during failure of the plate-end zone of beam SB04.1. The shots illustrate the different stages of plate separation, see Fig. 2.10. Still, shot 1 clearly shows that plate separation was initiated by a crack beyond the plate end. This observation might support the idea that conventional calculations are applicable.

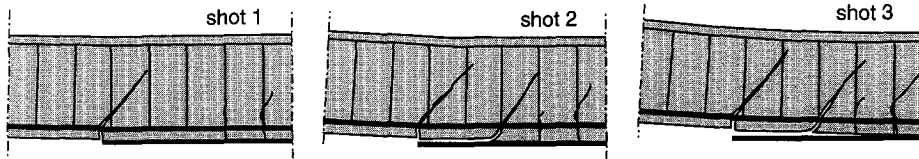


Fig. 2.10 Video shots of three stages of plate anchorage failure (Holzenkämpfer [1994]⁵)

Bolts at Plate End

The efficiency of different anchorage details has been investigated to overcome anchorage problems due to the high stress concentrations at the plate end (Jones, Swamy and Charif [1988]⁶). Bolts installed at the plate end did not prevent debonding, and as the load was increased more debonding took place. However, by virtue of the bolts the plate did not separate: the bolts were activated. This was confirmed by Roberts & Haji-Kazemi [1989]⁷, who tested under-reinforced beams strengthened with mechanically attached steel plates (thus only by bolts). They concluded that a significant improvement in stiffness and strength was achieved by fixing steel plates with bolts. However, no full composite action was present due to the influence of slip at the bolted connections. This slip was necessary to activate the bolts. Therefore, prior to debonding, the bolts did not contribute to the structural behaviour. This is visualised in Fig. 2.11 where a much stiffer load-slip response of the bonded plate is seen than for bolts (Münger, Ammann & Wicke [1991]¹¹).

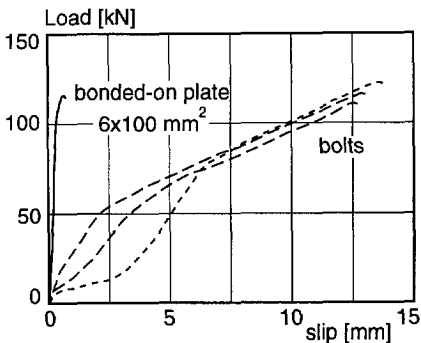


Fig. 2.11 Load-slip relations for bonded-on steel plate and for bolts (Münger, Ammann & Wicke [1991]¹¹)

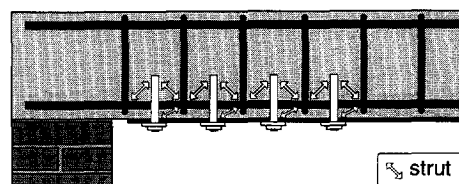


Fig. 2.12 Strut-and-tie model for plated member additionally anchored by bolts (Pichler [1993]¹¹)

Hussain et al. [1995a]¹⁰ investigated the influence of bolted end anchorage on the ductility and the ultimate load. Bolts were installed with a depth of 50 percent of the beam depth. They concluded that bolted anchorage could not prevent premature failure, however, improved ductility was obtained. Even so, they also stated that the additional anchorage had a marginal effect on improving the ultimate strength, which is contradicted by Pichler [1993]¹¹. From the same publication it emerged that shear problems played a dominant role.

The improved ductility by virtue of the bolts could be explained by Pichler's [1993]¹¹ strut-and-tie model. The plain concrete layer between the steel plate and the longitudinal bars is reinforced by the bolt and, therefore, follows the principles of the reinforced concrete theory: add reinforcement in zones of tensile stresses. With increasing normal stress applied to the plate by virtue of the pre-stressed bolts, the failure mechanism changed (Pichler [1993]¹¹). If a normal stress up to 5 N/mm² was applied, failure occurred in the concrete just above the epoxy layer. With higher normal stresses the adhesion between the epoxy and the plate broke, whereas at stresses of about 20 N/mm² the shear strength of the epoxy itself was exceeded.

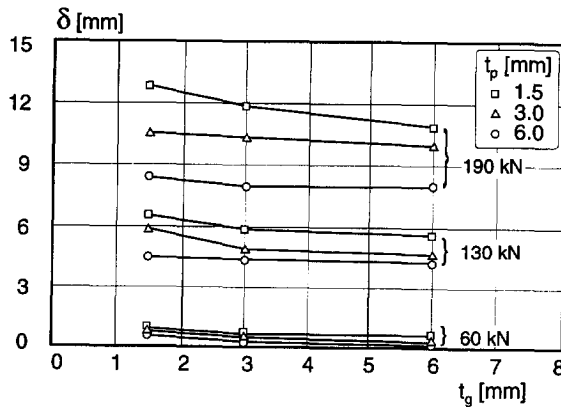


Fig. 2.13 Influence of flexural rigidity on central deflection (Swamy et al. [1987]⁶)

2.2 Serviceability Limit State

2.2.1 General

EC2 defines the serviceability limit state as that state beyond which specified service requirements are no longer satisfied. It includes deformations which affect the effective use of the structure and cracking of the concrete which is likely to affect durability and damage.

2.2.2 Structural Stiffness

The addition of bonded-on steel plates significantly influences the stiffness of the structural member at serviceability conditions (Swamy, Jones & Bloxham [1987]⁶). Experiments were carried out on beams with were reinforced with three 20 mm

diameter bars ($\rho_{s,0} = 2.76\%$) at an effective depth of 220 mm and plates with various thicknesses ranging from 1.5, 3.0 to 6.0 mm. Fig. 2.13 shows the influence of the plate thickness and the glue thickness on the deformational behaviour. Three load levels were considered, namely 60 kN, 130 kN and 190 kN, which represented approximately the initial cracking stage, the serviceability load stage and the non-linear stage at about 70 to 90% of the failure load. It emerged that with increasing plate thickness the central deflection was reduced. The thickness of the bonding layer had little effect, it only affected the rigidity due to the slightly increased lever arm of the plate.

2.2.3 Cracking Behaviour

Crack Spacing and Crack Widths

Jones, Swamy & Bloxham [1987]⁶ investigated the effect of externally bonded plates on the cracking behaviour of strengthened RC beams. The overall conclusions were that due to plating the crack development was delayed and the crack height was reduced. Consequently, the crack spacing of the strengthened member was larger at service load. However, at maximum load the total number of cracks and the ultimate crack spacing were equal. Accordingly, the number of cracks and ultimate spacing seemed relatively insensitive to the bonded-on amount of steel. However, in these tests the large amount of internal reinforcement played a dominant role. Holzenkämpfer [1994]⁵ remarked that in comparison with a conventionally reinforced beam the crack spacing of an externally plated beam was smaller. The mean crack width and the maximum crack width were reduced considerably by plating when the same load levels were considered. (Jones, Swamy & Bloxham [1987]⁶).

Formulations for Steel Strains and Crack Width

In Betonkalender [1996]¹³ expressions for RC members with steel plates are derived. The tensile force at which the first crack occurs, is expressed by:

$$F_r = F_{sr} + F_{pr} = 0.2 f_{ctm} A_c \quad (2.1)$$

For ranges at which the total tensile force $F_r < F_p < F_{py}$, the average strain of the bars and bonded-on plate equals:

$$\epsilon_m = \epsilon_{sm} = \epsilon_{pm} = \frac{F}{E_s A_s + E_p A_p} - \frac{F_r}{2(E_s A_s + E_p A_p)} \quad (2.2)$$

For the average crack spacing the following expression was derived:

$$s_{cr,m} = 50 + 0.1 \frac{f_{ctm}}{\tau_{sm} \rho_{sp^*}} \frac{d_s}{(1 + \eta \xi_1)} \quad (2.3)$$

$$\text{in which } \rho_{sp^*} = \frac{A_s + \xi_1 A_p}{b d_{sp}} \quad (2.4)$$

$$\eta = A_p / A_s < 2.0 \quad (2.5)$$

$$\xi_1 = \frac{\tau_{pm} E_s d_s}{\tau_{sm} E_p 4t_p} \quad (2.6)$$

$$\tau_{pm} = 1.25 f_{ctm} \quad (2.7)$$

$$\tau_{sm} = 1.8 f_{ctm} \quad (2.8)$$

The factor ξ_1 denotes a bond parameter which expresses the effectiveness of the glued plate due to the bond between the plate and the concrete. It must be noted that in other studies normally perfect bond is assumed. From the average crack spacing the average crack band width could be derived:

$$w_{cr,m} = \frac{F}{E_s A_s + E_p A_p} \left(1 - \frac{F_r}{2F} \right) s_{cr,m} \quad (2.9)$$

2.2.4 Long-term Behaviour of Bond

Much less research has been carried out on the long-term behaviour of bonded-on steel plates due to the time-consuming exposure tests. However, from tests carried out in the United Kingdom comprehensive data is available on the long-term performance and durability of strengthened beams. The main conclusion from these investigations is that with careful detailing, the plate bonding system to strengthen structures can be durable and reliable.

Calder [1979, 1988]² and Lloyd & Calder [1982]² reported on small specimens which were exposed under loaded and non-loaded conditions at sites for 1, 2 and 10 years representing high rainfall, industrial, marine and controlled (20°C, 65%RH) environment. The bonded-on plates were anchored beyond the support of the beams which had an effective span of 458 mm. It was found that the specimens exposed to natural conditions showed a considerable amount of corrosion at the steel-resin interface after 2 years. This corrosion was initiated by corrosive liquids and moisture that had penetrated through microcracks in the concrete and resin. As a consequence, compared to the controlled laboratory environment, some reduction in strength had taken place. However, compared to reference beams tested after 4 months, the beams exposed for 1 and 2 years were stronger due to natural ageing of the concrete strength, see Fig. 2.14.

After 10 years of exposure, the amount of corrosion was significantly increased compared to earlier tests. Despite this corrosion, a small increase of failure loads was observed (due to increased material strengths). Coating the steel plate with an epoxy primer reduced the degree of corrosion. Similar results were obtained by Calder [1989]² with large scale beams exposed to coastal environment for 8 years: using an appropriate resin the structural performance was still satisfactory despite the slight corrosion at the steel resin interface.

Hobbs & Swamy et al. [1995a]⁶ performed long-term exposure tests for periods of 11-12 years in an industrially polluted area on beams, as earlier reported in Swamy [1987]⁶. The strengthened beams, which were supported over an effective

span of 2300 mm, were kept under loaded and non-loaded conditions during the exposure period. Several geometrical variables were included, however, only beams with a single continuous plate are compared, see Fig. 2.15. With the exception of beam 109, which was incorrectly bonded, and 112, which failed in shear, the beams exhibited flexural flexure at loads higher than the reference beams 203/207/216/220/221 of Swamy & Jones et al. [1987]⁶. On the whole, the beams which were kept under sustained loading during the exposure period were stronger than the non-loaded ones (increased concrete maturity). These tests underline the satisfactory performance of the long-term behaviour of bonded-on plates.

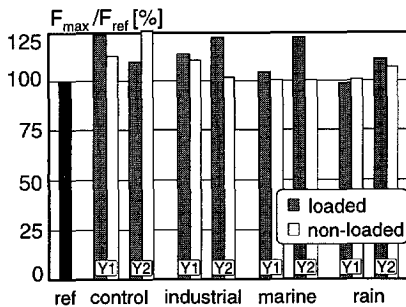


Fig. 2.14 Relative failure loads after exposure of 1-2 year (Calder [1979]²)

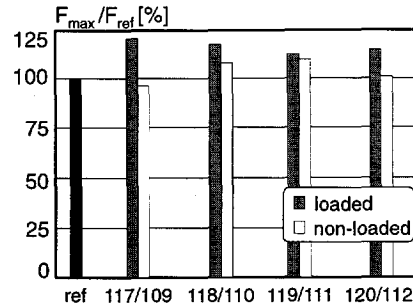


Fig. 2.15 Relative failure loads after exposure of 1-2 years (Hobbs & Swamy et al. [1995a]⁶)

2.2.5 Fire Conditions

At ambient temperatures higher than 50°C, the contribution of the stiffness of the epoxy becomes negligible. For strengthened structures, one must therefore always ascertain the safety against failure in the case of expected fire conditions. Then, if the safety of the structure is less than 1.1 or 1.2, fire protection provisions have to be installed covering the bonded-on plates to postpone heating up, Rutz [1995]¹³.

2.3 Detailing Provisions for Bonded-on Steel Plates

2.3.1 General

The anchorage behaviour of the partially bonded-on steel plates has always been of particular interest for most researchers. The peak stresses at the plate end and the interaction between the bonded-on plate and the concrete which could be described by stress-slip relations are the main topics of this section.

2.3.2 Peak Stresses at Plate End

When a strengthened beam is loaded in flexure, high stress concentrations and peeling forces are present at the end of a partially bonded-on steel plate. The significance of these anchorage stresses has always been the centre of attention. Roberts stressed in a discussion in Oehlers [1989]⁹ that: "It is therefore believed,

that rapid progress can be made only through the development of appropriate methods of analysis for predicting the (anchorage) stresses which are likely to initiate failure".

Various authors theoretically analysed these anchorage stresses. Roberts & Haji-Kazemi [1989b]⁷ derived formulations to describe the stresses that are imposed at the plate-epoxy-concrete interface when the plate is stopped before the support. The approximate solution expresses the shear and normal stress at the plate end:

$$\tau_{max} = \left(V_o + \left\{ \frac{K_s}{E_p b_p t_p} \right\}^{1/2} M^* \right) \frac{b_p t_p}{l b_g} (d_p - x) \quad (2.10)$$

$$\sigma_{max} = \tau_{max} t_p \left\{ \frac{K_n}{4E_p l_p} \right\}^{1/4} \quad (2.11)$$

$$\text{in which } K_s = G_g \frac{b_g}{t_g} \quad (2.12) \quad \text{and} \quad K_n = E_g \frac{b_g}{t_g} \quad (2.13)$$

$$V_o = F/2 \quad (2.14)$$

$$M^* = \text{bending moment at location } L + \frac{h+t_p}{2} \quad (2.15)$$

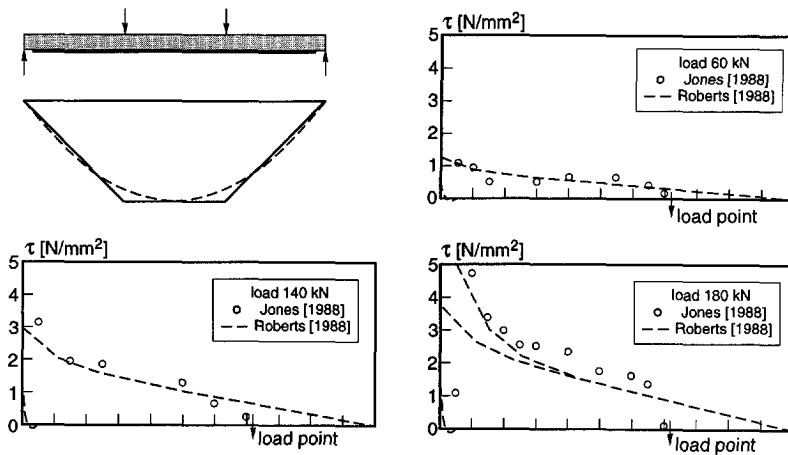


Fig. 2.16 Shear and normal stresses for F31 according to Roberts & Haji-Kazemi [1989]⁷

In a discussion on Jones, Swamy & Charif [1988]⁸, Roberts [1988]⁷ compared the results of the approximate solution with the experimental results for beam F31. Fig. 2.16 shows that up to load levels of 75% of the maximum load, there is correct agreement between theoretical and experimental results. By assuming that peeling failure had progressed over a distance of 50 mm along the epoxy joint, the theory

also shows a correct agreement at maximum load. A peeling stress of 1.5 N/mm^2 was calculated. With good reason Oehlers [1989]⁸ remarked that the theoretical method of analysis of Roberts & Haji-Kazemi [1988]⁷ could only be applied to *one* of the several modes of debonding as it models the failure zone at the plate-concrete interface only. Mostly, this only occurs if poor workmanship causes plate peeling.

Experimentally, Jones et al. [1988]⁶ found that the values for the bond stresses were very consistent and suggested a limiting value of 4.9 N/mm^2 . This indicated a limiting value of approximately $\sqrt{2} \times$ the tensile splitting strength of concrete. Also, they indicated that the anchorage stresses were increased as the length from the support to the end of the plate was increased. Although no experiments were carried out, they suggest that this dimension should be kept as small as possible. However, when a peeling crack started to initiate, it moved the effective cut-off of the plate away from the support, and thus increased the unplated length. Once this took place, the effect of peeling was magnified and the peeling crack extended rapidly. A progressive and brittle type of failure was the result.

A few tentative rules have been proposed for preventing peeling and ensuring a ductile behaviour by flexural failure. For peeling, the plate width over thickness ratio b_p / t_p seems dominant. It affects the bond stresses between the plate and the concrete at the anchorage zone. Macdonald [1982]² advised $b_p / t_p > 60$, Swamy et al. [1987]⁶ recommended as a rule of thumb $b_p / t_p > 50$ for design. Hence, broad and thin plates lead to sufficiently small bond stresses as experimentally proved.

However, even if all bonded plates satisfy the width-to-thickness requirement, there is also an overall limiting parameter for the plate thickness to ensure a ductile and flexural failure. A bonded-on steel plate might transform a conventionally designed under-reinforced beam in an over-reinforced beam. Thus, according to Swamy, Jones & Bloxham [1987]⁶, the neutral axis-effective depth ratio x/d_{sp} should be limited. Fig. 2.17 illustrates the strain distribution over the depth of an unplated and three plated beams. It was found that the transition from a ductile flexural failure to a brittle plate separation appeared to come between the beams with 1.5 and 3.0 mm plates. Then, the figure shows that between x/d_{sp} -values of 0.4-0.44 the transition took place. Hence, a limiting value of neutral axis over effective depth ratio of $x/d_{sp} < 0.4$ was therefore tentatively proposed.

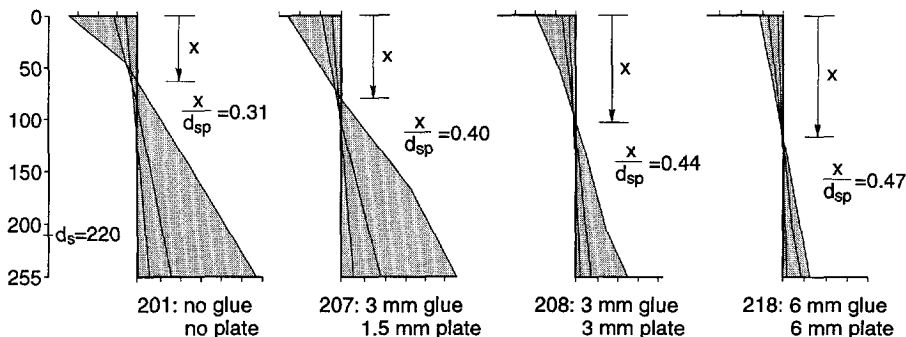


Fig. 2.17 Concrete strain distribution over depth of plated beams (Swamy et al. [1987]⁶)

2.3.3 Interaction Between Concrete and Steel Plate

Mechanism of Bond Failure

For the interaction between the concrete surface and the externally bonded plate, Hankers [1995]⁵ proposed a damage model for bond failure at the structural layer of concrete epoxy plate. Mostly, in the pull-off specimens bond failure occurred in the concrete just under the epoxy layer, because the imposed stresses are more critical to the tensile strength of concrete than that of epoxy.

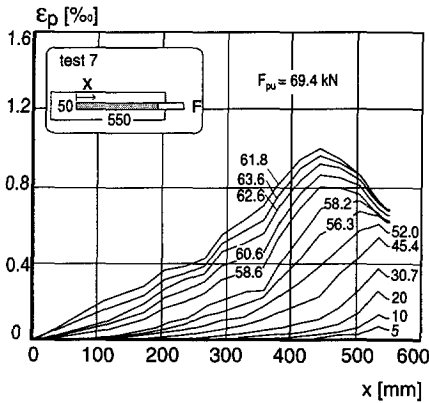


Fig. 2.18 Measured strains in steel plate as a function of the location and the load (Hankers [1995]⁵)

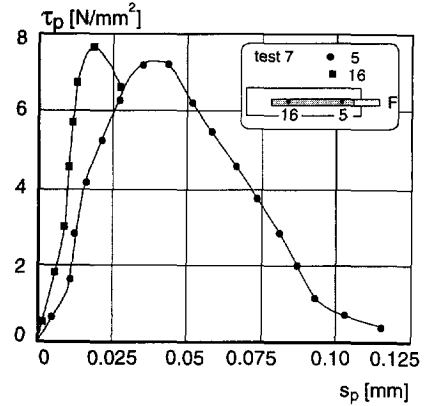


Fig. 2.19 Bond stress - slip relation derived from measured strains (Hankers [1995]⁵)

The mechanism of bond failure is explained by describing experiment no. 7 in detail. Fig. 2.18 shows the strains in the steel plate when a so-called pull-off specimen by tension compression was tested. This figure clearly illustrates the transfer length of the force which increases with increasing external load. On two locations at the steel plate (loaded and non-loaded side) the experimentally derived bond stress-slip relations were plotted, Fig. 2.19. These relations describe the non-reversible deformations in the vicinity of the bonding layer as a results of micro cracking. The reduced bond stress at the loaded side of the steel plate indicated that the bond between the concrete and the plate was completely destroyed; the shear stress amounted to zero with increased slip displacement. The bond at the non-loaded side was just in the post-peak branch at the onset of the maximum load when the plate separated.

The experimental observations were used to explain the mechanism of static bond failure as Fig. 2.20 depicts. It shows three stages of damage and marks these stages by dots in the τ - s graph. Because the concrete surface was grit blasted, a large amount of the coarse aggregate was anchored in the epoxy layer. Stage A shows the linear response of the epoxy bond due to deformations of the steel plate,

epoxy layer and concrete. With increasing external load, the principal stresses in the concrete equalled the maximum tensile strength: cracks of about 15 mm were initiated at an inclination of about 30°. The cracks went through the matrix just around the surface of a coarse grain. The bond stress-slip relation reached the maximum bond stress at stage B. Then, stage C showed the damage in the descending branch. A horizontal crack between the grains was initiated, some millimeters above the epoxy layer. Some more slip resulted in a total pull-out of the grains from the concrete and the ultimate bond was reached and exceeded.

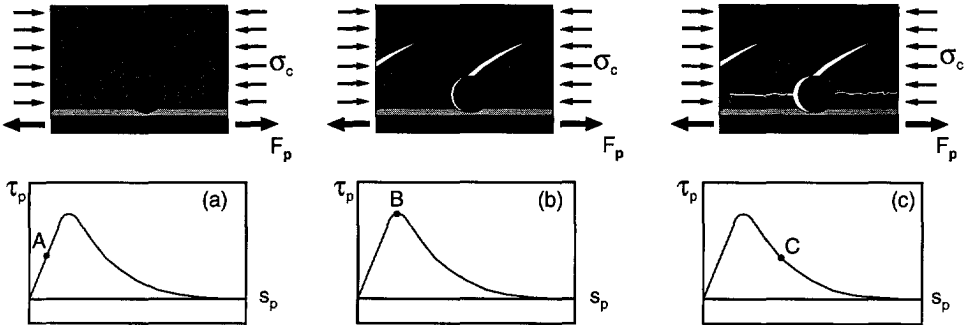


Fig. 2.20 Hankers's damage model of static bond failure (Hankers [1995]⁵)

Bond Stress-Slip Relation

In Holzenkämpfer [1994]⁵ a thorough overview was given on the theoretical analysis of bond stress-slip relations of externally bonded plates. Particularly, the bond-stress-slip relations of Holzenkämpfer and Pichler [1993]¹¹ are in accordance with conducted experiments. Fig. 2.21 graphically represents the relations.

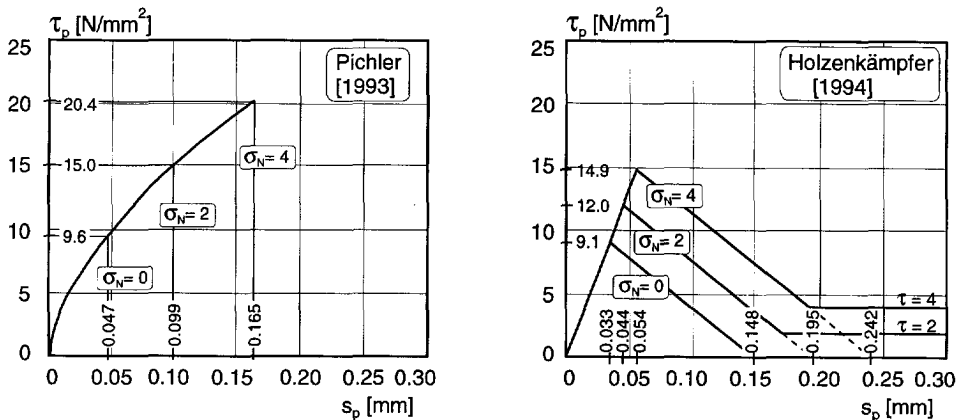


Fig. 2.21 Theoretical descriptions of bond stress-slip relations of externally bonded plates by Pichler [1993]¹¹ and Holzenkämpfer [1994]⁵

2.3.4 Maximum Plate Force and Anchorage Length

Equilibrium considerations of a part of a concrete-epoxy-plate connection, Fig. 2.22, lead to the following differential equation:

$$\frac{d^2 s_p}{dx^2} - \left\{ \frac{G_g \left(1 + \frac{E_p A_p}{E_c A_c} \right)}{t_g E_p t_p} \right\} s_p = 0 \tag{2.16}$$

with $\tau_p = \frac{G_g}{t_g} s_p$ (2.17)

The aforementioned various bond stress-slip relations were used as input to this differential equation by Holzenkämpfer [1994]⁵. Accordingly, the solved differential equation gave the maximum plate force F_{pu} and the anchorage length ℓ_a of the externally bonded plate, Table 2.II.

Table 2.II Maximum plate force and anchorage length (Betonkalender [1996]¹³)

based on Pichler [1993] ¹¹	Based on Holzenkämpfer [1994] ⁵
$F_{pu} = 13.7 b_p k_b k_c t_p^{\frac{1}{2}} \tau_{p1n}^{\frac{1}{3}}$ (2.18)	$F_{pu} = 0.35 \left\{ 1 + \frac{\sigma_n}{f_{ctm}} \right\} b_p k_b k_c \sqrt{f_{ctm} E_p t_p}$ (2.19)
$\ell_{a,max} = 66 t_p^{\frac{1}{2}} \tau_{p1n}^{\frac{1}{3}}$ (2.20)	$\ell_{a,max} = \sqrt{\frac{E_p t_p}{4 f_{ctm}}}$ with f_{ctm} of surface (2.21)

When both equations are graphically represented, Fig. 2.23, it emerges that a maximum for the anchorage length of the bonded-on plate exists. Moreover, a thicker plate results in an increased maximum force and a longer anchorage length.

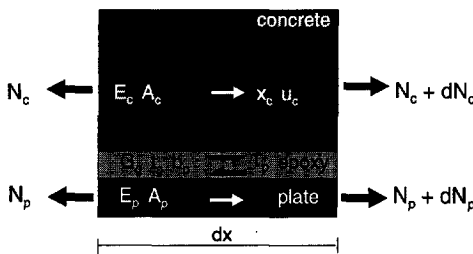


Fig. 2.22 Equilibrium of part of concrete, epoxy and plate (Holzenkämpfer [1994]⁵)

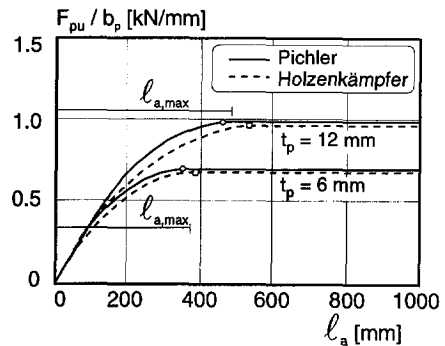


Fig. 2.23 Plate force and anchorage length (Holzenkämpfer [1994]⁵)

Bolt at Anchorage Zone

In practice, anchor bolts are often employed at the ends of the steel plate, which are intended to resist the normal and peeling forces. However, Roberts [1989b]⁷ indicated that high normal stresses occur on account of discontinuities at the plate ends. These stresses are therefore a stress concentration problem. He did not expect that the use of anchor bolts reduces the magnitude of the normal stresses. Also, it does not increase the strength of the plated beams. This had been experimentally verified by Jones et al. [1988]⁶. The use of anchor bolts did only increase the ductility of the plated beams.

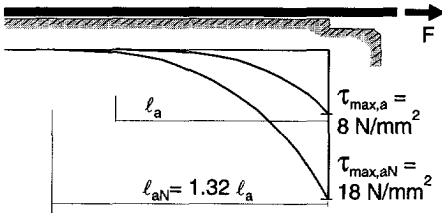


Fig. 2.24 Example of anchorage shear stresses with and without pre-stressed bolt (Münger, Ammann & Wicke [1991]¹¹)

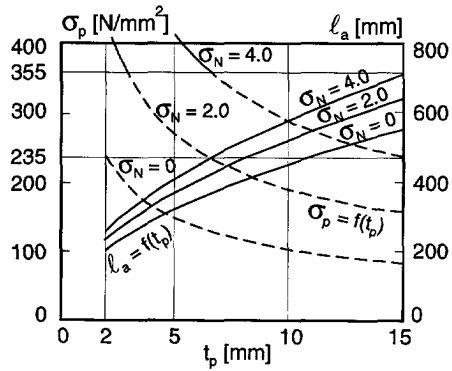


Fig. 2.25 Anchorage steel stress and anchorage length in relation to plate thickness and as a function of bolt action (Pichler [1993]¹¹)

Pichler [1993]¹¹, however, did show that by applying (pre-stressed) bolts at the end of the plates the anchorage capacity could be significantly increased, Fig. 2.24. By virtue of the bolt, the compressive stresses and friction at the interface increased the allowable shear stress. Hence, the advantage of bolts is that relatively thicker and narrower plates can be bonded showing a more ductile behaviour and allowing the steel plate to yield. Both Fig. 2.24 and Fig. 2.25 show that by applying a normal stress $\sigma_n = 4.0 \text{ N/mm}^2$, the anchorage capacity increases by 170%, whereas the anchorage length increases (only) by 30% compared with $\sigma_n = 0.0 \text{ N/mm}^2$.

2.4 Fatigue Limit State

2.4.1 General

On the fatigue response of members strengthened with externally bonded plates only a few tests have been carried out. Besides the well-known work of Ladner & Weder [1981]⁹, hardly any parameters concerning the dimensions of the bonded-on plates were investigated. Hankers [1995]⁵ recognised this lack of knowledge and investigated the fatigue response of structures and anchorage more thoroughly.

2.4.2 Structural Response of Strengthened Member

Ladner & Weder [1981]³ investigated the fatigue response of rectangular members strengthened with bonded-on plates in more detail. Eight beams and a reference beam (no. 6) were tested at four point loading with a total span of 2m. The beams ($b \times h = 250 \times 150 \text{ mm}^2$) were pre-cracked prior to bonding, the plates were bonded at a distance of 25 mm short of the support. The statically loaded reference beam failed at a maximum load of 50 kN. The results of the fatigue tests are summarised in Table 2.III. This table shows that the beams with plate stresses lower than the yield stress of the bonded-on plates ($f_{pym} = 196\text{-}242 \text{ N/mm}^2$) did not fail under the repeated loading conditions. However, when the plate tensile stresses were higher than the yield stress, two types of failure mechanisms were observed. Firstly, on three beams failure by plate separation was initiated at a flexural crack, and propagated towards the end of the plate with increasing load cycles; this failure type is characterised by Oehlers [1989]⁶ as reverse peeling cracking. Secondly, two beams suffered from fatigue in the bonded-on steel plate due to high plate stresses.

Table 2.III Results of fatigue tests (Ladner & Weder [1981]³)

beam no.	$F_{\max} - F_{\min}$ [kN]	$\sigma_{p,\max} - \sigma_{p,\min}$ [N/mm ²]	$\sigma_{p,\max} / \sigma_{py}$ [-]	cycles [-]	condition of beam
3	11.13 - 7.95	140 - 100	0.67	$10 \cdot 10^6$	intact bond
2	12.72 - 6.36	160 - 80	0.77	$10 \cdot 10^6$	intact bond
1	15.90 - 3.18	200 - 40	0.94	$10 \cdot 10^6$	intact bond
5	17.50 - 1.58	220 - 20	1.06	$2.22 \cdot 10^6$	reverse peeling cracks
4	18.28 - 0.80	230 - 10	1.17	$0.879 \cdot 10^6$	reverse peeling cracks
7	18.90 - 1.60	240 - 20	1.22	$1.26 \cdot 10^6$	fatigue of steel plate
8	19.60 - 1.60	260 - 20	1.07	$1.79 \cdot 10^6$	reverse peeling cracks
9	22.10 - 1.60	280 - 20	1.22	$0.238 \cdot 10^6$	fatigue of steel plate

An interesting failure type was obtained when, next to these rectangular beams, a T-beam (0.5 m high and span of 6 m) was tested with both bonded-on flexural and bonded-on shear plates. The flexural plate was stopped before the support to simulate the common practical case in which it is impossible to anchor the steel plate outside the support. This led to a crack in the section between the support and the end of the plate. Consequently, after surviving the first fatigue phase of $2 \cdot 10^6$ load cycles without damage, a 16 mm diameter reinforcing bar fractured at $1.64 \cdot 10^6$ load cycles in the second phase due to large stresses that occurred in this critical section. This indicated that high tensile bar stresses were present beyond the plate end in the unstrengthened part.

A diagonal crack at the end of the plate during fatigue testing was also observed by Mays [1985]². In these tests the plate was bonded 50 mm short of the support in the shear span that measured 300 mm. However, by virtue of the internal stirrups, failure was by plate separation at the level of the internal reinforcement.

Hankers [1995]⁵ performed tests to investigate the various failure mechanisms that may occur under repeated loading conditions in members strengthened with externally bonded plates. The failure mechanisms were characterised as follows:

- Plate separation by concrete failure. Failure occurred in the concrete in the vicinity of the plate-epoxy-concrete connection just above the epoxy layer.
- Plate separation by interface failure. Failure was initiated at the root of a flexural crack and subsequently grew to the end of the plate at the steel-epoxy interface (reverse peeling).
- Plate separation by epoxy failure. Failure occurred in the epoxy itself when the steel plate was highly stressed.
- Fatigue failure of steel plate. The bonded-on steel plate failed due to the fatigue loading.
- Plate separation at the level of internal reinforcement. When the unplated length between the plate end and the support was increased, the plate separated at the level of the internal reinforcement (shear and flexural shear peeling).

Hankers concluded from these preliminary tests that members strengthened in flexure are not sensitive to repeated loading conditions if the execution of bonding is correctly performed. When failure does occur, the most probable failure mechanism is plate separation through the concrete in the vicinity of the epoxy layer.

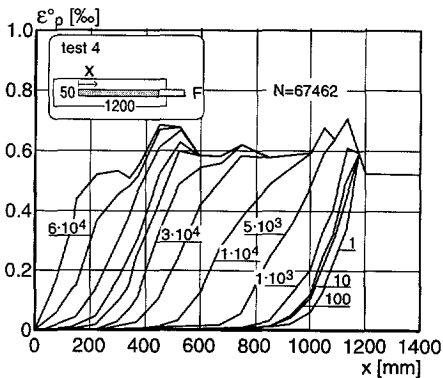


Fig. 2.26 Measured maximum strains in steel plate as a function of location and number of cycles (Hankers [1995]⁵)

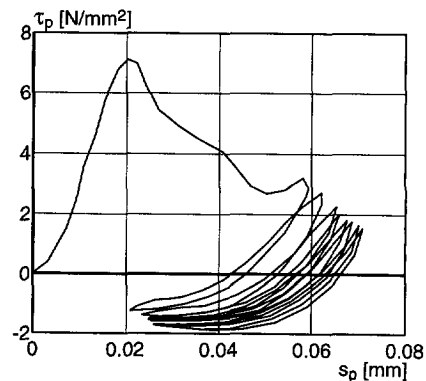


Fig. 2.27 Bond stress - slip relation derived from measured strains at last load cycles (Hankers [1995]⁵)

2.4.3 Anchorage Resistance of Externally Bonded Plate

Hankers [1995]⁵ also proposed a damage model for dynamic failure. The results of experiment no. 4 are plotted in Fig. 2.26 and Fig. 2.27. The measured strains in the steel plate clearly show that the force transfer length was approximately 300 mm for the maximum dynamic load. Also, the bond stress peak shifted from the loaded side to the non-loaded side with increasing number of load cycles. When the tail of the bond stress-slip relation during the last load cycles is examined, it emerges that

negative bond stresses were induced due to the reduction of the slip during an unloading cycle from maximum to minimum load. These negative bond stresses can only occur when compressive stresses were imposed in the steel plate.

The experimental observations were used for a damage model to describe the mechanism of dynamic bond failure, as Fig. 2.28 depicts. It shows three stages of dynamic damage which occur after the mechanism described in the static bond failure model. In the tail of the τ - s relation cracking has already been initiated. Stage (a) shows the stress-free bond with a large slip (path D-E). Then, in stage (b) the slip is reduced and secondary cracks are initiated at the other side of the grain (path E-F). The holes are filled with small damaged concrete particles. In stage (c) the bond is loaded again (F-G), and the bond capacity is reduced if compared to D.

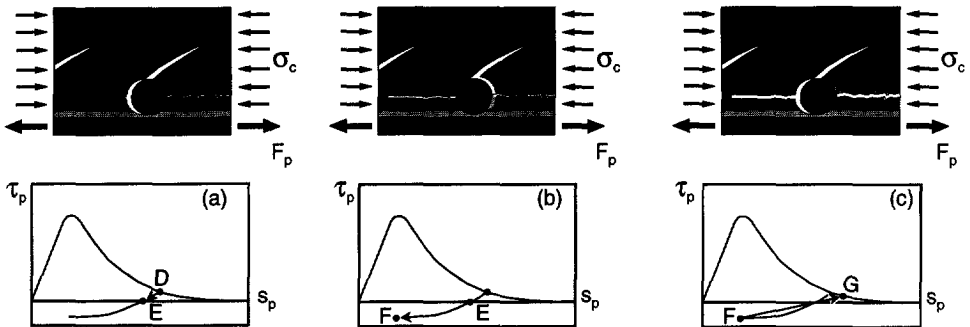


Fig. 2.28 Hankers's damage model for dynamic bond failure (Hankers [1995]⁵)

2.5 Conclusions

With respect to the literature overview on the structural behaviour of strengthened reinforced concrete structures, it is concluded that most studies focused on the flexural behaviour, the anchorage capacity, and shear strengthening. Accordingly, the basic mechanism of shear failure without shear reinforcement was hardly investigated. It is the author's opinion that shear plays a dominant role in a large number of tests on plate separation. Therefore, the research project will focus on the shear behaviour, in particular, plate-end shear. To start with, Chapter 3 shortly overviews the shear behaviour of conventionally reinforced concrete structures.

3. CONVENTIONALLY REINFORCED CONCRETE STRUCTURES - SHEAR BEHAVIOUR

For this study, shear is of great importance. This chapter therefore elaborates on the knowledge of the shear resistance of conventionally reinforced structures. §3.1 illustrates that the shear span-to-depth ratio a/d dictates the type of mechanism that contributes to the shear resistance of beams without stirrups. In §3.2, this is visualised by Kani's shear valley. Then, §3.3 compares empirical expressions of Rafta and CEB-FIP MC90 which formulate the shear resistance. This chapter concludes in §3.4 with the shear contribution of the web reinforcement.

3.1 Mechanisms of Shear Failure

3.1.1 Shear Span-to-Depth Ratio a/d

Failure of reinforced concrete beams without stirrup reinforcement is characterised by different mechanisms. A well-known publication by Leonhardt & Walther [1962]¹⁴ described tests on simply supported beams with $\rho_s = 1.88\%$. From the failure patterns depicted in Fig. 3.1 the transition into the different failure mechanisms clearly emerged for various a/d ratios. For $a/d > 7.0$ the beam failed in flexure: the internal reinforcement yielded and the concrete compression zone crushed. Due to shear failure, at lower a/d ratios (and various reinforcement ratios) the full flexural capacity is not reached. At very low ratios, this is $a/d < 1.0$, failure was caused by concrete crushing or diagonal splitting of the concrete strut which acted between the loading point and the support.

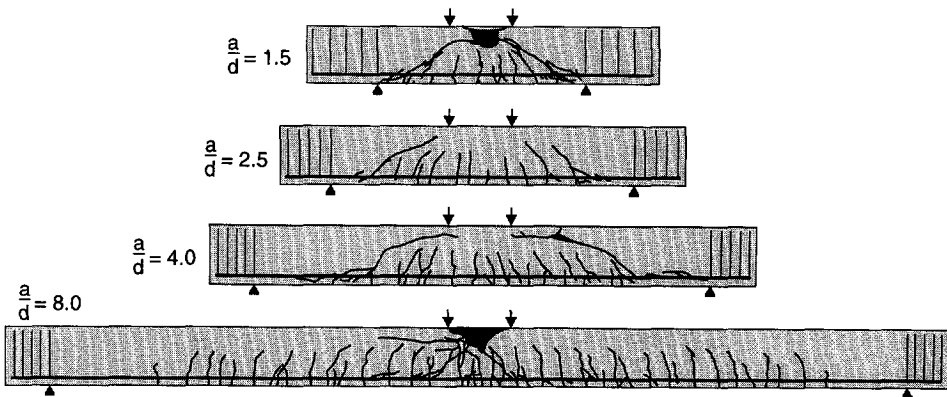


Fig. 3.1 Failure types for various ratios of a/d , $\rho_s = 1.88\%$ (Leonhardt & Walther [1962]¹⁴)

For $1.0 < a/d < 7.0$, shear failure dominated the above mentioned failure types. Within this range two types of shear failure were distinguished which are described in the subsequent sections. In general, the critical a/d ratio at which the transition between the two failure mechanisms occurs, lies around $a/d = 2.5$.

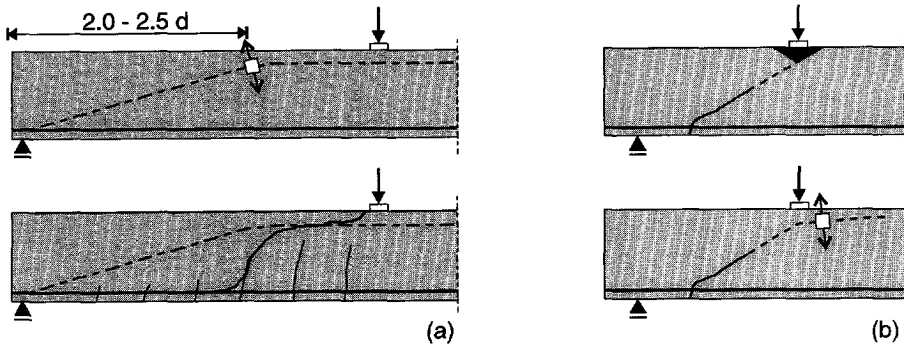


Fig. 3.2 Shear failure modes for (a) $2.5 < a/d < 7.0$ generally termed as flexural shear (b) $1.0 < a/d < 2.5$ generally termed as web shear (Kotsovos [1984, 1986]¹⁴)

3.1.2 Shear Failure Behaviour for $a/d > 2.5$

In the case of higher a/d ratios a beam fails at the load at which shear cracks develop. The shear failure crack develops from the tip of a flexural crack that was initiated due to tensile stresses in the concrete tensile zone. Thus, the inclined shear crack becomes unstable and extends through the concrete compression zone. The beam mechanism governs and shear failure is usually referred to as flexural shear failure, see Fig. 3.2.a. Sometimes, the term diagonal tension is inconsistently used.

A model that fairly well described this failure behaviour was first presented by Kani [1964]¹⁴ and known as Kani's comb-analogy, see Fig. 3.3. Due to the bending moment, cracks develop in the shear span. Accordingly, concrete teeth are formed between these cracks and are considered cantilevers fixed to the uncracked arch. By virtue of the bond between the concrete and the longitudinal reinforcement the cantilever is loaded. As the tensile strength at the root of a tooth is exceeded the flexural crack is transformed into a shear crack. As a result, the cantilever is separated from the arch, and because the remaining arch is not capable of resisting the external load, shear failure occurs.

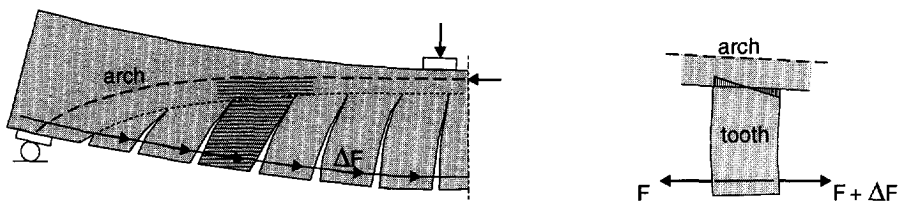


Fig. 3.3 Kani's comb analogy and equilibrium of concrete tooth (Kani [1964]¹⁴)

It is generally known that Kani's model underestimates the measured shear capacity because the contribution of the sliding crack faces is not taken into account. Taylor [1974]¹⁴ indicated that approximately 25 to 45% of the total shear force is transferred by the uncracked arch (beam action), 30 to 50% by the mechanism of aggregate interlock and 15-25% by dowel action of the longitudinal reinforcing bars.

3.1.3 Shear Failure Behaviour for $1.0 < a/d < 2.5$

In the case of lower a/d ratios inclined cracks in the shear span stabilise and the shear load could be increased. Then, failure is due to web shear or/and shear-compression failure (Russo et al. [1991]¹⁴). Web shear is adequately predicted by the principal stress computed in the web of an uncracked section because a web-shear crack is initiated before flexural cracks form in its vicinity. With respect to shear-compression failure, Kotsovos [1984]¹⁴ doubted the occurrence of the crushing mode in the region of the loading point because a multiaxial compressive state of stress is present. Instead, he stated that the path of branching of the diagonal crack is that according to the compressive stress trajectories. This is characterised by the presence of tensile stresses perpendicular to the compressive path near the diagonal crack tip, see Fig. 3.2.b. Hence, failure occurs in the middle span due to compression-tension failure.

3.2 Kani's Flexural Shear Valley

Kani [1964]¹⁴ graphically evaluated the relative strength of reinforced concrete beams over a wider range of different a/d ratios, see Fig. 3.4. The results of 14 beams showed that due to shear failure for $a/d = 2.5$ the maximum moment capacity, expressed as a percentage of the full flexural capacity, reached a minimum value of about 50%. Up to $a/d = 1.5$ and beyond $a/d = 5.2$ shear failure is not expected.

It has already been explained that shear failure for $a/d > 2.5$ is governed by the capacity of the concrete teeth. This capacity is influenced by the percentage of reinforcement, the ratio of the yield stress of the bars to the tensile strength of the concrete and on a so-called crack factor, describing the spacing and length of cracks (Kani [1964]¹⁴). When graphically represented, this appears to be a linear function of the shear span-to-depth ratio a/d .

For a/d values smaller than 2.5, if the beam is transformed into an arch, shear failure is governed by the capacity of this remaining arch. The relative beam capacity is influenced by the depth of the compressive zone in flexural failure to the reduced depth at shear failure, and seems to be equal to d/a (Kani [1964]¹⁴). By inserting a biaxial stress condition factor the theoretical capacity of the remaining arch shows good accordance with the experimental results, see Fig. 3.4.

After conducting an experimental program, Kani [1966]¹⁴ concluded that the shear strength of reinforced concrete beams is not dependent on the concrete strength. In that case, the region of shear failure is clearly visualised in a three-dimensional co-ordinate system in which M_{vcu} / M_{fl} , a/d and ρ_s are plotted on the

axes. This region is known as Kani's shear valley and is limited by the characteristic boundary lines D and T. With varying ρ_s , line D seems to be an approximate constant equal to $a/d = 1.0$. Line T varies. The deepest point of the valley appeared to occur at $a/d = 2.5$. For $\rho_s < 0.5\%$ the shear valley disappeared completely.

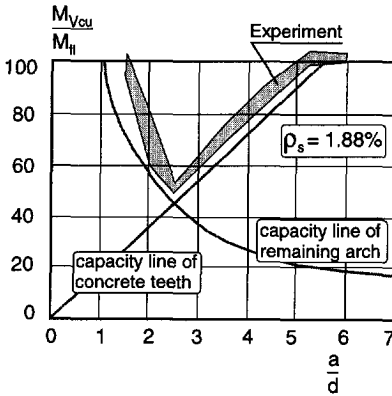


Fig. 3.4 Relative beam strength versus a/d at $\rho_s = 1.88\%$ (Kani [1964]¹⁴)

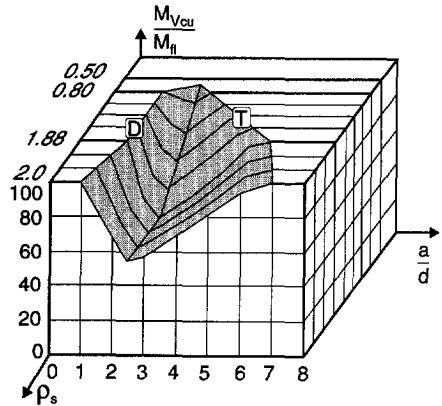


Fig. 3.5 Relative beam strength versus a/d and ρ_s (Kani [1966]¹⁴)

3.3 Formulations for the Shear Resistance

3.3.1 Expressions on Flexural Shear: Rafla and MC90

This section presents two expressions for the mean shear resistance for concrete members without shear reinforcement. This shear resistance forms the basis of the shear formulas and is used in some building codes. Hence:

$$\tau_{cum} = \tau_{cum} b d \tag{3.1}$$

$$\tau_{cum} = C_{m,Rafla} \alpha_u \sqrt{f_{cm}} \sqrt[3]{\rho_0} d^{-0.25} \tag{3.2}$$

[Rafla]

$$\text{where } \alpha_u = 6.0 - 2.2 \frac{a}{d} \tag{3.3}$$

$1.0 < \frac{a}{d} < 2.0$

$$\alpha_u = 0.795 + 0.293 \left(3.5 - \frac{a}{d} \right)^{2.5} \tag{3.4}$$

$2.0 < \frac{a}{d} < 3.5$

$$\alpha_u = 0.90 - 0.03 \frac{a}{d} \tag{3.5}$$

$3.5 < \frac{a}{d}$

$$\tau_{cum} = C_{m,MC90} \sqrt[3]{3 \frac{d}{a} \left(1 + \sqrt{\frac{200}{d}} \right)^3 \rho_0 f_{cm}} \tag{3.6}$$

[CEB-FIP MC90]

3.3.2 Evaluation of Mean Maximum Nominal Shear Stress

The mean nominal shear stress τ_{cum} was empirically determined by, amongst others, Rafla [1971]¹⁴ and CEB-FIP MC90 [1990]¹⁴. The factors $C_{m,MC90}$ and $C_{m,Rafla}$ are constants which have to be determined afterwards. $C_{m,MC90}$ is a constant of 0.15, however, the expression represents an estimation for the shear force *causing* cracking. To obtain an equation for the mean maximum nominal shear stress, a comparison with data of 170 tests was made to establish an improved factor. These data points were obtained from CEB bulletin 224 [1995]¹⁴ (results of Elzanaty et al. omitted) and from Taylor [1971]¹⁴, see Appendix A. Fig. 3.6 evaluates the maximum shear stress of both the Rafla and MC90 equations. It emerges that for $C_{m,Rafla} = 0.85$ and $C_{m,MC90} = 0.18$ the analytically calculated maximum nominal shear stresses are in good agreement with the empirically obtained stresses $\tau_{c,exp}$.

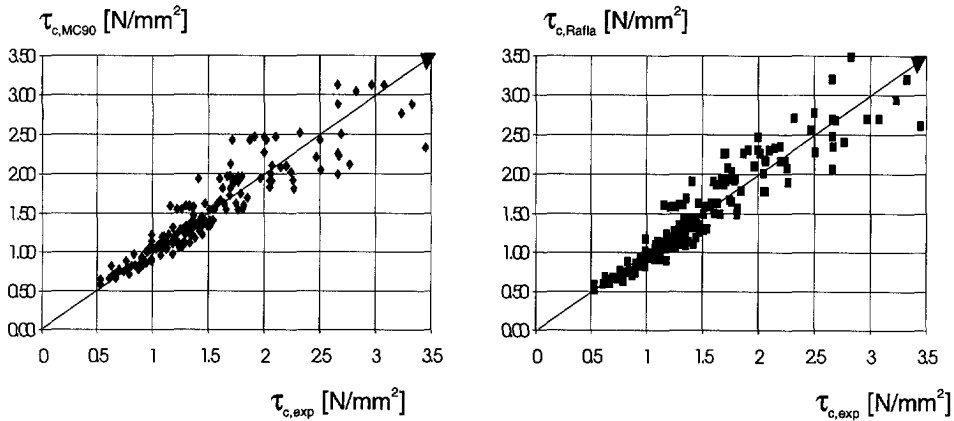


Fig. 3.6 Evaluation of maximum shear stress according to CEB-FIP MC90 and Rafla

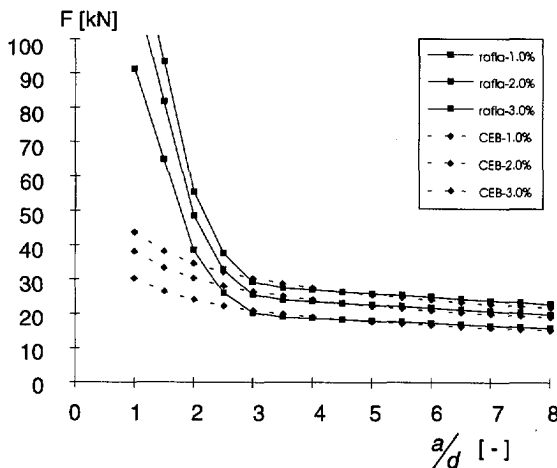


Fig. 3.7 Comparison between shear expressions according to CEB-FIP MC90 and Rafla

3.3.3 Comparison between Rafla and MC90

When the equations are mutually compared in Fig. 3.7, it is seen that for shear span-to-depth ratios $a/d > 3.0$ both equations are in correct agreement. However, for $a/d < 3.0$ the CEB-FIP MC90 equation does not fully take the contribution of arch action into account. On the contrary, Rafla's prediction for the shear capacity seems correct for all shear span-to-depth ratios and various reinforcement ratios.

3.4 Shear Resistance of Members with Web Reinforcement

3.4.1 Truss Analogy

When the shear capacity of a member is exceeded, web reinforcement is needed to increase the load bearing capacity. Consequently, brittle shear failure is excluded by virtue of the reinforcing bars bridging the shear cracks. As a result, the diagonal cracks fully develop as illustrated in Fig. 3.8. This crack pattern gave rise to the idea of the truss analogy of Ritter and Mörsch. A truss model is constructed with parallel top and bottom flanges at a distance of the internal lever arm. The truss members consist of compression struts inclined by definition at 45° to the beam axis (principal stresses in uncracked situation), and tension ties located at a distance z formed by a number of internal stirrups. Hence, according to the pure truss analogy, the amount of web reinforcement equals:

$$\frac{A_{sw}}{s} = \frac{V_{wd}}{z f_{ywd}} \quad (3.7)$$

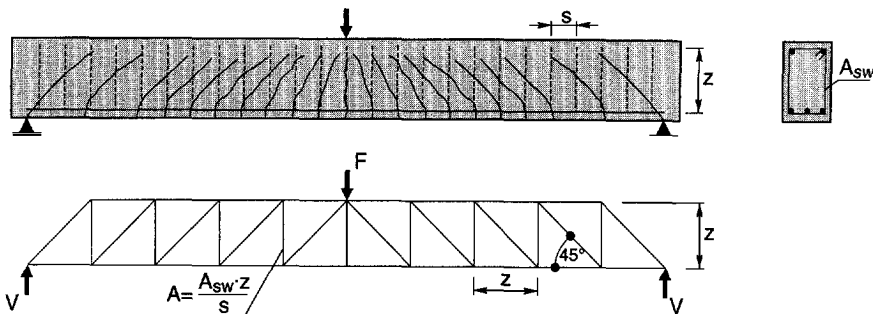


Fig. 3.8 Fully developed crack pattern and truss model of Ritter and Mörsch

3.4.2 Truss and Arch Contribution

Although the truss model fairly well describes the internal force distribution, experiments by Leonhardt [1977]¹⁴ indicated that the pure truss analogy overestimates the steel stress in the stirrups, see Fig. 3.9. It appeared that the difference in shear resistance ΔV between the predicted value by the pure truss

analogy and the measured value of the experiment equals the shear resistance of a beam without web reinforcement. Apparently, the concrete arch of the beam was capable of transferring a part of the shear load directly to the support. This is referred to as arch action, see Fig. 3.10. As a result of the small crack widths at the crack tips, the line of compression could be present just above or even through these crack tips.

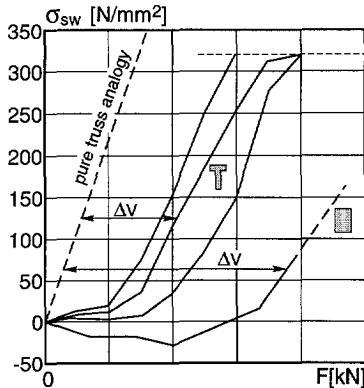


Fig. 3.9 Stress in stirrups as a function of shear load (Leonhardt [1977]¹⁴)

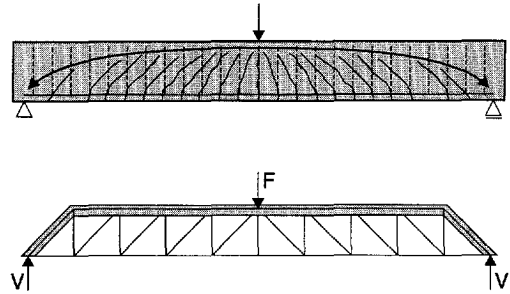


Fig. 3.10 Illustration of arch action

3.4.3 Elements Requiring Design Shear Reinforcement According to EC2

General

The method for shear design in EC2 is based on three values of design shear resistance:

- V_{Rd1} the design shear resistance of the member without shear reinforcement
- V_{Rd2} the maximum design shear force that can be carried without crushing of the notional concrete compressive struts
- V_{Rd3} the design shear force that can be carried by a member with shear reinforcement

For sections where the design shear force V_{Sd} exceeds V_{Rd1} , shear reinforcement should be provided such that:

$$V_{Sd} < V_{Rd3} \quad (3.8)$$

For cases where the design shear force exceeds the design shear resistance, two design methods could be used to calculate the shear reinforcement, namely the standard method or the variable strut inclination method.

Standard Method of EC2

The shear resistance of a section with shear reinforcement is given by:

$$V_{Rd3} = V_{Rd1} + V_{wd} \quad (3.9)$$

$$V_{wd} = \frac{A_{sw}}{s} 0.9d f_{ywd} \quad (3.10)$$

in which V_{wd} denotes the contribution of the vertical shear reinforcement. When the notional concrete compression struts are checked against crushing, the maximum design shear force for members with vertical stirrups is given by:

$$V_{Rd2} = \frac{1}{2} v f_{cd} b_w 0.9d \quad (3.11)$$

Variable Strut Inclination Method of EC2

The variable strut inclination method to design for shear is based on the concept of rotation of the concrete struts as a result of the transfer of shear stresses by means of friction between the crack faces (Walraven & Al-Zubi [1995]¹⁴, Stroband [1997]¹⁴), Fig. 3.11. The compressive stress of the struts is limited to $v f_{cd}$ in which v denotes a effectiveness factor. Accordingly, for elements with vertical shear reinforcement, the shear resistance is defined by the crushing strength of the concrete strut V_{Rd2} and the yield strength of the vertical shear reinforcement crossing a crack V_{Rd3} . Hence,

$$V_{Rd2} = b_w z v f_{cd} / (\cot\theta + \tan\theta) \quad (3.12)$$

$$V_{Rd3} = (A_{sw} / s) z f_{ywd} \cot\theta \quad (3.13)$$

In Eurocode 2, the inclination of the concrete struts is limited to $30^\circ < \cot\theta < 60^\circ$. The minimum amount of shear reinforcement is found when an angle of inclination of the struts is taken 60° . In experiments, if a certain amount of stirrup reinforcement is provided, both the inclination of the concrete strut at failure and the shear resistance are found by equalising V_{Rd2} and V_{Rd3} .

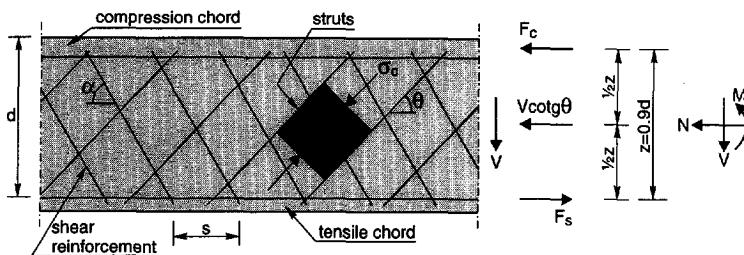


Fig. 3.11 Variable strut inclination method for members subjected to shear

4. FRAMEWORK OF EXPERIMENTAL STUDY

This chapter is the introductory chapter to Part II and deals with the framework of the experimental study. At first, it discusses the aim of the experimental program in §4.1. Then, §4.2 describes tests on two simply supported beams as a reference for further analyses. §4.3 deals with the experimental modelling, test set-up and testing procedure. It discusses the measuring system and describes the displacement controlled loading procedure. Then, §4.4 covers the material aspects and clarifies the preparation of the beam-ends. Finally, §4.5 presents a complete overview of the test series on plate anchorage and beam shear.

4.1 Aim of the Experimental Program

The main goal of the experimental program was to gain experimental evidence of and insight into the influence of the partially plated beam on plate anchorage and beam shear. Both the deformational behaviour and the failure mode are of particular interest. As described in the previous state-of-the-art survey, as far as the influence of plate length, bolted anchorage and repeated loading conditions are concerned, knowledge is still lacking. Also, the influence on beam shear of the plate length and the geometry of both the steel plate and the concrete member is still unclarified. The subsequent Chapters 5 and 6 therefore discuss in detail the laboratory experiments on plate anchorage and beam shear, respectively.

The experimental evidence obtained on plate anchorage and beam shear will form the first step into the direction of the development of a model. However, before the experiments on plate anchorage and beam shear are discussed, two initial tests on simply supported beams are described as a reference for further numerical and analytical analyses.

4.2 Reference Tests on Unplated and Plated Beams

4.2.1 Estimation of Flexural and Shear Capacity

Material Properties

An analytical study was first carried out to estimate the bearing capacity with respect to flexure and shear of beams with variable reinforcement ratio and shear span length. For the study the following material properties are assumed:

$$f_{cm} = 36 \text{ N/mm}^2, f_{sym} = 600 \text{ N/mm}^2 \text{ and } f_{pym} = 285 \text{ N/mm}^2$$

Flexural Capacity

For the design of reinforced concrete members the cross sectional area of the reinforcement is calculated. The internal reinforcement is assumed to be in horizontal equilibrium with the internal maximum force of the concrete compression zone at failure and the longitudinal reinforcement must yield before the concrete in the compression zone crushes. When full bond is assumed between the plate and the concrete the same analysis may also be carried out for a cross section with an external steel plate bonded on the tension side. Fig. 4.1 sketches the cross section of a plated beam. Table 4.1 lists the calculated flexural capacity for plated beams with various plate geometries. The beams that are considered measure 100×200 mm² and contain two 8 mm diameter bars ($A_s = 100.5 \text{ mm}^2$). The shear span is 800 mm. If a strengthening ratio of 5 (A_p / A_s) is applied by bonding a 5×100 mm² steel plate, it emerges that an increase of 3.4 of the flexural capacity could be expected. Then, both the internal bars and the external plate yield.

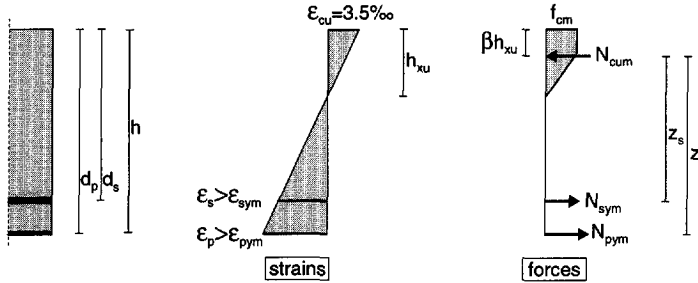


Fig. 4.1 Cross section of a beam with externally bonded plates

The flexural capacity of the cross section is calculated with:

$$M_{fl} = A_s f_{sym} (d_s - \beta h_{xu}) + A_p f_{pym} (d_p - \beta h_{xu}) \quad (4.1)$$

$$N_{cum} = \alpha b h_{xu} f_{cm} \quad (\beta = 0.388, \alpha = 0.75) \quad (4.2)$$

Table 4.1 Calculated results on flexural capacity

plate [mm ²]	unplated	2×40	3×60	4×80	5×100
d_{sp} [mm]	170	184.4	191.2	195.5	198.3
N_{pym} [N]	0	22800	51300	91200	142500
N_{sym} [N]	60318	60318	60318	60318	60318
h_{xu} [mm]	22.4	30.9	41.5	56.3	75.3
N_{cum} [N]	-60318	-83118	-111618	-151518	-202818
M_{fl} [kNm]	9730	13876	18873	25505	33396
$F_{fl, span}$ [kN]	12.16	17.34	23.59	31.88	41.75
$F_{fl} / F_{fl, unpl}$	1.00	1.43	1.94	2.62	3.43

Shear Capacity

If full bond is assumed between the concrete and the plate, just as between the concrete and the internal ribbed bars, the conventional expressions for the shear capacity may also be applied for plated members. For this purpose the flexural shear capacity for fully plated members is calculated with Rafla's expression (equations 3.1 and 3.2), see Table 4.II. It emerges that a strengthening ratio of 5 by bonding a 5×100 mm² plate results in only an increase of 2.0 of the shear capacity.

Table 4.II Calculated results on shear capacity (according to Rafla)

	unplated	2×40	3×60	4×80	5×100
d_{sp} [mm]	170	184.4	191.2	195.5	198.3
ρ [%]	0.59	0.98	1.47	2.15	3.03
a/d_{sp} [-]	4.71	4.34	4.18	4.09	4.03
α_u	0.76	0.77	0.77	0.78	0.78
$M_{V_{cum}}$ [kNm]	12224	15584	18432	21368	24256
V_{cum} [kN]	15.28	19.48	23.04	26.71	30.32
$V_{cum} / V_{cum,unpl}$	1.00	1.27	1.51	1.75	1.98

Comparison between Flexural Capacity and Shear Capacity

When Table 4.I and Table 4.II are compared in Fig. 4.2 and Fig. 4.3, it is seen that at lower reinforcement ratios the flexural capacity governs failure. However, at higher reinforcement ratios, failure is dominated by flexural shear. Accordingly, applying more flexural reinforcement has little effect on the shear capacity. Hence, one can conclude from the analytical study that if a beam is strengthened in flexure, and, thus, the reinforcement ratio increases, the shear capacity by flexural shear becomes more critical in comparison with the flexural capacity.

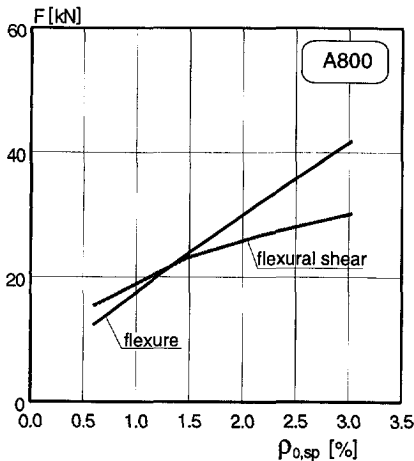


Fig. 4.2 Influence of reinforcement ratio on flexural capacity and flexural shear capacity

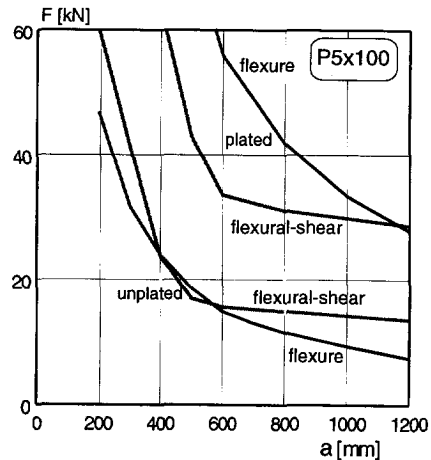


Fig. 4.3 Influence of shear span on flexural capacity and flexural shear capacity

4.2.2 Experimental Set-Up

Test Set-Up and Beam Geometry

As a reference for further tests, two beam tests are first described. Two simply supported reinforced concrete beams with an effective span of 2400 mm were tested by four point loading, Fig. 4.4. A conventionally reinforced reference beam BM0 ($\rho_s=0.59\%$) and a $5 \times 100 \text{ mm}^2$ plated beam BM1 ($\rho_{sp} = 3.03\%$) were tested. Table 4.III lists the specific geometries used for test series BM. Roller bearings were placed at the support to allow horizontal displacements. The vertical deflections were recorded by measurements at the loading point and at the support to take the setting of the rubber bearings into account. Both the test beams were provided with 6 mm diameter stirrups spaced 75 mm.

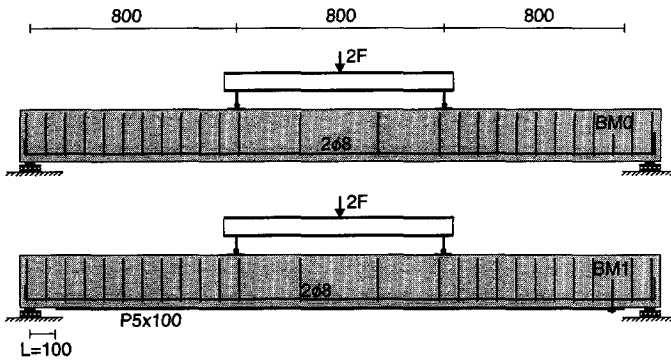


Fig. 4.4 Experimental set-up for simply supported beams

Table 4.III Details of test series BM

	A_s [mm ²]	A_p [mm ²]	A_{sw} [mm ²]	L [mm]	$b \times h$ [mm ²]	span [mm]
BM0	100.5 (2Ø8)	-	Ø6@75	-	100 × 200	2400
BM1	100.5 (2Ø8)	500 (5×100)	Ø6@75	100	100 × 200	2400

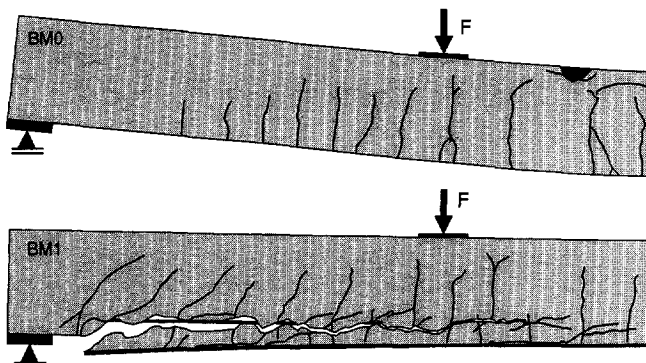


Fig. 4.5 Crack patterns of beams BM0 and BM1

4.2.3 Failure Behaviour

Crack Patterns

A clear difference in the failure behaviour of BM0 and BM1 was observed, Fig. 4.5 . The full flexural capacity was reached in the case of BM0. A ductile type of failure for BM0 occurred: yielding of the internal bars followed by crushing of the concrete compression zone at large deflections. The occurrence of large cracks at mid span and large deflections due to yielding of the internal reinforcement were clearly visible. On the contrary, the flexural capacity of BM1 was not reached. The bonded-on plate separated suddenly and, consequently, the failure response was a very brittle one. Plate separation by concrete cover rip-off was initiated at the end of the bonded-on plate. In Appendix C the crack pattern development for both beams at three loading stages is sketched more in detail.

Load-Deflection Diagram

In Fig. 4.6 the load-deflection relation for BM0 and BM1 are shown. BM0 failed due to flexure at a load $2F$ of 24.1 kN. The deflection of the beam was about 48 mm when the concrete compression zone crushed, about 3.7 times the deflection at which the reinforcement started to yield. The predicted analytical flexural load $2F$ of 24.3 kN calculated with $f_{\text{sym}} = 600 \text{ N/mm}^2$ appeared to be sufficiently accurate.

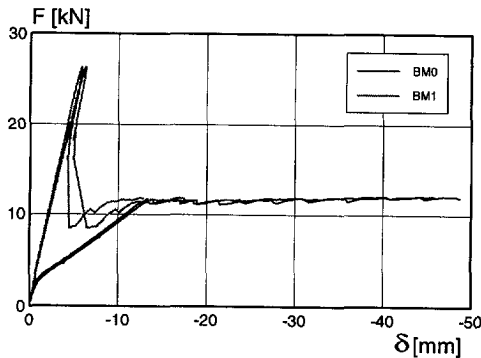


Fig. 4.6 Load-deflection response of unplated beam BM0 and plated beam BM1

The failure load of BM1 was $2F = 52.7 \text{ kN}$. Hence, the maximum flexural capacity of 83.5 kN (analytically calculated) was evidently not reached. Thus, instead of a strengthening factor of 3.4 for full flexural capacity only a ratio of 2.2 was obtained by applying an external plate of $5 \times 100 \text{ mm}^2$ with an unplated length of 100 mm. After separation of the external plate, the response of the deflection-controlled beam BM1 was similar to BM0 as it emerges from the load-deflection curves. Accordingly, the beam finally acted as an unplated beam. It must be remarked that the load-deflection curve for BM1, sketched in Fig. 4.6, is the response of a second loading. Due to an incorrect initial value of the control signal, the beam was already loaded with an initial load of about $2F = 38 \text{ kN}$, see Appendix C.

Modules of Toughness

The area under the load-deflection curve up to the failure load is defined as the modules of toughness as a criterion for measuring ductility, Hussain et al. [1995]¹⁰. This modules of toughness represents the energy absorbed by the beams up to failure. In order to compare the ductility of BM0 and BM1, the relative modules of toughness was derived, see Fig. 4.7. The area under the load-deflection curve for BM1 was only 0.18 times the magnitude of BM0. This means a tremendous decline of ductility occurred when the beam was partially strengthened by a 5×100 mm² steel plate. Hence, in practical designs an increase of the sustainable load by a ratio of 2.2 is only partly advantageous, because as a consequence of brittle failure, a higher safety factor should be taken into account.

Flexural stiffness of Beams

For a simply supported four-point loaded beam with continuous longitudinal reinforcement the (uncracked) flexural stiffness EI equals:

$$EI = \frac{5}{162} \frac{Fl^3}{\delta} \quad (4.3)$$

Despite the partially plated shear span, this relation is also used to derive the flexural stiffness for beam BM1. Fig. 4.8 shows the stiffness-load curves for BM0 and BM1. (Note that linear elastic is calculated $EI_{BM0} \approx 2000 \text{ kNm}^2$ and $EI_{BM1} \approx 3000 \text{ kNm}^2$). The initial stiffness of BM1 was (of course) higher than the initial stiffness of BM0. Due to flexural cracks the stiffness of BM0 reduced significantly with increasing load: at 50% of the maximum load the flexural stiffness EI was about 25% of the initial stiffness. On the contrary, with increasing load the flexural stiffness of BM1 hardly decreased due to a large cross sectional area of the steel plate and a large lever arm of the external reinforcement. However, after plate separation at the maximum load the stiffness EI clearly declined and amounted to that of the flexural stiffness of the reference beam BM0. The beam acted as an unplated beam.

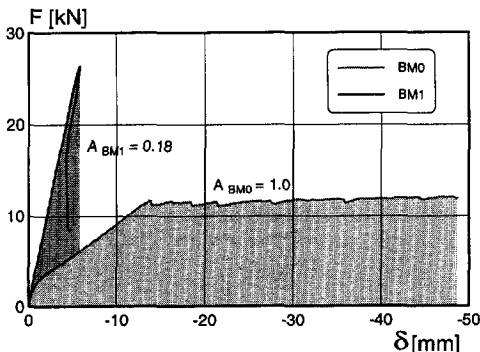


Fig. 4.7 Relative modules of toughness of BM0 and BM1 (Hussain et al. [1995]¹⁰)

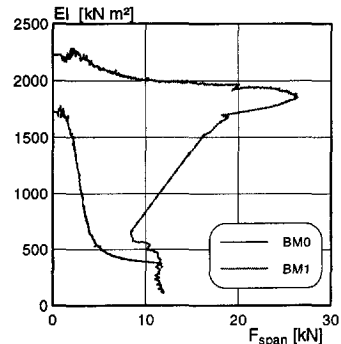


Fig. 4.8 Flexural stiffness as a function of the load

4.2.4 Development of Plate Stresses

Strain gauges were glued on the outside of the external plate of BM1, Fig. 4.9. The tensile stresses in the external plate as well as the shear stresses in the epoxy layer were derived by means of recorded strains. The tensile stresses in the bonded-on plate were determined using a Young's modulus of $E_p = 190000 \text{ N/mm}^2$.

In Fig. 4.10.a the tensile stresses in the steel plate are plotted for load stages up to $F=25 \text{ kN}$. The shape of the stress distribution was identical to the moment diagram. At a load of 25 kN the tensile plate stress in the constant moment region equalled $160\text{-}165 \text{ N/mm}^2$. After having reached $F=26.3 \text{ kN}$, the load dropped to about $F=12.5 \text{ kN}$ due to the initiation of a peeling crack. Accordingly, the plate stresses in the anchorage zone changed, see Fig. 4.10.b. At the end of the steel plate at the left span side no plate stresses were observed. When the load suddenly dropped to about $F=8.6 \text{ kN}$ and the plate fully separated, these zero stresses changed into compressive stresses due to a negative curvature of the separated plate. The tensile force in the external plate must be completely taken over by the internal bars. Accordingly, the internal reinforcement yielded and the load remained constant with increasing deflection.

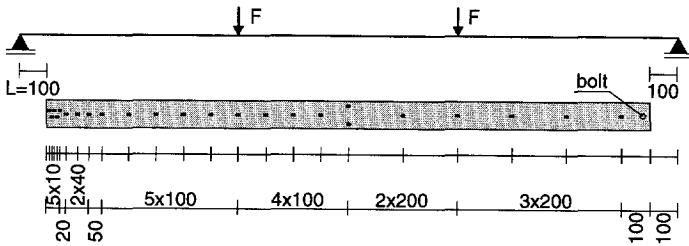


Fig. 4.9 Positions of strain gauges on bonded-on plate

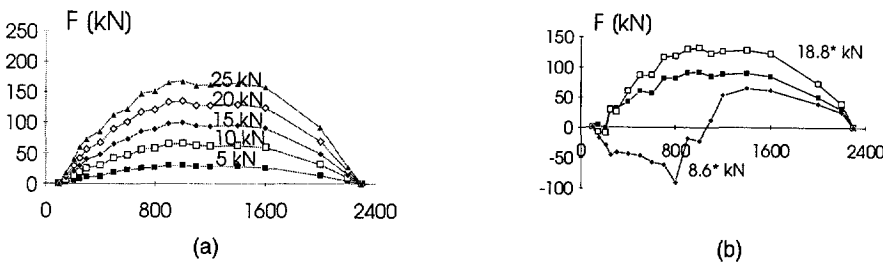


Fig. 4.10 Tensile stresses in external plate (a) before and (b) during plate separation

4.2.5 Conclusion

If a structural member is partly strengthened with a bonded-on steel plate, plate separation can occur. In the tested beam BM1 plate separation was very brittle and resulted in a load bearing capacity far less than the flexural capacity for which the beam was initially designed. After plate separation the beam responded similar to a conventionally reinforced concrete beam.

4.3 Test Set-Up and Testing Procedure

4.3.1 Experimental Modelling

Considerations for Experimental Modelling

Despite the fact that in practical situations about 90% of the strengthened structures are slabs, beam-ends have been tested in this study, see Fig. 4.11 and Fig. 4.12. The main reason for this is that the cracking and failure behaviour is better to follow on the front and back side of the specimen. A statically determined beam-end was obtained by clamping the external plate (A) and applying a hinge in the concrete compression zone (B) at 1/6 of the height of the beam. Support (B) as well as support (C) are knife-edge hinges for friction free rotation. The internal longitudinal reinforcement stopped at the clamped side. To prevent plate separation due to imposed deformations at the clamped side, the bonded-on plate was also additionally clamped by means of steel bars (D). The load was applied at (E).

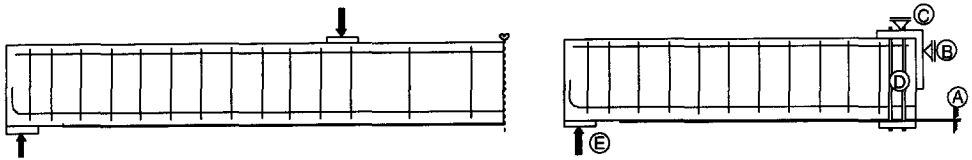


Fig. 4.11 Modelling of beam for experiments; arrangements for boundary provisions

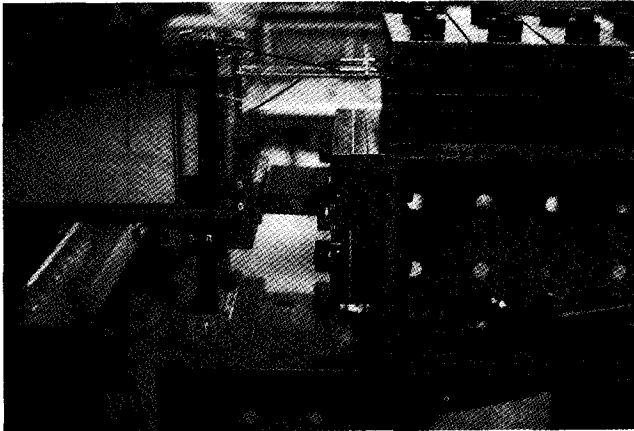


Fig. 4.12 Photograph of boundary provisions

Geometry of Beam-End

Concrete specimens with a cross section of $100 \times 200 \text{ mm}^2$ were reinforced with two 8 mm diameter ribbed bars ($\rho_s = 0.59\%$) at an effective depth d_s of 170 mm. The external plates used in the test series consisted of various cross sections, ranging

from $5 \times 100 \text{ mm}^2$ ($\rho_{sp} = 3.03\%$) to $3 \times 60 \text{ mm}^2$ ($\rho_{sp} = 1.47\%$). The epoxy layer (see §4.4.1) between the concrete surface and the bonded-on steel plate had an average thickness of approximately 1.5 mm. Accordingly, the effective depth d_p of the external reinforcement ranged between 203-204 mm. When provided, 6 mm diameter stirrups were spaced at 75 mm. The test set-up provided a shear span of 800 mm, thus modelling a beam with a total span of 2400 mm.

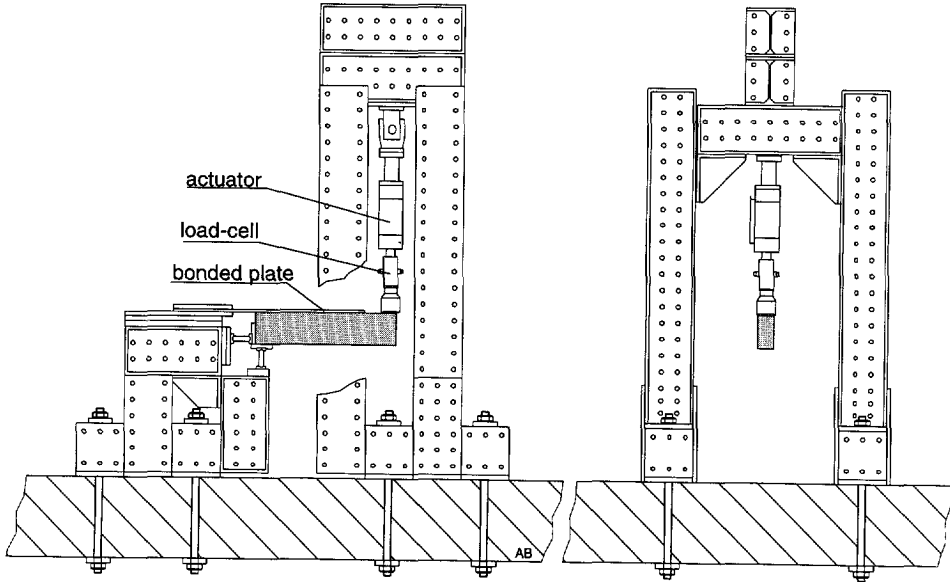


Fig. 4.13 Experimental set-up mounted on floor; side view and cross section

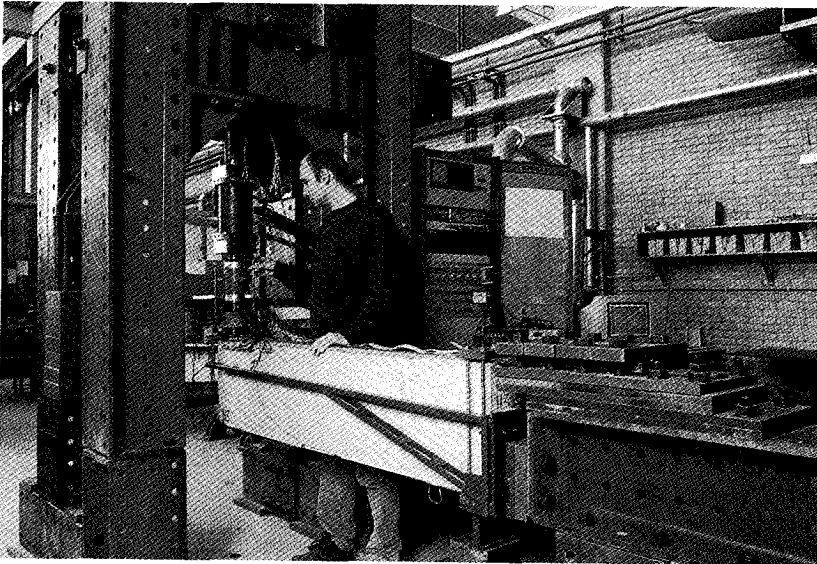


Fig. 4.14 Photograph of experimental set-up

4.3.2 Test Set-Up

To perform all the experiments; beams, beam-ends, static loading, repeated loading, one set-up was built in which all demands were satisfied. This resulted in a four-footed frame in which the load cell and the hydraulic actuator were mounted. The specimen was fixed to a different frame which was changed according to the required boundary conditions. Fig. 4.13 shows the set-up which was used for most of the experiments (series A and S-P), Fig. 4.14 shows a photograph (series S-H). The beam-end was tested up-side-down in order to clearly observe the steel plate.

4.3.3 Measurements

Measuring System

Two types of measurements were carried out: LVDT measurements in order to register (relative) displacements over cracks and strain-gauge measurements in order to register strains in the steel plate for deriving shear stresses in the epoxy layer. During the tests various measurements were carried out at different positions on the specimen. The measurements that were carried out on all beam-ends are shown in Fig. 4.15.

Load Deflection Measurements

The vertical overall displacement of the specimen at the loading point was measured by two 60 mm stroke LVDTs no. 2 and no. 3, which were directly connected to the four-footed frame. In these measurements displacements resulting from the elongation of the free part of the external plate at the clamped side (rotation) were also included and represent therefore not only the deflection of the shear span. Therefore, also the deflection of the beam-end was measured by LVDT no. 15 fixed to a frame, which was connected to the steel shoe at (B) and (C), see Fig. 4.11. When measurements of LVDT no. 15 were compared to results of no. 2/3, it was observed that particularly at failure no. 15 showed a snap-through, whereas no. 2/3 showed a snap-back behaviour.

Local Measurements with LVDTs

LVDTs no. 5 and no. 6 were positioned perpendicular to the plate at the anchorage zone. These LVDTs recorded a relative displacement when a peeling crack was initiated at the end of the plate. The main purpose for measurements of the LVDTs no. 2/3 and LVDTs no. 5/6 is test control, see next section. LVDTs no. 9 and no. 10 were positioned over the end of the plate to register the initiation of the bending/notching crack in the unstrengthened part.

Local Measurements with Strain Gauges

Strain gauges were glued at four locations on the plate at the clamped side to check for undesired yielding during the test execution. As mentioned earlier, during the tests various measurements were or were not carried out. The position of strain gauges will be shown in §5.2.4 as the specific anchorage tests are discussed.

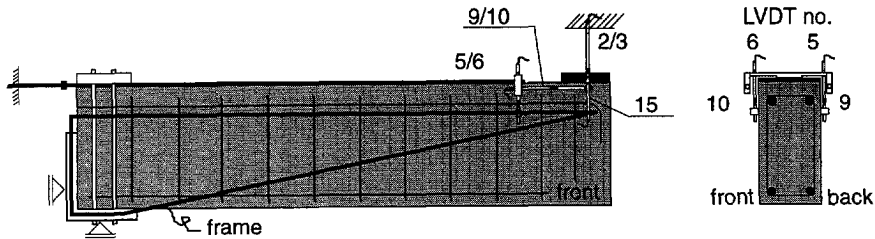


Fig. 4.15 Measurements on specimen by LVDTs and strain gauges

4.3.4 Test Control

Since failure of an externally plated specimen was expected to be sudden due to the plate peeling crack, and in order to study the failure mechanism thoroughly, deformation control was adopted as a loading procedure. The average of the sum voltage of the four measuring devices LVDTs no. 2/3 (overall displacement at loading point) and LVDTs no. 5/6 (deformation at crack localisation) was used to control the deformation rate. The summation of the voltage was such that up to peeling crack widening the overall deflection of the specimen was the controlling parameter, but during failure the crack widening rate measured by LVDTs no. 5/6 dominated the deformation rate. In such a way, peeling was well observed and the test was carried out in a rather stable way. However, sometimes a load drop of a few kN suddenly occurred as a result of either insufficient oil supply or the occurrence of a large crack at a position outside the measuring length of the LVDTs.

4.4 Specimen Preparation

4.4.1 Materials

Concrete

All the experiments were performed using a normal strength gravel concrete with 8 mm maximum aggregate, 375 kg/m³ Portland cement and a *w/c* ratio of 0.53. After 28 days the mean cube compressive strength $f_{cm,cube}$ amounted to 45.5 N/mm², the uniaxial compressive strength was $f_{cm} = 35.9$ N/mm². The mean cube tensile splitting strength $f_{ctm,sp}$ was 3.03 N/mm². The uniaxial tensile strength is assumed to be 0.9 the tensile splitting strength, so $f_{ctm,ax} = 2.75$ N/mm². Young's modulus was 32000 N/mm² and Poisson's ratio was assumed to be 0.2. See Appendix B for the concrete strengths during testing.

Ribbed bars

For the internal reinforcement ribbed bars FeB500 ($f_{sym} = 592$ N/mm²) were used. For the longitudinal reinforcement 8 mm diameter ribbed bars were used and 6 mm diameter ribbed bars for stirrup reinforcement. For series S-H 12 mm diameter ribbed bars were applied for the main longitudinal reinforcement. A Young's modulus of 200000 N/mm² was assumed, Poisson's ratio was 0.3.

Steel plate

For the steel plates a high quality steel St37K was applied with a mean tensile strength of 550 N/mm^2 to prevent yielding of the plate at the clamped side. Young's modulus averaged about 190000 N/mm^2 , Poisson's ratio was assumed to be 0.3.

Epoxy resin

The epoxy resin (AVENIT EP-Klebemörtel, Stahlton AG) consisted of two components: a filled resin and a hardener (mixed 7.75:1.00). The pot life is 45 min at 20°C . Properties given by the producer are (7 days hardening at 20°C): a mean compressive strength of 94 N/mm^2 , an Young's modulus of 11000 N/mm^2 and a flexural tensile strength of 27 N/mm^2 . Poisson's ratio was assumed to be 0.35.

4.4.2 Specimen Storage

After Concrete Casting

Two days after concrete casting, the beam-ends were stored in a curing room (20°C , 95%RH). Four weeks after concrete casting, the beam-ends were taken out of the curing room and stored in the testing hall ($18\text{-}22^\circ\text{C}$, 50-70%RH).

After Strengthening

After seven days of storage and drying in the testing hall, the beam-ends were strengthened. One day after strengthening (strength of epoxy about 70% of 7-days strength) the beam-ends were removed from the gluing frame and again stored in the testing hall. Between one or two weeks later the tests were carried out.

4.4.3 Strengthening Procedure

Surface Preparation

Before the beam-ends were externally strengthened, the concrete surface was grit-blasted to remove the (greasy) cement skin and to expose the coarse aggregates. Dust and grid remains were removed with high-pressure air. Also, the steel plate was grit blasted to remove the dirt film and to obtain a clean surface. In addition, the plate was also cleaned with high pressure air and thoroughly degreased with acetone. A primer was not applied on the plate because it was instantly bonded.

Bonding of the External Plate

A gluing frame was used with which the steel plate was placed and fixed. After mixing of the two component epoxy until a solid grey colour was obtained, the epoxy was spread roof-shaped on the plate with a spatula. With a crane the concrete specimen was placed on top of the steel plate and fixed. Due to the weight of the concrete, little pressure was applied on the epoxy layer. Then, the excess epoxy was removed with the spatula and the epoxy was left to harden for one day. Two beam-ends were strengthened at the same time.

4.5 Overview of Test Series

4.5.1 Design of Test Series

The experiments are divided into two main groups covering plate anchorage and beam shear. Plate anchorage is discussed in Chapter 5, and beam shear is discussed in Chapter 6. For reference to these tests the following capitals are used:

- A beam-ends tested for plate anchorage;
- S beam-ends tested for beam shear.

In the subsequent two sections a complete overview of the test series is listed. In the Tables the capitals denote:

- P plate geometry [mm^2];
- L unplated length [mm];
- B force in the bolt if a bolt is applied [kN] - \times number of bolts;
- W width of the concrete specimen [mm];
- H height of the concrete specimen [mm];
- A length of the shear span [mm].

4.5.2 Experiments on Plate Anchorage

Table 4.IV lists all tests carried out to investigate plate anchorage. Series A is subdivided into three series, namely tests on unplated length (A-L), tests on addition of bolt (A-B) and tests on repeated loading conditions (A-R). In series A, all beam-ends have been strengthened with a $5 \times 100 \text{ mm}^2$ steel plate.

Table 4.IV Series A - Plate Anchorage

test	P	L	B	W	H	A
<i>sub series L: Influence of unplated length</i>						
A-L1	5x100	100	-	100	200	800
A-L2	5x100	100	-	100	200	800
A-L3	5x100	200	-	100	200	800
A-L4	5x100	200	-	100	200	800
A-L5	5x100	300	-	100	200	800
A-L6	5x100	300	-	100	200	800
<i>sub series B: Influence of bolt</i>						
A-B1	5x100	100	-	100	200	800
A-B2	5x100	100	-	100	200	800
A-B3	5x100	100	00	100	200	800
A-B4	5x100	100	10	100	200	800
A-B5	5x100	100	10	100	200	800
A-B6	5x100	100	10-25?	100	200	800
A-B7	5x100	100	25	100	200	800
A-B8	5x100	100	25	100	200	800
A-B9	5x100	100	10-2x	100	200	800
A-B10	5x100	100	10-3x	100	200	800

<i>sub series R: Influence of repeated loading</i>						
A-R1	5×100	100	-	100	200	800
A-R2	5×100	100	-	100	200	800
A-R3	5×100	100	-	100	200	800
A-R4	5×100	100	-	100	200	800
A-R5	5×100	100	-	100	200	800
A-R6	5×100	100	-	100	200	800
A-R7	5×100	100	-	100	200	800
A-R8	5×100	100	-	100	200	800

4.5.3 Experiments on Beam Shear

Table 4.V lists all tests carried out to investigate beam shear. Series S is subdivided into three series, namely tests on plate cross-section and unplated length (S-P) and tests on geometry of concrete member (S-W and S-H).

Table 4.V Series S - Shear capacity

Test	P	L	B	W	H	A
<i>sub series P: Influence of plate cross-section and unplated length</i>						
S-P1	3×60	000	-	100	200	800
S-P2	3×60	100	-	100	200	800
S-P3	3×60	200	-	100	200	800
S-P4	3×100	000	-	100	200	800
S-P5	3×100	100	-	100	200	800
S-P6	3×100	200	-	100	200	800
S-P7	4×80	000	-	100	200	800
S-P8	4×80	100	-	100	200	800
S-P9	4×80	200	-	100	200	800
S-P10	5×60	000	-	100	200	800
S-P11	5×60	100	-	100	200	800
S-P12	5×60	200	-	100	200	800
S-P13	5×100	000	-	100	200	800
S-P13A	5×100	000	-	100	200	800
S-P14	5×100	100	-	100	200	800
S-P14A	5×100	100	-	100	200	800
S-P15	5×100	200	-	100	200	800
<i>sub series W: Influence of width of specimen</i>						
S-W1	4×80	100	-	200	200	800
S-W2	3×100	100	-	200	200	800
S-W3	5×60	100	-	200	200	800
S-W4	5×100	100	-	200	200	800
<i>sub series H: Influence of height of specimen</i>						
S-H1	4×80	200	-	100	400	1600
S-H2	3×100	200	-	100	400	1600
S-H3	5×60	200	-	100	400	1600
S-H4	5×100	200	-	100	400	1600

Note: In the next chapters a * will be used as superscript to indicate that the load which is listed, is a load after maximum load. For example: 10.8* kN indicates the maximum load has already been attained, and that the post-peak branch is considered.

5. EXPERIMENTAL OBSERVATIONS ON PLATE ANCHORAGE

This chapter describes experimental observations on the anchorage of bonded-on steel plates. §5.1 introduces the tests that are dealt with in this chapter. Then, the subsequent sections present the results of three test series. Firstly, §5.2 discusses the influence of the unplated length of the strengthened member on the failure and anchorage behaviour. Secondly, §5.3 describes the improvement of the anchorage capacity and the alteration in failure behaviour by virtue of a bolt installed at the plate end. Thirdly, §5.4 shows that repeated loading conditions hardly affect the anchorage capacity of a bonded-on steel plate. Finally, §5.5 concludes this chapter on plate anchorage.

5.1 Introduction to the Plate Anchorage Tests

This chapter presents test results on the anchorage capacity of steel plates which were bonded with the aim to strengthen for flexure. The purpose of these tests was dual. On the one hand, they were performed to investigate the influence of the plate geometry and the loading conditions on the anchorage capacity of steel plates. On the other hand, the tests were carried out to clarify whether anchorage failure of the steel plates is the primary mode of failure, or just a secondary effect.

In the literature many tests were published which dealt with the problems that arise when a plate is stopped at a short distance of the support. As already discussed in the literature overview, stress concentrations are imposed at the plate end. Although the existence of an anchorage stress concentration has been proven by many researchers, they still disagree on the actual value of the shear stresses that cause the plate to separate from the beam. Shear stress values ranging between 6 to 8 N/mm² were suggested by Swamy et al. [1986]⁶, and shear stress values ranging between 3 to 5 N/mm² combined with tensile stresses between 1 to 2 N/mm² were suggested by Roberts [1989c]⁷. Later, Swamy et al. [1989]⁸ related the maximum shear strength to the concrete quality and concluded that it equalled $\sqrt{2} \times$ the tensile strength of concrete. However, this value $\sqrt{2}$ could not be explained.

However, when the initial tests at the Delft University of Technology were carried out, doubt was raised if these stress concentrations really cause failure and, therefore, the significance of these maximum shear stresses was questioned. Then, like Oehlers [1992]⁸ stated that "*the formation of diagonal shear crack causes shear peeling,*" the idea arose that too much attention had been paid to the anchorage stress concentrations, and too little to the shear resistance of partially plated beams. Accordingly, during the research project the accent of the experimental program shifted from tests on plate anchorage (series A) to tests on beam shear (series S).

5.2 Influence of the Unplated Length

5.2.1 Contents of Test Series A-L

Because in practical situations it is mostly not possible to bond the external plate beyond the support, the plate is shorter than the total span of the concrete member to which it is bonded. Consequently, near the support the concrete member is partially unplated. As a result of the unplated length, stress concentrations at the end of the steel plate are induced. To investigate the influence of the unplated length on the plate anchorage capacity, beam-ends were tested with a plate stopped at distances of 100 mm, 200 mm and 300 mm before the centre of the support. Table 5.1 overviews the tests series. The beam-ends with a cross section of $100 \times 200 \text{ mm}^2$ were reinforced with two 8 mm diameter ribbed bars at an effective depth d_s of 170 mm. Internal 6 mm diameter stirrups spaced at 100 mm and 75 mm were provided in order to increase the shear resistance. In all the tests an external plate of $5 \times 100 \text{ mm}^2$ was bonded, so that the effective depth d_p was 204 mm. The effective depth d_p was calculated by $d_p = d_s + t_p + 0.5t_p$, with $t_p = 1.5 \text{ mm}$.

Table 5.1 Overview of test series A-L; maximum loads and mode of failure

Test	P [mm ²]	L [mm]	stirrups	F _{max} [kN]	mode of failure
A-L1	5×100	100	@ 100	23.4	plate separation by cover rip-off
A-L2	5×100	100	@ 100	23.9	plate separation by cover rip-off
A-L3	5×100	200	@ 75	16.1	plate separation by cover rip-off
A-L4	5×100	200	@ 100	18.9	plate separation by cover rip-off
A-L5	5×100	300	@ 100	14.7	plate separation by cover rip-off
A-L6	5×100	300	@ 75	14.3	plate separation by cover rip-off

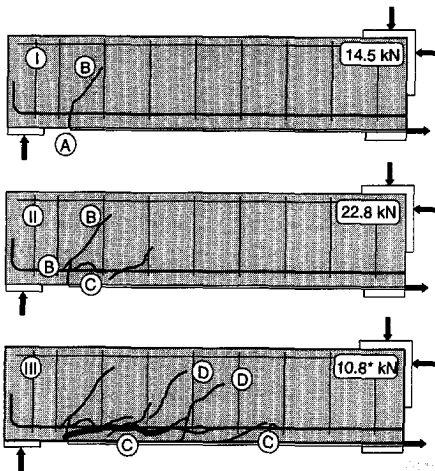


Fig. 5.1 Crack pattern development of A-L1 with unplated length of 100 mm

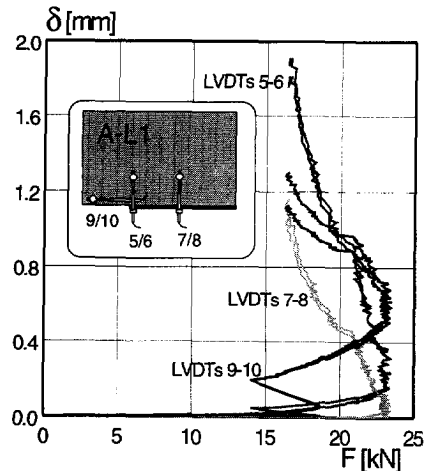


Fig. 5.2 Recorded relative displacement by LVDTs on beam-end A-L1

5.2.2 Failure Behaviour

Crack Patterns

For the test series A-L a crack-magnifier was not yet used, and, therefore, flexural cracks at the clamped side were not detected by the eye. Fig. 5.1 shows the crack pattern development of A-L1 with an unplated length of 100 mm. The sequence of the occurrence of cracks is discussed on the basis of this beam-end. Fig. 5.2 visualises LVDT measurements of A-L1 registered at the plate end.

The first stage is shown at a load of 14.5 kN, *just after* the first crack at the plate end had developed, as clearly emerges from the LVDTs 9/10 measurements of Fig. 5.2. At a load of 18.6 kN, at the end of the plate in the unstrengthened part a *plate-end crack* (A) initiated and partly developed into a shear crack (B). The occurrence of this crack was accompanied with a load drop to 14.0 kN. In this thesis, this shear crack will be referred to as a *plate-end shear crack*. By this name it explicitly indicates that the shear crack is located at the plate end.

The second stage was drawn at a load of 22.8 kN. It shows that the plate-end crack had further developed into a shear crack (B). This shear crack not only grew into the direction of the concrete compression zone, but also into the direction of the support. By virtue of the internal stirrups the plate-end shear crack was arrested. As a result, at the level of the internal bars a peeling crack (C) developed, confirmed by the recorded relative displacements of LVDTs no.5/6 (perpendicular to plate).

Fig. 5.2 shows that at the onset of the maximum load, LVDTs no.7/8 recorded a crack. So, the peeling crack had extended over about 100 mm. New shear cracks (D) formed in the shear span and the peeling crack kept growing. Finally, the maximum decreased and the maximum load capacity had been reached. The third stage was drawn when the test was stopped. As a result of the deformation control, the sequence of crack initiation could be well observed. Note that after force control only a large plate separation crack and small shear cracks would have been visible.

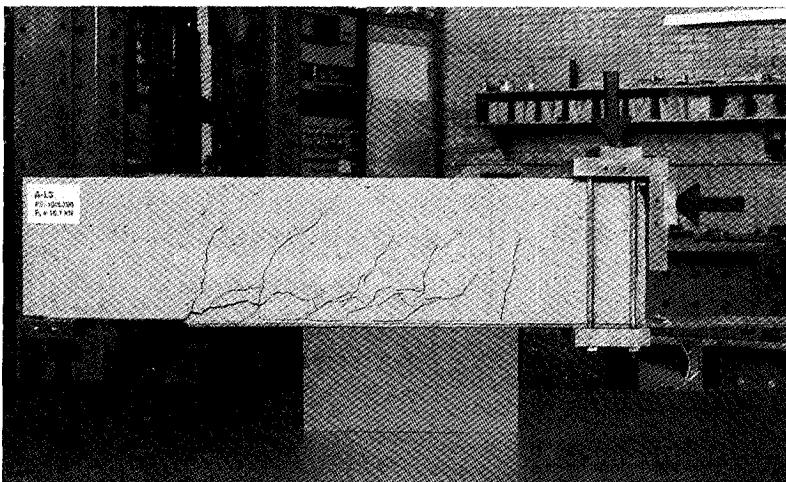


Fig. 5.3 Photograph of failure of beam-end A-L3 with unplated length of 200 mm (P5x100, L200, 2Ø8, Ø6@75)

Fig. 5.3 and Fig. 5.4 show crack patterns of the beam-ends with unplated lengths of 200 mm, and 100 mm, 200 mm and 300 mm, respectively. The failure behaviour of the various partially plated beam-ends was identical, namely, by plate separation through the concrete cover at the level of the internal longitudinal bars. Moreover, before the plate separated from the beam-end, a plate-end shear crack could clearly be distinguished beyond the plate end in the unstrengthened part. Particularly this plate-end shear crack arose the interest for the shear resistance of partially plated members. Crack pattern development and load-deflection responses of all beam-ends are shown in detail in Appendix C.

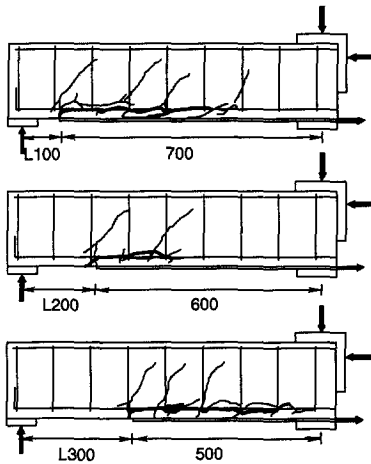


Fig. 5.4 Crack patterns of beam-ends with unplated lengths of 100, 200 and 300 mm (thick line represents failure crack)

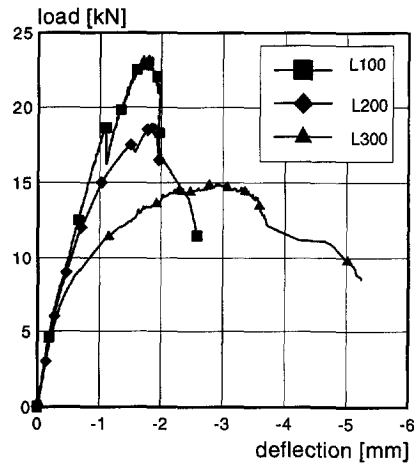


Fig. 5.5 Load-deflection responses of beam-ends with unplated lengths of 100, 200 and 300 mm

Load-Deflection diagrams

Fig. 5.5 shows the load-deflection responses of the partially plated beam-ends for which the crack patterns were depicted in Fig. 5.4. A difference in deflection at maximum load was observed. For the 100 mm and 200 mm unplated lengths the responses were brittle: at maximum load the load dropped very quickly. The response of the beam-end with the plate stopped at a distance of 300 mm before the support was less brittle. Concerning these observations, Oehlers [1990]⁸ mentioned the difference between shear peeling, shear-flexural peeling and flexural peeling. Accordingly, for the L300 beam-end peeling was more gradual due to a combined type of shear and flexural peeling. When the plate was stopped at a shorter distance from the support, the plate separated by brittle shear peeling.

When the load-deflection responses of A-L1 (L100) and A-L4 (L200) are more examined in detail, an unloading branch is already seen at about 18.5 kN and 17.2, respectively. Experimentally, it was observed that at these loads the plate-end shear crack developed from the plate-end crack, which was formed earlier at the

immediate plate end. Because the steering LVDTs were not placed over this plate-end shear crack, the deformation-controlled testing system was not able to react on the sudden progress of this crack. Nevertheless, after partly unloading, the internal stirrups that crossed the plate-end shear crack were activated and the load could be increased to a higher load level than that at which the plate-end shear crack developed, until the plate separated from the beam.

From the above mentioned discussion it may be concluded that plate-end shear played an important role. That plate separation was initiated by plate-end shear, was observed in the two tests in which the plate stopped 200 mm short of the support. Besides the difference in number of stirrups (@75 and @100), the location of the stirrups at the immediate plate-end differed. Fig. 5.6 shows the load-deflection responses. The unloading branches indicate that between 15 to 17 kN the plate-end shear crack developed. For A-L4 the load could be increased to 18.9 kN after this unloading branch. However, due to the fact that the unloading branch was much larger for A-L3, the maximum load sustained was significantly lower. These results may show that either a particular load or a particular deformation was needed after plate-end shear to initiate plate separation.

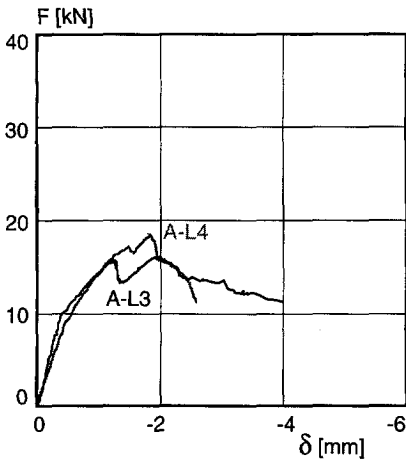


Fig. 5.6 Load-deflection responses of A-L3 and A-L4 with 200 mm unplated length

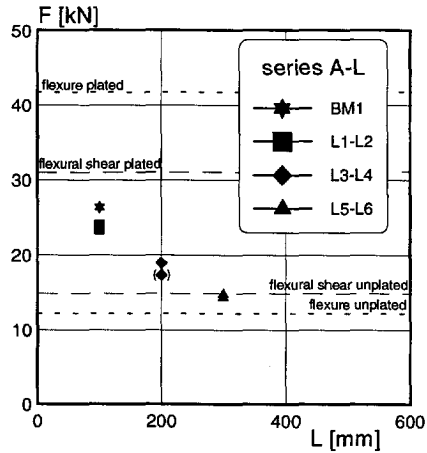


Fig. 5.7 Maximum loads of partially plated beam-ends in relation to unplated length

5.2.3 Maximum Loads in Relation to the Unplated Length

The experimental observations proved that the unplated length clearly affected the maximum load at which the plate separated. Fig. 5.7 depicts the maximum loads in relation to the unplated length. It clearly emerges that with increasing unplated length the maximum load decreases. Earlier in Chapter 4, it was derived that for the unplated beam BM0 and the plated beam BM2 the flexural loads were respectively 12.2 kN and 41.8 kN, and the flexural shear loads 15.3 kN and 30.3 kN. With lines, these are also plotted in Fig. 5.7. Compared to an unplated beam the maximum loads were increased, but this was hardly the case for the L300 plated beam-ends.

5.2.4 Anchorage Stresses

Strain measurements were carried out in order to derive the shear stresses that acted between the concrete and the steel plate. The location of the strain gauges is depicted in Fig. 5.8. As it is seen, measurements were carried out at both edges of the steel plate. At the end of the plate, a strain gauge was glued every 10 mm to get more detailed information at the plate-end. The strain gauges were glued at the outside of the steel plate. A linear stress distribution over the thickness of the steel plate is assumed. However, if cracks occur, this assumption is not correct. Then, strains at the outside are less than strains at the inside due to bending.

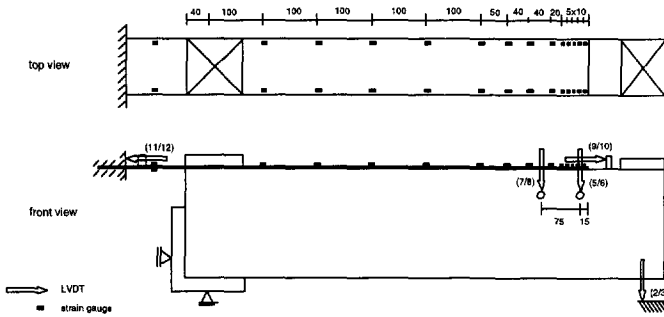


Fig. 5.8 Location of strain gauges for test series A-L, top view and front view

The magnitudes of the plate stresses were derived from the strain measurements. Fig. 5.9 presents the stresses in the external steel plates for the various unplated lengths, at 50% and 100% of the maximum loads. It is seen that at 50% of the maximum loads the plate stress is zero at the plate end. However, at 100 % of the maximum load, when plate separation started, the strain gauges measured compressive strains at the plate end. As mentioned, the strain gauges were glued on the outside of the steel plate, so these compressive stresses might only be explained by negative curvature of the steel plate. Due to sliding between the aggregates, the plate bends.

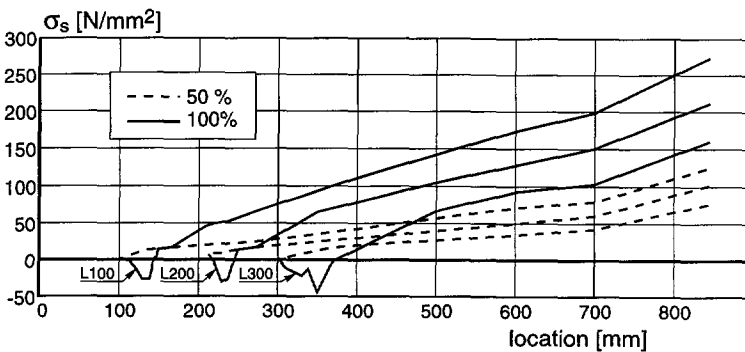


Fig. 5.9 Stresses in bonded-on plate at 50% and 100% of maximum loads

The plate stresses were used to derive the magnitude and distribution of the shear stresses between the external plate and the concrete face. The difference between the tensile stresses in subsequent plate cross-sections is transmitted to the concrete by shear stresses. The shear stresses are expressed by (Ladner & Weder [1981]⁹):

$$\tau_i = \frac{(\sigma_i - \sigma_{i-1})t_p}{x_i} \quad (5.1)$$

in which i and $i-1$ denote the subsequent cross sections that are considered. For all three plated beam-ends the shear stress distribution is plotted in Fig. 5.10a. It must be noted that the first strain gauge at 10 mm from the plate end hardly measured strains, probably because of the introduction of forces at the plate end over the plate thickness. Therefore, the shear stresses derived from the strain readings over these 10 mm did not represent the actual magnitude, but should be higher, see for example Täljsten [1994]⁹.

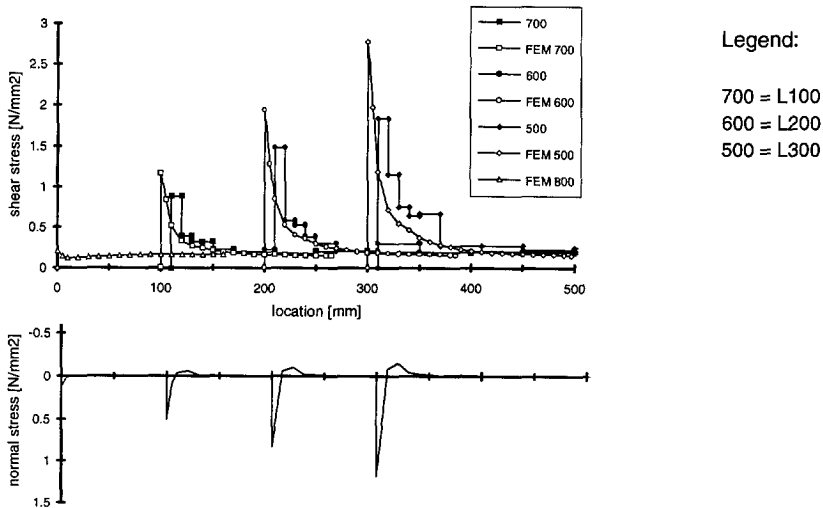


Fig. 5.10 Shear stresses (a) and normal stresses (b) along the bonded plate, experimental results and finite element calculation (at $F = 5.3$ kN)

For the sake of comparison with and validation of the experimentally derived shear stresses, results of a finite element (FEM) calculation are included. This FEM model will be dealt with in the numerical study in part III. The distributions of the measured and calculated shear stresses are quite similar. The results illustrate that the peak stresses increased as the unplated part of the beam-end was enlarged. However, due to the fact that experimentally the strains were measured at the outside of the bonded plate and numerically the stresses were calculated in the epoxy layer, the measured peak stresses at the plate end differed about 30%-50% from the calculated ones. At the same time, the calculated peak stress was dependent on the size of the FEM-mesh. As a result of the shear stresses, normal stresses were

imposed at the end of the plate as the finite element calculations showed, Fig. 5.10.b. With the approximate solution proposed by Roberts [1989c]⁷ the peak shear and normal stresses were analysed, see Table 5.II. It emerged that the results differed considerably. An explanation might be that in Roberts's derivation the Young's modulus of the epoxy was assumed to be 6 to 40 times lower than the stiffness used in this study.

Table 5.II Maximum anchorage stresses; experiment and according to Roberts [1989c]⁷

	L100	L200	L300	L100/L200/L300
τ_{\max} [N/mm ²]	1.16	1.94	2.77	$\sigma_{\max} = \pm 0.5\tau_{\max}$
τ_{Roberts} [N/mm ²]	3.18	4.62	6.06	$\sigma_{\max} = 0.87\tau_{\max}$

The linear anchorage stresses of Fig. 5.10 were deduced far before plate-end cracking. At plate-end cracking, the shear stress distribution changed completely. Fig. 5.11 presents the shear stress distribution of the partially plated beam-end with the plate stopped 100 mm before of the support. Two distributions of shear stresses are shown: the maximum shear stress ($F = 16.2$ kN) and the shear stress at maximum load ($F = 23.4$ kN). The shear stresses were derived with Eq. 5.1, as is mostly done, but it is questionable if these stresses really occur. It is seen that the stresses in the end zone decreased when the plate separated, and even, the sign of the shear stress changed. However, as mentioned, this resulted from negative curvature of the steel plate during separation. With respect to these observations, it is the authors opinion that these shear stresses do not initiate plate separation. Plate separation is caused by plate-end shear.

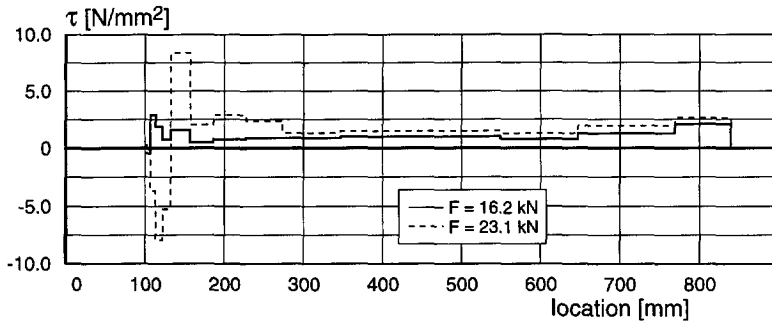


Fig. 5.11 Shear stress for beam-end with 100 mm unplated length; stress distribution before and after plate separation

5.2.5 Conclusions

By virtue of the deformation-controlled way of testing, the initiation and sequence of initiation of shear and peeling cracks was well observed. It emerged that a plate-end shear crack first formed, subsequently followed by a shear peeling crack which led to plate separation. Hence, plate-end shear dominated shear peeling. Normal and shear anchorage stresses at the end of the plate increased as the unplated part of the beam was enlarged. As a consequence, the anchorage capacity decreased.

5.3 Influence of the Addition of a Bolt

5.3.1 Contents of Test Series A-B

In order to increase the anchorage capacity and to obtain a more ductile failure response of the bonded-on plate, a bolt was added at the end of the anchorage zone. As already discussed in the literature overview, some different opinions on the effect of the addition of a (prestressed) bolt still exists. This section, therefore, discusses the series A-B which had the purpose of investigating the effect of the addition of a bolt.

Table 5.III lists an overview of the tests that were performed. Beam-ends with a cross-section of $100 \times 200 \text{ mm}^2$ were reinforced with two 8 mm diameter ribbed bars at an effective depth of 170 mm. Stirrups 6 mm diameter spaced at 75 mm were provided to increase the shear resistance. An external plate of $5 \times 100 \text{ mm}^2$ was applied for which the effective depth measured 204 mm. The bolt was 10 mm.

Beam-ends A-B1 and A-B2 were the so-called reference tests and were provided without a bolt. Beam-end A-B3 was provided with a bolt, however, no nut was applied. In this way, the influence of only a 'tie' in the unreinforced concrete cover could be investigated. The other beam-ends were provided with a bolt and nut that was tightened to obtain pre-stressing forces of 10 kN and 25 kN. Also, two beam-ends were provided with two and three bolts spaced at 75 mm.

Table 5.III Overview of test series A-B; maximum loads and failure modes

Test	P [mm ²]	L [mm]	B [kN]	F _{max} [kN]	mode of failure
A-B1	5×100	100	-	24.5	concrete plate separation
A-B2	5×100	100	-	24.4	concrete plate separation
A-B3	5×100	100	0	27.7	interface plate separation
A-B4	5×100	100	10	33.8	interface plate separation
A-B5	5×100	100	10	33.5	interface plate separation
A-B6	5×100	100	--- ¹⁾	28.9	interface plate separation
A-B7	5×100	100	25	32.0	interface plate separation
A-B8	5×100	100	25	33.4	interface plate separation
A-B9	5×100	100	2 10@75	37.9	interface plate separation
A-B10	5×100	100	3 10@75	43.4	interface plate separation

¹⁾ Due to a broken strain gauge on the bolt the prestressing force was not known

Anchor bolt

Before strengthening, at 25 mm from the plate end, a 12.5 mm diameter hole was drilled through the steel plate. After the concrete member was strengthened with the external steel plate, an approximately 90 mm deep hole was drilled in the concrete member. Then, the plate was additionally anchored by applying a bolt. After making the hole dust-free, a 10 mm diameter adhesive anchor bolt was installed (depth 80-85 mm) by using a two component epoxy capsule, see also Fig. 5.14. Just before testing the nut was tightened. During tightening of the nut the bolt strain was measured to derive the bolt force. To that end the bolt was provided with two strain gauges on opposite sides to exclude bending of the bolt in measurements. At the same time, these strain gauges were able to register the force variation in the bolt

during testing. The force in the bolt was determined by calculating the average of the values of the strain gauges multiplied by a calibrated factor. Fig. 5.12 illustrates details of the measuring device, which for the photograph was de-assembled.

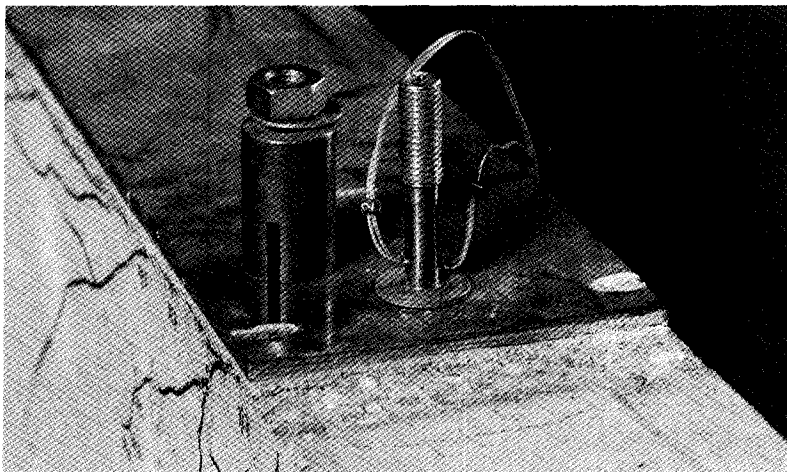


Fig. 5.12 Details of measuring device to register bolt force

5.3.2 Failure Behaviour

Crack Patterns

Appendix C gives various stages of crack patterns and load-deflection diagrams of the tested beam-ends. Fig. 5.13 sketches the crack patterns of A-B1, A-B3, A-B5 and A-B8. When the crack patterns at ultimate load are compared it is seen that the addition of a bolt was very effective. The development of the first cracks was quite similar to that discussed in the previous section concerning test series A-L. A plate-end crack also formed beyond the plate end and developed into a plate-end shear crack at a higher load. By virtue of the internal stirrups this shear crack was arrested and the load could be increased. Then, for beam-ends with a bolt the maximum load and the failure mechanism were different compared to the reference tests.

In Fig. 5.13 it is seen that in the case of the reference beam-end plate separation occurred at the level of the internal reinforcement. In contrast to cover rip-off, in the case of the bolted beam-ends plate separation occurred at the epoxy-concrete interface. By virtue of the bolt, the peeling crack in the unreinforced concrete cover was arrested and plate separation by concrete cover rip-off could not extend. In that case, the load could be increased and as a result of the increased anchorage stresses at the plate end interface failure occurred. High shear stresses at the concrete-epoxy interface led to interface plasticity as reported in Jansze [1996b] and as shown in Fig. 7.13. When a relatively larger normal compressive stress was applied, the resistance of the interface increased. It was also observed during the experiments that in the region at a distance from the bolt interface failure did not take place anymore. There, away from the influence of the bolt, the peeling crack jumped to the level of the internal bars, see Fig. 5.13.

The inner sides of the bonded-on plates are drawn in Fig. 5.13. Fig. 5.14 shows a photograph. After the tests were stopped, and the plates were completely removed from the beams, the surface of the inner side of the steel plates confirmed interface plasticity. Normally, either the full concrete cover or the concrete aggregates anchored in the epoxy were present at the inner side of the steel plate. In contrast, if a bolt was applied at the plate end, concrete free areas were observed. Because on the concrete surface of the beam-ends epoxy was not left behind, it was obvious that the areas did not result from failure in the epoxy itself (cohesion), but did result from plasticity failure at the concrete-epoxy interface (adhesion).

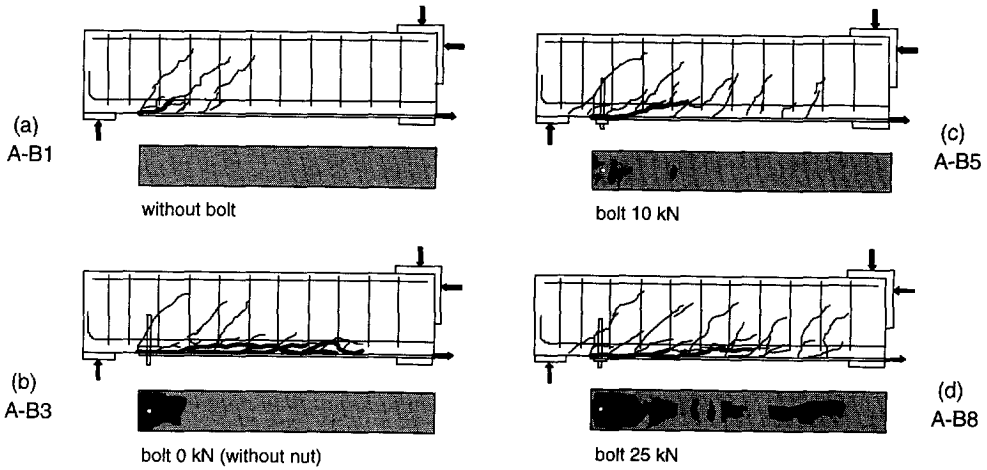


Fig. 5.13 Crack patterns of beam-ends. (a) A-B1 without a bolt (b) A-B3 with bolt without nut (c) A-B5 with force in the bolt of 10 kN and (d) A-B8 with force in bolt of 25 kN (light grey = concrete failure, dark grey = interface failure)

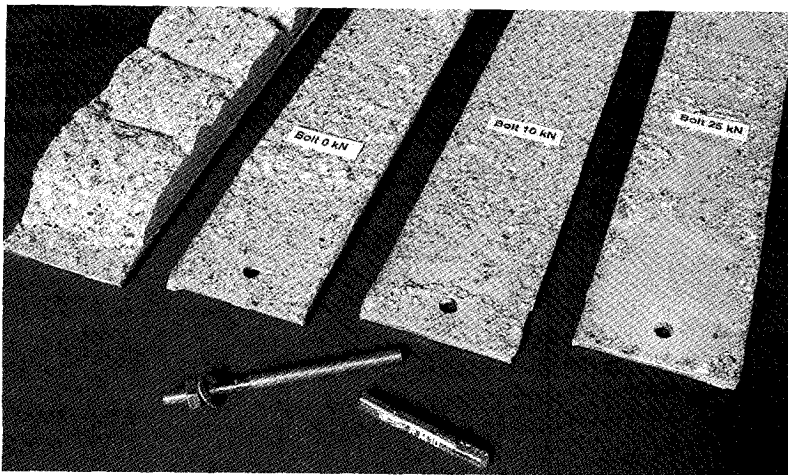


Fig. 5.14 Photograph of innersides of steel plates; with increasing bolt force it shows plate separation by concrete cover rip-off and plate separation by interface failure

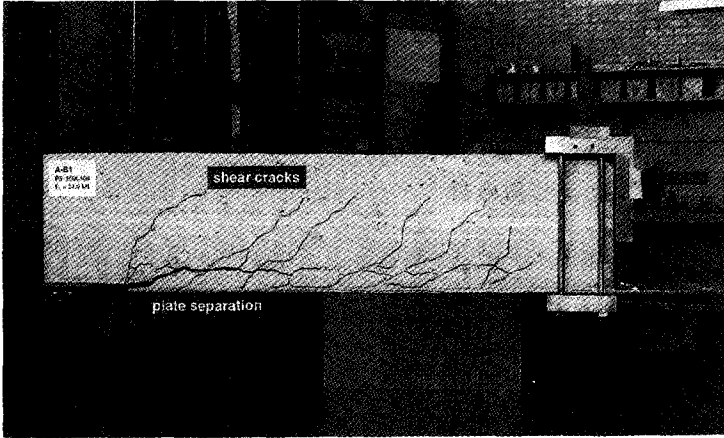


Fig. 5.15 Photograph of A-B1; concrete cover rip-off (P5x100, L100, 2Ø8, Ø6@75, no bolt)

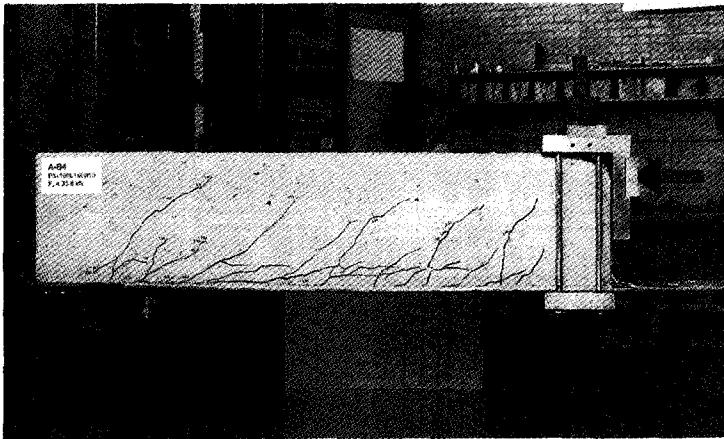


Fig. 5.16 Photograph A-B4; interface plasticity (P5x100, L100, 2Ø8, Ø6@75, B10)

If more than one bolt was installed, the load could be increased to 37.9 kN (two bolts spaced at 75 mm) and 43.4 kN (three bolts spaced at 75 mm). Fig. 5.17 shows the crack patterns and innersides of the plates. By virtue of the larger prestressed zone with increased normal compressive stresses, the interface failed at a higher load.

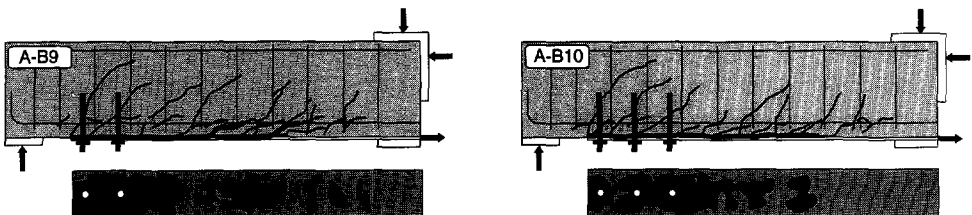


Fig. 5.17 Crack patterns and inner sides of plates if more than one bolt is installed

Maximum Loads and Load-Deflection Diagrams

The reference beam-ends failed at a maximum load of 24.5 kN. By applying a bolt without a nut (0 kN), the maximum load was increased to 27.7 kN. By virtue of the bolt which crossed the concrete cover rip-off crack, it was arrested. When bolt forces of respectively 10 kN and 25 kN were applied, the maximum loads were increased up to 33.6 kN and 32.7 kN, an average increase of about 35%.

From the load-deflection responses shown in Fig. 5.18 it is seen that the initial stiffness was equal for all beam-ends. But, when the load-deflection responses in Fig. 5.18 of the various bolted beam-ends are considered at a load level at which the reference beam-end failed, it was observed that also a plate-end shear crack developed. Then, the load-deflection responses became different in comparison with the reference tests. For all, partly unloading branches were distinguished. Unloading was accompanied by widening of the plate separation crack. However, the load could be increased after the bolt was activated by the opened concrete separation crack. Then, through plasticity the interface crack propagated gradually what could be visually well followed. By virtue of the installed bolts the response of the bolted beam-ends at failure was much more ductile.

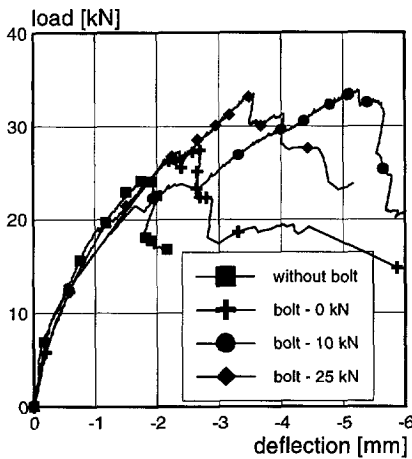


Fig. 5.18 Load-deflection responses of beam-ends without a bolt and initial bolt forces of 0 kN, 10 kN and 25 kN (A-B1 A-B3, A-B5 and A-B8)

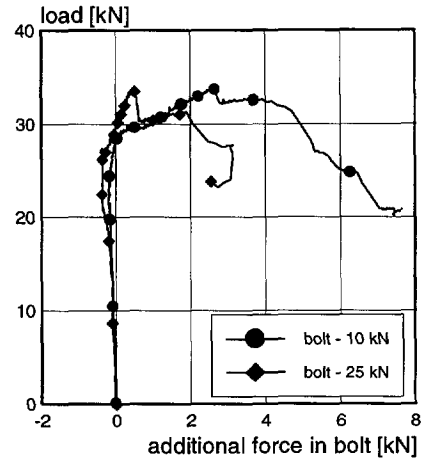


Fig. 5.19 Additional force in the bolt when initial bolt forces of 10 kN and 25 kN were applied (A-B5 and A-B8)

Bolt Forces

For beam-ends A-B5 and A-B8, which were provided with bolts with initial forces of 10 kN and 25 kN, the variation of the force in the bolt is plotted as a function of the load, see Fig. 5.19. It is seen that the initial force in the bolts nearly remains constant up to a load of approximately 25 kN at which the reference beams failed. This observation confirmed that up to plate separation the bolts played a passive role. Hence, the plate-concrete connection by epoxy responded much stiffer than

the plate-concrete connection by the prestressed bolt (Münger [1991]¹¹). From 25 kN up to the maximum load the force in the bolt was significantly increased. Ultimately, in the initial 10 kN bolt, the bolt force was increased with 6 kN (60%), in the initial 25 kN bolt, the bolt force was increased with 3 kN (12%). This underlines the observation that the bolt was only activated after the peeling crack developed (either at the level of the internal bars or at the concrete-epoxy interface).

5.3.3 Anchorage Capacity

When the anchorage capacity is compared to that obtained in the reference tests A-B1 and A-B2, and the tests A-L, one must conclude that it is considerably improved. This could partly be attributed to the application of additional reinforcement in the unreinforced concrete cover so that the failure mode changed from concrete cover rip-off to interface plasticity. But also, this occurred by virtue of applying a prestressing force in the bolt, so that additional compressive stresses acted at the anchorage zone of the bonded-on plate. Consequently, higher shear stresses could be resisted, so that the external load could be increased. However, when the prestressing force was increased from 10 kN to 25 kN, the anchorage capacity was not increased. You might question yourself if pretensioning the bolt is really needed. Fig. 5.20 visualises that as a result of plate separation concrete struts were formed. Due to the absence of suspension reinforcement that crossed the separation cracks, the plate peeled off. The most important function of the bolt is to apply reinforcement. It is, therefore, better to install more bolts instead of one bolt with a high force.



Fig. 5.20 Concrete cover between internal bars and steel plate; concrete struts are visible

5.3.4 Conclusions

By virtue of a bolt at the plate end, the anchorage capacity of the bonded plate was significantly increased. The bolt was activated when the plate separated, which altered the mechanism from brittle plate separation by concrete cover rip-off to a more ductile type of failure by interface plasticity between the concrete and the epoxy. Installing a number of bolts was more effective than one pre-stressed bolt.

5.4 Influence of Repeated Loading

5.4.1 Contents of Test Series A-RL

Finally, in the research program some repeated loading tests were carried out in order to get a first impression of the influence of repeated loading on the anchorage capacity. Tests were carried out with plates of $5 \times 100 \text{ mm}^2$ and an unplated length of 100 mm. A loading frequency of 6 Hz was adopted for all the tests. At first, the pilot test A-RL0 was carried out to investigate critical lower and upper load levels. It emerged that an upper level of 80% of the static load of the reference beam-ends A-B1 and A-B2 was needed to initiate cracks at the anchorage zone. Hence, for the other test a 35%-80% load interval was chosen (8.6 kN to 19.6 kN).

Table 5.IV Overview of test series A-R; maximum load cycles and mode of failure

Test	lower-upper level [%]	N [-]	mode of failure	remark
A-RL0	30-60,30-70, 30-80	$1.36 \cdot 10^6$	-	followed by statical test
A-RL1	35-80	$2.67 \cdot 10^6$	-	
A-RL2	35-80	$3.40 \cdot 10^6$	-	
A-RL3	35-80	$2.35 \cdot 10^6$	-	followed by statical test
A-RL4	30-70,30-80	$2.83 \cdot 10^6$	plate fracture	
A-RL5	35-80	110000	fault in control	
A-RL6	35-100	$9.6 \cdot 10^5$	plate yielding	additional bolt applied

5.4.2 Failure Behaviour

Load Cycles

In most tests the beam-ends resisted the required number of load cycles. The pilot test A-RL0 was stopped after $1.36 \cdot 10^6$ load cycles, after which the beam-end was tested statically. In the tests A-RL4 the plate fractured at the clamped side, because a hole was drilled in the plate for a measuring device. Despite, $2.83 \cdot 10^6$ load cycles could be resisted. In the anchorage zone of A-RL6 an additional bolt was applied, and therefore the upper level load was 100% of that of the reference beams. Due to a fault in the load control beam-end A-RL5 failed at 11000 load cycles.

Crack patterns

Fig. 5.21 and Fig. 5.22 show the load-deflection response and crack pattern development of specimen RL3, as well as the response of the reference test. During testing it was observed that the plate-end crack (I) initiated and the plate-end shear crack (II) developed with increasing number of load cycles. Also, a plate separation crack (III) was initiated. However, anchorage failure was not observed during the applied load cycles. Anchorage failure was also not observed in the other repeated loading tests. On the contrary, the plate-end shear crack propagated gradually.

After the repeated loading test, beam-end A-RL3 was statically tested up to failure. Failure was by plate separation alike test series A-L. The failure load amounted to 26.2 kN which was more than in case of the reference beams A-B1 and A-B2, thus indicating that the anchorage capacity of the externally bonded plate was not negatively influenced by repeated loading.

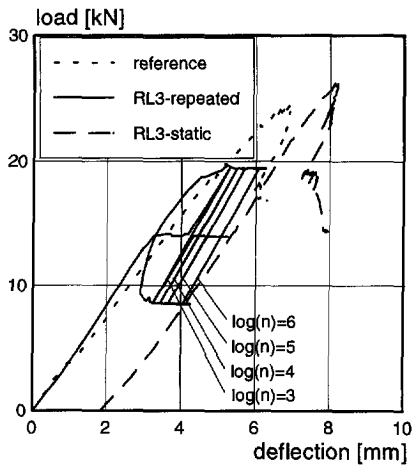


Fig. 5.21 Load-deflection responses of repeated loading and static loading tests

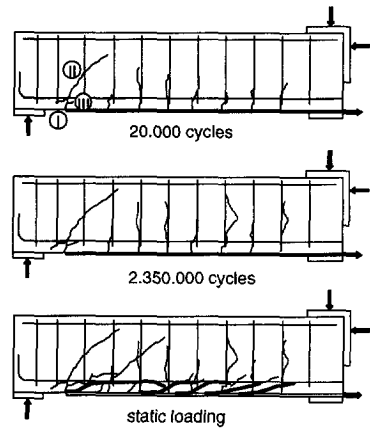


Fig. 5.22 Crack patterns of specimen RL3 after repeated and static flexural loading ($P5 \times 100$, L100, $2\varnothing 8$, $\varnothing 6 @ 75$)

5.4.3 Conclusions

With an upper load level of 80% of the static load, the anchorage capacity of externally bonded plates was not sensitive to repeated loading conditions. Particularly growth of the plate-end shear crack was observed.

5.5 Conclusions

This chapter covers results of experiments on the anchorage behaviour of externally bonded steel plates to strengthen reinforced concrete beam-ends. The unplated length considerably influenced the maximum plate separation load. A longer unplated length led to a decrease of the maximum load bearing capacity. The maximum load was increased if the bonded plate was additionally anchored by a (prestressed) bolt. By virtue of this bolt, the mechanism of plate separation changed from brittle concrete cover rip-off to a more ductile type of failure at the interface between the concrete and the epoxy. This occurred in spite of the fact that the bolt was only activated at the onset of the maximum load. Finally, it was concluded that the anchorage capacity of the externally bonded plates tested was not sensitive to fatigue under repeated flexural loading.

On the whole, it was observed that plate separation took place after the development of the plate-end shear crack, which grew from the initiated plate-end crack. Hence, plate-end shear played a dominant role in the failure behaviour. It seems, therefore, that plate separation is a secondary effect of plate-end shear, because by virtue of the internal stirrups the plate-end shear crack itself could not localise. Shear deformations cause plate separation at the level of the internal bars.

6. EXPERIMENTAL OBSERVATIONS ON BEAM SHEAR

This Chapter describes experimental observations on the shear capacity of concrete members strengthened only in bending. §6.1 introduces this chapter. Results of the three test series are presented in the subsequent sections. Firstly, the influence of the geometry of the plate is investigated in §6.2. It discusses the influence of the unplated length and the external reinforcement ratio. Then, the influence of the geometry of the concrete member is analysed. §6.3 presents results on the width of the concrete member. §6.4 investigates the height of the concrete member. Finally, §6.5 concludes this chapter on beam shear.

6.1 Introduction to the Beam Shear Tests

This chapter presents experimental results on the shear capacity of beam-ends strengthened only in bending. The purpose of the experiments was to investigate the influence of the geometry of the steel plate and the concrete member on the shear capacity. To that end, concrete beam-ends without internal stirrups were strengthened in bending with various plate cross sections and unplated lengths.

Rafia's expression on the flexural shear resistance is used for reference if the shear span of the beam-end is fully plated. Despite the fact that the equation was developed for specimens with ribbed bar reinforcement, the bonded-on plates are also treated as conventional reinforcement. It is known that both reinforcement types have different stress-bond slip characteristics (see Fig. 7.21), however, this was not of influence on the maximum flexural shear load as the experiments showed. If the shear span is fully plated, the influence of the plate mainly emerges in the expression for flexural shear by the larger effective depth.

In Chapter 4 it was deduced that for a $5 \times 100 \text{ mm}^2$ plate, an increase of the flexural reinforcement resulted in an increase of 3.4 of the maximum flexural capacity. The maximum flexural shear resistance was only increased by a factor 2.0. Thus, when large plate cross sections are bonded (and anchored beyond the support), the flexural shear resistance becomes more critical in comparison with the flexural capacity. Hence, the failure behaviour will change from ductile yielding of the reinforcement to a more brittle type of shear failure. Of course, this conclusion is only valid if shear reinforcement (stirrups or glued shear plates) is not provided in the shear span of the member.

The mentioned important finding only concerns the flexural shear resistance of a plated member. As already observed in Chapter 5, plate-end shear seemed the governing type of failure if a member is only partially plated. To that end, it is important to know what the influence of the plate-end shear resistance is on the maximum load bearing capacity of a partially plated member.

6.2 Influence of Unplated Length and Plate Cross Section

6.2.1 Contents of Test Series S-P

A total of 17 beam-ends were tested to investigate beam shear. Table 6.1 lists the contents of test series S-P. Five different plate geometries were tested with variable lengths of the steel plate. An unplated length of 0 mm indicates that the plate is stopped beyond the support and, thus, sufficiently anchored. The beam-ends with a cross section of $100 \times 200 \text{ mm}^2$ were reinforced with two 8 mm diameter ribbed bars at an effective depth of 170 mm. Stirrups were not applied in the shear span, apart from practical reinforcement near support and loading point. The effective depth of the plates ranged between 203 and 204 mm for the 3 mm and the 5 mm plate thicknesses, respectively.

Table 6.1 Overview of series S-P

test	P [mm ²]	L [mm]	F _{max} [kN]	mode of failure
S-P1	3×60	0	±22.5 ¹⁾	none
S-P2	3×60	100	20.6	plate-end shear
S-P3	3×60	200	17.8	plate-end shear
S-P4	3×100	0	26.7	flexural shear
S-P5	3×100	100	20.9	plate-end shear
S-P6	3×100	200	16.7	plate-end shear
S-P7	4×80	0	26.8	flexural shear
S-P8	4×80	100	20.2	plate-end shear
S-P9	4×80	200	16.9	plate-end shear
S-P10	5×60	0	26.3	flexural shear
S-P11	5×60	100	20.7	plate-end shear
S-P12	5×60	200	17.2	plate-end shear
S-P13	5×100	0	32.1 ²⁾	flexural shear
S-P13A	5×100	0	35.3 ²⁾	flexural shear
S-P14	5×100	100	20.1 ²⁾	plate-end shear
S-P14A	5×100	100	19.6 ²⁾	plate-end shear
S-P15	5×100	200	16.1 ²⁾	plate-end shear

¹⁾ at the clamped side the steel plate yielded outside the beam-end
²⁾ additional stirrup was present in the shear span that influenced flexural shear

6.2.2 Failure Behaviour

During a test, cracks were marked on the beam-ends at various stages of the external load. Appendix C shows the crack pattern development of all the performed tests. Four typical cases will be discussed to provide more insight into the shear failure behaviour: a fully plated beam-end, namely S-P13A (L0) and three partially plated beam-ends, namely S-P14A(L100), S-P8 (L100) and S-P3 (L200).

Fully Plated Beam-End (L0)

On beam-end S-P13A an external plate measuring $5 \times 100 \text{ mm}^2$ was bonded beyond the support. Fig. 6.1 shows the development of cracks at three loading stages, the load-deflection diagram is shown on the right. At first, cracks developed in the shear span with increasing external load, see stage I and II. Then, at the onset of the maximum load, a shear crack suddenly initiated in the shear span at the tip of a flexural crack at a location of 60%-40% of the shear span. This shear crack propagated nearly horizontal towards both the loading point and the support and caused failure at a load of 35.3 kN. The type of failure was typically *flexural shear failure* as defined by Kani [1964]¹⁴.

Stage III sketches the failure pattern at a load when the test was stopped. Widening of the shear crack had occurred. Note that by virtue of the practically applied stirrups near the loading point the maximum load could be increased from 35.3 kN to 37.3 kN. Even so, the maximum load was marked as 35.3 kN.

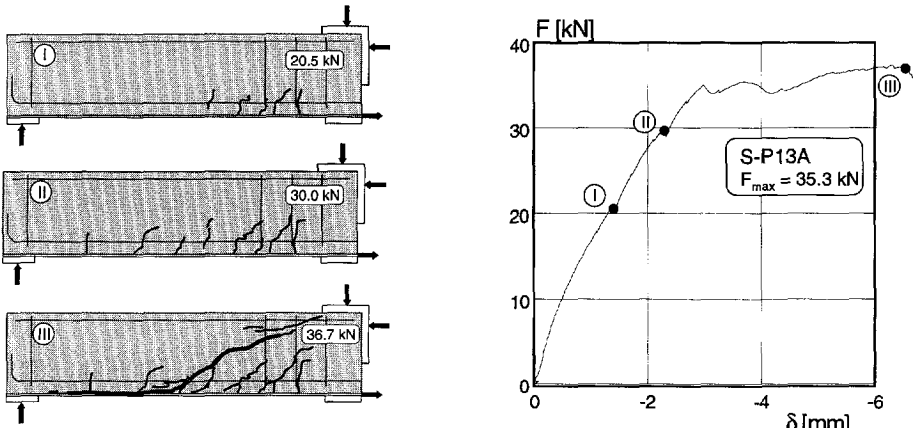


Fig. 6.1 Crack pattern development and load-deflection diagram of beam-end S-P13A (P5 \times 100, L0, W100, H200, 2 \varnothing 8, no stirrups)

Partially Plated Beam-End (L100)

Fig. 6.2 shows stages of crack development and the load-deflection diagram of beam-end S-P14. Three stages are considered in the post-peak branch of the load-deflection diagram. The maximum shear load resisted by the specimen was 20.1 kN.

Before the maximum load, at about 15 kN, a *plate-end crack* initiated just beyond the bonded-on plate in the unplated part of the concrete specimen. This crack grew quickly into the concrete and was visually well followed as a result of the deformation controlled steering control of the test. Then, at maximum load this plate-end crack had developed into a *shear crack*, referred to as *plate-end shear crack*. The plate-end shear crack grew into the concrete compression zone. At nearly the same moment, at the level of the internal reinforcement a *shear peeling crack* initiated. This crack resulted from the large shear deformations of the web (beam shear) and the flexural rigid concrete cover stiffened by the bonded-on steel plate.

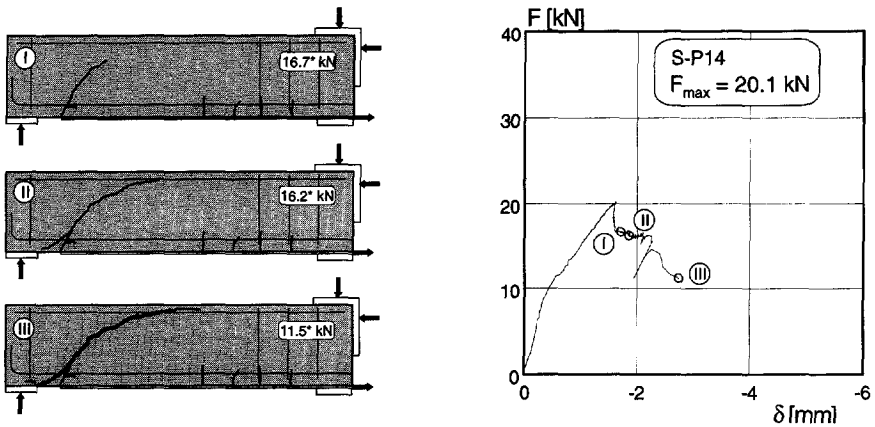


Fig. 6.2 Crack pattern development and load-deflection diagram of beam-end S-P14 (P5×100, L100, W100, H200, 2Ø8, no stirrups)

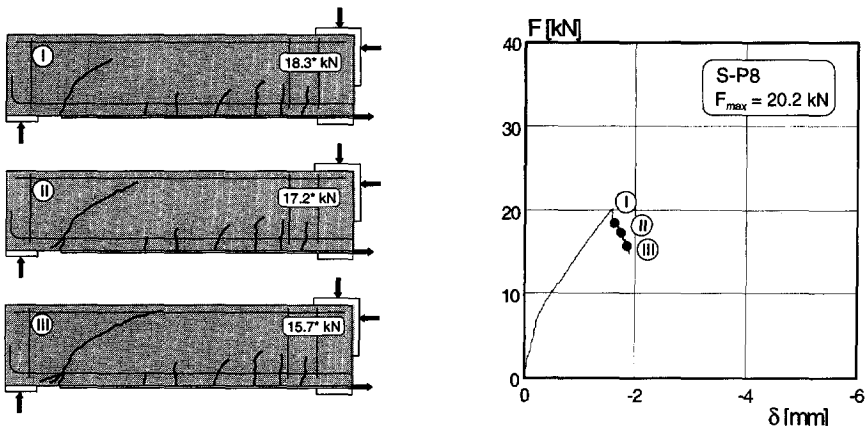


Fig. 6.3 Crack pattern development and load-deflection diagram of beam-end S-P8 (P4×80, L100, W100, H200, 2Ø8, no stirrups)

Stage I was drawn at a load of 16.7* kN after the maximum load had been attained. It shows what was just discussed. Stage II shows further growth of the crack at the plate end into the concrete compression zone. The tip of the crack grew further into the direction of the applied shear load at the level of the top reinforcement. Also, at the plate end, a new crack tip formed from the plate-end crack which grew towards the support. It was the result of dowel action activated by shear deformations. By virtue of the dowel action mechanism the bars pushed the unreinforced concrete cover away from the concrete.

Stage III shows the final stage at which the test was stopped. Widening of the plate-end shear crack was observed. Failure clearly appeared to be plate-end shear. The shear resistance of the unplated area of the beam was exceeded. Observations indicated that the plate-end crack (at the immediate plate end) played a contrasting

role in the failure behaviour. Although the plate-end crack initiated plate-end shear, some tests taught that this part of the crack closed during widening of the plate-end-shear crack.

In beam-end S-P8, the bonded-on plate was $4 \times 80 \text{ mm}^2$ and was stopped at a distance of 100 mm from the support. Failure of this beam-end was identical to that of S-P14, despite the smaller plate cross section. Stage I in Fig. 6.3 depicts cracks in the shear span of the beam-end after the maximum load of 20.2 kN had been reached. It was observed that at this stage the plate-end shear crack had developed. Also, a new tip had initiated near the root of the plate-end crack and grew to the support, see stage II. Stage III shows the ultimate stage when the test was stopped. As in beam-end S-P14, plate-end shear governed failure.

Partially Plated Beam-End (L200 mm)

For specimen S-P3 the bonded-on external plate $3 \times 60 \text{ mm}^2$ was stopped at a distance of 200 mm from the support. The type of failure was identical as for S-P8 and S-P14: *plate-end shear failure*. However, some differences between the L100 and L200 can be observed from the sketched crack patterns in Fig. 6.4.

In stage I we distinct a plate-end crack and a plate-end shear crack in the same cross section which were *not* connected. Hence, it seemed likely that when the unplated length of the plate increased a more combined shear flexural crack played a role. Another difference is that at stage III more clearly peeling and dowel cracks were observed at the level of internal reinforcement. The dowel crack in the unplated part occurred due to dowel action of the internal bars. Because the peeling crack was initiated after the plate-end shear crack developed, the peeling crack in the plated part at the level of the internal bars seemed to result from the plate-end shear deformations and the stiff bonded-on steel plate.

Fig. 6.5 shows a photograph of S-P12 which failed like S-P3 by plate-end shear. The shear crack, dowel crack and peeling crack are clearly visible.

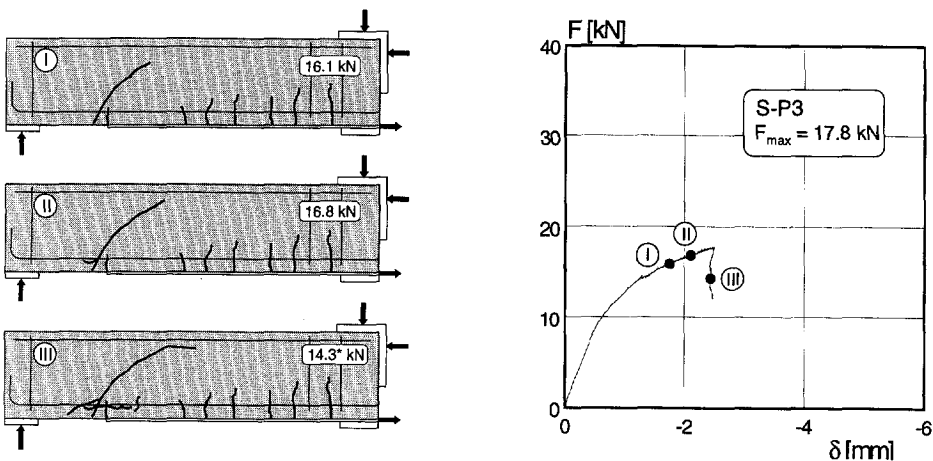


Fig. 6.4 Crack pattern development and load-deflection diagram of beam-end S-P3 (P3 \times 60, L200, W100, H200, 2 ϕ 8, no stirrups)

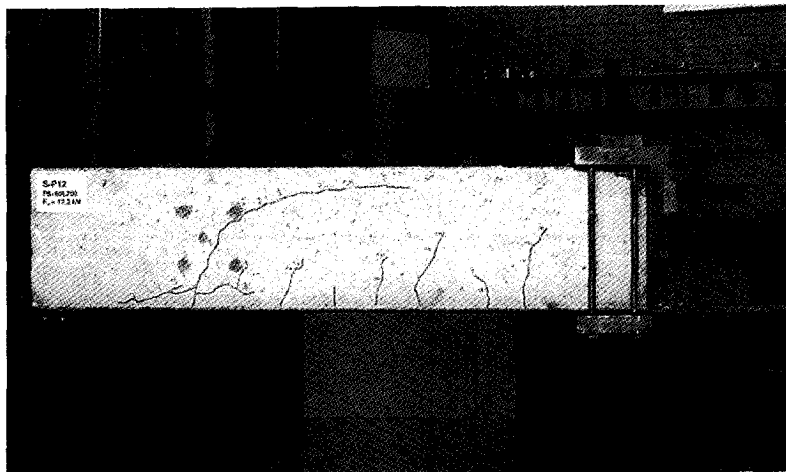


Fig. 6.5 Photograph of plate-end shear failure of beam-end S-P12 (P5×60, L200, W100, H200, 2Ø8, no stirrups)

6.2.3 Maximum Loads in Relation to Unplated Length

The maximum loads from Table 6.1 are graphically represented in Fig. 6.6 as a function of L . With regard to the unplated length the following conclusions are drawn:

- If the steel plate was anchored beyond the support (fully plated), shear failure occurred by flexural shear;
- If the steel plate was partially bonded, shear failure occurred by plate-end shear. The shear resistance by plate-end shear was clearly less than the shear resistance by flexural shear of the fully plated member;
- If the unplated length of a partially plated member increased, the plate-end shear resistance decreased. Accordingly, the unplated length had a major influence on the plate-end shear load;
- Despite plate-end shear, the shear resistance of the partially plated beam-ends L100 and L200 was still higher than the flexural shear resistance of an unplated beam. Apparently, the section at which plate-end shear of partially plated members takes place is more advantageous than that at which flexural shear of unplated members occurs.

6.2.4 Maximum Loads in Relation to External Reinforcement ratio

The maximum loads listed in Table 6.1 are graphically represented in Fig. 6.7 as a function of the total reinforcement ratio ρ_{sp} . Four lines are sketched; three lines connect the experimental results of the tests L0, L100 and L200, the fourth line represents the analytically calculated flexural shear resistance according to Rafla (shear span fully plated). In this graph it is assumed that the reinforcement ratio is defined by the total amount of bar and plate reinforcement present in the constant moment span. Nevertheless, despite the fact that additional reinforcement is bonded to the beam, still a (small) part of the beam remains unstrengthened.

The following conclusions with respect to the external reinforcement ratio are drawn:

- the experimental results on the flexural shear resistance of the fully plated beam-ends are in good agreement with the expression of Rafia and MC90. Hence, bonded-on plate reinforcement can also be treated as conventional longitudinal reinforcement when the shear resistance is calculated. Then (only), of course, the effective depth of the reinforcement is calculated by the weighted effective depth of the cross sectional areas of the bonded-on plate and internal bars;
- If the steel plate is stopped at a distance of 100 mm or 200 mm short of the support, the shear resistance slightly decreases with increasing reinforcement ratio. Accordingly, the external reinforcement ratio hardly influences the magnitude of the plate-end shear load. At this point, it is not yet clear if the small difference is affected by the difference in the amount of external reinforcement, the thickness of the steel plate or the effective depth of the reinforcement;
- a larger amount of external plate reinforcement results in a larger difference between the flexural shear resistance and the plate-end shear resistance.

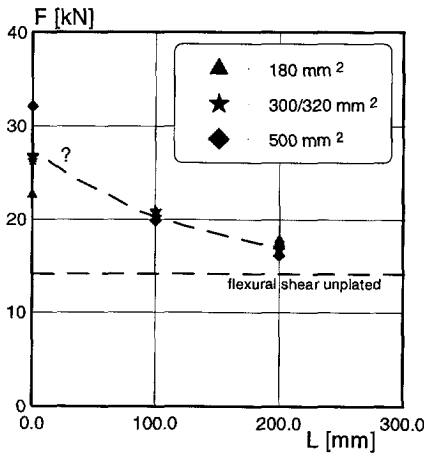


Fig. 6.6 Maximum load as a function of unplated length of steel plate

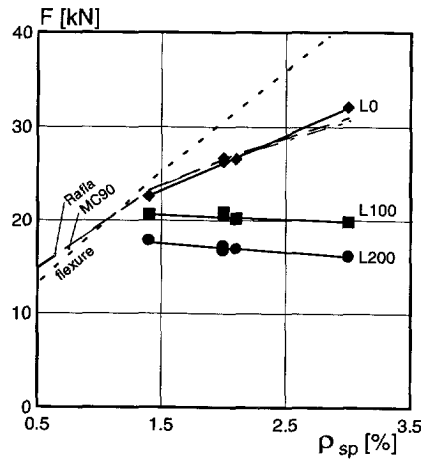


Fig. 6.7 Maximum load as a function of total reinforcement ratio

6.2.5 Initiation of Plate-End Crack

It is interesting to analyse whether the plate thickness has any influence on the initiation of the plate-end crack (note: not plate-end *shear* crack). As during the tests the crack width had been registered by LVDTs no. 9 and no. 10, the measurements were used to analyse the influence of the thickness of the steel plate. However, looking at the obtained measurements it was concluded that the tests results did not give a clear indication on the *initiation* of the plate-end crack.

The L200 measurements were more suitable for a comparison because they gave clearer results of the load on *growth* of the initiated crack at the plate end. Table 6.11 shows the results. As the magnitude of the maximum load, it emerged that

also the crack growth load is influenced by the thickness, because the crack growth load over maximum load ratio decreases from 78% to 70%.

Table 6.11 Tests results of growth of crack at plate end

L200 tests	P [mm ²]	F _{max} [kN]	F _{growth} [kN]	F _{growth} / F _{max}
S-P3	3×60	17.8	13.9	78%
S-P6	3×100	16.7	12.9	77%
S-P9	4×80	16.9	13.1-11.5 ¹⁾	78%-68%
S-P12	5×60	17.2	12.1	70%
S-P15	5×100	16.1	11.4	71%

¹⁾ exact crack growth load was not clearly registered

6.2.6 Aggregate Interlock

Earlier, it was remarked that in test S-P14 the plate-end crack closed after plate-end shear failure. A possible explanation may be given by aggregate interlock. Therefore, measurements over the plate-end shear crack were carried out. On the beam-ends that were partially plated, triangled measuring devices with LVDTs were located at the plate end to recalculate the sliding of the plate-end shear crack faces, Fig. 6.8. By doing so, stresses generated by aggregate-interlock could be derived between the crack faces to get an insight in the state of stress at the crack faces during plate-end shear. The LVDTs were located only at the front side of the beam.

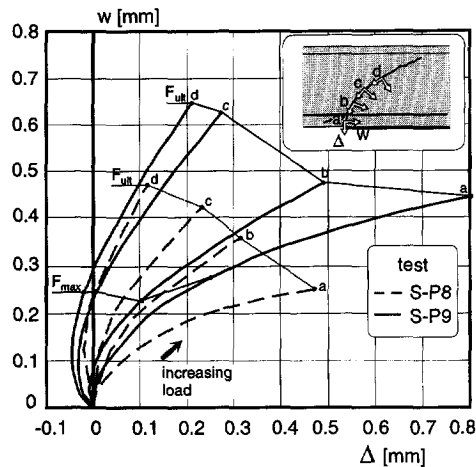
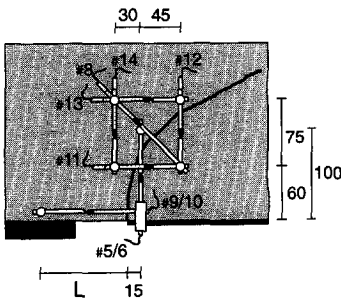


Fig. 6.8 Triangled measuring devices with LVDTs placed over plate-end shear crack

Fig. 6.9 Recalculated normal and shear displacements of plate-end shear crack

Fig. 6.9 shows the recalculated relative displacements by transforming the measured displacements into a normal displacement w and a shear displacement Δ . This was done for S-P8, with a 100 mm unplated length, and S-P9, with a 200 mm unplated length. The lines in Fig. 6.9 represent the opening and sliding of the crack

faces with increased loading. In this figure it can be seen that at the root of the plate-end shear crack (a) mainly shear displacements were registered, and near the tip of the plate-end shear crack (d) mainly normal displacements were measured. Hence, the region in which the plate-end shear crack was inclined to 45° , the crack opened gradually and at the root of the crack the faces slid over each other.

Accordingly, particularly the root of the shear crack should have contributed to internal equilibrium. This was further analysed with the aggregate interlock model of Walraven [1980]¹⁴. This model couples normal- and shear displacement at crack faces to normal and shear stresses imposed by the aggregates, which is influenced by the maximum diameter of the aggregate and the concrete compressive strength. To that end, of test S-P9 at maximum and ultimate load (when the test was stopped), and of test S-P8 at ultimate load, the normal and shear displacements were plotted in the displacement-stress diagram to obtain the contributions of the crack face stresses resulting from aggregate interlock. Fig. 6.10 shows the w - Δ - σ and w - Δ - τ relations. The derived crack stresses are visualised in Fig. 6.11. As it emerges from this figure, the contribution by virtue of aggregate interlock is significantly and dominantly present in the lower part of the beam at the root of the shear crack. Due to sliding of the crack faces, shear and compressive normal stresses developed. Also, in the range where the shear crack was inclined, stresses were not present. This was due to the fact that the inclined shear crack mainly opened in the normal direction, so that aggregate interlock was not developed.

In the case of beam-end S-P9, it is seen that the interlock stresses were considerably increased from maximum to ultimate load, but were still transferred over the same length of the crack. Ultimately, the observations show that closing of the plate-end crack was needed to activate aggregate interlock stresses to obtain internal equilibrium after the maximum plate-end shear load was reached. Also, the dowel force V_{dowel} and the concrete arch force V_{arch} contribute to the total shear load.

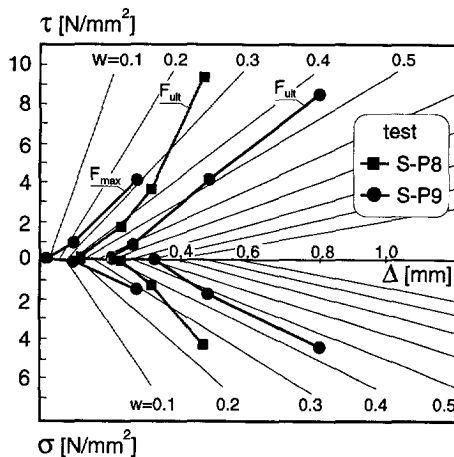


Fig. 6.10 Contributions to the transfer of stresses at the crack face (Walraven [1980]¹⁴, $d_{\text{max}} = 16 \text{ mm}$ and $f_{\text{cm,cube}} = 37.6 \text{ N/mm}^2$)

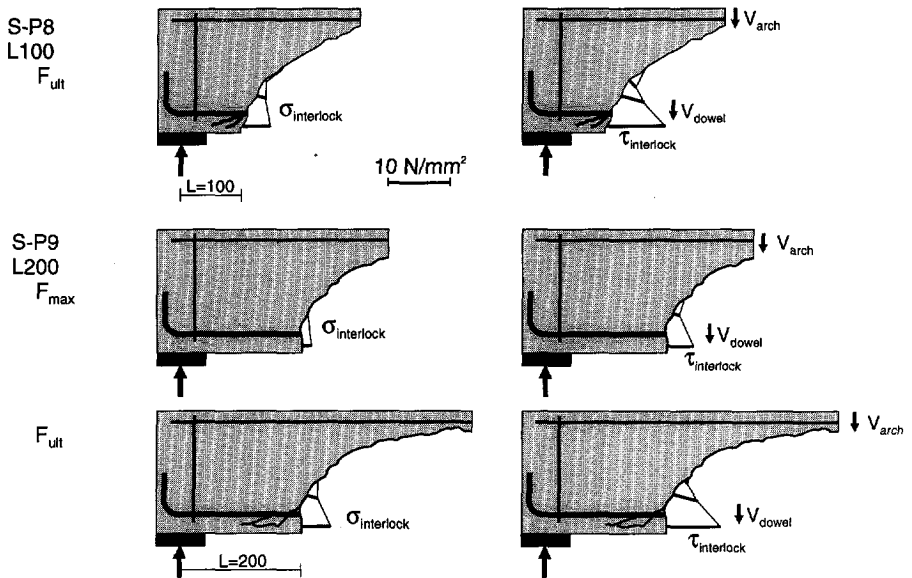


Fig. 6.11 Beam-ends at support; contribution of normal (compression) and shear stresses in crack by virtue of aggregate interlock, and contributions of dowel action force and concrete arch force

6.2.7 Conclusions

From this section main conclusions could be drawn with respect to the shear capacity of members strengthened in bending by externally bonded steel plates:

- If the steel plate was bonded beyond the support, failure occurred by flexural shear. The shear capacity of the fully plated member was significantly increased when the external reinforcement ratio was enlarged. Flexural shear could be predicted by using the shear resistance formulations of Rafia or CEB-FIP MC90;
- If the member was only partially plated, and if the steel plate was stopped at a short distance before the support, failure occurred by plate-end shear;
- Plate-end shear was mainly governed by the unplated length of the shear span, or, in other words, the length of the shear span that was not strengthened influenced plate-end shear. Plate-end shear was hardly influenced by the external reinforcement ratio, because the load bearing capacity decreased slightly when the external reinforcement ratio was enlarged;
- No effect of the thickness of the plate on the initiation of the plate-end crack could be deduced;
- Aggregate interlock stresses at the root of the plate-end crack provided internal equilibrium after the maximum shear load had been reached.

6.3 Influence of Width of Concrete Cross Section

6.3.1 Contents of Test Series S-W

A total of 4 beam-ends were tested to investigate the influence of the width of the concrete member and various plate geometry's on plate-end shear. Table 6.III lists the contents of the test series S-W. The beam-ends with a concrete cross section of $200 \times 200 \text{ mm}^2$ were reinforced with four 8 mm diameter bars at an effective depth of 170 mm. The unplated length of the applied bonded-on steel plates was 100 mm.

Table 6.III Overview of test series S-W

test	P [mm ²]	L [mm]	F _{max} [kN]	mode of failure
S-W1	4×80	100	35.9	plate-end shear
S-W2	3×100	100	36.5	plate-end shear ¹⁾
S-W3	5×60	100	35.8	plate-end shear
S-W4	5×100	100	36.9	plate-end shear

¹⁾ because epoxy-resin was badly mixed, at maximum load interface failure occurred

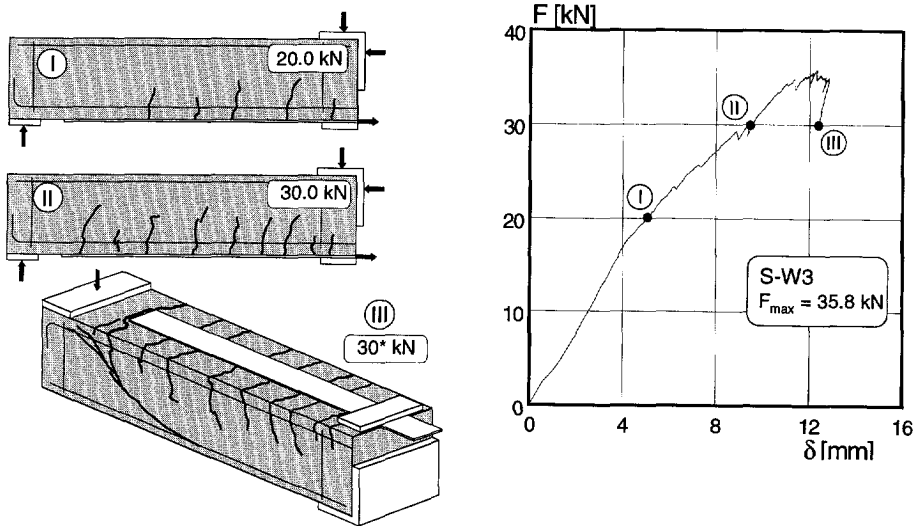


Fig. 6.12 Crack pattern development and load-deflection diagram of beam-end S-W3 (P5×60, L100, W200, H200, A800, 4Ø8, no stirrups)

6.3.2 Failure Behaviour

Despite the different plate cross sections that were bonded, the failure behaviour of the four beam-ends was identical. Failure was by plate-end shear, also for S-W2 which ultimately showed interface failure due to bad mixing of the epoxy. Appendix C shows crack patterns and load-deflection diagrams for all the tests.

Fig. 6.12 depicts the crack pattern development of test S-W3, on which a $5 \times 60 \text{ mm}^2$ plate was bonded. The first stage shows flexural cracks at an external

load of 20 kN. Then, the next stage at 30 kN shows the initiated plate-end crack. Note that the plate-end crack at the bottom side propagated around the plate-end of the steel plate. This is clearly seen in the third load stage, which was drawn up at a load of 30* kN, after the maximum load had been reached. The plate-end shear crack caused shear failure of this beam-end. So, despite the fact that only 60 mm of the width of the concrete member of 200 mm was plated (1 : 3.3), plate-end shear still dominated. Of course, as a result of the increased concrete width, the contribution of the concrete to the shear load was higher than that of the smaller beam-ends S-P14 and S-P14A. Accordingly, the failure shear load of test series S-W was much higher than those of test series S-P.

6.3.3 Maximum Loads in Relation to External Reinforcement Ratio

Fig. 6.13 shows the experimental results of the test series S-W. Also, the flexural and flexural shear capacity lines are drawn. As it emerges from the graph, the maximum loads of the beam-ends S-W1, S-W2 and S-W3 equalled the flexural capacity of the cross section. However, because experimentally a high-quality steel plate was applied, yielding was not observed during the test. All the beam-ends failed by plate-end shear. Compared to an unplated member with a flexural shear capacity of about 30 kN, the maximum load by plate-end shear was significantly higher. Like the test series S-P, the external reinforcement ratio hardly affected the maximum plate-end shear load.

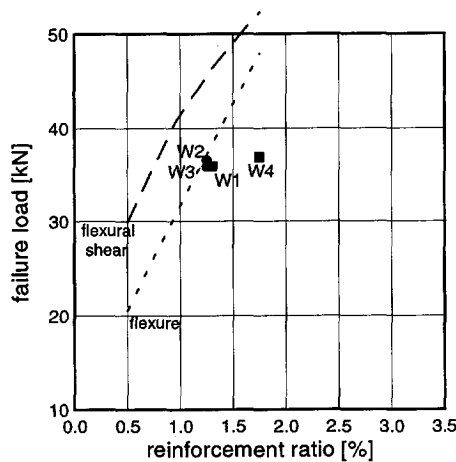


Fig. 6.13 Maximum load as a function of total reinforcement ratio $\rho_{sp,0}$

6.3.4 Conclusions

The contribution of the concrete to the shear load increased when wider beam-ends were strengthened. However, if the concrete width-over-plate width was increased (up to a ratio of 3.3), plate-end shear still dominated failure. The amount of external reinforcement hardly influenced the plate-end shear load.

6.4 Influence of Height of Concrete Cross Section

6.4.1 Contents of Test Series S-H

A total of 4 beam-ends were tested to investigate the influence of the height of the concrete member and various plate geometry's on plate-end shear. Table 6.III overviews the test series S-H. The beam-ends with a concrete cross section of $100 \times 400 \text{ mm}^2$ were reinforced with two 12 mm diameter bars at an effective depth of 366 mm. The top bars consisted of two 8 mm diameter bars. The unplated length of the bonded-on steel plates was 200 mm from the centre of the support. The test set-up provided a shear span of 1600 mm.

Table 6.IV Overview of test series S-H

test	P [mm^2]	L [mm]	F _{max} [kN]	mode of failure
S-H1	4×80	200	38.1	plate-end shear
S-H2	3×100	200	40.6	plate-end shear
S-H3	5×60	200	40.3	plate-end shear
S-H4	5×100	200	34.4	plate-end shear

6.4.2 Failure Behaviour

Also, in the test series S-H plate-end shear dominated failure. At 30* kN in the post-peak branch, Fig. 6.14 shows a photograph of beam-end S-H3 externally strengthened with a $5 \times 60 \text{ mm}^2$ plate. The maximum load was 40.3 kN. At an external load of 25 kN, flexural cracks had developed in the shear span. Then, at 38.5 kN, the load suddenly dropped to 35.8 kN. A plate-end crack had initiated. The load was further increased to a maximum load of 40.3 kN, at which the plate-end crack had developed into a plate-end shear crack. A dowel crack had formed at the plate-end, and a plate shear peeling crack had formed at the level of the internal bars. Appendix C shows crack patterns and load-deflection diagrams of series S-H.

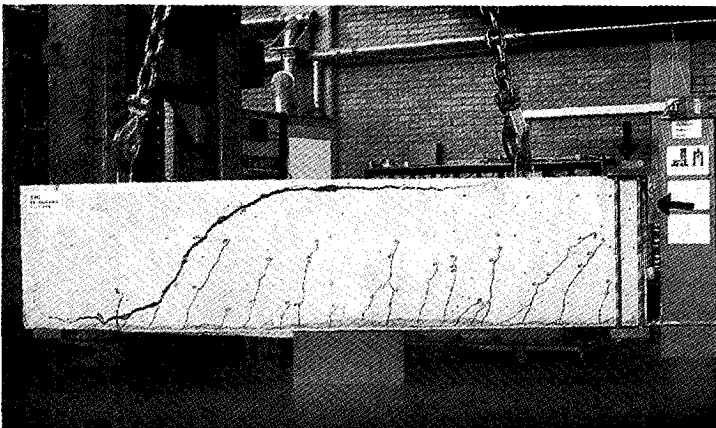


Fig. 6.14 Photograph of crack pattern of beam-end S-H2 (P3×100, L200, W200, H200, A1600, $\varnothing 12$, no stirrups)

6.4.3 Maximum Loads in Relation to External Reinforcement Ratio

Fig. 6.15 shows the maximum loads of test series S-W as a function of the total reinforcement ratio. The plate-end shear loads were nearly equal to the flexural and flexural shear capacity. The plate-end shear load of S-H4 was much lower than those of the other tests. Accordingly, the amount of external reinforcement did influence the plate-end shear load. A beam with a larger height is generally more sensitive to the initiation of cracks than a beam with a height of 200 mm or less.

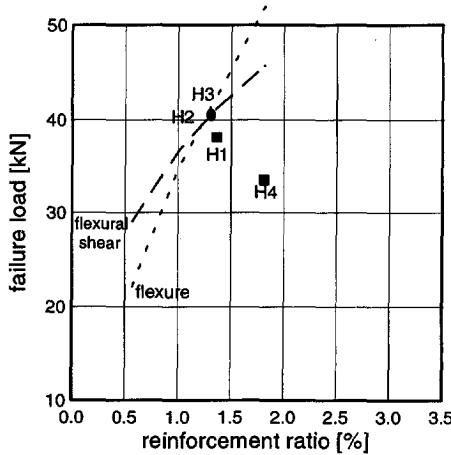


Fig. 6.15 Maximum loads as a function of total reinforcement ratio $\rho_{sp,0}$

6.4.4 Conclusions

Plate-end shear dominated failure for relatively high beams and an unplated length of 200 mm. The external reinforcement did influence the plate-end shear load.

6.5 Conclusions

This chapter dealt with the shear resistance of beam-ends strengthened in flexure with externally bonded steel plates. The shear resistance of beams with externally bonded plates over the support was in agreement with Rafla's and CEB-FIP's MC90 expression for flexural shear. Failure occurred in the shear span due to the development of a flexural shear crack. On the contrary, when the shear span was only partially plated, a crack initiated at the end of the steel plate. As a result of this plate-end crack, shear failure was forced to occur in the unstrengthened part beyond the plate end. Then, the plate-end shear resistance of the partially plated member was significantly decreased compared to the flexural shear resistance of beam-ends with steel plates bonded over the support. The experiments proved conclusively that the unplated length of the shear span governed failure. For nearly all tests, the amount of external reinforcement did not influence the plate-end shear load.

7. DEVELOPMENT OF SMEARED-DISCRETE CRACK MODEL

Numerical simulations play an important role in this study. Thus, this introductory chapter on Part III is fully dedicated to the development of the finite element model and the validation of the simulations. Firstly, §7.1 deals with the aim of the simulations. §7.2 presents macro material models for concrete, reinforcement and epoxy-resin. Then, §7.3 introduces the initial finite element model. Solution techniques and numerical problems are also dealt with. §7.4 extensively discusses the development and calibration of the smeared-discrete crack model. Finally, this chapter concludes in §7.5 and summarises the adopted material models.

7.1 Aim of Numerical Simulations

Until now only little has been published on finite element calculations in the field of strengthening with externally bonded steel plates. Some analyses have been carried out on the normal- and shear stress distribution at the plate end. For example, Pichler [1993]¹¹ performed simulations on beams additionally anchored with bolts, however, these were only intended to show that the flexural capacity of a cross section could be reached. Non-linear simulations on beam shear or plate anchorage were rarely carried out. Although carrying out experiments as well as numerical simulations is time-demanding, both complementary studies are indispensable to gain insight into the failure behaviour of a strengthened concrete member.

A lot of experiments on strengthened members are described in the literature. Mainly, the amount of bonded-on plate reinforcement was varied. In some cases, the influence of the length of the bonded-on plate on the anchorage capacity was investigated. Hardly any tests were found in which the shear span was varied. Experimentally, this requires a lot of effort, in contrast to numerical simulations. In the latter case, the boundary conditions can be quickly changed and a non-linear calculation can be performed within approximately 20 hours. Because shear plays a dominant role in the failure behaviour in this study, an extensive part of the simulations was dedicated to varying the length of the shear span.

By performing numerical simulations complementary to experiments, additional results were obtained. Accordingly, as a result of the simulations and experiments, better founded conclusions could be drawn on the influence of the unplated length, the reinforcement ratio and the length of the shear span.

The simulations described in this thesis were performed with the finite element program DIANA (version 5.1). This program particularly models the non-linear characteristics of concrete well. The calculations were carried out on two Silicon Graphics workstations.

7.2 Macro Material Models

7.2.1 Concrete

Linear Elastic Properties

For concrete a Young's modulus $E_c = 32000 \text{ N/mm}^2$ and a Poisson's ratio $\nu = 0.20$ were assumed as linear input parameters.

Plasticity

For the compressive regime the Mohr-Coulomb yield criterion was applied, Fig. 7.1. In the Mohr-Coulomb formulation one calculates the cohesion c by:

$$c = \frac{1 - \sin \phi}{2 \cos \phi} f_{cm} = 10.4 \text{ N/mm}^2$$

A typical value for the internal angle of friction for concrete is $\phi = 30^\circ$. Associated plasticity was assumed, so the dilatancy angle $\psi = \phi$. Hence, $\sin(\phi) = \sin(\psi) = 0.5$. Furthermore, the control tests of the concrete used in the experiments showed a mean uniaxial compressive strength of $f_{cm} = 35.9 \text{ N/mm}^2$, whereas the mean cube compressive strength was $f_{cm,cube} = 45.5 \text{ N/mm}^2$.

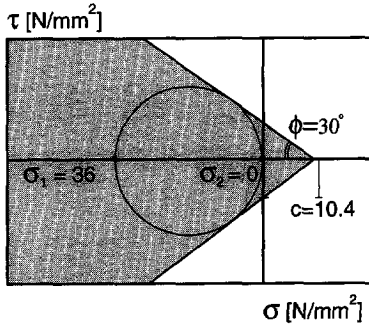


Fig. 7.1 Mohr's stress circle for uniaxial compression and Mohr-Coulomb yield criterion as an envelope

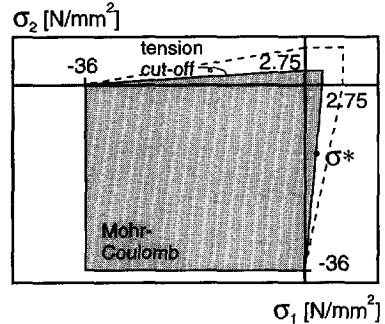


Fig. 7.2 Mohr-Coulomb yield surface for plane stress conditions and linear tension cut-off

Cracking

In the tensile regime the smeared crack concept was used to model cracking of the continuum elements. Cracking occurs in the integration points. There, the stress-strain relation is modified in order to account for the stiffness and strength degradation that accompanies cracking. The smeared crack approach is specified by tension cut-off, tension softening and shear retention.

A linear tension cut-off was applied. A crack arises if the principal stress exceeds the minimum of f_{ctm} or $f_{ctm} \{1 - |\sigma^*/f_{cm}|\}$, see also Fig. 7.2.

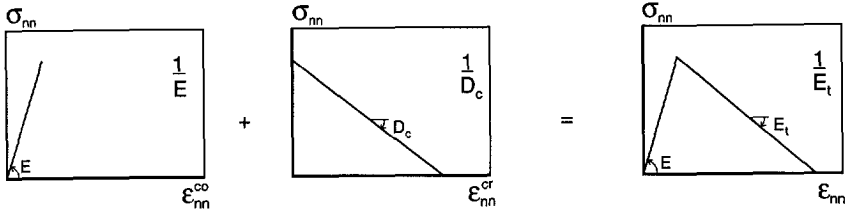


Fig. 7.3 Normal stiffness after concrete cracking

For tension softening, Rots's [1985]¹⁴ modelling approach is implemented in DIANA. The total strain is decomposed into a concrete part ϵ^{co} and a crack part ϵ^{cr} to allow more cracks in one integration point and to still obey the stress-strain relation, Fig. 7.3. The softening modulus D_c was determined from a tensile test carried out by Hordijk [1991]¹⁴, see Fig. 7.4. To approach the softening tail, a bilinear descending branch was applied, as proposed by Petersson [1981]¹⁴ and Hillerborg [1984]¹⁴, Fig. 7.5. A fracture energy of $G_f = 0.120 \text{ N/mm}^1$ was initially assumed for the simulations.

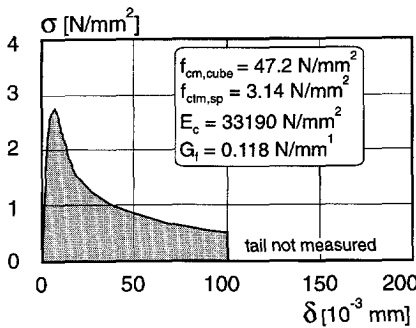


Fig. 7.4 Load-deformation for concrete with $f_{cm,cube} = 47.2 \text{ N/mm}^2$ (Hordijk [1991]¹⁴)

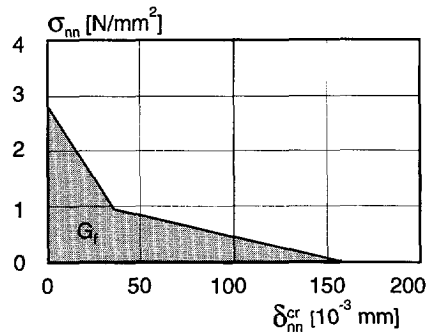


Fig. 7.5 Bilinear tension softening model according to Hillerborg [1984]¹⁴

The axial tensile stress was derived from the mean tensile splitting strength determined by standard tests (see Chapter 4). According to Eurocode 2 the magnitude of the axial tensile stress is a function of the tensile splitting strength:

$$f_{ctm} = 0.9 f_{ctm,sp} = 2.75 \text{ N/mm}^2$$

The ultimate deformation δ_u , or the maximum crack width at which the opened crack does not transfer any stresses equals:

$$\delta_u = \frac{18 G_f}{5 f_{ctm}} = 0.1575 \text{ at } f_{ctm} \text{ and } \frac{2}{9} \delta_u = 0.0350 \text{ at } \frac{1}{3} f_{ctm} \text{ (for } G_f = 0.120 \text{ N/mm}^1\text{)}$$

The stress-deformation relation from Fig. 7.5 was used to derive the stress-smeared strain relation which has a similar shape. In this relation, the fracture energy is

smeared out over a crack band width h . Thus, the volumic fracture energy g , equals G_c / h . However, for the value of the volumic fracture energy g , a parameter study was needed to determine correct magnitudes of the fracture energy and crack band width in order to obtain a satisfactory ultimate smeared crack strain.

Finally, for the smeared crack model the shear stiffness of cracked concrete was specified, represented by a shear retention factor β . The shear retention factor indicates the percentage of elastic shear capacity retained after cracking, see Fig. 7.6. In advance, a shear retention factor of $\beta = 0.2$ was assumed.

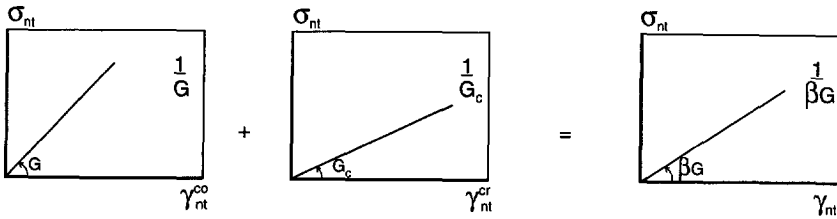


Fig. 7.6 Shear stiffness after concrete cracking

7.2.2 Ribbed Bar Reinforcement

Linear Elastic properties

In the linear branch of the load-deformation diagram, the stiffness defined as the modulus of elasticity ranges between 195000-210000 N/mm² according to Rußwurm [1989]¹⁴. Hence, $E_s = 200000$ N/mm² and $\nu = 0.30$ were adopted for the simulations.

Plasticity

The mean yield and the mean maximum stress of hot-rolled and cold-worked steel are respectively 580/690 N/mm² and 630/665 N/mm². In this numerical study a mean yield stress of 600 N/mm² was utilised, comprising an ideal plastic branch at yielding (Fig. 7.7). Also, a Von Mises yield surface had to be defined (Fig. 7.8).

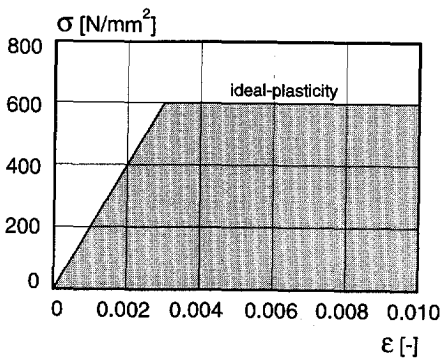


Fig. 7.7 Stress-strain relation for bars

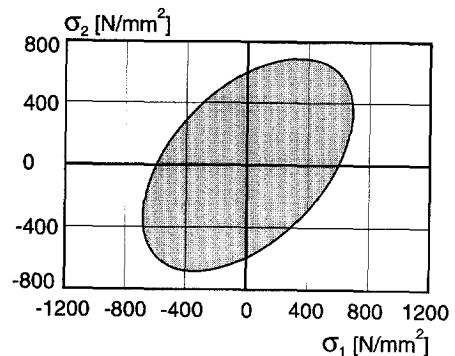


Fig. 7.8 Von Mises yield surface for bars

7.2.3 Steel Plate Reinforcement

Linear Elastic properties

The modulus of elasticity for the external steel plates was 190000 N/mm², Poisson's ratio was assumed to be $\nu = 0.30$.

Plasticity

Although a high quality steel was used in the experiments, a normal steel quality was considered in the numerical analyses because this is commonly used for strengthening. A mean yield stress of 285 N/mm² and a Von Mises yield surface were adopted, see Fig. 7.9 and Fig. 7.10. Furthermore, for the steel plate it was assumed that the yield function not only depended on stresses, but also on plastic strains. Accordingly, work-hardening was adopted in which the yield surface expanded. Fig. 7.11 shows the stress-strain relation used and Fig. 7.12 shows the hardening relation derived from Fig. 7.11.

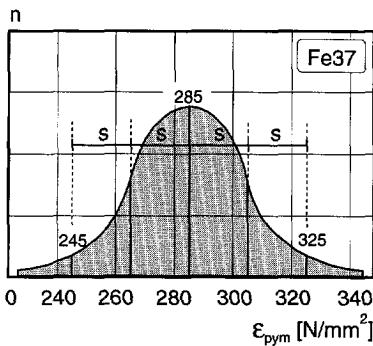


Fig. 7.9 Gaussian representation of yield stress of normal quality steel

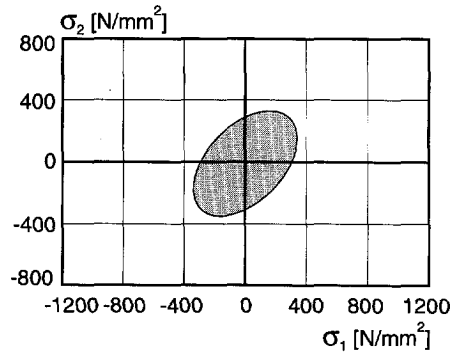


Fig. 7.10 Von Mises yield surface for steel plate

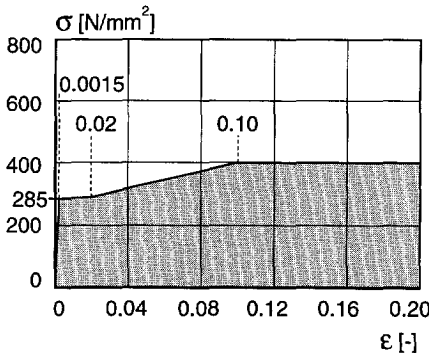


Fig. 7.11 Stress-strain relation for steel plate

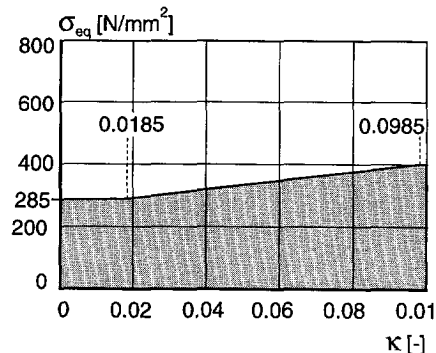


Fig. 7.12 Stress-equivalent plastic strain relation for steel plate

7.2.4 Epoxy Resin

Linear Elastic properties

According to the technical information of the epoxy resin, the modulus of elasticity was 11000 N/mm^2 after seven days of hardening. Poisson's ratio was assumed to be $\nu = 0.35$. Because an interface element was generated for the epoxy layer, a normal stiffness D_{11} and a shear stiffness D_{22} were required. Hence:

$$\begin{bmatrix} t_n \\ t_t \end{bmatrix} = \begin{bmatrix} D_{11} & 0 \\ 0 & D_{22} \end{bmatrix} \begin{bmatrix} \Delta u_n \\ \Delta u_t \end{bmatrix} \quad (7.1)$$

These stiffnesses are dependent on the normal- and shear stiffness of the epoxy and the thickness of the interface element which amounted to $t_g = 1.5 \text{ mm}$:

$$D_{11} = \frac{E}{t_g} = 7350 \text{ N/mm}^3 \text{ and } D_{22} = \frac{E}{2(1+\nu)t_g} = 2700 \text{ N/mm}^3.$$

Friction

To model bond and plasticity, a friction model was assumed based on the Mohr-Coulomb yield criterion. Jansze [1996b] conducted experiments on prismatic specimens comprising an inclined filled epoxy-resin joint to determine these strength characteristics of the interface. Despite the use of high strength concrete in the study, the failure envelope would hardly change if a normal concrete quality was used. This is mainly explained by the fact that the epoxy resin itself characterises the bonding strength and the friction in the interface. The concrete itself hardly played a role. The study concluded that the Mohr-Coulomb yield surface for the epoxy and high strength concrete was defined as (Fig. 7.13):

$$\tau_{max} = 24.0 + 0.33\sigma \quad (7.2)$$

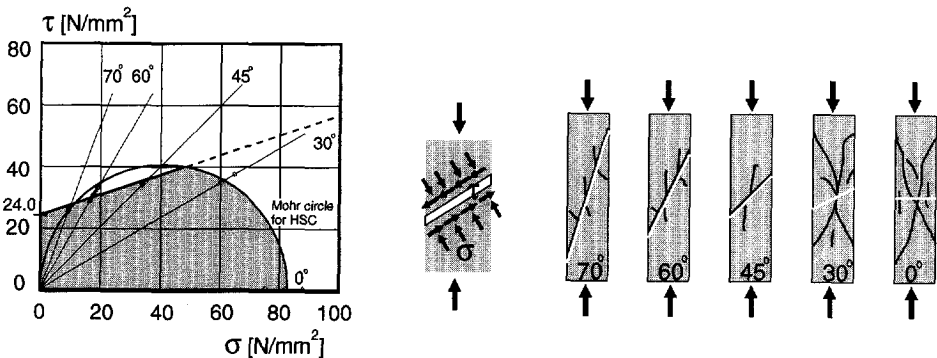


Fig. 7.13 Mohr-Coulomb yield surface for interface layer between concrete and epoxy, experimentally determined on specimens as shown on the right (Jansze [1996b])

7.3 Finite Element modelling

7.3.1 Design of Continuum Finite Element Model

Two-Dimensional Approach

The strengthening of a structural element is a three-dimensional problem. In laboratories it is possible to approach this by three-dimensional tests, however, in a computational approach the numbers of freedom must be limited to reduce the calculation time. At the same time, most three-dimensional problems can be approached by two-dimensional models, in which the z-direction is of significance for the state of stresses or strains. A two-dimensional model is based on either a plane-stress or plane-strain approach.

By definition, a plane stress approach is applied to schematise walls or deep beams. Accordingly, the thickness of the elements is equal to the thickness of the specimen. Despite the fact that the thickness of the beam is not small in relation to the height, namely 1:2, the plane-stress approach was used for the simulations. Then, the in-plane thickness of the finite elements equalled 100 mm.

Element types

In the continuum model the specimen is subdivided into a finite number of plane elements that are connected in nodes by equilibrium- and compatibility relations. The CQ16M element was used for the concrete, the steel plate and the supports. To explicitly model the internal bar reinforcement and the stirrups, the truss element CL6TR was used. Both epoxy and bond (between concrete and epoxy) were jointly modelled by the discrete interface-element CL12I. Later on, it turned out that this discrete element could also be applied for discrete cracking in concrete.

The plane stress element CQ16M is a quadrilateral plane-stress element with 8 nodes (Fig. 7.14). Due to the quadratic interpolation accurate results are obtained. A 3×3 Gauss-integration scheme was applied.

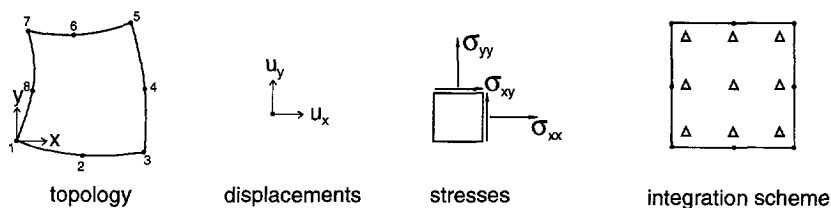


Fig. 7.14 Plane stress elements CQ16M

The truss element CL6TR is a 2-D curved uniaxial-stress element with 3 nodes (Fig. 7.15). A quadratic interpolation with a 3 point Gauss integration scheme was applied.

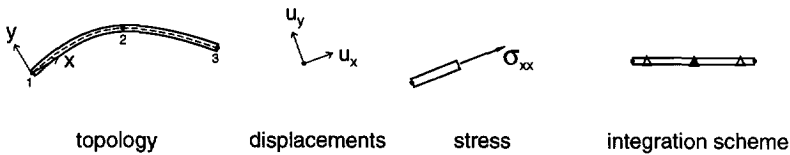


Fig. 7.15 Truss element CL6TR

The interface element CL12I is an interface between two lines in a 2-D configuration (Fig. 7.16). A quadratic interpolation with a 3 point Lobatto scheme was applied. This element describes a relation between tractions t and relative displacements Δu .

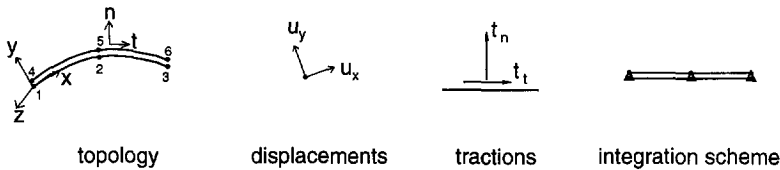


Fig. 7.16 Interface element CL12I

Continuum Model and Boundary Conditions

Taking advantage of the symmetry of the problem, only half the beam was modelled in the numerical finite element model. In such a way, yielding of the internal and/or external reinforcement in the constant moment span could be taken into account.

Fig. 7.17 shows the generated initial finite element mesh. Element sizes of $20 \times 20 \text{ mm}^2$ were applied. It comprises a shear span of 800 mm and half a moment span of 400 mm. The thick line in the mesh represents the ribbed bar reinforcement at an effective depth of 170 mm. The fully bonded-on plate measured $5 \times 100 \text{ mm}^2$. Between the concrete and the steel plate, discrete interface elements were generated to model the epoxy resin. The geometrical thickness of the epoxy layer between the concrete and the steel plate equalled 1.5 mm. In anticipation, it must be mentioned that the configuration of this initial mesh will change.

Finally, kinematic and dynamic boundary conditions were applied. At the symmetry-axis of the beam every element node was tied to a boundary which only allowed a displacement in the vertical direction. The roller bearing on the left side supported the beam. A unity load of $F = 1 \text{ kN}$ acted in the vertical direction. This unity load F was scaled and incremented during the non-linear simulations.

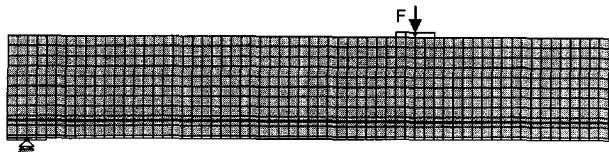


Fig. 7.17 Generated initial finite element mesh and boundary conditions of a reinforced concrete beam fully strengthened with an externally bonded steel plate

7.3.2 Solution Techniques

Incremental-Iterative Solution Procedure

The non-linear relation between load and displacement asks for an incremental-iterative solution procedure, in which the load is incrementally increased (in steps) and within an increment equilibrium is iteratively achieved (De Borst [1991]¹⁴). Iteration is repeated until internal equilibrium conditions are sufficiently fulfilled and convergence is obtained. In this study, the regular Newton-Raphson iteration procedure was used, in which the tangential stiffness matrix is set up before each iteration. Regular Newton-Raphson iteration is graphically shown in Fig. 7.18.

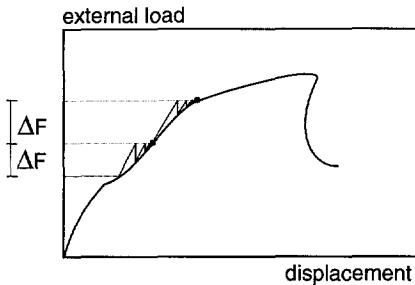


Fig. 7.18 Incremental-iterative solution procedure to obtain converged equilibrium (De Borst [1991]¹⁴)

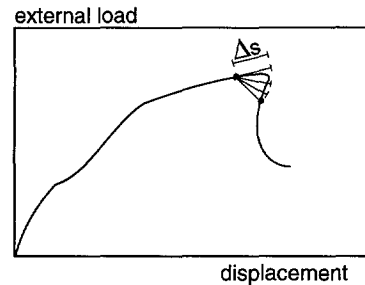


Fig. 7.19 Linearised arc-length control (De Borst [1991]¹⁴)

Arc-Length Control

At maximum load, a pure load controlled procedure fails, because an additional load step does not find an intersection point with the load-displacement diagram. Hence, divergence of the iterative procedure will occur. A solution, however, would be found with a clever modification of load control. Therefore, an arc-length control procedure was used, Fig. 7.19 (De Borst [1991]¹⁴). With this path-following technique, the maximum load could be determined and (the first part of) the post-peak branche.

Convergence Criterion

For convergence, internal equilibrium based on internal energy was checked by 0.0001. The maximum number of iterations within a step ranged between 15 and 25. With the purpose to accelerate the numerical simulation, the convergence criterion was sometimes increased to 0.001.

Localisation of Failure

In the case of plate-end shear and plate separation a snap-back response in the post-peak branch was calculated, but after some steps a converged solution could not be obtained anymore. Consequently, the post-peak behaviour could not be numerically reproduced. But, because the behaviour up to the maximum load was of interest, and the failure response was already thoroughly investigated in the tests, no real effort had been put into further analysis of the post-peak branch.

7.3.3 Model uncertainties

Tension Stiffening

After flexural cracks are formed in an RC member loaded in bending, the cracked concrete tensile zone still contributes to the stiffness of an RC member. This phenomenon is generally known as tension stiffening, Fig. 7.20. In tension stiffening the bond-slip behaviour between the reinforcing bars and the concrete, and the tension softening characteristics of the concrete play a major role. Rots [1988]¹⁴ distinguishes bond-slip into three approaches with decreasing degree of precision:

- computational determination of bond-slip. Bond-slip is characterised by the tangential relative displacement between the bar and the concrete. Longitudinal cracks and secondary transverse cracks cause this relative displacement;
- interface with bond-slip characteristics. The traction-slip behaviour is lumped into an interface element to predict the spacing and width of primary flexural cracks;
- tension stiffening with perfect bond. If distributed cracking occurs as in densely reinforced concrete, the bond characteristics are accounted for in an indirect manner, namely, by adjusting the descending concrete tension softening branch.

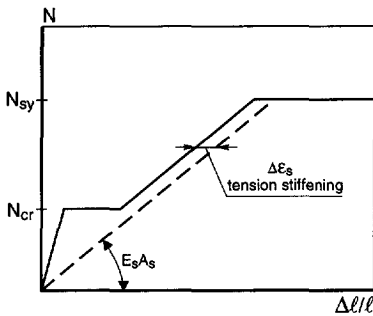


Fig. 7.20 Tension stiffening: concrete contribution after cracking

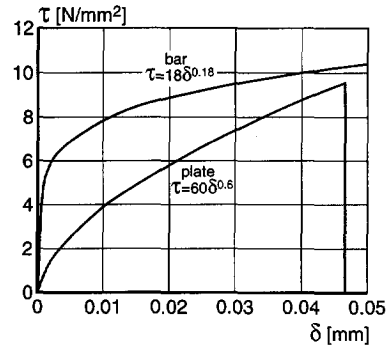


Fig. 7.21 Bond-slip relations for cast-in ribbed bar and bonded-on steel plate

For the engineering practice, the third approach is recommendable. The second one is more for research purposes. The addition of interface elements with bond-slip characteristics improve the localisation of primary cracks in structures with concentrated layers of bars. Conversely, perfect bond generally causes a diffuse crack pattern. Even so, with perfect bond convergence is easier reached.

In Fig. 7.21 the bond-slip relations of a cast-in ribbed bar (Noakowski, DIANA Manual [1993]¹⁴) and a bonded-on plate (Pichler [1993]¹¹) are compared. It emerges that at identical slip, the bond stresses of the plate are lower than the bond stresses of a ribbed bar. Hence, the crack distance as dictated by the bonded-on plate, is much larger compared to that dictated by the bar. Accordingly, the flexural crack distance of an externally plated member is mainly dominated by the internal bars. Moreover, the experiments provided evidence that beam shear and plate anchorage

were hardly influenced by flexural cracking. The stress condition and notching crack at the plate end mainly dominated plate-end shear failure. For these reasons, it was decided not to apply bond-slip characteristics, but to apply perfect bond between the bar and the concrete. Because tension softening was already adopted to the continuum elements surrounding the bar, tension stiffening is partly taken into account. As will emerge from the performed simulations, the response of the beams will be a little too stiff, see Fig. 7.24, but the outcome satisfies.

Smeared Crack Band Width

With the smeared crack approach, a local discrete crack is distributed over a certain width of the finite elements. Then, the volumic fracture energy, which equals the area g , under the tensile stress-crack strain curve, is calculated by dividing the fracture energy G_f by the crack band width h . Rots [1993]¹⁴ emphasised that h is not a material parameter, but a discretisation parameter that depends on the finite element configuration. Mainly, the width of the crack band depends on the element size, the element type, the element shape, the integration scheme, and on the problem considered (Rots et al. [1985]¹⁴). For determining the crack band width, a distinction between three cases was made, see Fig. 7.22. Mode I cracks for which the crack path is parallel (1), or approximately parallel (2) to the mesh and known in advance, and cracks for which the crack path does not follow the mesh (3) and not known in advance. The crack is smeared out over a number of integration points.

Rots [1993]¹⁴ indicated that localisation must take place in a single element, and that element dimensions of about three times the aggregate size should work optimally. As opposed to this constant value correlation to the maximum aggregate size, Ozbolt [1993]¹⁴ showed that the optimum values of the crack band width, by Ozbolt called the characteristic length, in relation to the maximum aggregate size varied substantially for various types of analysed structures. Fig. 7.23 depicts that for bending a width of $3d_{max}$ and for shear a width of $8d_{max}$ was calculated.

Accordingly, it follows that the smeared crack band width should range between 1.0 and $\sqrt{2}$ times the element size, and the element size should range between 24 mm and 64 mm. This will be calibrated in the next section.

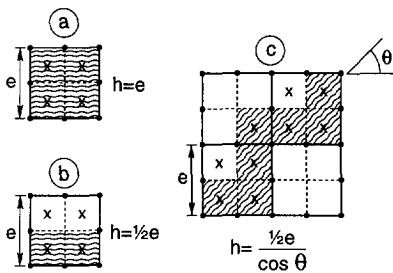


Fig. 7.22 Estimates of crack band width (a) symmetric mode I (b) non-symmetric mode I (c) zig-zag crack band (Rots [1993]¹⁴)

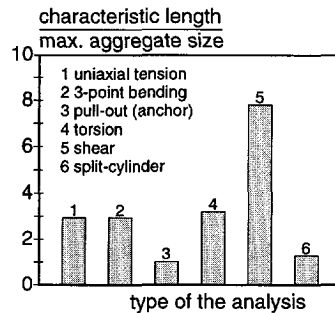


Fig. 7.23 Characteristic length in relation to aggregate size at various cases (Ozbolt [1993]¹⁴)

7.4 Development and Calibration of Finite Element Model

7.4.1 Design of Stages for Development of Model

Three stages were considered to calibrate the outcome of the simulations and to develop the geometry of the finite element mesh. During these stages, choices concerning the smeared crack band width and shear retention factor had to be well founded. Firstly, simulations on an unplated and plated beam with respect to flexural cracking were performed where the influence of the crack band width was investigated. Secondly, plate-end shear cracking was simulated and values for the crack band width, shear retention factor and mesh size were analysed. Thirdly, simulations on plate separation were carried out for which the configuration of the initial mesh was altered. By following these stages, overall and local cracking and failure were accounted for and a sound finite element model was developed.

7.4.2 Stage 1: Simulations on Flexural Cracking

Influence of Softening Quantities

For the deformational behaviour up to failure of the finite element model, flexural cracking was analysed. The volumic fracture energy G_f/h was investigated by varying the ultimate smeared crack strain. Because bond-slip elements were not included in the model (perfect bond), the real crack distance should emerge. Experimentally, the unplated beam BM0 had an average crack distance of about 90 mm, the partially plated beam BM1 65 mm. But, how does variation of smeared crack strain affect the crack pattern and crack distance in the numerical simulations?

Table 7.1 Influence of crack band width on distance between flexural cracks

$\epsilon_u = \delta_u/h$ [-]	$g_f = G_f/h$ [N/mm ²]	$l_{cr, BM0}$ [mm]	$l_{cr, BM2}$ [mm]
0.00785 ¹⁾	0.00600	62	73
0.00450	0.00343	73	67
0.00315	0.00240	73	62
0.00243	0.00185	73	57
0.00198	0.00150	no convergence	50

¹⁾ $G_f = 0.120$ N/mm² and $h = 20$ mm (equals element size)

Five calculations were carried out for both an unplated (BM0) and a fully plated (BM2) beam with stirrups. The shear retention factor was 0.2. Table 7.1 shows the results of the calculations. It emerged that the distance between the flexural cracks for the various smeared strains was not so different for an unplated beam, but was different as far as it concerned the plated beam. This was also confirmed by the crack patterns as depicted in Fig. 7.25. Fig. 7.24 shows that the influence on load-deflection behaviour was not so distinct. For BM0 the tension stiffening effect was clearly visible. The influence on the stability of the numerical calculations was noticeable. For larger smeared crack strains, convergence was easier reached. Particularly, for beam BM0 smaller smeared crack strains showed a much more brittle and unstable response after initiation of the first cracks.

Because plated members were investigated in this study, and stable simulations were preferable, an ultimate smeared crack strain of 0.00315 was found to be favourable for simulating flexural cracking. Actually, as far as flexural cracking was concerned, the outcome of the simulations was not dependent on this value.

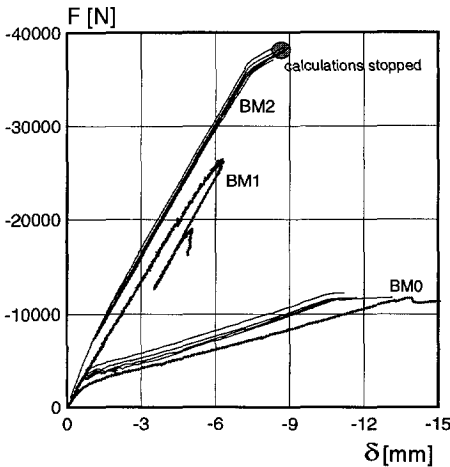


Fig. 7.24 Load-deflection responses of BM0, BM1 and BM2; simulations and experiments (dotted lines)

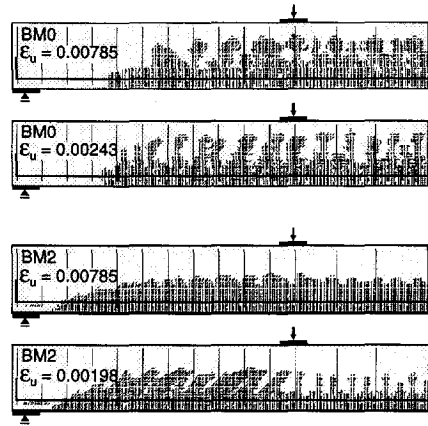


Fig. 7.25 Influence of ultimate smeared crack strain on flexural cracking for BM0 and BM2

7.4.3 Stage 2: Simulations on Plate-End Shear Cracking

Influence of Crack Band Width

A strengthened beam without stirrups and with an unplated length of 100 mm was considered (S-P14(A)). Five crack band widths were investigated, see Table 7.II. In contrast to flexural cracking it emerged from the numerical simulations that the crack band width had a great influence on the maximum load at which plate-end shear led to failure. Fig. 7.26 and Fig. 7.27 show the results of the simulations. As expected, the deformational behaviour due to flexural cracking was quite similar for the various simulations. However, the load at which plate-end shear led to failure differed significantly and ranged between 27.16 kN for $h = 20$ mm and 17.20 kN for $h = 80$ mm. Experimentally, maximum loads of 20.1 kN and 19.6 kN were attained by S-P14 and S-P14A, respectively. Compared to the average load of these tests the outcome of the simulations ranged between 137% to 87%.

When the crack patterns at failure were examined for the 20-50-80 mm cases, identical plate-end shear crack configurations were noticed. So, the fracture energy consumed in the shear crack caused the difference in maximum load. Because plate-end shear plays a dominant role in the failure behaviour of partially plated members, the finite element model had to be calibrated to obtain correct results. A crack band width of $h = 50$ mm was, therefore, chosen. It stands to reason that a crack band width of $h = 50$ mm leads to a correct outcome only if $\beta = 0.2$ and $e = 20 \times 20$ mm². Other values for β and e are investigated in the next sections.

Table 7.11 Influence of crack band width on maximum plate-end shear load

$\epsilon_u = \delta_u / h$ [-]	$g_t = G_t / h$ [N/mm ²]	F_{max} [kN]	F_{max} / F_{exp} [%]
0.00785	0.00600	27.16	137
0.00450	0.00343	23.06	116
0.00315 ¹⁾	0.00240	20.40	103
0.00243	0.00185	18.08	93
0.00198	0.00150	17.20	87

¹⁾ $G_t = 0.048$ N/mm¹ and $h = 20$ mm

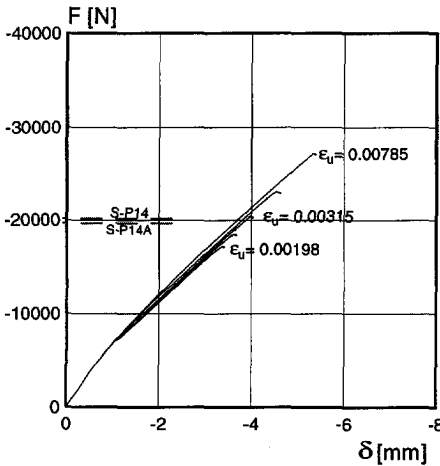


Fig. 7.26 Load-deflection responses of numerical simulations on SP14(A) with various crack band widths

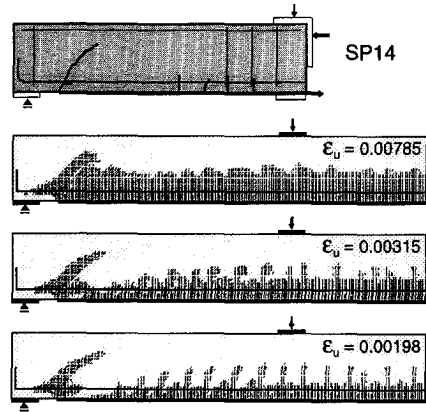


Fig. 7.27 Influence of ultimate smeared crack strain on plate-end shear cracking; reference is test S-P14(A)

The numerical simulation with $\epsilon_u = 0.00315$ is examined more in detail to analyse plate-end shear. Fig. 7.28 depicts the crack pattern development of four stages, namely, 9.35 kN, 16.45 kN, 20.27 kN and 20.26* kN (after maximum load). Actually, the simulated crack pattern development was identical as observed in the experiments. At first, with increased loading flexural cracks formed in the constant moment and shear span. Then, at a load in the order of magnitude of 15 kN, a plate-end crack initiated and gradually developed into a plate-end shear crack at maximum load (20.27 kN). Finally, after the maximum load was reached, the external load decreased and the plate-end shear crack tip grew further towards the loading point and towards the support. Localisation of the flexural cracks and plate-end shear crack are sketched on the right side in Fig. 7.28. These graphs show smeared crack strains larger than $2/9 \epsilon_u$. It clearly emerges that at the onset of the maximum load localisation in the plate-end shear crack had occurred.

As stated earlier, it was very difficult to proceed the numerical simulation beyond the maximum load in the snap-back branch. Particularly, the steps in the post-peak branch were accompanied by the initiation of numerous cracks at the tip of the plate-end crack. Hence, in most of the simulations divergence occurred.

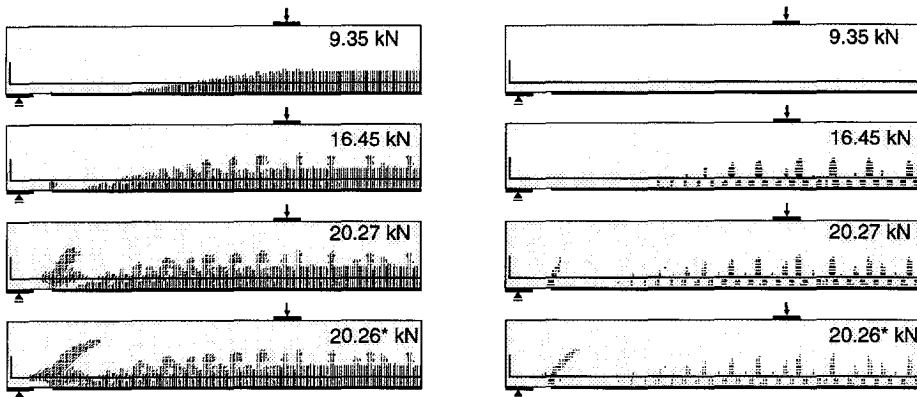


Fig. 7.28 Crack pattern development for partially plated beam for various stages; left - all cracks, right - cracks with smeared crack strain $> 2/9 \epsilon_u$

Influence of Shear Retention Factor

With a constant smeared crack strain of $\epsilon_u = 0.00315$, the shear retention factor was varied to investigate the influence of the percentage of elastic shear capacity that was retained after cracking. In addition to $\beta = 0.2$, simulations with $\beta = 0.1$, 0.05 and 0.01 were carried out. From the simulations, it emerged that much more iterations were needed for smaller values of β . Maximum loads were respectively 20.40 kN for $\beta = 0.2$, 19.25 kN for $\beta = 0.1$ and 19.12 kN for $\beta = 0.05$. For $\beta = 0.01$ convergence could not be reached after the first flexural cracks. Also, at low β hardly any shear cracking occurred until divergence stopped the simulation. Accordingly, a difference in maximum load was visible for the investigated shear retention factors.

It was decided to take $\beta = 0.2$. Then, the simulations performed well and showed good convergence as well as regular crack patterns. In addition, it must be noted that it was experimentally shown in §6.2.6 (aggregate interlock) that shear stresses between the crack faces significantly contributed to internal equilibrium after plate-end shear cracking. This may not be underestimated by a low β .

Influence of Mesh Size

Finally, the size of the finite element mesh was changed to investigate the influence on localisation of the plate-end shear crack. Three rectangular sizes were analysed, namely the mentioned 20×20 mm², and both 10×10 mm² and 40×40 mm². The volumic fracture energy and ultimate smeared crack strain were kept constant for the three different meshes. However, by changing the size of the mesh, the crack band width should also have been changed, but this was not done. Hence, for $e = 10$ mm the response will be too brittle, and for $e = 40$ mm too ductile.

Fig. 7.29 shows the result of the three simulations. Basically, the three crack patterns were identical, however, the width of the flexural and plate-end shear cracks differed. In all cases the plate-end shear crack went through about 1.5 elements. Maximum loads of 26.38 kN for $e = 40$ mm and 17.82 kN for $e = 10$ mm were calculated, indeed different with respect to 20.40 kN ($e = 20$ mm).

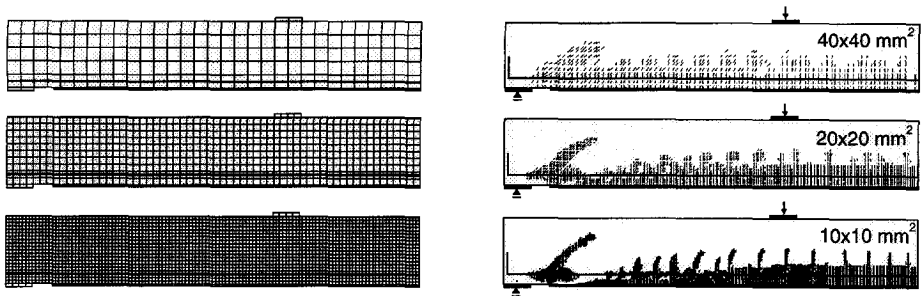


Fig. 7.29 Influence of mesh size on localisation of the plate-end shear crack

7.4.4 Stage 3: Simulations on Plate Separation Cracking

Smeared-Discrete Crack Model

This section describes the alteration of the initial finite element mesh with the purpose to simulate both plate-end shear and plate separation. The modification of the mesh is inevitable to enable plate separation. Simulations containing only continuum elements with smeared cracking revealed that plate separation at the level of the internal bars could not sufficiently be modelled. After the development of the plate-end shear crack, horizontal cracks, that is to say second cracks, were initiated in the integration points due to peeling at the plate end. However, localisation followed by plate separation could not clearly be simulated.

To simulate plate separation, *peeling interface elements* were added to the continuum mesh parallel to the internal bars at a depth of 20 mm. These distinct elements were provided with the discrete cracking material model. In addition, to allow the concrete cover to peel away without any restraints due to element locking, *plate end interface elements* were also generated. These interface elements were placed perpendicular to the aforementioned peeling elements.

Fig. 7.30 shows the configuration of the adapted mesh. For all the interface elements an element width of 90 mm was applied to model the effective width of the concrete at the level of the internal reinforcing bars. The developed so-called *smeared-discrete crack model* comprises continuum elements for smeared cracking to model flexural and shear cracks, and interface elements for discrete cracking to model plate separation.

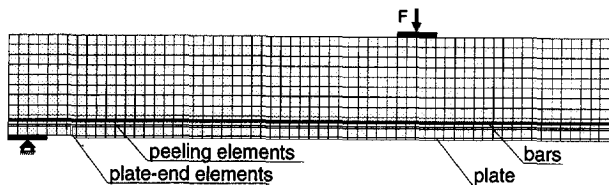


Fig. 7.30 Continuum finite element mesh with additional discrete elements at level of internal bars for the simulation of plate separation

For the *plate-end interface elements* brittle cracking (no softening) was adopted to enable the initiation of a plate end crack without crack stresses. The shear stiffness of a cracked interface element was assumed 0 N/mm^3 . For the *peeling interface elements* the bilinear tension softening model was adopted as depicted in Fig. 7.5. Furthermore, the influence of the shear stiffness after cracking was investigated. It emerged that a shear stiffness after cracking caused problematic shear locking of the interface elements, because shear stresses were still transferred through the plate separation crack. Further peeling was prevented. It was, therefore, also decided to apply no shear stiffness after cracking for the peeling interface elements.

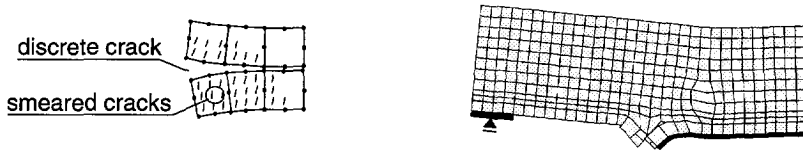


Fig. 7.31 Smeared-discrete crack concept; localisation for multi-directional cracking

Despite this, in simulations on plate separation, problems still occurred due to the initiation of horizontal second cracks in the continuum elements, see Fig. 7.31-right. Hence, as a consequence of the smeared-discrete crack approach, no multi-directional smeared cracks were allowed in the integration points of the continuum elements (option TD=90.0). Then, as depicted at Fig. 7.31-left, the plate separation crack could localise. Although no multi-directional cracking limited the initiation of second cracks in the integration points of elements at another location of the mesh, analyses showed that hardly any effect was noticeable on the outcome of the simulations when plate separation was simulated. So, only when plate separation was simulated (not shear), second cracks were not allowed in the integration points.

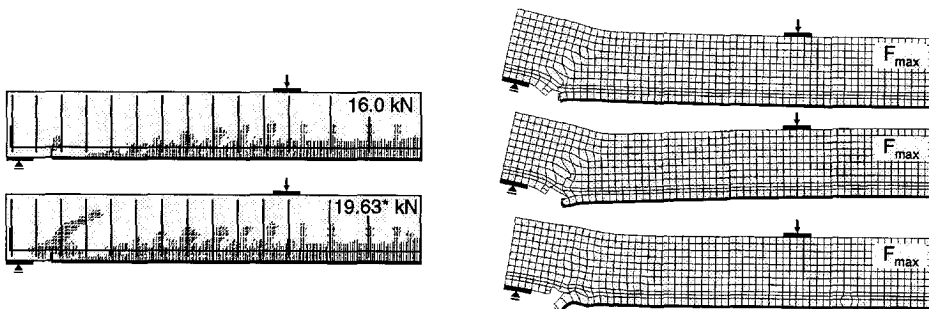


Fig. 7.32 Smeared-discrete crack model: simulation of flexural crack and plate-end shear crack; initiation and development of plate separation at the level of the internal reinforcement at the onset of maximum load (displacements enlarged)

Finally, with the developed smeared-discrete crack model a simulation with respect to plate separation was performed. The left side of Fig. 7.32 shows two stages of crack development, the right shows incremental displacements at the onset of the

maximum load. It clearly demonstrates the initiation of plate separation at the level of the internal reinforcement. Peeling started at the end of the plate, and grew along the level of the internal bars.

Influence of Tensile Strength on Plate-end Shear Load

Because the configuration of the initial mesh had been changed, the influence of both the adapted mesh and the tensile strength on plate-end shear was investigated. The modification of the initial mesh did not influence the initiation and development of the plate-end shear crack. Two simulations without shear reinforcement were performed in which the tensile strength of the concrete was 3.00 N/mm² and 2.5 N/mm², respectively, a variation of about 10% compared to 2.75 N/mm². The outcome of the simulations was 20.32 kN and 19.09 kN, 102.5% and 96.5% compared to the reference simulation in which the tensile strength was 2.75 N/mm². Hence, it was concluded that the tensile strength affected the maximum load, however, not so much as the tensile strength was varied (10%).

7.5 Conclusions

In this chapter a numerical model has been developed to simulate beams strengthened with an externally bonded steel plate. Calibration of the numerical model concerning the ultimate smeared crack strain was needed to obtain correct results. Furthermore, a smeared crack approach combined with discrete cracking was needed to enable the finite element model to simulate both plate-end shear and plate separation. Fig. 7.33 schematically overviews the adopted material models.

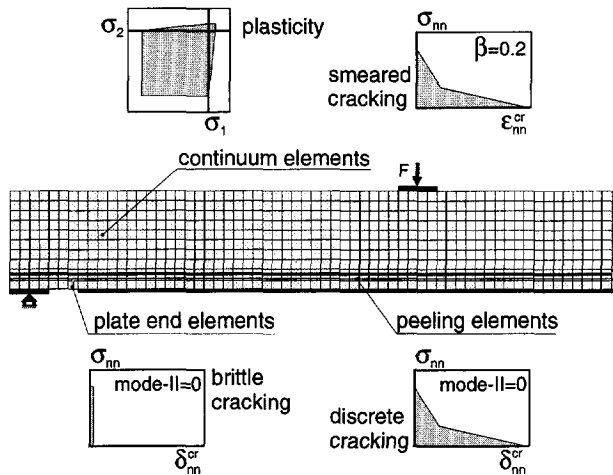


Fig. 7.33 Concrete material models adopted to the various element types

8. SIMULATIONS WITH SMEARED-DISCRETE CRACK MODEL

This Chapter discusses numerical simulations with the smeared-discrete crack model on the shear resistance of strengthened members and the anchorage capacity of the steel plates. §8.1 introduces the numerical simulations. §8.2 overviews the various types of failure that the smeared-discrete crack model could simulate. Then, §8.3 analyses the mechanism of plate-end shear and plate separation. Further, §8.4 discusses the influence of the unplated length and §8.5 analyses the influence of the external reinforcement ratio. The length of the shear span is dealt with in §8.6. Finally, conclusions in §8.7 end this chapter.

8.1 Introduction on Numerical Simulations

The previous chapter was fully dedicated to the development of the smeared-discrete crack model. This Chapter elaborates on numerical simulations with the developed model. Insight into the failure mechanisms of beam shear and plate anchorage and additional results contribute to the foundation of a design model. The smeared-discrete crack model is capable of simulating various types of failure. Thus, this gives the researcher the opportunity to analyse the influence of different parameters. Also, with the numerical model simulations outside the range of experiments could be performed. In particular, one must think of varying the length of the shear span, which was not investigated in the experiments.

8.2 Simulation of Types of Failure

8.2.1 General

This chapter analyses variables with the smeared-discrete crack model. The analyses comprise about fifty numerical simulations. Accordingly, before showing the influence of the variables, it is necessary to show that the results of the simulations were objectively obtained, or, that the type of failure was correctly simulated. This section shows that various failure mechanisms can be simulated with the smeared-discrete crack model by changing the geometry of the steel plate.

8.2.2 Flexure

With the smeared-discrete crack model the flexural capacity of the tested unplated beam (BM0) and an imaginary fully plated beam (BM2) were investigated. The internal reinforcement consisted of two 8 mm diameter bars and stirrups spaced 75 mm, BM2 was additionally fully provided with a plate $5 \times 100 \text{ mm}^2$. Fig. 8.1 shows

the results of both numerical analyses including the test results of BM0. Compared to the test, it emerged for BM0 that the maximum flexural capacity was simulated with sufficient accuracy. With regard to BM2, the external plate yielded before the yield stress of the internal bars was reached. A comparison of the flexural crack development between BM0 and BM2 showed that in the case of the unplated beam, the cracks developed much deeper into the concrete compression zone at maximum load. Hence, the height of the concrete compression zone was much smaller as could be expected on the basis of simple linear stress analyses.

The stiffness of the unplated member was significantly reduced after the occurrence of the first flexural cracks in the constant moment region (4.0 kN), whereas the stiffness of the plated member was maintained. This demonstrates that the external plate significantly contributed to the flexural stiffness, particularly after flexural cracking.

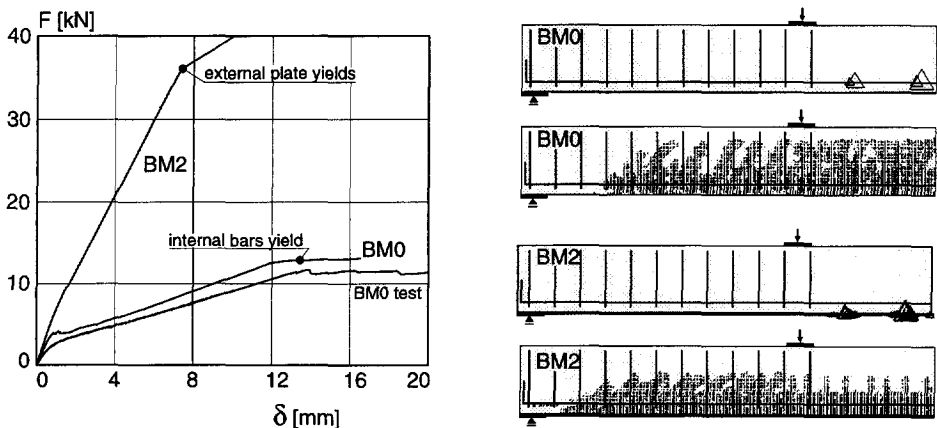


Fig. 8.1 Load-deflection diagram for BM0 (test and simulation) and BM2 (simulation); plasticity status and partially and fully open cracks (12.8 kN (BM0) and 36.0 kN (BM2))

8.2.3 Flexural Shear

To verify the flexural shear behaviour, a simulation was performed in which beam BM2 was not provided with stirrups, Fig. 8.2. It emerged that at a load of 33.6 kN flexural shear cracks formed in the shear span of the fully plated beam. This was clearly illustrated by the incremental displacements. Inclined deformations as a result of shear cracks were visible, however, the numerical model was not capable of indicating a distinct maximum load during the formation of these inclined cracks.

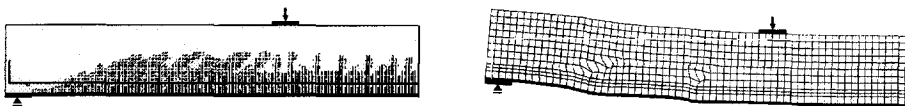


Fig. 8.2 Fully plated, no stirrups: partially and fully open cracks and incremental displacements at 33.6 kN; initiation of flexural shear cracks

8.2.4 Plate-End Shear

If a strengthened member was partially plated and stirrups were not present in the shear span, a shear crack at the end of the plate in the concrete governed failure. Fig. 8.3 depicts typical results of the simulation on test S-P14. It is clearly seen that at a load of about 10 kN, flexural cracks had developed in the shear span. Then, when the load was further increased, a plate-end crack initiated at a load of about 14 kN. This plate end crack had developed into a plate-end-shear crack at maximum load (20.6 kN). When the incremental displacements in the load steps after the maximum load are analysed, it is obvious that this shear crack dominated failure. This plate-end-shear crack was well simulated with the use of the smeared crack approach for concrete. Also, it emerged from the incremental displacements that at the onset of the maximum shear load the tip of a peeling crack at the level of the internal reinforcement was initiated. The initiation of this peeling crack during plate-end shear failure will further be analysed in this chapter.

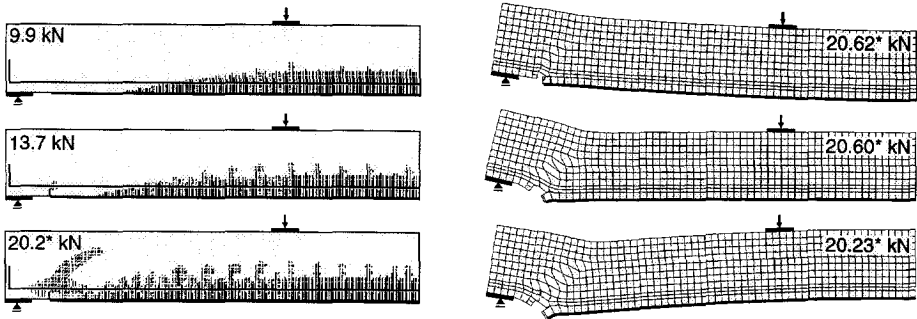


Fig. 8.3 L100, no stirrups: partially and fully open cracks at various loading stages and incremental displacements at maximum load; failure by plate-end shear

8.2.5 Plate Separation by Shear Peeling

If a strengthened member was partially plated, but the plate was stopped at the very short distance of 50 mm from the support, and stirrups were provided in the shear span, shear peeling governed failure. Fig. 8.4 shows the crack pattern and incremental displacements at maximum load. It was observed that a plate-end shear crack developed with increased load, but it was arrested by virtue of the internal stirrups. Accordingly, plate-end shear failure could not take place and the load was increased. Finally, plate separation at the level of the internal reinforcement led to failure. The reader is also referred to Fig. 7.32, there the unplated length is 100 mm.

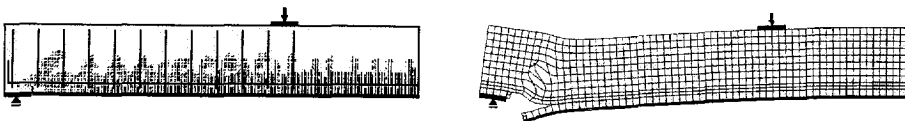


Fig. 8.4 L50, stirrups: partially and fully open cracks and incremental displacements at maximum load (27.3 kN); failure by shear peeling crack

Like the experiments, the numerical simulation showed that shear peeling was a very brittle type of failure: a severe snap-back was observed in the post-peak branch of the load-deflection diagram of the simulation.

8.2.6 Plate Separation by Shear Flexural Peeling

If the bonded-on plate strengthened only a small part of the shear span and the plate was stopped at a long distance from the support, a combined shear flexural peeling type of failure as defined by Oehlers [1992]⁸ was observed. Shear flexural peeling was independent from whether stirrups were applied or not. Fig. 8.5 depicts the incremental displacements at maximum load at which plate separation due to shear flexural peeling clearly emerged of a simulation with a 500 mm unplated length. Generally, for various unplated lengths the shear flexural peeling mechanism was correctly simulated, but the maximum peeling load was slightly underestimated.

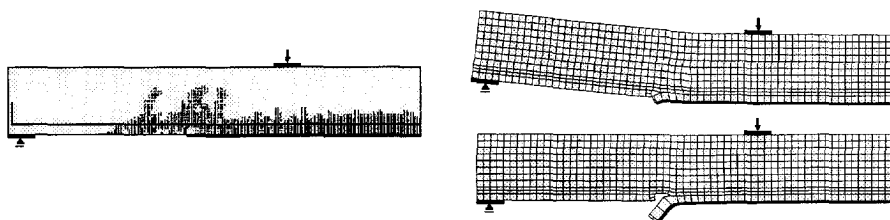


Fig. 8.5 L500, no stirrups; partially and fully open cracks at maximum load; incremental displacements at various loads; failure by shear flexural peeling crack

8.2.7 Conclusion

In the previous sections, various types of failure were simulated. With respect to these simulations, one must draw the conclusion that the smeared-discrete crack model is capable of numerically simulating various failure types of a member, externally strengthened with a bonded-on steel plate. Also, the model proved conclusively that the failure load could be satisfactorily predicted.

8.3 Mechanism of Plate-End Shear

8.3.1 Stresses in Strengthened Members before Cracking

Concrete Stresses

The principal stresses (uncracked) in a strengthened beam provide a good insight into the state of stress, and particularly, they show regions where cracks are likely to initiate. Also, when the principal stresses for structures strengthened in flexure by an externally bonded steel plate are visualised, one becomes aware of the alternative internal equilibrium system that is present in such a structural member. Fig. 8.6 displays the principal stresses of the unstrengthened beam BM0 and a partially strengthened member L200 with the steel plate stopped at a distance of 200 mm

before the support. The figure shows the maximum principal stress σ_1 , and the minimum principal stress σ_2 .

The principal stresses in BM0 are as expected. However, the principal stresses in the partially plated beam differ. In the constant moment region the minimum principal stresses clearly indicate the tensile zone and the compression zone. Conversely, in the shear span two compression systems are distinguished: firstly, an arch acts between the loading point and the support by virtue of the internal reinforcement. Secondly, an additional arch acts between the loading point and the end of the steel plate by virtue of the external reinforcement.

Accordingly, an additional equilibrium system is present in members strengthened with externally bonded plates. Due to this second equilibrium system, large tensile stresses act at the end of the steel plate as clearly emerges from both the minimum and maximum principal stresses as depicted in Fig. 8.6. These concrete tensile stresses are necessary to connect the "external" force system to the support to obtain equilibrium. Consequently, these zones of increased tensile stresses have a pronounced effect on cracking of partially plated members.

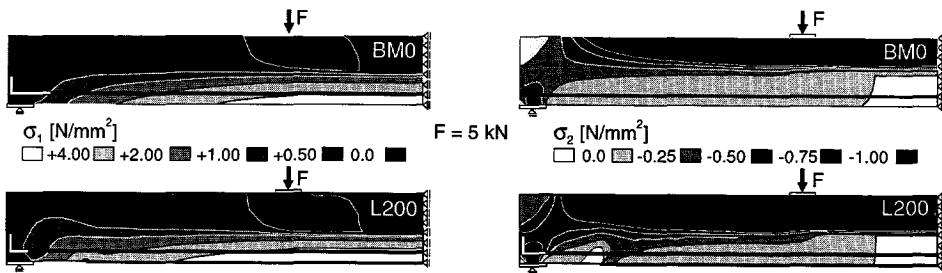


Fig. 8.6 Principal stresses in continuum finite element models; the unstrengthened beam BM0 and a beam with the bonded-on plate stopped 200 mm short of the support (σ_1 = maximum stress, σ_2 = minimum stress)

Reinforcement Stresses

The reinforcement stresses of both the internal bars and the bonded-on plate were calculated for a plate cross section of $5 \times 100 \text{ mm}^2$ and various unplated lengths. The reinforcement stresses were considered at an external load of 1 kN, before cracking. Fig. 8.7 and Fig. 8.8 show the tensile stresses for a fully plated beam L0 and three partially plated beams; L100, L200 and L300. The analyses demonstrated that in the constant moment region the magnitude of the reinforcement stresses was similar for all the cases. But, in the shear span at the vicinity of the support the reinforcement stresses differed considerably. This could only be explained by the discontinuity of the bonded-on plate. If the plate was bonded beyond the support (L0), the tensile stresses in both the bars and the plate decreased linearly into the direction of the support. However, if the plate was stopped before the support, an increase of the bar tensile stress was observed at the plate end. As a result of the interruption of the external plate, the internal bars had to transfer the additional force to the support. Hence, at the plate end, the stress in the internal bars increased.

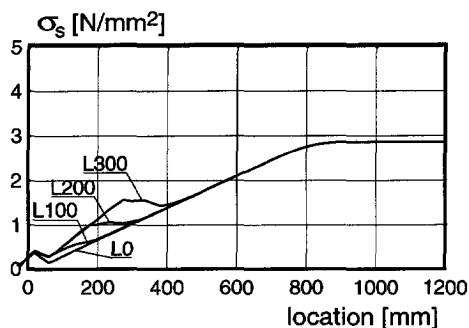


Fig. 8.7 Tensile stress in bars (100 mm²) in relation to unplated length

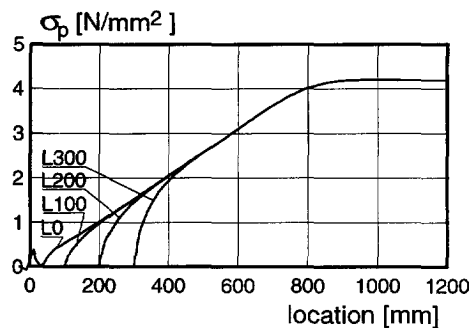


Fig. 8.8 Tensile stress in bonded-on plate (5x100 mm²) in relation to unplated length

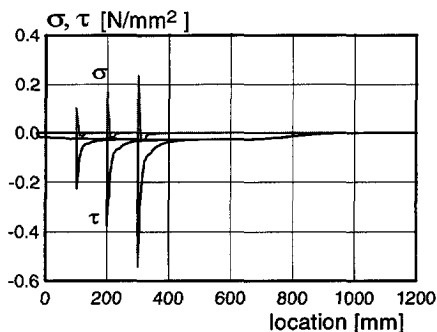


Fig. 8.9 Anchorage stresses at plate-end (5x100 mm²) in relation to unplated length

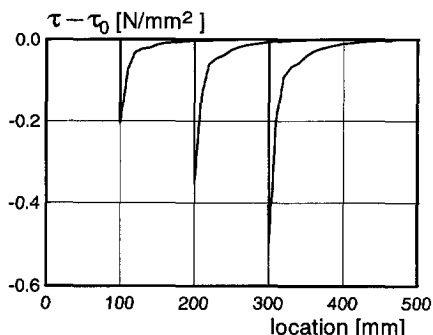


Fig. 8.10 Shear stress difference between partially and fully bonded plates

Anchorage Stresses at Plate-End

As a consequence of stopping the bonded-on plates at a distance from the support, peak anchorage stresses between the steel plate and the concrete were introduced. Fig. 8.9 shows normal and shear stresses in the epoxy layer.

In the case of a fully plated beam, normal stresses were not present between the plate and the concrete. In the shear span only shear stresses were present with an average magnitude of about $\tau_{avg} = 0.025 \text{ N/mm}^2$ ($F = 1 \text{ kN}$). In the case of a partially plated beam, if the plate was stopped before the support, normal and shear stresses were introduced at the plate-end to anchor the plate. Table 8.1 lists the peaks of these anchorage stresses. As a rule of thumb, the normal peak stress was about half the shear peak stress.

Fig. 8.10 shows the difference between the peak shear stress τ_{peak} and the average shear stress τ_{avg} calculated with the fully plated beam (L0). In Table 8.1, this difference is indicated by $\tau_{avg} - \tau_{peak}$. Logically, $\tau_{avg} - \tau_{peak}$ increases with increasing unplated length. When $\tau_{avg} - \tau_{peak}$ of the three partially plated beams are compared with the volumetric shear stresses $\tau_{avg,L}$ of a fully bonded plate (τ_{avg} over distance L), it must be concluded that the two are indeed equal. Hence, the magnitude $\tau_{avg} - \tau_{peak}$ is

equal to the shear stress $\tau_{avg,L}$ as if the plate was fully bonded. From Fig. 8.10 the anchorage length ℓ_a was also calculated. The simulations show that the anchorage lengths for the three cases were 165 mm despite the different unplated lengths. As Holzenkämpfer [1994]⁵ derived, the anchorage length is dependent on the thickness and material properties of the plate, which were the same for all three. A maximum anchorage length of 293 mm was calculated with Holzenkämpfer's Eq. 2.21 ($f_{clm,ax}=2.75 \text{ N/mm}^2$) and 308 mm with Pichler's Eq. 2.20 ($\tau_{pin}=9.1 \text{ N/mm}^2$)

Table 8.1 Normal- and shear stresses at plate end

	σ_{max} [N/mm ²]	τ_{max} [N/mm ²]	ℓ_a [mm]	$\tau_{avg}-\tau_{peak}$ [N]	$\tau_{avg,L}$ [N]
L000	0	0.025 ¹⁾	-	-	
L100	0.102	0.228	165	309	325
L200	0.167	0.378	165	563	575
L300	0.237	0.540	165	836	825

¹⁾ not maximum shear stress, but average shear stress

8.3.2 Stresses in Strengthened Members at Plate-End Shear

Reinforcement Stresses

A considerable alteration of the tensile stress in the reinforcement took place after plate end cracking. It caused a significant increase of the tensile stresses. At various loading stages, Fig. 8.11 depicts the plate stresses and Fig. 8.12 depicts the tensile stresses in the internal bars. See also Fig. 8.3 for the accompanying crack patterns at certain loading stages.

As a result of the incremented external load, the tensile stress in the reinforcement increased. Due to flexural cracking the distribution of stresses is not linear. Up to plate-end cracking (<13 kN) the tensile stresses in the bars at the plate-end hardly changed. However, a considerable increase of the tensile stress in the internal bars at the plate end was observed after plate-end cracking. With increased loading and development of the plate-end shear crack, this tensile stress rose. Even at maximum load the tensile stress at the plate end was higher than that in the constant moment region. This observation is highly significant. Concerning the considerable increase of this tensile stress at the plate end, one must always be certain that the amount of longitudinal reinforcement at the support is sufficient to avoid yielding of the bars. Particularly in practice, this could hold true for floors in buildings, where the amount of longitudinal bar reinforcement might be reduced at the surrounding support of the wall.

Fig. 8.11 shows the plate stresses. As for the internal bars, the plate stress distribution is neither linear at higher loads due to flexural cracking. The figure illustrates what was also found in the experiments. At the onset of the maximum load, after plate-end shear cracking, the plate starts to separate from the concrete beam. As a result, the plate curves at the plate-end. This was also registered during the experiments. In the simulation at 20.2* kN, the plate started to separate and negative curvature of the plate-end was calculated.

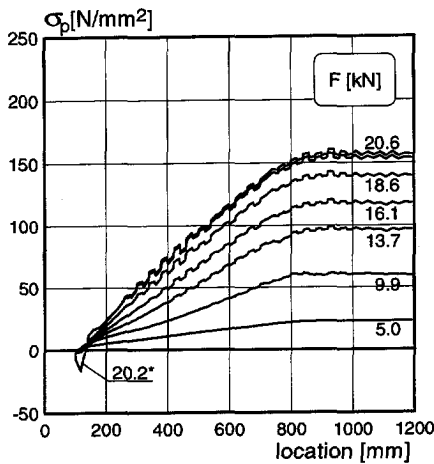


Fig. 8.11 Plate stresses

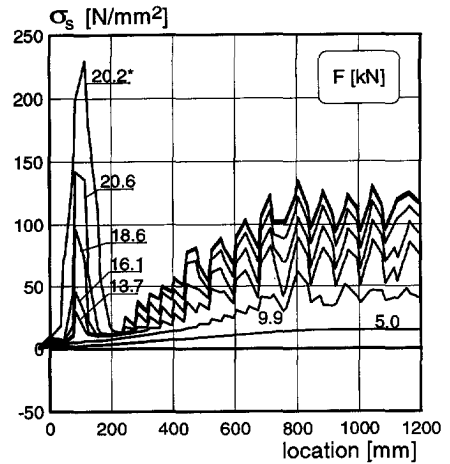


Fig. 8.12 Bar reinforcement stresses

Bond Stresses Between Reinforcement and Concrete

During initiation of the plate-end crack, the cracked concrete was not able to transfer the concrete tensile stresses which were imposed at the plate end. Consequently, it was shown in the last section that the stress in the reinforcement bridging the plate-end crack increased. As a result, the bond stresses between the reinforcement and concrete also increased. Fig. 8.13 shows the bond stresses at the plate end as a function of the external load (crack initiated at 95 mm). It is seen that after initiation of the plate-end crack up to failure, the bond stresses were constantly increased due to the growth of the plate-end shear crack. As a result of the high bond stresses, the shear stress was increased in a horizontal cross section in the concrete in the zone parallel to the internal reinforcement.

Shear Stress Distribution in Vertical Cross Section

Due to plate end cracking, also the shear stress in the vertical cross section altered. Fig. 8.14 shows the shear stress in a vertical cross section beyond the plate end at a location of 90 mm from the support (the plate end crack was located at 95 mm). Before the plate end crack was initiated, the shear stress distribution was parabolic. However, after the initiation of the plate end crack, the shear stress distribution changed. Due to the development of the plate-end shear crack, the peak of the shear stress distribution shifts more and more vertically to the concrete compression zone because a concrete arch clearly developed between the loading point and the support. As a result, the shear stress distribution in the vertical cross section changed significantly as the various stages of Fig. 8.14 show.

Magnification of Shear Stress beyond Plate End Crack

The previous sections showed that due to the plate end crack the shear stress distribution in a section beyond the plate end changed considerably. As a result, large tensile stresses were imposed which initiated the development from the plate

end crack into the plate-end shear crack. The important point is, therefore, that the plate end crack ultimately caused failure. In other words, plate end cracking was the precondition for the development of plate-end shear. Actually, this is also the case for flexural cracking and flexural shear. In analogy, the flexural crack is the precondition for flexural shear. As shown in Kim & White [1991]¹⁴, at the tip of a flexural crack just above the internal reinforcement the magnification of the shear stress may amount to more than a factor 3 due to increased bond stresses and arch action. Hence, from these observations may be concluded that the failure mechanism of plate-end shear is analogous to flexural shear.

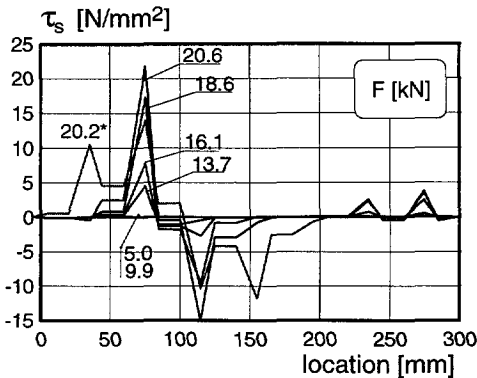


Fig. 8.13 Bond stresses between internal bars and concrete at plate end

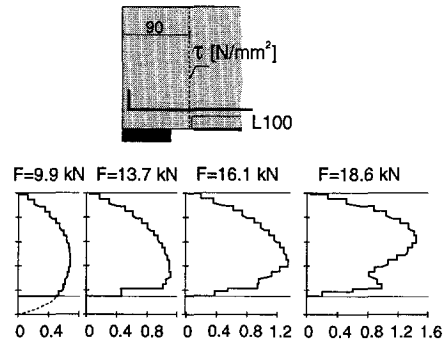


Fig. 8.14 Alteration of shear stress in vertical cross section beyond plate end crack

8.3.3 Conclusions

When structural members are strengthened in flexure with partially bonded steel plates, an additional arch acts between the loading point and the support. By virtue of this arch anchorage stresses are developed at the plate end and peak stresses are imposed in the concrete beyond the plate end. Due to these peak stresses a plate end crack is initiated. Plate end cracking substantially magnifies the shear stress beyond the plate end crack. As a result, a plate-end shear crack develops which leads ultimately to plate-end shear, a mechanism identically to flexural shear.

8.4 Influence of Unplated Length

8.4.1 Contents of Simulation Series

In this section, the influence of the unplated length of the bonded-on plate on the failure behaviour is investigated. A fully plated beam fails either by flexure (with stirrups) or by flexural shear (without stirrups). However, it is not known what the effect of an increased unplated length on the type of failure is. Also, applying internal stirrups influences the failure mechanism. Hence, two series of simulations were carried out on beams strengthened with a plate cross section of $5 \times 100 \text{ mm}^2$ and a

shear span of 800 mm. Table 8.II overviews the series of the simulations, and lists the results of the outcome. Although unplated lengths of half or more of the length of the shear span (400 and 500 mm) are not common for practical applications, it is interesting to investigate the effect of these large unplated lengths on failure.

Table 8.II Overview of simulations on unplated length

L [mm]	without stirrups		stirrups	
	F_{max} [kN]	failure type	F_{max} [kN]	failure type
0	33.6	flexural shear	-	flexure
50	23.76	plate-end shear	27.41	shear peeling
100	20.62	plate-end shear	22.64	shear peeling
200	15.36	plate-end shear	16.85	shear peeling
300	13.03	shear flex peeling	13.34	shear flex peeling
400	9.52-10.70	shear flex peeling	11.03	shear flex peeling
500	7.89-8.97	shear flex peeling	7.87	shear flex peeling

8.4.2 Simulations on Unplated Length

The outcome of the range of the performed simulations was surprising. It emerged that the influence of stirrups was evident, as long as plate-end shear governed failure. If stirrups were not provided, plate-end shear led to failure. If stirrups were provided, plate separation due to plate-end shear deformations led to failure. However, from a particular unplated length on ($L > 300$ mm), plate-end shear did not govern failure anymore.

Fig. 8.15 depicts crack patterns of the series of simulations without stirrups. It shows the results of the range of simulations from $L=50$ mm to $L=500$ mm. When the large crack at the plate end is observed more in detail for the various simulations, one sees a clear difference. In the range of 50-300 mm, the plate-end shear crack was a diagonal one and, thus, implied shear failure. However, from unplated lengths from 300 mm up, the plate-end crack developed more vertically, thus implying this crack was a flexural crack. Then, plate separation, due to shear flexural peeling, did occur resulting from curvature of the strengthened member. This curvature was primarily caused by the bending moment distribution, which increases between the support and the loading point, and amplified by cracking. So, at larger unplated lengths, plate separation resulted not from plate-end shear, but from increased curvature of the beam, whether stirrups were provided or not. Increased curvature was defined as the basic mechanism for flexural peeling by Oehlers [1990, 1992]⁹. The fact that for shear flexural peeling the maximum failure load was much lower than the flexural shear capacity or plate-end shear capacity of the partially plated member is likely to be explained with this mechanism.

With respect to the aforementioned discussion concerning Fig. 8.15, a conclusion of great importance was drawn. Namely, it emerged that deformations mainly dominated failure, either by shear deformations as a result of plate-end shear or by beam curvature as a result of the bending moment and amplified by flexural cracking. With respect to these deformations, one must bear in mind that by bonding a plate externally, a stiff member is added on the beam.

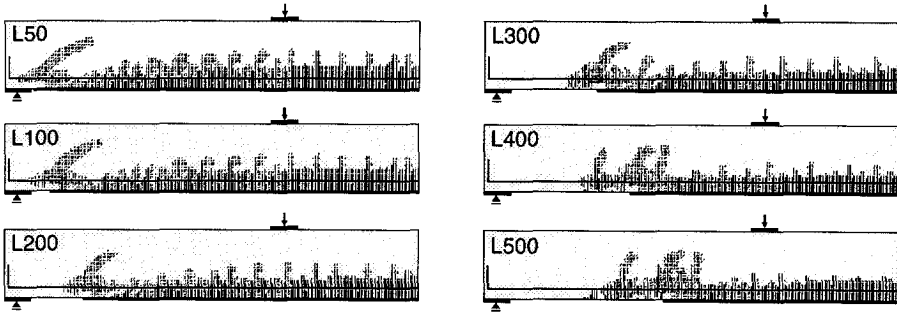


Fig. 8.15 Influence of unplated length of partially plated beam without stirrups

8.4.3 Maximum Loads

Fig. 8.16 represents the maximum calculated failure loads listed in Table 8.II. It emerges clearly that if the unplated length L increases, the calculated maximum load decreases. This was explained by the fact that when the unplated length increased, the plate-end crack initiated at lower external loads. The figure also shows that up to unplated lengths of 300 mm the maximum loads of plate separation were higher than those of plate-end shear. This is logical, because plate separation is governed by plate-end shear deformations. Hence, only after the internal stirrups were activated by deformations the plate-end shear crack was arrested, and consequently, at a higher load the bonded-on plate separated.

If only a small part of the shear span was plated (L400-L500), the maximum load was less than the flexural capacity or flexural shear capacity of an unstrengthened beam due to shear flexural peeling. Then, the beam was not strengthened but weakened. Then, it would be better not to strengthen the concrete beam. It also followed from the numerical study that whether stirrups were provided or not, failure was always by shear flexural peeling.

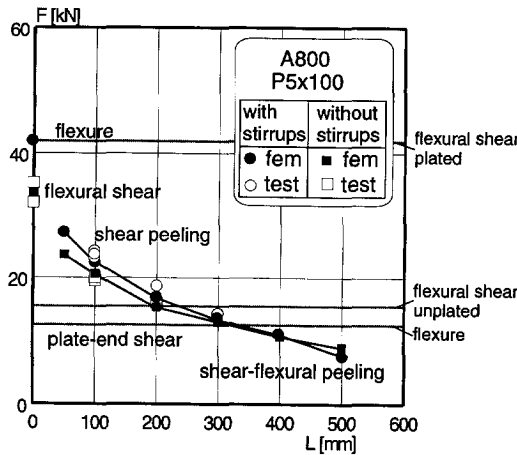


Fig. 8.16 Results of simulations on the influence of the unplated length

8.4.4 Conclusions

The main conclusion from the case study on the unplated length is that this variable had a significant influence on the failure behaviour and failure load of the partially strengthened member. Failure was dependent on the unplated length and stirrup provision, and was by plate-end shear or plate separation.

8.5 Influence of External Reinforcement Ratio

8.5.1 Contents of Simulation Series

In this section, the influence of the amount of external reinforcement on the failure behaviour is investigated. Only a few simulations are of interest, because experimentally this variable was thoroughly investigated in series S-P. Here, the outcome of the simulations on partially plated beams with their plates bonded at a very short distance of 50 mm from the support are of interest. Three plate geometries of 3×60, 4×80 and 5×100 were analysed. Also, beams with an unplated length of 100 mm strengthened with these plate geometries were simulated to verify the correctness of the outcome of the simulations, because the model was initially calibrated on a 5×100 mm² plate cross section. Table 8.III overviews the simulations.

Table 8.III Overview of simulations on unplated length

P [mm ²]	L50		L100	
	F _{max} [kN]	failure type	F _{max} [kN]	failure type
P3×60	24.1	bar/plate yield	21.55	plate-end shear ¹⁾
P4×80	24.52	plate-end shear	20.93	plate-end shear
P5×100	23.76	plate-end shear	20.62	plate-end shear
¹⁾ yielding of plate at 17 kN				

8.5.2 Simulations on External Reinforcement Ratio

The outcome of the simulations on the amount of external reinforcement was as expected. Simulations with the model comprising a 100 mm unplated length were satisfactory simulated compared to the results of the experiments. As far as the L50 beam with the 3×60 mm² plate was concerned, instead of brittle plate-end shear a ductile type of failure by yielding of the internal bars was observed. Thus, when the amount of external reinforcement was reduced to 3×60 mm², plate-end shear was overruled by the flexural capacity of the strengthened beam. Although a crack at the plate end was initiated, yielding of both the external plate and the internal bars prevented the development of this plate-end crack into a plate-end shear crack. In the case of the 3×60 mm² plate of the L100 beam, only the external plate yielded, so that plate-end shear still dominated failure. Accordingly, the total amount of reinforcement of the beams with a 4×80 mm² plate was too large to obtain yielding of the reinforcement and, thus, plate-end shear dominated failure.

8.5.3 Maximum Loads

Fig. 8.17 shows the results on the variation of the external reinforcement ratio. The experimental results are also included in the graph. The maximum loads of the partially plated beams with the plate bonded 50 mm short of the support were considerably higher than the L100 and L200 loads. Bonding the plate closer to the support had, therefore, a positive effect on the magnitude of the bearing capacity. For the L50 loads, the difference between the flexural shear and plate-end shear loads became smaller, however, a clear discrepancy still remained at higher reinforcement ratios.

Also, the numerically calculated results show the same tendency as the experimental ones. The plate-end shear load decreases a little with enlargement of the amount of external reinforcement. This can be explained by the fact that a larger amount of external reinforcement led to a larger discontinuity between the plated and unplated section. Also, the increase of the tensile stress in the internal bars at the plate end was larger compared to smaller external reinforcement ratios. Accordingly, as explained in the section on mechanism of plate-end shear, due to the increased tensile stress in the bars, the shear stress at the plate end was magnified and, thus, leading to earlier inclined shear cracking.

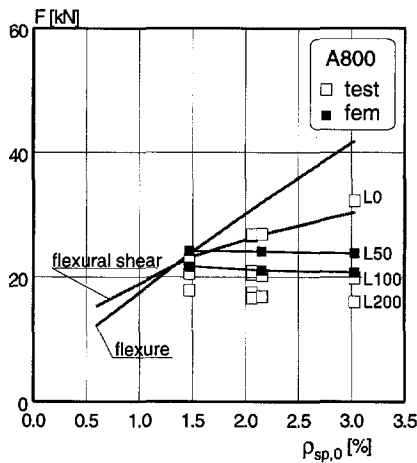


Fig. 8.17 Results of simulations on the influence of the external reinforcement ratio

8.5.4 Conclusions

The main conclusion from the case study on the external reinforcement ratio is that this variable hardly influenced the magnitude of the plate-end shear load. Nevertheless, it did influence the type of failure, because at certain reinforcement ratios plate-end shear might not occur as a result of the flexural capacity of the strengthened member. Then, yielding of the reinforcement governed the type of failure. With respect to this, chapter 11 elaborates on the interaction between shear and flexure as influenced by this ratio.

8.6 Influence of Shear Span Length

8.6.1 Contents of Simulation Series

The last case study with the smeared-discrete crack model studies the influence of the length of the shear span on the failure behaviour. As known from the literature, the shear span-to-depth ratio has a major effect on the shear load. The question is whether this also holds true for plate-end shear. Shear span-to-depth ratios up to 6 were investigated, thus implying shear span lengths from 100 up to 1200 mm. It was simply varied by changing the position of the external load. Accordingly, the length of the constant moment span was varied during the various simulations. Even so, this did not influence the failure behaviour. Beams with unplated length of 50 mm, 100 mm and 200 mm were analysed in which plate-end shear played a dominant role. Table 8.IV overviews the series of simulations and lists the outcome.

Table 8.IV Overview of simulations on length of the shear span

A [mm]	L50	L100	L200
	F_{\max} [kN]	F_{\max} [kN]	F_{\max} [kN]
100	36.85 ²⁾	41.44 ³⁾	^{1) 3)}
200	25.78	22.73	45 ^{2) 3)}
300	24.52	20.56	26.46 ³⁾
400	23.56	20.37	15.18
500	23.60	20.48	15.07
600	23.68	20.55	15.14
800	23.76	20.62	15.36
1000	23.79	20.50	15.10
1200	24.02	20.54	15.16

¹⁾ not calculated ²⁾ calculated/estimated ³⁾ failure not by plate-end shear

8.6.2 Simulations on Shear Span Length

Fig. 8.18 depicts the crack patterns of the simulations by the influence of the length of the shear span, in the case of an unplated length of 100 mm. Generally, it is seen that the plate-end shear crack is distinctly present. Failure was as expected by plate-end shear, however, not in the simulations marked with ³⁾ in Table 8.IV. When the pattern of the flexural cracks in the case of shear span length of $a > L + d$ (here $a > 270$ mm) is observed, it is seen that by increasing shear span the cracks developed deeper into the concrete compression zone, because the bending moment increased. But, with increasing length of the shear span it is also observed that the configuration of the plate-end shear crack remained identical. Accordingly, the length of the shear span did not influence plate-end shear and, consequently, it also did not influence the maximum plate-end shear load, see Table 8.IV.

In the case of short shear spans ($a < L + d$), the plate-end shear crack also developed but plate-end shear failure did not occur. After the development of this crack, the external load could be increased by virtue of the strut that acted between the loading point and the support. It was not cut by the plate-end shear crack. This is

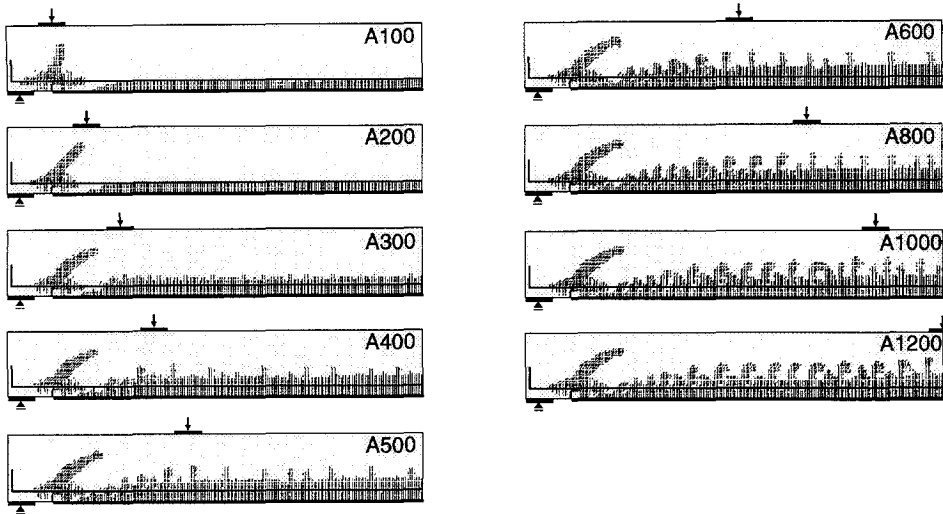


Fig. 8.18 Overview of crack patterns of simulations on the influence of the shear span; plate cross section $5 \times 100 \text{ mm}^2$ and unplated length of 100 mm

visualised in Fig. 8.19 for a shear span length of 300 mm and an unplated length of 200 mm. As a result of the direct strut, the maximum load could increase to 26.46 kN instead of 15.1-15.3 kN due to plate-end shear. When the plate stopped at 50 mm distance from the support, as depicted for the L50 case in Fig. 8.19, the strut between the loading point and the support was cut by the plate-end shear crack. Hence, plate-end shear governed the maximum load of 24.52 kN. Notice that this load is less than when the plate was stopped 200 mm short of the support. Accordingly, in the case of short deep beams, one must be aware of the fact that a possible plate-end shear crack cuts the direct transfer of the shear load to the support. Also, this holds true when a life load, for example, a driving vehicle approaches the vicinity of the support. Then, the strengthening of the structure needs additional analyses concerning shear (web shear or shear compression). In some cases, it might even be necessary to apply additional shear reinforcement (externally bonded plates or internal bolts) in order to increase the shear resistance. In practical situations with distributed loads, the assumed shear span-to-depth ratio commonly ranges between 3.0 up to 6.0. Then, the condition $a > L + d$ is fulfilled.

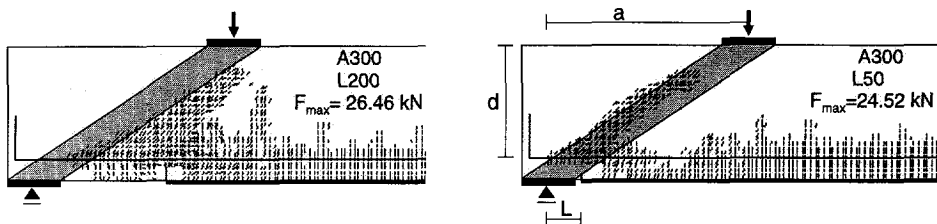


Fig. 8.19 Direct concrete strut between loading point and support (L200); if plate is bonded at a short distance from the support, the strut is cut by plate-end shear crack (L50)

8.6.3 Maximum Loads

The loads of Table 8.IV are graphically represented in Fig. 8.20. As remarked in the previous section, the influence of the length of the shear span is not noticeable for lengths of $a > L + d$. For all the three cases, the lines connecting the simulated loads are nearly horizontal and parallel to each other. Only for short, deep beams the maximum load was significantly increased. From this figure, it is concluded that the length of the shear span does not influence the plate-end shear load.

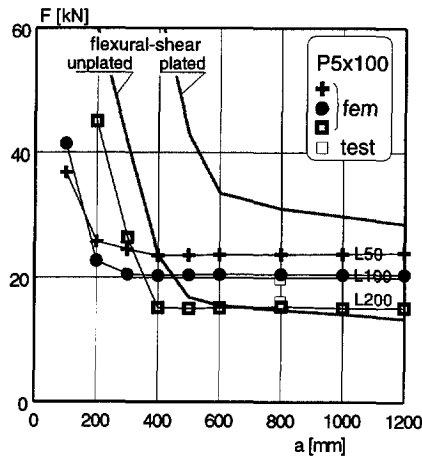


Fig. 8.20 Results of simulations on the influence of the shear span length

8.6.4 Conclusions

The main conclusion from the case study on the length of the shear span is that this variable did not influence the plate-end shear load. This held true for the majority of practical applications in which the length of the shear span fulfils the following condition $a > L + d$. The plate-end shear crack configuration was identical for various cases of the shear span length, and the maximum load remained constant. On the contrary, for short deep beams the maximum load could be increased after the development of the plate-end shear crack. For these cases, the web shear mechanism should be investigated separately.

8.7 Conclusions

In this chapter numerical simulations with the smeared-discrete crack model were carried out. Plate-end shear dominated failure. The mechanism of plate-end shear is identical to the classical flexural shear mechanism. If stirrups were provided, plate separation by shear peeling occurred due to shear deformations. The unplated length mainly influenced the plate-end shear load. The external reinforcement ratio and the shear span length for $a > L + d$ did not influence plate-end shear.

9. PLATE-END SHEAR MODEL

Chapter 9 interprets the results of the experiments and numerical simulations to develop a model for plate-end shear. At first, §9.1 introduces this chapter on the plate-end shear model. Then, §9.2 summarises the experimental and numerical studies on the influence of the unplated length, the external reinforcement ratio and the length of the shear span. Also, it quantifies the influence of these variables. In addition, §9.3 proposes a model for plate-end shear based on a fictitious shear span. A comparison in §9.4 with results from literature on both beam shear and plate separation shows the accuracy of the plate-end shear model. After a final evaluation, §9.5 concludes this chapter.

9.1 Introduction on the Plate-End Shear Model

The experimental and numerical studies showed that plate-end shear plays a dominant role in the failure behaviour of members partially strengthened with steel plates, for beam shear as well as for plate separation. The importance of plate-end shear has been unnoticed in the literature and, therefore, a design method is not available. Accordingly, it is necessary to develop an analytical model to enable one to design for plate-end shear.

In the numerical study in chapter 8 it was proved that the basic mechanism of plate-end shear was identical to the mechanism of flexural shear as described by Kim & White [1991]¹⁴. Despite this agreement, the analytical expressions for flexural shear have to be modified to obtain correct results as far as the plate-end shear load is concerned. In this chapter the plate-end shear model proposed will be based on the critical crack section analyses of Kim & White. By analogy between this critical crack section for conventionally reinforced beams and the unplated length for partially plated members, a fictitious shear span is introduced. By using the fictitious shear span in combination with the CEB-FIP MC90 expression for flexural shear, the plate-end shear load is correctly predicted. At the same time, the plate-end shear model may be used for plate separation by concrete cover rip-off for steel and fibres.

9.2 Summarising: Quantification of Variables

In chapters 4 to 6, the experiments were elaborately discussed, whereas chapter 7 and 8 dealt with the numerical simulations. For an analytical model which is capable of predicting maximum plate-end shear loads, the results concerning failure are of particular interest. When the experimentally determined and numerically simulated

maximum loads are graphically represented, the following main conclusions with respect to the variables can be drawn:

- The unplated length L governs the magnitude of the maximum plate-end shear or plate separation load, see Fig. 9.1;
- The shear span a does not influence the maximum shear load if $a > L+d$, see Fig. 9.2. Most practical applications for uniformly distributed loads satisfy this condition, exceptions are moving concentrated loads and short, deep beams;
- The amount of plate reinforcement ρ_p has little effect on the maximum plate-end shear load in comparison with classical flexural shear ($L0$), see Fig. 9.3.

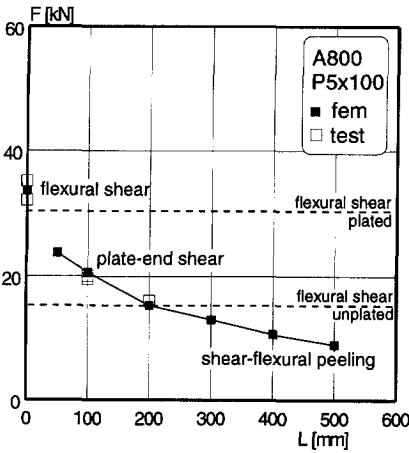


Fig. 9.1 Influence of unplated length L on beam shear and plate separation

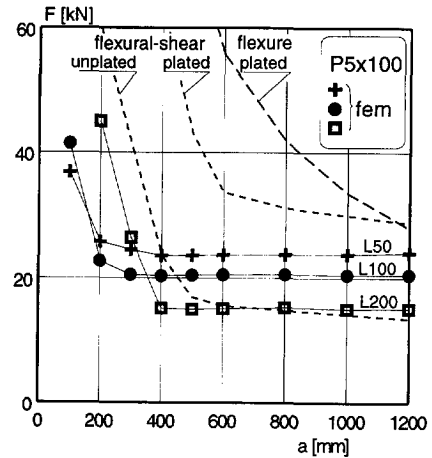


Fig. 9.2 Influence of shear span a on shear capacity as a function of L

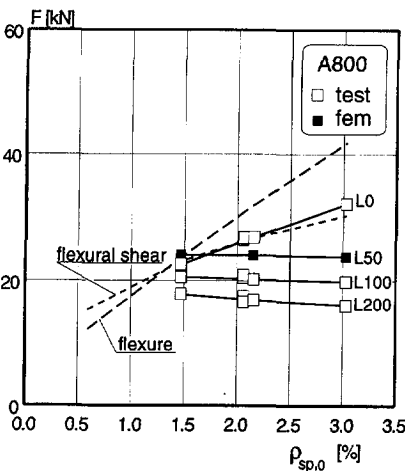


Fig. 9.3 Influence of reinforcement perc. $\rho_{sp,0}$ on shear capacity as a function of L

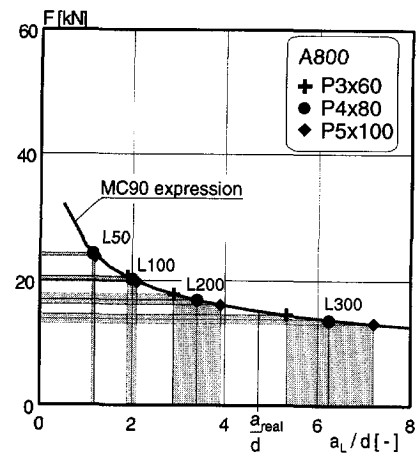


Fig. 9.4 Fictitious a_l / d_s according to tests and analysis based on MC90

With respect to these conclusions regarding the investigated variables, it is conclusively proven that the most important influencing variable is the unplated length. The unplated length L dominates the plate-end shear load.

The model for plate-end shear that will be derived consists of a fictitious shear span and the CEB-FIP MC90 expression on flexural shear. For the derivation of the fictitious shear span only the influence of the unplated length L is taken into account. If this expression is assumed to be applicable for $a > L + d$, the influence of the real shear span a may be omitted. The influence of the amount of plate reinforcement ρ_p is neglected. In the plate-end shear expression the unplated length, the amount of internal reinforcement, the effective depth of the beam with regard to the bars, and the concrete quality will be considered.

9.3 Derivation of Plate-End Shear Model

9.3.1 Fictitious Shear Span

The plate-end crack causes a drastical change of the internal stress distribution as elaborated in Chapter 8. The numerical simulations showed that as a result of the plate-end crack the tensile stress in the internal bars in the vicinity of the crack increased significantly. Consequently, large bond stresses between the bars and the concrete developed, and as a result alteration of the principal stresses caused the formation of diagonal cracks, that is to say, shear cracks.

The development of the plate end crack into a plate-end shear crack also influenced the load transfer. Namely, the plate-end shear crack prevented the partially plated beam-end to take full advantage of arch action since the crack cut through the compressive-force path, see Fig 8.19. Kotsovos [1984, 1986]¹⁴ showed that this compressive force path is directly present between the shear load and the support. Thus, during growth of the plate-end crack into the plate-end shear crack, this compressive force path is gradually cut through and, therefore, in partially plated beams arch action might not be fully taken into account. Only the contribution of beam action activated by the fully anchored internal bars may be accounted for.

The literature survey showed that, in comparison with Rafla's expression, the CEB-FIP MC90 expression on flexural shear insufficiently takes full arch action into account (§3.3). As arch action may neither be fully accounted for in partially plated beams, the MC90 expression on flexural shear is of particular interest for this study.

Fig. 9.4 shows a graphical representation of the CEB-FIP MC90 expression on flexural shear for an *unstrengthened* member as a function of the shear span-to-depth ratio. When the maximum plate-end shear load plotted on the vertical axis is taken as the input into this graph, a fictitious shear span-to-depth ratio can be defined on the horizontal axis by using the flexural shear line. So, despite the fact that a real shear span-to-depth ratio is present, an a_L/d_s is fictitiously present (definitions see Fig. 9.7). The model derived will work in the reverse direction: then a_L/d_s is calculated and is subsequently used as an input for the MC90 flexural shear expression. Hence, it predicts the mean maximum plate-end shear load.

Accordingly, because the effective depth d_s of the unplated part is considered, which is a constant, a fictitious shear span a_L can be deduced from a_L/d_s . Table 9.1 lists this fictitious shear span for the various unplated lengths and various cross-sections of the external plate. From this table it follows that the fictitious shear span a_L increases considerably with increasing unplated length L . At the same time, the fictitious shear span also increases with increasing cross sectional area of the steel plate. However, as earlier stated, this influence is neglected in the derivation of the analytical formulation for the fictitious shear span. It is actually assumed that this parameter is of little influence on the outcome of the maximum load if the unplated length is already accounted for.

For an unplated length of 50 mm the fictitious shear span equalled approximately 200 mm. Hence, this indicates that when a RC beam with a shear span of 800 mm without web reinforcement is partially strengthened with an unplated length of 50 mm, a fictitious external load is located at about 200 mm from the support. In analogy, then the plate-end shear load equals the flexural shear load of a conventionally reinforced beam with a real shear span of 200 mm. Notice that for an unplated length of 300 mm the fictitious shear span calculated is about 1000 mm, which is larger than the real shear span of 800 mm. Thus, the plate-end shear load is less than the unplated flexural shear load.

Table 9.1 Fictitious shear span a_L deduced from maximum plate-end shear load and MC90

unplated length	L50		L100		L200		L300	
	a_L/d_s [-]	a_L [mm]	a_L/d_s [-]	a_L [mm]	a_L/d_s [-]	a_L [mm]	a_L/d_s [-]	a_L [mm]
P3x60	1.1	187	1.9	325	2.9	495	5.3	901
P4x80	1.15	195	2.0	340	3.4	580	6.2	1054
P5x100	1.2	205	2.1	355	3.9	665	7.2	1225

9.3.2 Modelling Analogy with Critical Crack Section

General

By introducing the fictitious shear span, an analogy was found with flexural shear described by Kim & White [1991]¹⁴. There, an expression was developed for conventionally reinforced members to predict the location of the critical flexural crack which develops into a shear crack when the flexural shear resistance is reached. Variables in the study were those mainly used in shear studies, namely ρ , a and d . Based on both equilibrium considerations and experimental observations, a theoretical formulation was derived. To provide information on this interesting study, the main considerations of Kim & White [1991]¹⁴ are cited in the following section.

Reinforced Concrete Beam

In a homogeneous beam, the average distribution of the shear stress τ_{avg} over the surface in a horizontal cross section at the level of the internal bars is constant. The distribution of the shear stress τ in a vertical cross section is parabolic and is:

$$\tau = \frac{VS}{bl} \quad (9.1)$$

Fig. 9.5 shows a reinforced concrete beam with a flexural crack at the critical shear crack distance a_c . Equilibrium of an element $pp'm'n'$ is considered, with the reinforcement tension force T acting in the flexural crack. The average shear stress τ acting on the horizontal plane pp' is:

$$\tau = \frac{T}{ba_c} \quad (9.2)$$

However, after the formation of flexural cracks, the shear stresses do not remain constant but change considerably, see Fig. 9.5.(c) and (d). Formulation (9.2) needs careful consideration because of the discontinuities caused by cracking and the complexities in stress distribution caused by the composite action of steel and concrete. More specific, these discontinuities are caused by the effect of bond between the concrete and the bar and the effect of the development of arch action.

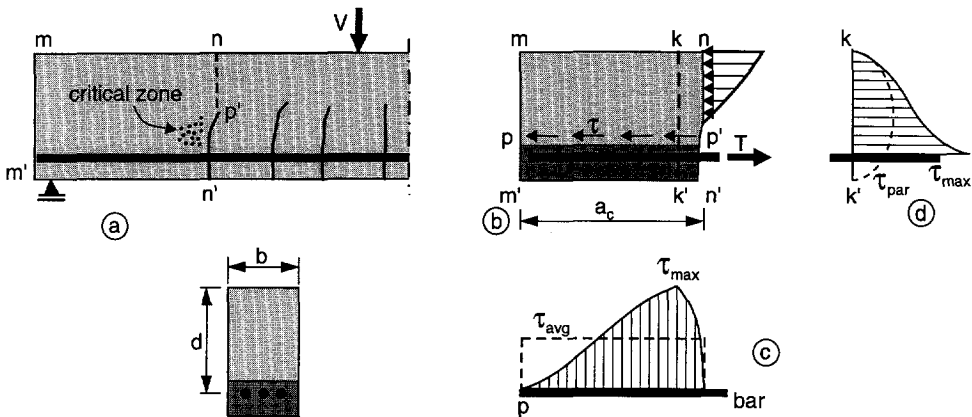


Fig. 9.5 Shear stress in reinforced concrete beam (Kim & White [1991]¹⁴)

Effect of Bond

The reinforcement force is transferred to the concrete through bond. As a result, the shear stress along the surface pp' varies along the length, Fig. 9.5(c) and along the height, see (d). Immediately after the flexural crack $n'p'$ forms, bond phenomena lead to highly concentrated shear stresses in the zone above the internal bars, adjacent to the flexural crack. In the critical zone a maximum shear stress is present, with a value of 2 or more of the average shear stress. Hence, a magnification factor m_{bond} is introduced which, according to Kim, equals 2 or more the average stress.

Effect of Development of Arch Action

The neutral axis shifts down-ward after the occurrence of flexural cracks, see Fig. 9.6.a. With the internal lever arm, the uncracked-section beam theory adequately

predicts the reinforcement force variation along the beam. In cracked-section analyses, however, the lever arm tends to be smaller than the calculated one in the shear span. Kim explains this by the fact that when the flexural cracks extend, the compressive stress distribution becomes more uniform. Accordingly, the neutral axis shifts down-ward. This is attributed to the development of arch action. As a result of the reduction of the internal lever arm from z_0 to z_c , the reinforcement force T in the shear span is consistently higher than the calculated value. Kim even remarks that in some experimental studies it was found that in the middle of the shear span the measured bar tension exceeded the calculated value by a factor up to 1.5 or more. Hence, a magnification factor m_{arch} is introduced, which equals the actual internal moment arm length z_c over the calculated moment arm z_0 . With regard to Kim's explanation, it is remarked that the increased reinforcement force is normally accounted for by the so-called "shift-rule": in a cross section it is calculated with the higher shear load acting at the concrete compression zone at a distance z , at the tip of the flexural crack, see Fig. 9.6.c.

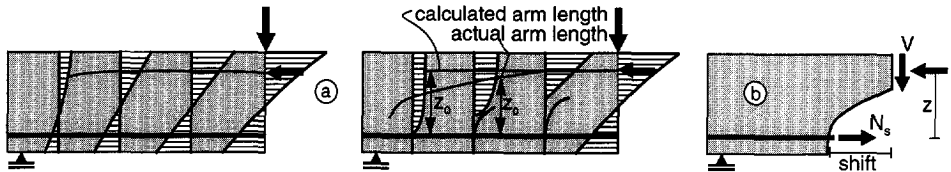


Fig. 9.6 (a) Reduction of internal moment arm length due to the development of arch action by flexural cracks based on finite-element analyses, before flexural cracking (left) and after flexural cracking (right), Kim & White [1991]¹⁴; (b) shift rule: reinforcement force is dependent on the shear force acting at a distance z

Shear Cracking Load

On the basis of these considerations Kim derived two crack criteria. Criterion (9.3) describes the flexural shear cracking load, when the shear stress τ reaches the tensile stress f_t of the concrete. Then, a shear crack may initiate at a point in the critical zone in which m_{arch} and m_{bond} only have a meaning after flexural cracking. For a simply supported beam under point loads, criterion (9.4) describes the shear force as a function of the flexural cracking moment at a section a_c from the support.

$$V_{cr} = \frac{1}{m_{arch} m_{bond}} f_t b z_0 \quad (9.3)$$

$$V_{cr} = \frac{M_{cr}}{a_c} \quad (9.4)$$

Critical Crack Position

By equilibrating criteria (9.3) and (9.4), a probable flexural shear load and a flexural shear crack position a_c emerge. The critical crack position is:

$$a_c = k_3 \left[\frac{\rho \left(\frac{d}{a} \right)^2}{(1-\sqrt{\rho})^2} \right]^{1/3} a \quad (9.5)$$

Because only limited experimental data had been found on the exact location of the critical crack position a_c , Kim used a statistical analysis to determine the constant k_3 in formulation (9.5). Hence, Kim & White proposed (9.6) for the critical crack location. (note: $\rho = \rho_s =$ reinforcement ratio $= A_s/bd$).

Modelling analogy

If RC members are partially strengthened by means of externally bonded steel plates, a plate-end shear crack is forced to occur at the plate-end location. Hence, the position of the unplated length L is analogous to the location of the critical shear crack a_c of Kim & White. This is depicted in Fig. 9.7. On the left side the critical crack section of Kim & White is depicted, the right side shows a partially plated beam-end. As a result of the analogy between a_c and L , the shear span a belonging to a_c is analogous to the fictitious shear span a_L belonging to L . Taken this modelling analogy into account, (9.6) can be interpreted as (9.7):

$$a_c = 3.3 \left[\frac{\rho \left(\frac{d}{a} \right)^2}{(1-\sqrt{\rho})^2} \right]^{1/3} a \quad (9.6) \quad \xrightarrow{\text{modelling analogy}} \quad L = 3.3 \left[\frac{\rho_s \left(\frac{d_s}{a_L} \right)^2}{(1-\sqrt{\rho_s})^2} \right]^{1/3} a_L \quad (9.7)$$

Fig. 9.7 Location a_c of governing flexural shear crack according to Kim & White [1991]¹⁴. Modelling analogy with fictitious shear span a_L and unplated length L for partially plated member for which plate-end shear crack is analogous to flexural shear crack

Calibration of Fictitious Shear Span

The fictitious shear span a_L as expressed by (9.7) is used as an input parameter to compute the shear resistance on the basis of MC90-expression. Essential is that with this MC90-expression the unstrengthened part is considered, so the effective depth of the internal reinforcement d_s and the internal reinforcement percentage $\rho_{s,o}$ have to be taken into account. In Fig. 9.8 the calculated shear resistance is compared with the experimental and simulated results. It is obvious that the

expression (9.7) with the constant $k_s = 3.3$ of Kim & White incorrectly predicts the maximum load. So, this constant value 3.3 is not satisfactorily defined.

To satisfy the prediction of the maximum shear load, the formulation has been adjusted. Analyses showed that by replacing the constant 3.3 in (9.7) by the fictitious shear span-to-depth ratio a_L/d_s , a correct agreement was obtained between the plate-end shear loads based on the fictitious shear span and the experimental and numerically calculated results. This is again shown in Fig. 9.8. The adjusted fictitious shear span and MC90 are now capable of predicting the maximum plate-end shear loads. Thus, by substituting constant 3.3 in (9.7) with a_L/d_s , it can be rewritten into formulation (9.8) that objectively expresses the fictitious shear span:

$$a_L = \sqrt[4]{\frac{(1 - \sqrt{\rho_s})^2}{\rho_s}} d_s L^3 \tag{9.8}$$

When this formulation is used to calculate the fictitious shear span of the strengthened beams with the various unplated lengths of the 5×100 mm² steel plate, the outcome is in accordance with the experimental and simulated shear loads. Table 9.II lists the analytically predicted and earlier derived fictitious shear spans. At larger unplated lengths the difference increases, even so, this hardly influences the plate-end shear load, because at larger shear spans the calculated shear load remains nearly constant.

Table 9.II Comparison of outcome of fictitious shear spans for P5×100

unplated length	L50	L100	L200	L300
fictitious shear span	a_L [mm]	a_L [mm]	a_L [mm]	a_L [mm]
test /simulation	205	355	665	1225
prediction (9.8)	235	395	665	900

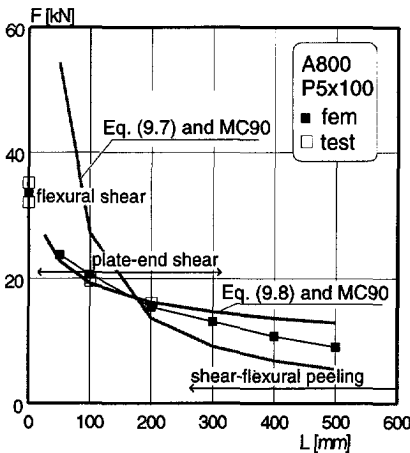


Fig. 9.8 Plate-end shear resistance by tests, simulations and model

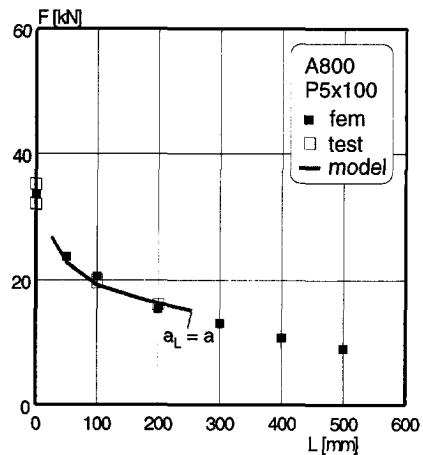


Fig. 9.9 Prediction of plate-end shear load in relation to unplated length L

9.3.3 Validation and Application of Plate-End Shear Model

Finally, the results of the simulations and experiments on the unplated length, reinforcement ratio and shear span length, presented in Fig. 9.1, Fig. 9.2 and Fig. 9.3, are recalculated with the plate-end shear model. Fig. 9.9, Fig. 9.10 and Fig. 9.11 show the outcome of the analyses. The thick grey lines represent the analytical model. As it emerges from the graphs, all the recalculated cases are in correct agreement with the results. It is hereby proven that the plate-end shear model is able to satisfactorily predict the plate-end shear loads.

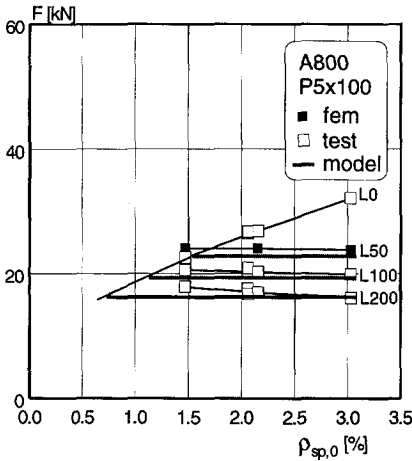


Fig. 9.10 Prediction of plate-end shear load in relation to reinforcement percentage $\rho_{sp,0}$

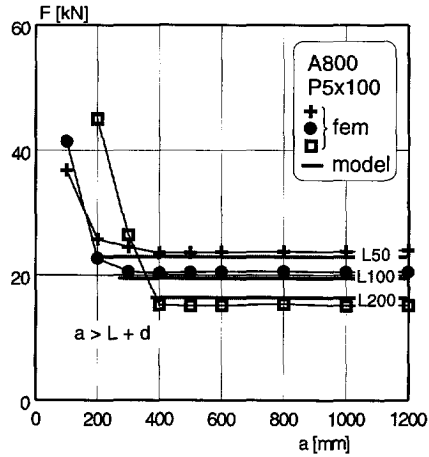


Fig. 9.11 Prediction of plate-end shear load in relation to shear span a

Experiments were also carried out on different concrete sections. In test series S-W the width of the concrete member was 200 mm, in test series S-H the height of the concrete member measured 400 mm. Hence, when (9.8) is used in combination with the MC90 flexural shear expression to predict the plate-end shear resistance of these concrete cross sections, as listed in Table 9.III, the conclusion is drawn that the plate-end shear model is definitely capable of calculating the plate-end shear load of partially plated members with various cross sections.

Table 9.III Shear resistance of additional tests according to plate-end shear model

tests series	S-W (200x200)	S-H (100x400)
d_s [mm]	170	366
L [mm]	100	200
a [mm]	800	1600
a_L [mm]	395	795
V_{exp} [kN]	35.9, 36.5, 35.8, 36.9	38.1, 40.6, 40.3, 34.4
V_{model} [kN]	39.9 ¹⁾	37.2 ¹⁾

¹⁾ calculated with $f_{cm} = 40 \text{ N/mm}^2$ after 45 days

Application Restrictions

Finally, it is mentioned that one must take the range in which the plate-end shear model is applicable into account. The model was derived for $a > L + d$. Furthermore, the model is applicable when a plate-end shear crack develops at the plate-end position. This sounds logical, but it means the unplated length of the shear span must not be too large, otherwise a flexural crack will form from the plate-end crack. Accordingly, a limiting value of $a_L < a$ is proposed. With this condition, the calculated plate-end shear load is not higher than the flexural shear load of an unstrengthened member. Mostly, this implicates that $0.0a < L < 0.25a$ to $0.4a$, which indicates a limiting value for the unplated length.

9.3.4 Summarising: Expressions for Plate-end Shear

In the previous section the plate-end shear model was derived. To complete this section, the most important expressions are summarised. Again, it must be remarked that in the plate-end shear model only the internal reinforcement in the unplated region is considered.

PLATE-END SHEAR MODEL: MEAN MAXIMUM SHEAR LOAD	
fictitious shear span	$a_L = \sqrt[4]{\frac{(1 - \sqrt{\rho_s})^2}{\rho_s} d_s L^3}$
mean nominal maximum shear stress	$\tau_{cum} = 0.18 \sqrt[3]{3 \frac{d_s}{a_L} \left(1 + \sqrt{\frac{200}{d_s}}\right) \sqrt[3]{\rho_{s,0} f_{cm}}}$
mean maximum shear capacity	$V_{cum} = \tau_{cum} b d_s$
application restrictions	$a > L + d$ $a_L < a$
in which	<p>ρ_s bar reinforcement ratio (A_s/bd_s) [-]</p> <p>$\rho_{s,0}$ bar reinforcement perc. ($100A_s/bd_s$) [%]</p> <p>d_s effective depth of internal bars [mm]</p> <p>L unplated length of bonded plate [mm]</p> <p>a_L fictitious shear span [mm]</p> <p>f_{cm} <u>uniaxial</u> compressive strength [N/mm²]</p> <p>b width of concrete section [mm]</p>

9.4 Validation of Plate-end Shear Model with Literature

9.4.1 Beam Shear Tests

The prediction of the shear capacity with the plate-end shear model has proven to be correct for the tests carried out in this research study. Even so, the number of results was limited and it is, therefore, useful to validate the model with results from literature. However, only a limited number of tests was carried out without stirrups. The only reference found on plate-end shear were tests reported by Oehlers [1992]⁸.

He investigated peeling due to shear forces and the interaction between shear peeling and flexural peeling. To that end, the distance from the centre of the support to the end of the plate was varied to change the moment-to-shear force ratio at the plate end. A number of 6 beams in test series 1 and 2 beams in test series 2 were not provided with stirrups. Fig. 9.12 shows the experimental loads as a function of the relative unplated length L/a (see also §2.1.3). Beam 2/1N showed a flexural type of failure, the others failed in shear. Oehlers concluded that "the extent of plating L/a did not affect the shear strength V_{cum} ." This conclusion is likely to be based on the apparent scatter of the experimental shear loads. But the results and scatter could be fully explained with the plate-end shear model.

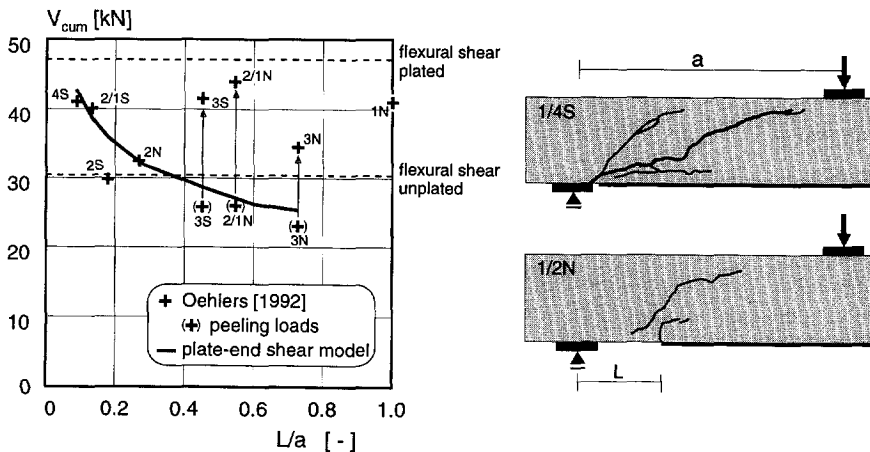


Fig. 9.12 Beam shear according to Oehlers [1992]⁸ and plate-end shear loads predicted by plate-end shear model; crack patterns of beams 1/4S and 1/2N

For that reason, lines of the calculated plate-end shear loads and flexural shear loads (unplated and plated beam) are also drawn in Fig. 9.12. Then, the following conclusions may be drawn with respect to the range of application.

Actually, within the range $a_L < a$, three of the four maximum loads are correctly predicted by the model, namely 4S, 2/1S and 2N. Of 4S and 2N crack patterns were given, and they show plate-end shear as the model predicted. The shear load of beam 2S is about 17% too low. It is questionable whether this beam failed too early either by flexural shear or by the scatter in material properties. But on the whole, for $a_L < a$ the maximum loads are in correct agreement with the model.

In the range $a_L > a$, the maximum loads of 3S, 3N and 1N are not correctly predicted. However, Oehlers also listed the load V_p , which is "the shear load at the end of the plate when the plate peeled away from the reinforced concrete beam as signified by a rapid drop in the longitudinal strain in the plate." When these loads are plotted in the figure, it is seen that the load at which this occurred lies in the vicinity of the plate-end shear prediction. The drop is probably caused by plate-end shear. Hence, the plate-end shear model adequately predicts the peeling loads for $a_L > a$.

Even so, for $a_L > a$ the peeling loads could be considerably increased before the maximum load was attained. This observation contradicts the simulations carried out in the numerical study, see §8.4. There, as it emerges from Fig. 8.16, the load was not increased after $a_L > a$. However, in the numerical simulation shear-flexural peeling occurred, and in Oehlers study shear failure (flexural-shear?) took place. For that reason these two study's could not be compared. Generally, it might only be concluded that for $a_L > a$ additional influences of the bending moment started to play a more dominant role than influences of shear.

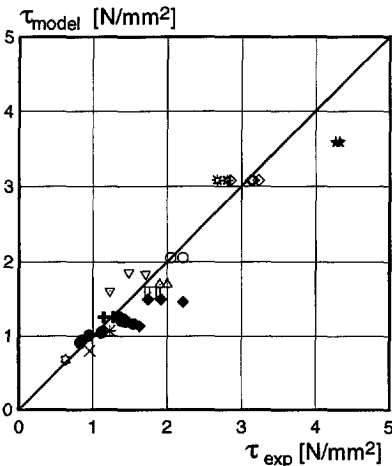


Fig. 9.13 Maximum shear stresses, experimental and according to plate-end shear model; legend in Fig. 9.15

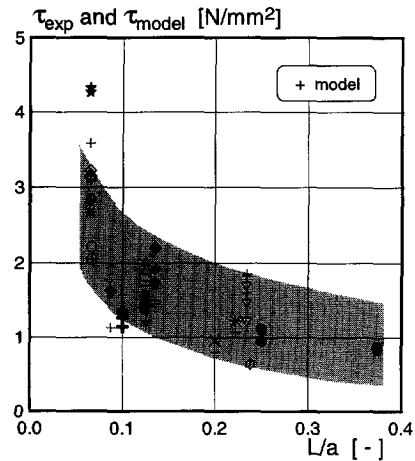


Fig. 9.14 Experimental and model maximum shear stresses as a function of L/a ; legend in Fig. 9.15

9.4.2 Steel Plate Separation Tests

The numerical study concluded that plate separation by concrete cover rip-off was initiated by the plate-end shear deformations. Oehlers [1992]⁹ also concluded that "the formation of the diagonal shear crack causes shear peeling." Accordingly, there must exist a consistency between the analytically predicted plate-end shear load and the experimental plate separation load. From literature, 42 tests with steel plate separation by concrete cover rip-off were found and analysed, see Appendix D. Fig. 9.13 shows the relation between the experimental shear stress and the shear stress predicted by plate-end shear ($\tau = V_{\text{um}}/bd_s$), which seems linear. Fig. 9.14 shows that for plate separation the same dependence on the L/a ratio exists as emerged from

the shear tests conducted by Oehlers. With increasing unplated length as a proportion of the shear span, the maximum concrete shear stress and thus the external shear load decreases.

Finally, in Fig. 9.15 the results from literature are once again plotted as a function of L/a . Now, the experimental maximum load is represented as a proportion of the load predicted with the plate-end shear model. It is calculated that the mean value of the literature results is $x = 1.08$ with a standard deviation of $s = 0.15$. Of course, because plate separation takes place after the formation of a plate-end shear crack and shear deformations, it is obvious that the plate separation load is higher than the plate-end shear load. The standard deviation explicitly means that 90% of the literature results on steel plates are ranged between $(x-1.64s) = 0.84$ and $(1+1.64s) = 1.33$ of the predicted plate-end shear load ($V_{exp} / V_{model} = 1.0$). The deviation would even be smaller if the predictions of Van Gemert [1980]⁴ and Täljsten [1994]⁹ would be omitted. It is questionable, if the prediction is incorrect, or that parameters that played a role in the experiments, are not considered.

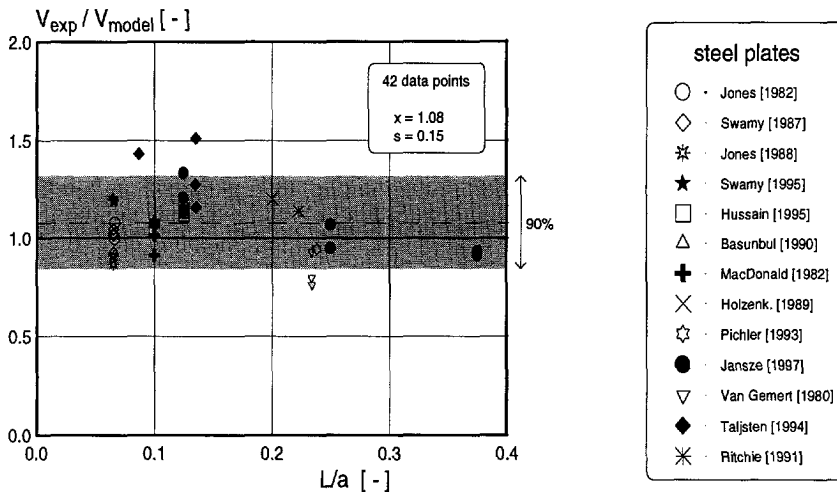


Fig. 9.15 Relative load of steel plate separation in relation to relative unplated length

9.4.3 FRP Plate Separation Tests

Identical to steel plate separation, 17 tests were found in literature in which plate separation of FRP sheets (carbon, glass) by concrete cover rip-off led to failure. Also, the experimental maximum loads are compared with the plate-end shear loads, Appendix D. It is calculated that the mean value of the literature results is $x = 1.17$ with a standard deviation of $s = 0.21$. The standard deviation means that 90% of the results on FRP plates are ranged between 0.83 and 1.51 of the predicted plate-end shear load ($=1.0$). A large scatter due to a small number of results.

The mean value of the literature results and the higher upper bound supports the idea that due to the lower value of Young's modulus (12000-40000 N/mm²) the sheet peels away at a higher shear load. In contrast to steel plates ($E_p = 190000$

N/mm²), the FRP sheets have a smaller stiffening effect on the concrete cover, so that larger shear deformations are needed to initiate plate separation by concrete cover rip-off. Nevertheless, when FRP sheets are used, additional shear problems could also give rise to problems over the plated part of the beam. Namely, Kaiser [1989]³ concluded that special attention must be paid to the formation of flexural shear cracks in the concrete and recommended shear crack formation as a design criterion. Sliding of the shear crack faces lead to irregularities of the concrete surface, that generally causes a peeling-off of the FRP sheet.

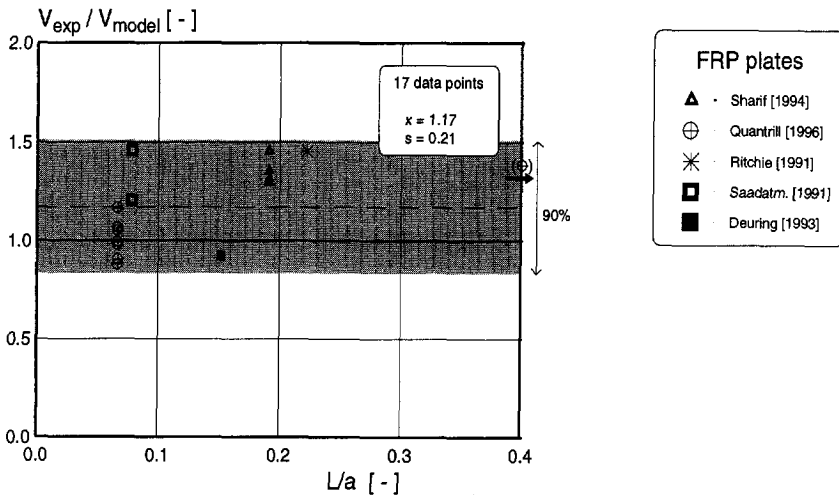


Fig. 9.16 Relative load of FRP plate separation in relation to relative unplated length

9.4.4 Evaluation of Plate-End Shear Model: Additional Parameters

After the thorough comparison with results from literature, the plate-end shear model could be evaluated. For the purpose of predicting plate-end shear for which the model was developed, it performs well. If plates are stopped at a short distance from the support, the maximum shear load is correctly predicted. The plate-end shear model could also be used to predict the plate separation load. The results are very satisfactory, because 90% of the peeling loads could be predicted in a range of 84% to 133% of the calculated plate-end shear load. However, the model only considers the unplated length L , the effective depth d_s and the reinforcement ratio ρ_s of internal bars and the concrete quality f_{cm} . It is actually surprising that the amount and geometry of the external reinforcement hardly influences the outcome of the results. Of course, the end of the plate initiates the plate-end crack, and without this plate-end crack, the plate-end shear crack would not extend. Despite, the model proves that the maximum load could be predicted by, basically, conventional analyses. Nevertheless, some last analyses on plate separation are carried out to investigate the influence of some parameters on the prediction of the maximum plate separation load with the plate-end shear model.

In this thesis, it is stated several times that the stiffness of the steel plate influences the plate separation load. Because the plate geometry is not accounted for in the plate-end shear model, the experimental-over-predicted maximum load was analysed in relation to the stiffness of the steel plate expressed by the second moment of inertia, Fig. 9.17. In fact, it shows the tendency that, with increased second moment of inertia, the maximum plate separation load decreases. Hence, the stiffness of the steel plate influences the maximum load.

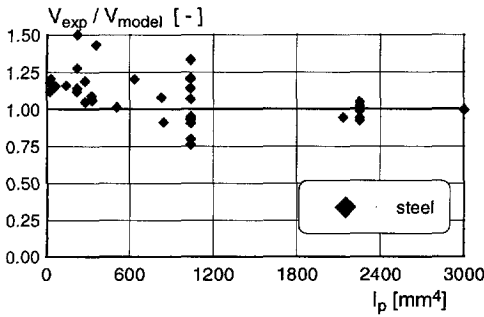


Fig. 9.17 Relative load of plate separation in relation to second moment of inertia

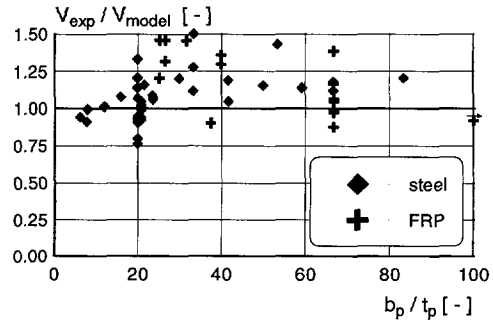


Fig. 9.18 Relative load of plate separation in relation to plate width-over-thickness

Actually, in literature the plate geometry was considered by the plate width-over thickness ratio. MacDonald [1982]² and Swamy et al. [1987]⁶ recommended plate geometry values of $b_p/t_p > 60$ and > 50 , respectively. Fig. 9.18 illustrates the relation of the analysis with respect to the plate width-over-thickness ratio. It indicates that for relatively thin steel plates the experimental peeling loads are higher than the predicted loads. Relatively thicker steel plates peel-off at loads lower than the predicted load. From Fig. 9.18 it can be concluded that if the plate-end shear model is used to predict the maximum load at which the plate separates, a limiting value of $b_p/t_p > 25$ is recommended. Because maximum plate widths of 300 mm are common, maximum plate thicknesses of 12 mm may be used. At the same time, it can be concluded that the plate geometry which is not taken into account in the plate-end shear model, does influence the outcome of the predicted loads.

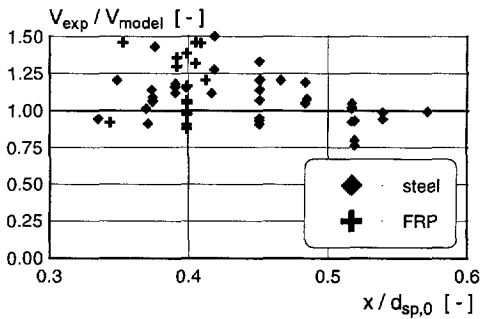


Fig. 9.19 Relative load of plate separation in relation to neutral axis-effective depth

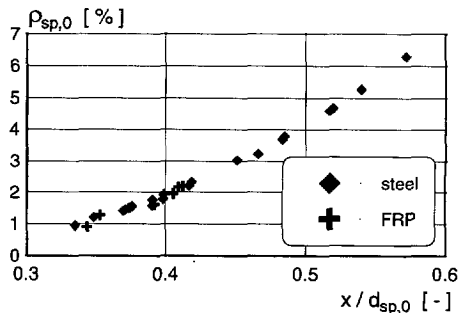


Fig. 9.20 Neutral axis-effective depth ratio and total reinforcement ratio relation

Swamy [1987]⁶ linked the neutral axis-over-effective depth ratio to the transition from a ductile flexural failure to a brittle type of plate separation. He proposed a limiting value of $x/d_{sp} < 0.4$. Because the amount of additional external reinforcement, and thus implicitly neutral axis-over-effective depth, is also not accounted for in the model, this value was investigated. When the test results as a proportion of the predicted plate-end shear loads are analysed, see Fig. 9.19, a tendency emerges that with increasing x/d_{sp} the peeling loads become smaller than the predicted plate-end shear loads. Accordingly, also this ratio influences the magnitude of the plate separation load. With reference to the described experimental and numerical studies it was already observed that with increasing external reinforcement the plate-end shear load decreases. Fig. 9.20 shows that the neutral axis-over-effective depth ratio is linearly dependent on the amount of external reinforcement. The external reinforcement ratio was not taken into account in the fictitious shear span and plate-end shear model because it had only little effect on the results. Hence, it may be concluded that the neutral axis-over-effective depth and related external reinforcement ratio influence the outcome of the predicted load, but the effect is only little.

Concerning the external reinforcement ratio, a study was also carried out that analysed the strengthening ratio. Fig. 9.21 shows the influence of the strengthening ratio on the prediction of the plate-end shear model. The strengthening ratio is defined by $S = A_p / A_s$. In Germany, for example, a maximum strengthening ratio of 2.0 is prescribed (Holzenkämpfer [1994]⁵). However, concerning the factor itself it may only be concluded from Fig. 9.21 that for various strengthening ratios the prediction with the plate-end shear model does not show a particular tendency. Of course, absolutely spoken, the amount of external reinforcement is of great importance, because the flexural capacity could only be reached when the amount of bonded-on reinforcement is not too high.

Finally, the influence of the width of the bonded-on plate in relation to the concrete member was investigated. Fig. 9.22 shows the outcome of the analyses. It indicates that no negative tendency could be indicated on the prediction with the plate-end shear model concerning the plate width-over-concrete width. The width of the concrete member is taken into account in the plate-end shear model.

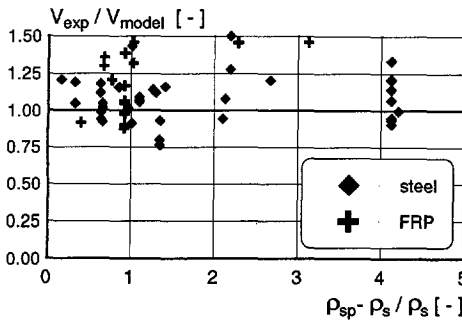


Fig. 9.21 Relative load of plate separation in relation to strengthening ratio

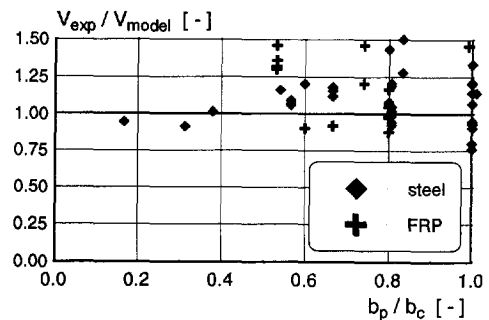
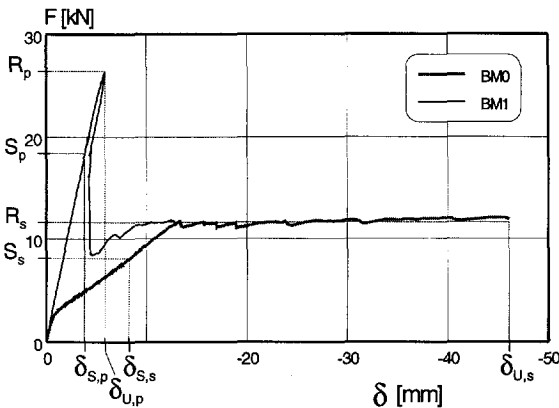


Fig. 9.22 Relative load of plate separation in relation to plate width-concrete width

9.5 Design Method for Plate-End Shear

In this section, the plate-end shear model is modified for a design method for plate-end shear. This ultimate limit state design method may be used for both plate-end shear and plate separation. A good design not only takes the ULS into account, but it guarantees also a ductile behaviour to allow for a stress redistribution.

Throughout the various studies on plate-end shear and plate separation, tests proved that the failure response of the member and the bonded-on plates was characterised as very brittle. So, when one should design for these brittle failure types, a lower bound approach of the maximum plate-end shear load is advisable. Fig. 9.23 illustrates this on the basis of the tested beams BM0 and BM1 (see Chapter 4). The safety against failure is expressed as the ultimate limit resistance load R over the serviceability limit load S . According to the codes this safety factor should be taken R/S , generally about 0.6. However, when the safety factor was defined as the ultimate deformation δ_u over the deformation δ_s at the serviceability state, a clear difference is observed between the brittle failure behaviour of BM1 and ductile yielding of BM0. The safety against failure for the brittle one is then too small. For a design method for plate-end shear an additional safety factor on the characteristic lower bound should, therefore, be taken into account.



$$\frac{R_s}{S_s} = \frac{R_p}{S_p} = \gamma_R$$

$$\gamma_{\delta,s} = \frac{\delta_{U,s}}{\delta_{S,s}} \neq \frac{\delta_{U,p}}{\delta_{S,p}} = \gamma_{\delta,p}$$

Fig. 9.23 Schematic representation of strength- and deformation safety factors for ductile flexural failure of conventionally reinforced concrete beam BM0 and brittle plate separation of partially plated beam BM1

For the described plate-end shear loads, test 2S of Oehlers [1992]⁸ was estimated 17% too low, so at a percentage of 83% of the predicted one. For the described plate separation loads, it was calculated that the lower bound variation ($x-1.64s$) was 0.84 for the steel plates and 0.83 for the FRP plates. Hence, 95% of the predicted loads was higher than 0.83 times the predicted one. Only the worst predicted loads of Van Gemert [1982]⁴ were not part of this interval (0.76 and 0.80). Accordingly, based on the above mentioned observations a characteristic lower bound of 0.83

times the mean maximum shear load is advised by the author. Then, the plate-end shear model should be multiplied by a factor 0.83 for safe design. Hence, in the modified MC90 expression the factor 0.18 should be replaced by the design factor $0.83 \times 0.18 = 0.15$. At the same time, the mean value of the concrete cylinder compressive strength should be replaced by the characteristic compressive cylinder strength of the concrete at 28 days. Then, for the design method for plate-end shear and plate separation the following expressions are obtained:

DESIGN METHOD FOR PLATE-END SHEAR AND PLATE SEPARATION	
fictitious shear span	$a_L = \sqrt[4]{\frac{(1 - \sqrt{\rho_s})^2}{\rho_s} d_s L^3}$
design nominal maximum shear stress	$\tau_{Rd1} = 0.15 \sqrt[3]{3 \frac{d_s}{a_L} \left(1 + \sqrt{\frac{200}{d_s}}\right) \sqrt[3]{\rho_{s,0} f_{ck}}}$
design maximum shear capacity	$V_{Rd1} = \tau_{Rd1} b d_s$
application restrictions	$a > L + d$ $a_L < a$

Surprisingly, then the modified MC90 expression equals the shear cracking load as recommended by the MC 90 code in section 6.3.3.2 "Reinforced concrete beams". It is concluded that the plate-end shear model is a lower bound model for the maximum shear load and for plate separation by concrete cover rip-off.

9.6 Conclusions

This chapter discusses the plate-end shear model. Based on the simulations and the experiments a fictitious shear span has been formulated. The fictitious shear span is in combination with a modified MC90 formulation on the flexural shear capacity successfully used to predict the maximum shear load for plate-end shear. The plate-end shear model is only applicable within certain ranges, namely for $a > L + d$ and $a_L < a$. Also, it is concluded that the plate-end shear model may also be used to design for plate separation.

10. DETAILING PROVISIONS FOR PLATE-END SHEAR

This chapter presents a design method for detailing provisions for strengthened structures which are partially plated. §10.1 introduces the detailing provisions. On the basis of the truss analogy, §10.2 illustrates the internal force distribution in a partially plated beam. The truss model analyses plate-end shear and plate separation. Furthermore, it visualises the necessarily addition of bolts as suspension reinforcement. Then, §10.3 provides design rules for detailing for plate-end shear and plate separation. §10.4 concludes this chapter.

10.1 Introduction to the Detailing Provisions

The previous chapter elaborated on a plate-end shear model and also presented a design method for plate-end shear. However, if the shear resistance V_{Rd1} of the member is less than the design plate-end design shear load V_{Sd} , additional shear reinforcement should be provided. A design method could be carried out according to the Standard Method of shear reinforcement as described in §3.4.3. But, before doing so, the location and configuration of the detailing provision must be analysed.

Pichler [1993]¹¹ sketched a strut-and-tie model for a bonded-on plate, additionally anchored by bolts, see Fig 2.10. The short bolts are stopped beyond the longitudinal bars to activate strut action, the bolts act as ties. This simple model gave rise to the idea to develop a truss model to analyse plate-end shear as well as plate separation. Such an analysis could be successfully carried out on the basis of truss analogy. The classical truss analogy ($\theta=45^\circ$) provides a simple model which enables it to gain more insight in the distribution of forces in a structure. Despite, in analysing shear, this model underestimates the contribution of the concrete. By virtue of the strength and stiffness of the concrete, it is capable of carrying the load directly to the supports. One must therefore split the force transfer in a part contributed by the truss and a part contributed by the concrete, see Fig 3.9. With respect to this, Leonhardt [1977]¹⁴ observed that the contribution of the concrete was constant during testing and equalled the flexural shear capacity of the concrete member.

10.2 Truss Analogy for Internal Force Distribution

10.2.1 General

As a train of thought, beam shear and plate anchorage are dealt with on the basis of truss analogy. Such a truss model is a simple representation of a more complicated

reality. Moreover, this engineering model provides a very good understanding of the internal force distribution. As a matter of fact, the truss analogy is based on equilibrium of forces in the ultimate limit state of an RC member when large cracked areas are formed: reinforcement bridging the cracks is considered to act as ties, concrete under compression is represented by struts. Even so, in this paper concrete under tension is also modelled by trusses analogous to Reineck [1991]¹⁴.



Fig. 10.1 Minimum principal stresses in finite-element model for a beam with a bonded-on plate stopped 200 mm short of the support

10.2.2 Configuration of Truss Model

The configuration of a conventional truss model is based on the truss analogy of Ritter and Morsch. According to this modelling approach, the shear force is transferred by concrete compressive struts and steel tensile bars. The model comprises parallel top and bottom flanges, for which the distance between the two flanges equals the internal lever arm. When such a truss model is configured for structures strengthened in flexure by an externally bonded steel plate, one must be aware of an alternative internal equilibrium system. This was already discussed in section 8.3.1. Fig. 10.1 displays the minimum principal stresses acting in a strengthened member with an unplated length of the shear span of 200 mm. Two main compression struts are distinguished: one arch acts between the loading point and the support, and, by virtue of the external reinforcement, an additional arch acts between the loading point and the anchorage zone of the steel plate.

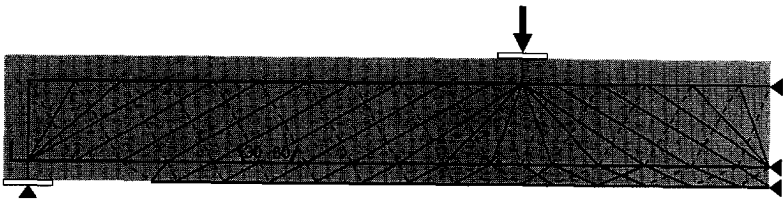


Fig. 10.2 Truss model for externally plated member with a $5 \times 100 \text{ mm}^2$ bonded-on plate stopped 200 mm short of the support

On the basis of the truss analogy and the two arches distinguished above, a truss model is developed. This truss model represents the stress field in the web of a strengthened member without stirrups, and is based on the model developed by Reineck [1991]¹⁴. There, the truss members are connected with hinges and inclined

at 30° and 60°. Of the same kind, Fig. 10.2 shows the truss model for a partially strengthened member. Besides, the truss configuration between the internal bars and external plate is based on experimental observations as Fig 5.20 depicts. The photograph clearly shows inclined strut action in the concrete cover at about 30°. and tie action at about 60°. However, in the photograph cracks have already formed in the notional concrete ties.

10.2.3 Stiffness of the Truss Members

An important parameter for this truss model is the normal stiffness EA of the truss members. The proportion of stiffnesses of the members determines the internal load distribution and the load transfer to the support. The normal stiffness is characterised by Young's modulus E and the cross section A . Quantities are assumed of $E_c = 32000 \text{ N/mm}^2$, $E_s = 200000 \text{ N/mm}^2$ and $E_p = 190000 \text{ N/mm}^2$, the cross section A is determined by dividing the structure into notional parts. Table 10.1 lists the stiffnesses EA for the various truss members used in this study.

Table 10.1 Stiffness characteristics of load-bearing systems of truss model

truss member	name truss	h [mm]	b [mm]	EA [MN]
arch and tensile zone	EA_c	80	100	250
inclined strut	EA_{strut}	65	100	210
inclined tie	EA_{tie}	37.5	100	120
bars 2Ø8	EA_s	$A_s = 100 \text{ mm}^2$		20
plate 5x100	EA_p	5	100	95
stirrups Ø6-75 (when provided)	EA_{ss}	$A_{\text{sw}} = 57 \text{ mm}^2$		11
tensile failure	EA_{cr}	-	-	≈ 0

Both the concrete compression zone and the concrete tensile zone are assumed to be 80 mm in height and 100 mm in width. Then, a normal stiffness EA_c of approximately 250 MN is derived. The internal lever arm measures 130 mm, the external lever arm is 164 mm. The longitudinal bar and plate reinforcement are modelled separately from the concrete tensile zone in order to be able to directly deduce reinforcement stresses. The concrete tensile zone truss member is assumed to be present at the level of the internal bars.

To model tensile failure of the concrete, a truss member comprising an approximately zero normal stiffness is assumed. Due to the low normal stiffness a member with such stiffness would not contribute to the force distribution. Thus, to simulate failure in the truss model, this zero stiffness is assigned to a concrete truss member with the largest tensile stress, and a new analysis is carried out to determine the next truss member with the highest tensile stress. Accordingly, simulation of failure is carried out as if the truss members with the highest tensile stress are successively removed from the truss model. In such a way the truss member could remain in the truss model to avoid instabilities of the model and to avoid divergency of the element program.

10.2.4 Analyses with Truss Model

Linear Distribution of Reinforcement Stresses

An external load of 1 kN is considered to act on the truss model and concrete cracking is not assumed in the tensile zone. Fig. 10.3 compares the derived stresses of the internal bars and external plate of the truss model with results of a linear calculation with the smeared-discrete crack model as discussed in chapter 7 and 8. Fig. 10.3 clearly shows that the truss model satisfactorily predicts the reinforcement stresses. Accordingly, it may be concluded that the developed truss model adequately calculates the total internal force distribution of a member strengthened with an externally bonded steel plate. Hence, plate-end shear and plate separation will be analysed with the truss model to visualise the internal force transfer.

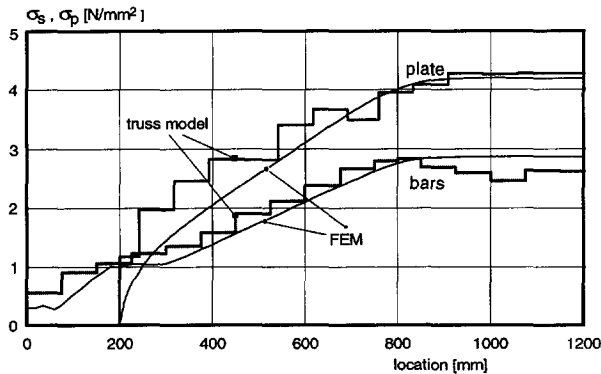


Fig. 10.3 Comparison of reinforcement stresses of truss model with reinforcement stresses obtained by linear finite-element calculation at external load $F = 1$ kN

Plate-End Shear Failure

Fig. 10.4 shows five stages of the configuration of the truss model during the development of the plate-end-shear crack. Stage A shows the initial truss configuration of the strengthened member as depicted in Fig. 10.2. Also, it shows the locations of the numbered truss members ties 1 to 6 and struts 7 and 8, which are of particular interest. The bar is located at the plate end. Table 10.11 lists the forces in the numbered truss members.

Relative high forces in tie 2 and strut 8 in the uncracked stage A indicate the active role of these members which also emerged from the minimum principal stresses depicted in Fig. 10.1. However, as stage B indicates, the initiation of the crack at the plate end drastically changes this linear force distribution. Due to failure of concrete ties at the plate end, tie 2 and strut 7 are unloaded and tie 3, strut 8 and the bar are subsequently activated. Then, it is likely that in stage C, due to the large tensile force, tie 3 fails. As a consequence, the following tie 4 is activated. Stage D and stage E show that eventually all ties would subsequently fail due to development of the plate-end-shear crack. At the same time, the external load should decrease due to progressive failure of the concrete web ties during plate-end

crack development. Stages A up to E also illustrate that in the unstrengthened part of the beam beyond the plate-end shear crack, the force in strut 7 continually increases to transfer the shear load by truss action directly to the support.

Recapitulating, the analysis with the truss model shows that concrete ties successively fail due to the development of the plate-end-shear crack. As a result, the internal forces redistribute to obtain internal equilibrium.

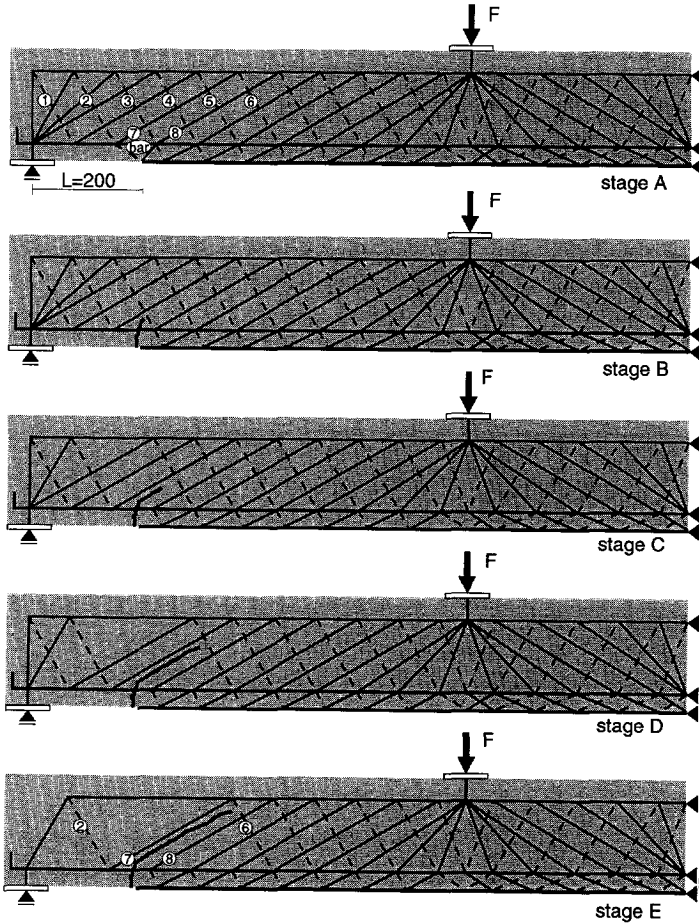


Fig. 10.4 Modification of the configuration of the truss model during the development of the plate-end shear crack

Table 10.II Distribution of relative forces in truss members at external load of 1.0 F

stage	1	2	3	4	5	6	7	8	bar
A	0.242	0.524	0.188	0.201	0.242	0.215	-0.373	-0.501	0.106
B	0.132	-0.031	0.815	0.239	0.132	-0.031	+0.053	-0.703	1.359
C	0.309	0.094	0	0.752	0.309	0.003	-0.162	-0.005	1.978
D	0.768	0.387	0	0	0.768	0.387	-0.670	+0.338	2.501
E	0	1.154	0	0	0	1.154	-2.000	+1.154	2.885

Plate Separation

Fig. 10.5 shows a final stage in which the structural member is provided with web reinforcement. The plate-end shear crack had developed and the plate had separated. The main difference with plate-end shear failure from Fig. 10.4 lies in the fact that stirrups are activated after failure of the concrete web ties. Hence, the internal stirrups act as suspension reinforcement to contribute to the load bearing capacity. However, due to plate-end shear, the stiffness of the structural member at the plate end reduced considerably. More specifically, instead of the inclined tie stiffness of 120 MN, only the stiffness of the stirrups of 11 MN had to be accounted for. This implies a reduction by a ratio 10. The local deformations of the truss model in the zone at the plate end therefore increased considerably. Although the truss model does not translate imposed deformations into increased member forces, it is likely that a plate separation crack forms at the plate end. As a result, the ties between the bonded-on plate and internal bars fail and the steel plate separates from the strengthened member. With respect to this, the strut and tie action depicted in Fig 5.20 is once more referred to.

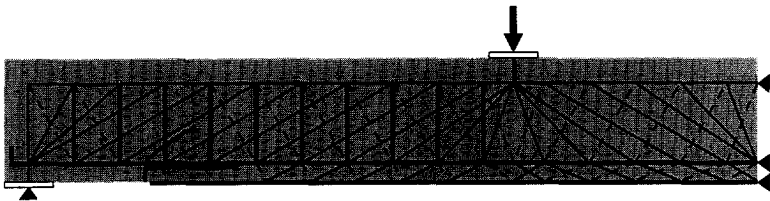


Fig. 10.5 Truss model configuration as a result of plate separation by shear peeling

10.2.5 Suspension Reinforcement by Bolts at Plate End

The two described cases on plate-end shear and plate separation showed both that the absence of ties resulted in the loss of internal equilibrium. Hence, reinforcement should be added to the strengthened member. Moreover, it emerges that the arch at the plate end activated by the external reinforcement has to be suspended up to the concrete compression zone. Only then truss action develops and the load could be directly transferred to the support.

With this knowledge, the solution to detail for plate-end shear and plate separation seems quite simple. Fig. 10.6 depicts two configurations in which equilibrium is obtained after the development of the plate-end-shear crack and/or plate separation crack. Large bolts are installed at the anchorage zone of the steel plate and anchored in the concrete compression zone to enable them to fully suspend the load. This holds true for both cases, when internal web reinforcement is provided or not. In such a way, internal equilibrium is always assured in partially plated members after plate-end shear cracking or plate separation. Notice that this proposed provision is different from that of Pichler [1993]¹¹, see Fig. 2.12. There, the suspension provision is correct but not so transparent. By virtue of the short bolts,

the load is suspended beyond the internal bars. Then, it is transferred to the internal stirrups by struts. Eventually, the load is really suspended by virtue of the internal web reinforcement.

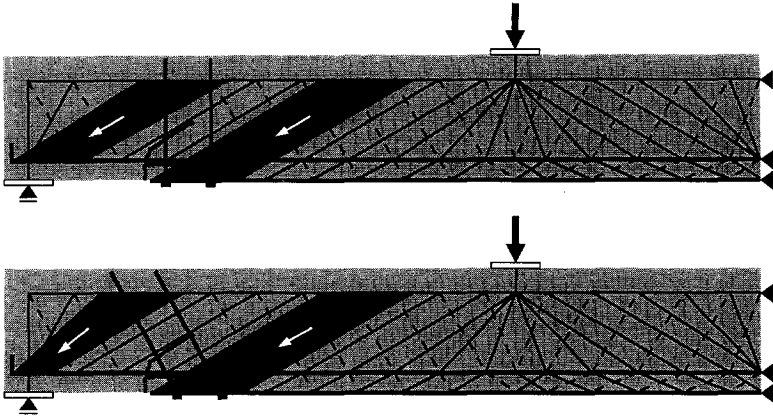


Fig. 10.6 Equilibrium in truss model by virtue of two configurations of, in this case, two bolts acting as suspension reinforcement for the concrete arch activated by the externally bonded steel plate

10.3 Design Method for Bolts for Plate-End Shear

General

As a result of the increased flexural capacity by flexural strengthening with partially bonded steel plates, the shear capacity of the strengthened member may be insufficient. A strengthened structural member without shear reinforcement might, therefore, be critical for either flexural shear or plate-end-shear failure. For flexural shear design the EC2 design code could be advised. But also for plate-end shear the same code could be used, even so, in an adjusted form. This section, therefore, provides a design method for bolts installed at the plate end in accordance with EC2. As explained, this design method is also valid if stirrups are provided in the web of the structural member. Then, plate-end shear is followed by plate separation. Still, correctly designed suspension provisions by bolts are needed at the plate end. Fig. 10.7 illustrates the configuration of the bolts at the plate end with accompanying notations for the proposed design method.

Design Method for Plate-End Shear

The method for shear design is based on three values of design shear resistance, namely V_{Rd1} , V_{Rd2} and V_{Rd3} , see §3.4.3.

Any member of which the design shear strength V_{Sd} is less than the design resistance V_{Rd1} of the member without shear reinforcement, requires no design shear reinforcement. In this case, V_{Rd1} is the design plate-end shear resistance.

Hence:

$$V_{Sd} \leq V_{Rd1} \quad \text{no bolts required}$$

The design plate-end shear resistance V_{Rd1} is calculated with:

$$V_{Rd1} = 0.15 \sqrt[3]{3 \frac{d_s}{a_L} \left(1 + \sqrt{\frac{200}{d_s}} \right) \sqrt[3]{\rho_{s,0} f_{ck}} b d_s}$$

$$\text{in which } a_L = \sqrt[4]{\frac{(1 - \sqrt{\rho_s})^2}{\rho_s} d_s L^3}$$

For members where V_{Sd} exceeds V_{Rd1} bolts should be provided so that:

$$V_{Sd} \leq V_{Rd2}$$

In any member, the design shear force V_{Sd} should not exceed the maximum design shear force that can be carried without crushing of the notional concrete compression struts. Hence:

$$V_{Sd} \leq V_{Rd2}$$

$$\text{in which } V_{Rd2} = \frac{1}{2} v f_{cd} b 0.9 d_s$$

$$v = 0.7 - \frac{f_{ck}}{200} > 0.5$$

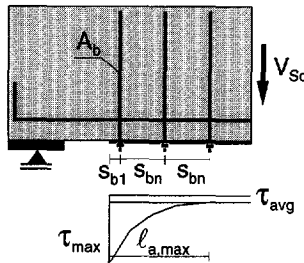


Fig. 10.7 Suspension reinforcement by virtue of a bolt; configuration and notations

Design Method for Members Requiring Bolts

The design of bolts at the plate end is carried out analogously to EC2 - Standard method of shear design.

The design shear resistance V_{Rd3} is:

$$V_{Rd3} = V_{cd} + V_{bd}$$

in which V_{cd} is the contribution of the concrete. The contribution of the concrete is equal to the plate-end shear resistance V_{Rd1} .

The contribution of the vertically installed bolts is given by the equation:

$$V_{bd} = n A_b (f_{ybd} - \sigma_{bd,0})$$

in which n is the number of bolts;
 A_{bw} is the cross-sectional area of one bolt;
 f_{ybd} is the design yield strength of the bolt;
 $\sigma_{bd,0}$ is the initial (pre)stress in the bolt;

Position of Bolts

The bolts should be installed in the anchorage zone of the bonded-on plate, as close to the end of the plate taking a minimum distance s_{min} into account which is related to the diameter of the hole in the plate. For an approximation of the length of the anchorage zone, Holzenkämpfer's [1993]⁵ expression for the maximum anchorage length may be used. Hence:

$$s_{b1} = s_{min} = 2.5 d_{hole} \text{ or } = 6.0 t_p$$

$$s_{bn} = \frac{\ell_{a,max} - s_{min}}{n-1} > 2.5 d_{hole}$$

$$s_{max} = 0.7 d_s \text{ only within } \ell_{a,max}$$

$$\text{in which } \ell_{a,max} = \sqrt{\frac{E_p t_p}{4 f_{ctm,ax}}}$$

Other Relevant Limit States

Ofcourse, if bolts are additionally provided at the anchorage zone of the bonded-on plate, and thus, if the design capacity of the strengthened member is once more increased, one must be aware that no other relevant limit states could be exceeded. Other limit states are, for example:

- flexural shear. When the maximum load could be increased by virtue of the bolts, the flexural shear capacity may become critical. Therefore, this limit state must be checked, and, if necessary, additional bolts must be installed over the full length of the shear span;
- Shear. Shear beyond plate end and support, if the unplated length is too large;

- yielding of the internal reinforcement. At the location of the plate-end shear crack, it emerged that the magnitude of the tensile stress in the bars increased significantly when the load was increased. By the addition of bolts at the plate end, the amount of internal longitudinal reinforcement must be sufficient to prevent yielding of the bars. Particularly at the support, where the steel plate stops, the amount of tensile bar reinforcement may be reduced by the structural engineer in the design as a result of the smaller bending moment.
- epoxy-concrete interface plasticity. It emerged from the test series A-B that, if bolts are additionally provided and the internally applied reinforcement (longitudinal bars and stirrups) is sufficient, the maximum load bearing capacity is mainly dominated by interface plasticity. As a result of the increased shear stresses at the anchorage zone of the steel plate, the strength of the interface at the anchorage zone is exceeded.

10.4 Conclusions

A truss model was developed to analyse plate-end shear and plate separation. It emerged that an internal redistribution of forces took place during the development of the plate-end shear crack. The truss model clearly showed that suspension reinforcement by large bolts installed at the plate end is needed to ascertain equilibrium after plate-end cracking. By virtue of these bolts the strut activated by the external reinforcement is suspended up to the concrete compression zone, and transferred directly by strut action to the support. A design method analogous to the Standard method of EC2 was proposed to detail the bolts.

11. APPLICATION: SHEAR FLEXURE INTERACTION

This last chapter of Part IV merges the most important topics concerning plate bonding, namely shear and flexure, into an interaction graph. §11.1 introduces this interaction graph, which represents shear and flexural failure by a shear valley as a function of the reinforcement ratio and the shear span-to-depth ratio. §11.2 summarises the expressions on which the interaction graph is based. Then, §11.3 treats case studies to visualise the influence of the unplated length and the strengthening ratio on the shear valley. Finally, §11.4 concludes this chapter.

11.1 Introduction to the Shear-Flexure Interaction Graph

A lot of experimental and numerical evidence on beam shear and plate anchorage was collected in the foregoing chapters. Insight into the failure behaviour has been gained and parameters influencing the type and mechanism of failure were systematically investigated. However, for the structural engineer, a simple tool to visualise the design of externally strengthening members is indispensable. Mostly, members are strengthened to increase the flexural capacity. It is, therefore, logical to develop a shear-flexure interaction graph which covers the most important design topics when dealing with the strengthening of structures, namely, the capacities in flexure and shear. Particularly, the latter one has proven to be of great significance when beams with partially bonded plates are considered. It is, therefore, interesting to visualise how shear influences flexure.

The shear-flexure interaction graph is an extension of Kani's flexural shear valley and is a graphical representation for illustrating the influence of the amount of longitudinal reinforcement and the shear span-to-depth ratio on the type of failure. The interaction graph is based on the flexural capacity, the flexural shear capacity and the plate-end shear capacity. Because the ratio shear moment-to-flexural moment is represented, one must be aware of the fact that the interaction graph indicates the dominance of shear over flexure. Moreover, the various graphs contain different absolute values of the flexural capacity.

Flexural shear can be described with the conventional expressions for the shear capacity. In this case, Rafta's expression is used. Plate-end shear is described with the plate-end shear model derived in Chapter 9. It is based on the modified CEB-FIP MC90 flexural shear expression and a fictitious shear span. This fictitious shear span is activated by the unplated length of the partially plated member. It should be noted that the interaction graph is worked out with mean values of the material properties to indicate whether shear or flexure governs failure. For design, material and safety factors have to be taken into account.

11.2 Expressions for Shear Flexure Interaction

11.2.1 Flexural Capacity

The flexural capacity of the strengthened cross section is calculated with the following expressions, which assume that the steel yields before the compressive stress of the concrete is attained (see also Fig. 1.7).

$$M_n = A_s f_{sym} (d_s - \beta h_{xu}) + A_p f_{pym} (d_p - \beta h_{xu}) \quad (11.1)$$

$$N_{cum} = \alpha b h_{xu} f_{cm} \quad (11.2)$$

$$\alpha = 0.75 \text{ and } \beta = 0.388 \quad (\text{Dutch code})$$

11.2.2 Shear Capacity

Flexural Shear Capacity

The flexural shear capacity of members without shear reinforcement is expressed as a function of the weighted effective depth for internal and external reinforcement:

$$V_{cum} = \tau_{cum} b d_{sp} \quad (11.3)$$

$$\tau_{cum} = 0.85 \alpha_u \sqrt{f_{cm}} \sqrt[3]{\rho_{sp,0}} d_{sp}^{-0.25} \quad (11.4)$$

$$\alpha_u = 6.0 - 2.2 \frac{a}{d_{sp}} \quad \text{for} \quad 1.0 < \frac{a}{d_{sp}} < 2.0 \quad (11.5)$$

$$\alpha_u = 0.795 + 0.293 \left(3.5 - \frac{a}{d_{sp}} \right)^{2.5} \quad \text{for} \quad 2.0 < \frac{a}{d_{sp}} < 3.5 \quad (11.6)$$

$$\alpha_u = 0.90 - 0.03 \frac{a}{d_{sp}} \quad \text{for} \quad 3.5 < \frac{a}{d_{sp}} \quad (11.7)$$

Plate-End Shear Capacity

The plate-end shear capacity of members without shear reinforcement is expressed as a function of the effective depth related to the unplated part:

$$V_{cum} = \tau_{cum} b d_s \quad (11.8)$$

$$\tau_{cum} = 0.18 \sqrt[3]{3 \frac{d_s}{a_L} \left(1 + \sqrt{\frac{200}{d_s}} \right)} \sqrt[3]{\rho_{s,0} f_{cm}} \quad (11.9)$$

$$a_L = \sqrt[4]{\frac{(1 - \sqrt{\rho_s})^2}{\rho_s} d_s L^3} \quad (11.10)$$

11.3 Case Studies on Shear Flexure Interaction

11.3.1 Assumptions for Case Studies

General

To describe shear flexure interaction, the shear moment capacity-over-flexural moment capacity of the beam is calculated with the equations of section 11.2. The flexural capacity is a property of the strengthened section. The shear capacity is calculated by determining the maximum shear load and multiplying it by the length of the shear span.

For the case studies, strengthening ratios are assumed. If a strengthening ratio of 1.0 is assumed, it means that the amount of external reinforcement equals the amount of internal reinforcement. Always, the total reinforcement ratio is related to the effective depth of the strengthened cross section. Hence, $\rho_{sp} = (A_s + A_p) / bd_{sp}$. The effective depth of the cross section is calculated on the basis of the weighted average of the cross-sectional areas of the internal bars and the bonded-on plates.

The shear span a was varied to obtain shear span-to-depth ratios a/d_{sp} up to 8.0. Values between 0 and 1.0 were considered, however, it must be remarked that flexural shear only applies for $a/d_{sp} > 1.0$ and plate-end shear only for $a > L + d_s$. Shear span-to-depth ratios between 0 and 1.0 represent short deep beams, for which web shear or shear compression dominate failure. Nevertheless, a horizontal plateau was assumed in the shear flexure graph equal to Kani.

Geometry

The case studies were carried out with the beam geometry used in the experimental and numerical studies and depicted in Fig. 11.1. The beam measures $100 \times 200 \text{ mm}^2$ in cross section and is reinforced with A_s at an effective depth of 170 mm. The bonded-on reinforcement A_p had a constant width of 100 mm, equal to the width of the beam. Hence, the effective depth of the external plate varied between 202 and 204 mm, depending on the amount of reinforcement.

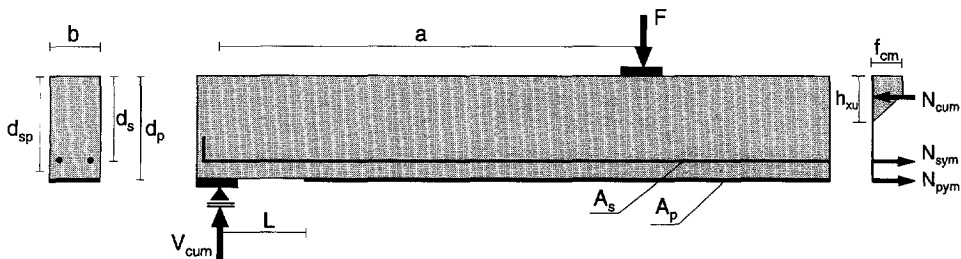


Fig. 11.1 Geometry of beam used for case studies

Material Properties

For concrete, a mean uniaxial strength of 36 N/mm^2 was assumed. Mean yield stresses of 600 N/mm^2 and 285 N/mm^2 were adopted for the internal and external reinforcement, respectively. For both, an ideal plastic branch was assumed.

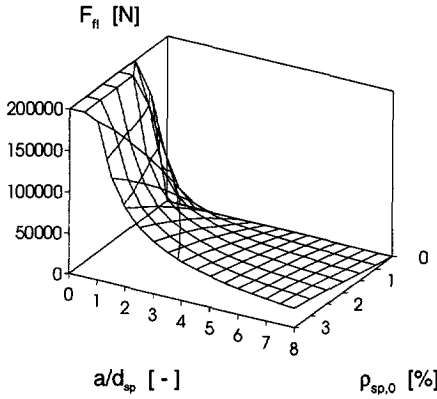


Fig. 11.2 Flexural load

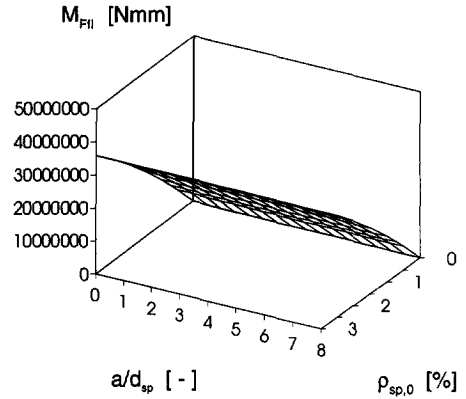


Fig. 11.3 Flexural moment

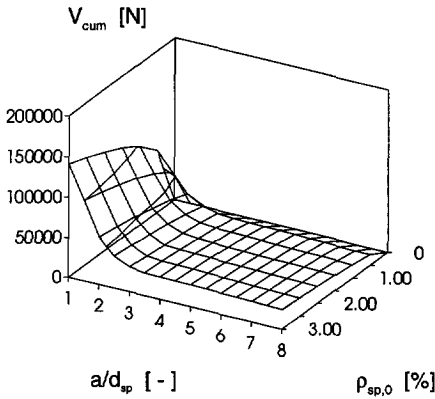


Fig. 11.4 Flexural shear load

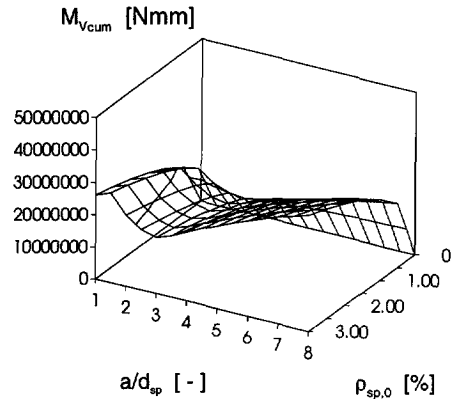


Fig. 11.5 Flexural shear moment

11.3.2 Variation of Unplated Length for Strengthening Ratio 1.0

General

The first case study investigates the influence of the unplated length in relation to the reinforcement ratio and the shear span-to-depth ratio. Two unplated lengths are analysed, namely the one of 50 mm and that of 200 mm. However, fully plated beams are first considered to construct the flexural shear valley. Later, this valley is used as a reference for the partially plated beams. With the purpose of clearly showing how the shear valley was constructed, this section elaborately discusses the case in which the unplated length is 50 mm. For this case, a strengthening ratio of 1.0 is assumed, so $A_p / A_s = 1.0$.

Fully Plated Members

At first, fully plated members are analysed. When the external plate is bonded beyond the support, only flexure and flexural shear have to be considered. Fig. 11.2 shows the external flexural load at which both the internal bars and the external plate yield. With decreasing shear span the flexural load increases. Fig. 11.3 shows the flexural moment capacity of the concrete cross section. Because the flexural moment capacity is a property of the concrete cross section, it increases with enlargement of the reinforcement ratio, but it is constant in relation to the shear span-to-depth ratio. At a reinforcement ratio of 3.0 the concrete compression zone crushes before the reinforcement yields, because for $A_p = 1.0 A_s$ ρ_{\max} equals 2.8%.

The flexural shear capacity in relation to the total reinforcement ratio and shear span-to-depth ratio is depicted in Fig. 11.4 and Fig. 11.5. Fig. 11.4 sketches the flexural shear load as predicted by Rafia's expression. For a/d_{sp} ratios less than 2.5, the shear load increases significantly by virtue of direct strut action. Fig. 11.5 shows the flexural shear moment capacity. At a ratio $a/d_{sp} = 2.5$ the flexural shear moment shows a minimum. For smaller and higher shear span-to-depth ratios the flexural shear moment increases. As mentioned earlier, values between 0 and 1.0 are not considered to be realistic for flexural shear. There, web shear or shear compression failure dominates failure, but these are not taken into account in the shear-flexure interaction graph.

After the flexural moment capacity and the flexural shear moment capacity have been analysed, Fig. 11.3 and Fig. 11.5 are merged to visualise the flexural-shear flexure interaction. To that end, the flexural shear moment is expressed as a percentage of the flexural moment. By doing so, Fig. 11.6 is constructed. In this graph the horizontal plateau indicates that flexure governs failure and the flexural shear valley indicates that flexural shear dominates flexure and, thus, governs failure. As expected, for fully bonded plated members, the flexural shear valley is identical to the valley known for RC members as constructed by Kani.

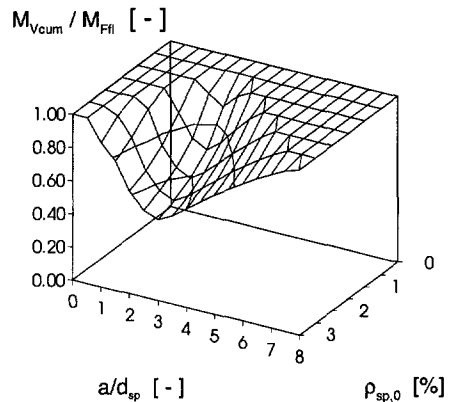


Fig. 11.6 Flexural shear valley for fully plated member and strengthening ratio 1.0

Partially Plated Members

When partially plated members are analysed, plate-end shear has to be accounted for. However, at first in this analysis, only flexure and plate-end shear are considered. Fig. 11.7 illustrates the plate-end shear load of a member with its plate stopped 50 mm short of the support. Hence, $L/a = 1/16$. The plate-end shear model is only applicable for $a > L + d_s$, so the maximum load could only be predicted for a/d_{sp} ratios higher than 1.5. The graph clearly indicates that the plate-end shear load is dependent on the (internal) reinforcement ratio, and independent of the shear span-to-depth ratio. Fig. 11.8 illustrates the plate-end shear moment capacity of the partially plated member. By virtue of the increased shear span, the moment bearing capacity increases.

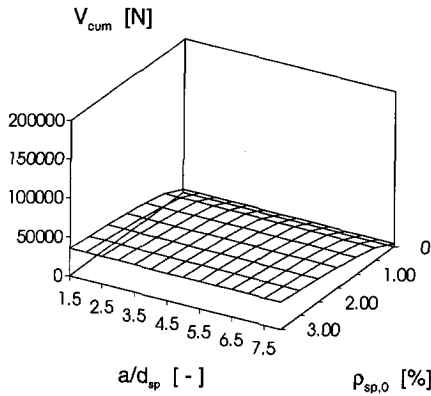


Fig. 11.7 Plate-end shear load for $L/a=1/16$

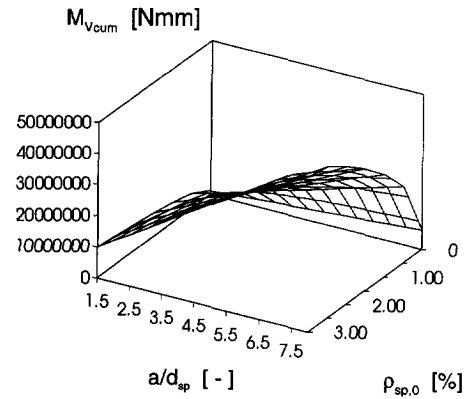


Fig. 11.8 Plate-end shear moment for $L/a=1/16$

After the flexural moment and the plate-end shear moment have been calculated, the plate-end shear moment is expressed as a percentage of the flexural moment. Accordingly, Fig. 11.9 is constructed. It evidently shows a very steep plate-end shear valley in comparison with the flexural shear valley of fully plated beams. The deepest point of the valley is reached at an a/d_{sp} ratio of 1.5. This value results from the restriction of the range of application, namely that $a > L + d$.

To visualise full shear flexure interaction, both types of shear failure have to be taken into account. Not only plate-end shear failure is likely to occur in partially plated members, it is also possible that flexural shear failure dominates plate-end shear failure. Hence, Fig. 11.6 and Fig. 11.9 are merged into Fig. 11.10. It sketches the interaction between plate-end shear, flexural shear and flexure of the L50 member. It is seen from the shape of the shear valley that both plate-end shear and flexural shear play an important role in the failure behaviour. Generalising, at lower shear span-to-depth ratios plate-end shear dominates flexure and flexural shear, at higher ratios flexural shear dominates plate-end shear and flexure. Furthermore, it is concluded that only at low reinforcement ratios the member exhibits flexural failure by yielding of both the internal and external reinforcement.

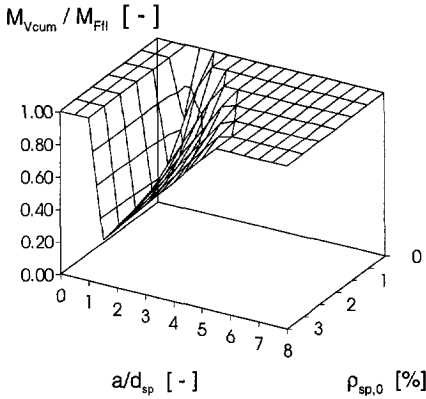


Fig. 11.9 Plate-end shear valley for $L/a=1/16$

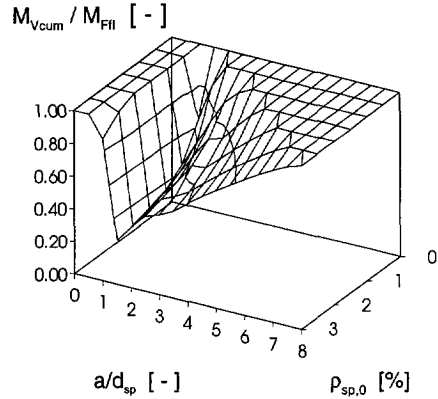


Fig. 11.10 Shear flexure interaction for $L/a=1/16$

The same analyses is carried out for a partially strengthened beam with the plate stopped at a distance of 200 mm before the support. Accordingly, $L/a = 1/4$. Then, Fig. 11.11 and Fig. 11.12 are constructed. For this configuration, the deepest point of the plate-end shear valley lies at a shear span-to-depth ratio of 2. Concerning shear flexure interaction, flexural shear hardly occurs at the various combinations of reinforcement ratio and shear span-to-depth ratio, so plate-end shear is dominant. Flexural failure only occurs at the lower reinforcement ratios.

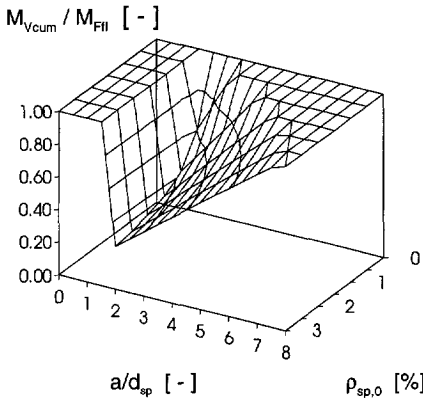


Fig. 11.11 Plate-end shear valley for $L/a=1/4$

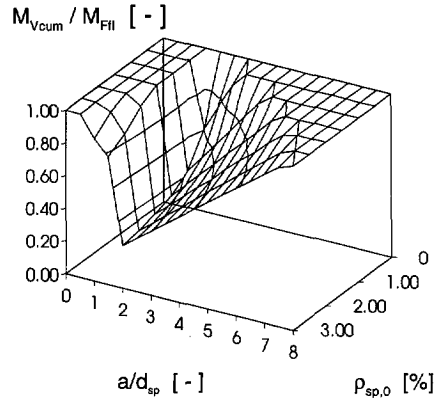


Fig. 11.12 Shear flexure interaction for $L/a=1/4$

When the shear-flexure interaction graphs of the L50 and the L200 beams are mutually compared, one may draw the conclusion that, compared to flexural shear and flexure, plate-end shear is more dominant if the bonded-on plate is stopped at a larger distance from the support. Then, also at higher shear span-to-depth ratios, for which beams fail normally in flexure, plate-end shear dominates failure.

11.3.3 Variation of Unplated Length and Strengthening Ratio

General

Now that shear flexure interaction is established for a strengthening ratio of 1.0, it is interesting to investigate the influence of the strengthening ratio on the interaction if the two unplated lengths are compared. Strengthening ratios of 0.5 and 2.0 are analysed. Notice that in comparison with the case in which the strengthening ratio was 1.0, the total amount of reinforcement remains constant. However, in the case of a ratio of 0.5, one third of the total reinforcement is externally bonded, and two thirds consists of internal bars. In the case of a ratio of 2.0, two thirds of the total amount of reinforcement is external and one third is internal. Because the yield stresses of the steel plate and the internal bars are distinct, a variation in the strengthening ratio directly means that the maximum flexural capacity is different for the two cases. At a reinforcement ratio of 1.0%, the flexural capacity for $A_p = 0.5A_s$ is 15.0 kNm, but only 12.7 for $A_p = 2.0A_s$. Hence, when the results of the interaction between shear and flexure for 0.5 and 2.0 are mutually compared, one might get the wrong impression as far as the depth of the shear valley is concerned. In other words, a ratio shear moment-to-flexural moment of 1.0 seems identical for a 0.5 and a 2.0 strengthening ratio, but are dissimilar when the absolute values are compared.

Fully Plated Members

Fig. 11.13 and Fig. 11.14 show the flexural shear valleys for strengthening ratios of 0.5 and 2.0, respectively, if the plates are fully bonded. The flexural shear valleys indicate that at higher reinforcement ratios the flexural shear capacity dominates. Note that the maximum reinforcement ratio for $A_p = 2.0A_s$ is 3.2% and for $A_p = 0.5A_s$ is 2.5%. In the latter case the concrete compression zone crushes before yielding.

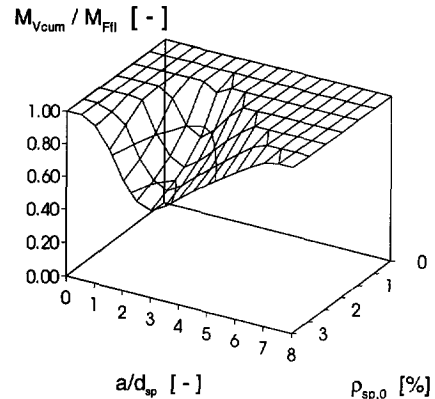
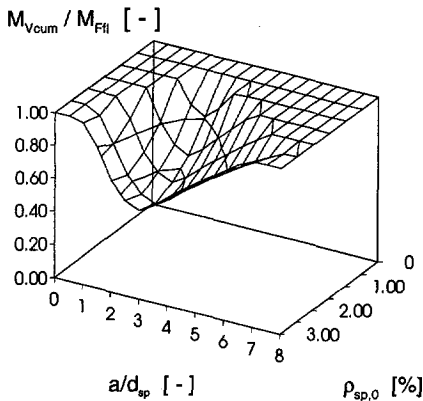


Fig. 11.13 Flexural-shear valley $A_p = 0.5 A_s$ Fig. 11.14 Flexural-shear valley $A_p = 2.0 A_s$

Partially Plated Members

For the partially plated members, plate-end shear is analysed. For the beam with the 50 mm unplated length, the plate-end shear load is higher than that of the beam with

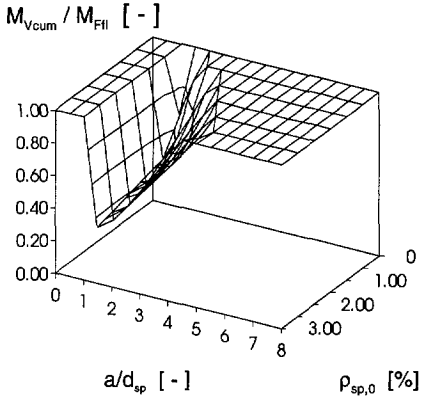


Fig. 11.15 Plate-end shear valley for $A_p = 0.5 A_s$ and $L/a=1/16$

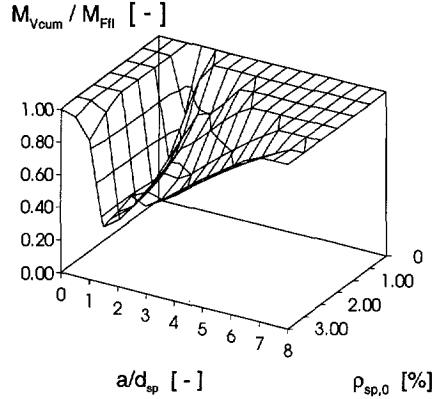


Fig. 11.16 Shear flexure interaction for $A_p = 0.5 A_s$ and $L/a=1/16$

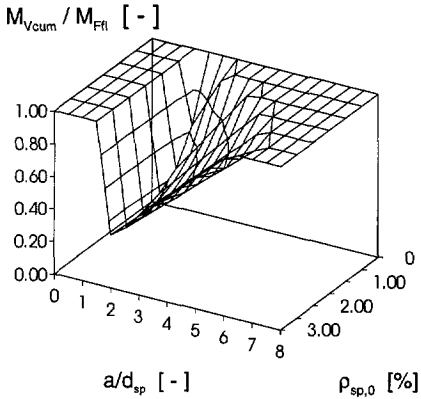


Fig. 11.17 Plate-end shear valley for $A_p = 0.5 A_s$ and $L/a=1/4$

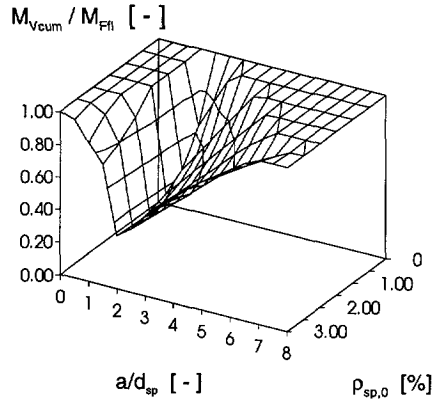


Fig. 11.18 Shear flexure interaction for $A_p = 0.5 A_s$ and $L/a=1/4$

the 200 mm unplated length. The figures with the odd numbers, Fig. 11.15 up to and including Fig. 11.21, sketch the interaction between plate-end shear and flexure for 50 mm and 200 mm unplated length, with strengthening ratios of 0.5 and 2.0. If the shapes of the plate-end shear valleys of the four graphs are compared, it may be concluded that lower strengthening ratios are more favourable over higher strengthening ratios. Moreover, smaller unplated lengths are more favourable than larger unplated lengths.

The even figures Fig. 11.16 up to and including Fig. 11.22 visualise a complete overview of shear flexure interaction. For the case in which the strengthening ratio is 0.5, flexural shear could mainly give rise to shear problems. Nevertheless, the figures show that plate-end shear could be very dominant compared to flexural shear and flexure. Even, for the case of a strengthening ratio of 2.0 and $L/a = 1.4$, plate-end shear fully dominates flexural shear.

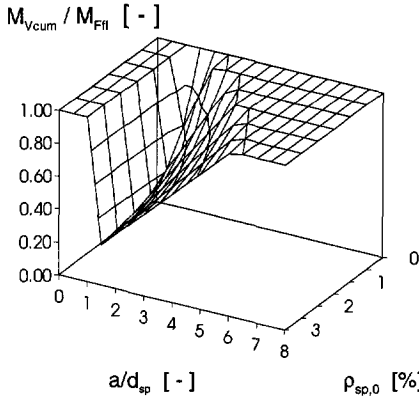


Fig. 11.19 Plate-end shear valley for $A_p = 2.0 A_s$ and $L/a=1/16$

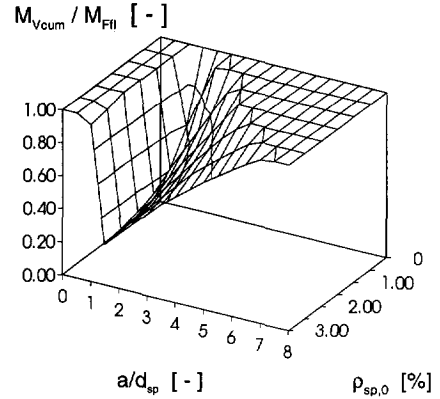


Fig. 11.20 Shear flexure interaction for $A_p = 2.0 A_s$ and $L/a=1/16$

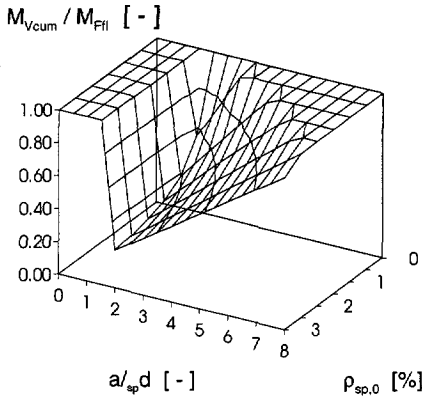


Fig. 11.21 Plate-end shear valley for $A_p = 2.0 A_s$ and $L/a=1/4$

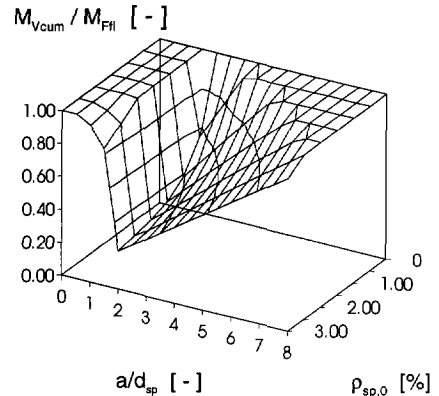


Fig. 11.22 Shear flexure interaction for $A_p = 2.0 A_s$ and $L/a=1/4$

Interaction between Plate Separation and Flexure

In practice, structural members are mostly provided with internal web reinforcement. Consequently, the above mentioned flexural shear and plate-end shear will not play a role by virtue of these stirrups. But, in Chapter 9 it was proven that the plate-end shear load is a lower bound load for the maximum load at which the externally bonded plate separates. Accordingly, in case of stirrup provision, the interaction graph could also be used to determine whether plate separation or flexure governs failure. Of course, then failure by flexural shear could not occur. Then, plate separation and flexure interact like Fig. 11.15, Fig. 11.17, Fig. 11.19 and Fig. 11.21 depict. The graphs show the lower bound capacity of plate-end shear in relation to flexure. Hence, at lower strengthening ratios and smaller unplated lengths, the response of a partially plated beam shifts more to the flexural capacity.

11.3.4 Discussion: Initial Stresses and Unloading

In the previous section, the interaction between shear and flexure was investigated. With respect to these graphs, some remarks must be made with regard to the validity of the outcome of the results in practical situations.

When existing concrete structures are strengthened, they already carry dead and live loads. Hence, initial stresses are present in the structure. Before actual strengthening, the structure could be unloaded down to a certain resulting flexural moment M_o . But even then, certain stresses remain in the structure. Presently, Brosens & Van Gemert [1997]⁴ deal with this subject, see also section 2.1.2. After strengthening, the beam could be loaded up to a maximum flexural moment M_p , which is much higher than the initial flexural moment M . At the maximum flexural moment M_p the new stress situation could be calculated to indicate whether the reinforcement yields or the concrete compression zone crushes, but this situation is very dependent on the unloading situation. With respect to reinforcement yielding, two extremes could be considered, namely fully unloading, $M_o / M = 0$, or no unloading, $M_o / M = 1$. For the first situation, it is likely that the external plate yields at a flexural moment much lower than M_p . Conversely, for the second situation it is likely that the internal bars yield before the ultimate moment M_p is attained. After yielding of either the internal bars or external plate, a redistribution of reinforcement stresses will take place, and both reinforcements will ultimately yield.

In the shear-flexural interaction graphs the horizontal plateau at M_{Vcum} / M_{Fl} indicates yielding of both the internal bars and the external plate. However, with reference to the above mentioned discussion, the question may rise if the shear-flexural interaction graph might change if the initial stresses and unloading would be taken into account. With respect to the flexural capacity, it is possible that the concrete compression zone crushes before the maximum flexural capacity is attained. With respect to plate-end shear, the author wants to underline that this failure type is not dependent on the initial stress situation. Plate-end shear expresses the shear capacity of the unstrengthened part of the beam beyond the plate end. This shear capacity is not dependent on the initial stress situation, but is only dependent on the shear load which acts on the strengthened member. This conclusions also holds true for flexural shear. Whether the flexural shear capacity is exceeded or not, is only dependent on the acting shear load.

With reference to the question raised above, the following answer can be given. Given that crushing of the concrete compression zone is not taken into account, the shear-flexure interaction graphs do not modify due to either the initial stress situations or unloading of the structure.

11.4 Conclusions

In this chapter, an application of the plate-end shear model is worked out. The plate-end shear model is used together with the flexural shear model of Rafla to visualise the interaction between shear and flexure. The analyses clearly showed that low strengthening ratios and short unplated lengths of the bonded-on steel plate are

preferable. Then, the influence of the brittle plate-end shear mechanism or separation of the steel plate is not so dominant. Conversely, if a large amount of external reinforcement is bonded to strengthen for flexure, plate-end shear or plate separation can be very dominant. Then, it fully dominates flexural shear and at the same time, it dominates flexure in a large range of reinforcement ratios and shear span-to-depth ratios.

12. RETROSPECTIVE VIEW, SUMMARY AND OUTLOOK

This last chapter concludes this thesis on the design of beam shear and plate anchorage of members strengthened with externally bonded steel plates. It summarises the research described in this thesis and resumes the most important findings. In addition, it gives an outlook on the development of the strengthening technique and recommends topics to be investigated.

Introduction

Both the serviceability and the ultimate load bearing capacity of an existing concrete structure may be inadequate to meet the users demands. An attractive solution is the strengthening of the existing structure by means of externally bonded steel plates. Research into the plate bonding technique started in the 1960's. Nowadays, strengthening of existing reinforced concrete structures by this plate bonding technique is accepted in Europe as an efficient way of improving the serviceability limit or/and ultimate limit state. Still, in the Netherlands in practical applications this method is not often used. The strengthening technique is mainly applied to increase the flexural capacity: steel plates are bonded to the tension side of an RC member, thus providing it with additional longitudinal reinforcement. Besides, also applications concerning shear strengthening are reported in literature.

Research Objective

The research study aims at developing a design method for beam shear and plate anchorage, and aims to describe the interaction between the flexural capacity, shear capacity and premature failure of the externally plated member.

State-of-the-Art

A review of the available literature showed that particularly the shear capacity of members has hardly been investigated. Attention had been paid to applying bonded-on shear plates for shear strengthening, however, the role of shear when concrete members were only strengthened in flexure with externally bonded plates, still remained unclear. This was only recognised by Oehlers [1992] in his investigation on shear flexure interaction. In spite of this research program, no firm conclusions concerning beam shear could be drawn. Even so, he did conclude that plate anchorage was dependent on the formation of shear cracks. Also, until now only little has been published in the field of the plate bonding technique regarding the use of finite element analyses. In comparison with analytical analyses, the use of a numerical model enables us to gain more insight into the deformational behaviour and the stress redistribution during failure. The current research study was,

therefore, conducted to provide more information on beam shear and plate anchorage, since it was believed that the two failure modes were inseparable.

Experimental Study

To gain insight into the failure behaviour of reinforced concrete members strengthened with externally bonded steel plates, a test program was developed. Experiments were carried out on beam-ends with regard to plate anchorage and beam shear.

In the plate anchorage tests, three parameters have been investigated, namely, the unplated length, the addition of a bolt and the influence of repeated loading. The unplated length is defined as the distance between the plate end and the centre of the support. A larger unplated length showed that the maximum load bearing capacity decreased. At the plate end, a typical *plate end crack* initiated which developed into a shear crack. However, by virtue of the internally applied stirrups, this shear crack was arrested and the bonded-on plate separated from the concrete member at the level of the longitudinal reinforcement. Hence, by applying a bolt at the anchorage zone of the plate, the maximum load bearing capacity could be increased. At the same time, it was clearly observed that the failure mechanism changed from brittle concrete cover rip-off to a more ductile type of interface failure. Two effects played a role. On the one hand, by applying the bolt through the unreinforced concrete cover, actually a reinforcing bar was applied which arrested the concrete peeling crack. Then, by the developed shear stresses at the concrete-epoxy interface, the interface yielded. On the other hand, as a consequence of applying the bolts with an initial force, a normal compressive stress acted at the anchorage zone. Hence, the combined compressive-shear stresses increased the load for which at the interface the plasticity criterion was reached. Furthermore, experiments with repeated loading showed no negative effect on the anchorage capacity. Conversely, it did affect the growth of the shear crack at the plate end.

In the beam shear tests, the influences of the geometry of the steel plate and the concrete members on the shear resistance were investigated. Two types of shear failure were distinguished, namely *flexural shear* and *plate-end shear*. Flexural shear was observed when concrete beam-ends were fully plated, that is to say, with their plate bonded beyond the support. Failure occurred by the development of a flexural crack into a flexural shear crack. Conversely, plate-end shear was observed when the concrete beam-ends were partially plated, that is, with their plate stopped at a certain distance from the support. During the tests, it was observed that after the initiation of the plate end crack, this crack developed into a plate-end shear crack. This plate-end shear crack grew into the direction of the loading point and the support. At the same time, the initial plate end crack closed and transferred stresses as a result of aggregate interlock. The unplated length clearly affected the maximum plate-end shear load. Concerning plate anchorage, a larger unplated length led to a decrease of the maximum shear load capacity. Variation of the external reinforcement ratio by varying the plate area hardly affected the maximum shear load.

Numerical Study

Complementary to the experimental program, numerical simulations have been performed. In order to analyse both plate-end shear and plate separation, the smeared-discrete crack model has been developed. This finite-element model enabled the analyses of various failure types of members strengthened in flexure by means of fully or partially bonded steel plates. Moreover, by the choice of smeared and discrete cracking combined with softening, the model proved to be very accurate. The simulations confirmed the experimental observation that particularly the unplated length influenced the plate-end shear load. It also provided numerical evidence that the length of the shear span did not affect the maximum plate-end shear load for practical shear span-to depth ratios. The mechanism of plate-end shear was thoroughly analysed. It showed that the plate end crack imposes large bond stresses between the internal reinforcement and the concrete, and caused an alteration of the vertical distributed shear stress. Hence, the shear stress increased substantially in the horizontal and vertical cross section beyond the end of the plate. As a consequence, it gave rise to the development of the plate end crack into a plate-end shear crack. Basically, the numerical simulations proved that the plate-end shear mechanism is identical to the flexural shear mechanism, and that the location of the shear crack is forced to occur at the plate end.

Interpretation of Results

The experiments and numerical simulations provided clear evidence that plate-end shear plays a dominant role in the failure behaviour of strengthened beams, also in the case of plate separation. In order to predict the plate-end shear load, a design method has been derived based on observations from the experiments and the simulations. In analogy with Kim & White [1991], who analytically described the mechanism of flexural shear, a fictitious shear span is defined. The fictitious shear span is activated by the unplated length of the partially strengthened member. This fictitious shear span is calculated on the basis of this unplated length, the reinforcement ratio of the unstrengthened part and the effective depth of the beam with regard to the internal bars. The design method for plate-end shear is based on the CEB-FIP MC90 expression on flexural shear and the fictitious shear span:

plate-end shear capacity

$$V_{cu} = \tau_{cu} b d_s$$

nominal maximum shear stress

$$\tau_{cu} = \xi \sqrt[3]{3 \frac{d_s}{a_L} \left(1 + \sqrt{\frac{200}{d_s}} \right) \sqrt[3]{\rho_{s,0} f_c}}$$

$$\xi = 0.18 \text{ for mean stress, } f_c = f_{cm}$$

$$\xi = 0.15 \text{ for design stress, } f_c = f_{ck}$$

fictitious shear span

$$a_L = \sqrt[4]{\frac{(1 - \sqrt{\rho_s})^2}{\rho_s}} d_s L^3$$

application restrictions

$$a > L + d$$

$$a_L < a$$

The plate-end shear model satisfactorily predicts the mean maximum shear load, so that an expression for the design shear load of a partially plated beam could be derived. Moreover, it was shown that the plate-end shear mechanism not only affected beam shear, but in the case of stirrup reinforcement, it also affected the plate anchorage capacity. A comparison with experimental results on plate separation from the literature showed that the plate-end shear model may be used as a lower bound model for the ultimate load at which the plate separates. By virtue of suspension bolts installed at the plate end and anchored into the concrete compression zone, one could correctly detail for plate-end shear and plate separation.

Now that expressions are available to predict flexural shear as well as plate-end shear, shear flexure interaction was visualised by means of shear valleys. Compared to the flexural shear capacity and the flexural capacity, strengthening applications with an incorrect design of the bonded-on plates leads to the dominance of plate-end shear. In particular, due to smaller shear span-to-depth ratios and larger unplated lengths of the partially plated shear span, the maximum load bearing capacity decreased in comparison with flexure and flexural shear.

Application for Engineering Practice

The developed plate-end shear model is very useful for the engineering practice. About 90% of the existing concrete structures strengthened are concrete slabs in buildings or bridges. Hence, no shear reinforcement is provided. Although it is mostly memorised that the deformational restrictions and not the shear capacity play a role in these structural concrete members, this study has revealed that plate-end shear must be accounted for. The engineering practice is not familiar with plate-end shear, and compared to the well-known flexural shear, plate-end shear is a much more dominant type of shear failure. Particularly this holds true for higher strengthening ratios and larger unplated lengths. This thesis provides a design method for plate-end shear which is very transparent for the structural engineer, who does not have a lot of experience with the plate bonding technique. Moreover, this study also provides a design method for provisions to detail for plate-end shear by the addition of suspension reinforcement (bolt anchored in compression zone).

Recommendations

Four years of experience by the author with research on the plate bonding technique, asks for some recommendations.

Structural engineers are often reluctant to utilise epoxies for structural applications. The structural long term contribution of this material is mostly underestimated. Therefore, the structural applications of epoxies in concrete structures is still scarce in comparison with the use in timber structures, even more in comparison with applications in the aircraft and car industry. In addition to bonding plates, adhesive bonded joints are utilised for example in the field of precast segmental construction. Still, the overall application remains scarce. There is enough experimental evidence that shows that concrete itself by the low tensile

strength is the weakest link, and that shows that the epoxy contributes to the structural performance.

By reviewing literature on the plate bonding technique and performing theoretical and numerical analyses, a lot of information was obtained. However, to gain real and very useful experience within the field of plate bonding, one is almost obliged to conduct experiments. By performing plate bonding operations and carrying out experiments, observing the sequence of crack initiation, development, and localisation, very valuable information is gathered which is indispensable for a researcher. Such practical experiences positively influence the way of thinking of the researcher and, thus, contributes to a satisfactory outcome of the project.

One must be aware that, if existing concrete structures are strengthened with externally bonded steel plates, additional failure mechanism are introduced. Peeling of the bonded-on plate by plate separation is well known, but the possibility of plate-end shear was hardly or not recognised. It is often remarked that shear failure hardly plays a role in the failure behaviour of strengthened members, but then flexural shear or web shear is meant. Plate-end shear is a newly discovered type of failure, which is fully understood as a result of this research project. It is therefore advised to take plate-end shear into account and to design for plate-end shear as well.

It is advisable to bond thin, wide steel plates, which are stopped as close as possible to the support. To reduce the area of grit-blasting and the amount of epoxy, a optimum steel cross section of plate width-over-thickness ratio of 25 may be applied when the plate-end shear model is used to calculate the maximum load bearing capacity.

When structures are strengthened externally, it is strongly recommended to apply bolts at the end of the plate, anchored in the concrete compression zone. The research study showed that these bolts are needed to provide additional suspension reinforcement at the plate end, where the concrete compression strut of the external plate system stops. In such a way, the compressive strut could be suspended to the concrete compression zone and, subsequently, transferred to the support. In this way, internal equilibrium is always ascertained after plate-end shear cracking.

Development of Plate Bonding Technique

The attractiveness of the plate bonding technique concerning the structural performance and cost-effective application will increase its demand in the forthcoming years. And, although the technique has already existed for thirty years, new developments still take place.

For several years, research has been carried out in which the steel plates are replaced by so-called carbon fibre reinforced plastic (CFRP) sheets. Mainly, the high tensile strength, the relatively small thickness of the sheets and the non-corrosive character of the non-metallic material are advantages. Also, CFRP is much easier to apply, because it is lighter and not restricted in length. And, although steel is cheaper than CFRP, labour and operational costs also have to be considered, which are more favourable for the CFRP sheets. Despite these clear advantages, steel plates are still used in practice because the material has proven its performance (high stiffness) and the costs are very competitive. Beams strengthened with

externally bonded CFRP sheets show a very similar failure behaviour in comparison with steel plates. However, additional failure modes were observed such as CFRP sheet rupture and debonding due to peeling of the sheet as a result of shear cracking. Also, the contribution of the CFRP sheets to the shear resistance must be neglected compared to steel plates.

With the use of composite CFRP materials, the plate bonding technique has been extended to pretensioning. Unidirectional CFRP sheets are pretensioned and applied with epoxy to the concrete structure. However, only laboratory tests have been carried out, which also indicated that additional mechanical anchorage systems are needed to efficiently anchor the pretensioned CFRP sheets.

Needs for Future Work

Although the main objective of this research project was achieved, some additional questions were raised during the work. Two questions will be dealt with as an encouragement for future work.

In the Netherlands, an estimated percentage of about 90% of the strengthening works carried out consists of concrete slabs in buildings or flyovers. Despite this large amount, hardly any research has been carried out on the strengthening of floors. Beams are easier to handle in the laboratory. The results are expected also to hold true for slabs, and results are extrapolated from beams to slabs. However, the question is raised if this is true, because experiments showed that width effects do play a role. With respect to the plate-end shear model, the influence of the width of the bonded-on plate with regard to the concrete width is not analysed. Rules for minimum and maximum distances between the bonded-on plates must be derived.

If existing concrete structures are strengthened, they are already stressed by the dead load of the structure. If such a structure is not unstressed by supporting scaffolding during the strengthening work, a non-uniform stress distribution exists over the height of the structure when it is loaded. This non-uniform stress distribution is often neglected during experimental research, but design calculations have to take these initial stresses into account.

REFERENCES

Note: primary and secondary literature are grouped into the research institutes, and referred to in the text by a number in superscript

1) L'Institut technique du Bâtiment et des Travaux Publics, France

- L'Hermite, R. and Bresson, J (1967a). Béton armé d'armatures collées. *Rilem International Symposium Synthetic Resins in Building Construction*. Paris 4-6 Sept 1967, pp 175-203.
- L'Hermite, R (1967b). l'Application des colles et résines dans la construction - Le béton à coffrage portant. *Annales d'Institut Technique de Bâtiment et des Travaux Publics, série béton et béton armé*. No 239, Nov 1967, pp 1481-1498.
- Bresson, J. (1971). Nouvelles recherches et applications concernant l'utilisation des collages dans les structures. Béton plaqué. *Annales d'Institut Technique de Bâtiment et des Travaux Publics, série béton et béton armé*. No 278, Feb 1971, pp 22-55.
- L'Hermite, R (1977). Use of bonding techniques for reinforcing concrete and masonry structures. *Materials and Structures*, Vol 10, No 56, 1977, pp 85-89.
- Theillout, J.N. (1986). Repair and strengthening of bridges by means of bonded plates. *RILEM International Symposium on adhesion between polymers and concrete*. Aix-en-Provence, Sept 1986, pp 601-621.
- Poineau, D, Theillout, J. and Cusin, F. (1992). Réparation et renforcement de structures de bâtiments et d'ouvrages d'art - application des techniques de tôles collées et de précontrainte additionnelle. *Annales de l'Institut Technique du Bâtiment et des Travaux Publics, série technique générale de la construction*. No 501, Feb 1992, pp 26-46.

2) Transport and Road Research Laboratory, Crowthorne, England

- Calder, A.J.J. (1979). Exposure tests on externally reinforced concrete beams - First two years. *Transport and Road Research Laboratory, Crowthorne*. Report SR529, 1979.
- Raithby, K.D. (1980). External strengthening of concrete bridges with bonded steel plates. *Transport and Road Research Laboratory, Crowthorne*. Digest of Report SR612, 1980.
- Raithby, K.D. (1982). Strengthening of concrete bridge decks with epoxy-bonded steel plates. *International Journal of Adhesion and Adhesives*. Vol 2, No 2, 1982, pp 115-118.
- MacDonald (1981). Strength of bonded shear joints subjected to movement during curing. *International Journal of Cement Composites and Lightweight Concrete*. Vol 3, No 4, 1981, pp 267-272.
- Macdonald, M.D. (1982a). The flexural performance of 3.5 m concrete beams with various bonded external reinforcements. *Transport and Road Research Laboratory, Crowthorne*. Digest of Report SR728, 1982.
- MacDonald, M.D., Calder, A.J.J. (1982b). Bonded steel plating for strengthening. *International Journal of Adhesion and Adhesives*. Vol 2, No 2, 1982, pp 119-127
- Lloyd, G.O. and Calder, A.J.J. (1982). The microstructure of epoxy bonded steel-to-concrete joints. *Transport and Road Research Laboratory, Crowthorne*. Report SR705, 1982.
- Mays, G. and Calder, A. (1988). External plates extend reinforcement's reach, *Concrete*. Nov 1988, pp 25-28.

Calder, A.J.J. (1988). Exposure tests on externally reinforced concrete beams - Performance after 10 years. *Transport and Road Research Laboratory, Crowthorne*. Digest of Report RR129, 1988.

Calder, A.J.J. (1989). Exposure tests on 3.5 m externally reinforced concrete beams - The first eight years, *Transport and Road Research Laboratory, Crowthorne*. Digest of Report RR191, 1989.

3) EMPA, Dübendorf and ETH Zürich, Swiss

Ladner, M. Flüeler, P. (1974). Verstärken von Tragkonstruktionene mit geklebter Armierung. Telefongebäude Füsslistrasse in Zürich. Umbau und Renovation. Versuche an Stahlbetonbauteilen met geklebter Armierung. *Schweizerische Bauzeitung*. 92. Jahrgang, Heft 19, Mai 1974, pp 463-470.

Ladner, M. and Weder, Ch. (1981). Concrete structures with bonded external reinforcemen. *EMPA*, Report No 206, 1981, Dübendorf.

Weder, Ch. and Ladner, M. (1981). Application of epoxy adhesives in the field of bonded externally reinforced concrete structures. *IABSE British National Group, Colloquium on the effective use of materials in structures*. Imperial College, London, 7/8 Sept 1981, pp 123-135.

Ladner, M. and Weder, Ch. (1983). Belastungsversuche an 12 fünfjährigen Stahlbetonbalken mit aufgeklebter Bewehrung. *EMPA*, Bericht nr. 37'846/4, Februar 1983, pp 1-15.

Holtgreve, K. (1986); A contribution in regard to behaviour of Reinforced Tee-beams with bonded flatsteel componenets under fatigue loads, *RILEM International Symposium on Adhesion between Polymers and Concrete*, Aix-en-Provence, 1986, pp 528-533.

Ladner, Holtgreve (1989); Verstärken von Stahlbetonbauten mit angeklebte CFK-lamellen, *Report*, IABSE Symposium, Lissabon, 1989, pp677-682.

Meier, U. (1987); Bruckensanierung mit hochleistungs Faserverbindstoffen, *Material + Technik*, 15. Jahrgang, Dez 1987, pp 125-128.

Meier, U. (1988); Design and producing materials by combination, *Materials and Structures*, 21, 1988, pp 85-89.

Kaiser, H.P. (1989); Bewehren von Stahlbeton mit Kohlenstoffverstärkten Epoxidharzen, *Dessertation*, ETH Zürich, 1989.

Ladner, M., Pralong, J. and Weder, Ch. (1990) Geklebte Bewehrung - Bemessung und Erfahrungen, *EMPA Dübendorf*, Bericht Nr 116/5, April 1990.

Meier, U. (1992); Carbon fiber-reinforced polymers - Modern materials in bridge engineering, *Structural Engineering International*, Science and Technology, No 1, 1992, pp 7-12.

Deuring, M. and Meier, U; Projekt Ibachbrücke, *EMPA*, Switzerland.

Deuring, M. (1993); Verstärken von Stahlbeton mit gespannten Faserverbundwerkstoffen, *Dissertation*, ETH Zürich, 1993.

4) Katholieke Universiteit Leuven, Leuven, Belgium

Van Gemert, D. (1979) Versterken en herstellen van betonconstructies met oplijmwapening, *Cement*, nr. 10, 1979, pp 437-451.

Van Gemert, D., De Buck, J., Van Aelst, J. and Van der Mijnsbrugge, J. (1980a); Krachtoverdracht in gelijmde beton-staal verbindingen, *Tijdschrift der Openbare Werken van België*, Nr 6, 1980, pp 493-505.

Van Gemert, D. (1980b); Force transfer in epoxy bonded steel/concrete joints, *International Journal of Adhesion and Adhesives*, Vol 1, No 2, 1980, pp67-72.

- Van Gemert, D. (1980c); Reparatie van brandschade aan een gewapend-betonplaat, *Cement*, XXXII, Nr 8, 1980, pp 444-446.
- De Buck, J., Van Essche, Th., Van Gemert, D. and Gamski, K. (1981); Conceptie, berekening en proefprogramma voor de herstelling van twee bruggen in voorgespannen beton, *Tijdschrift der Openbare Werken van België*, Nr 2, 1981.
- Van Gemert, D. and Van den Bosch, M. (1982a); Dimensionering van gelijkde wapeningen bij op buiging belaste elementen, *Tijdschrift der Openbare Werken van België*, Nr 1, 1982.
- Van Gemert, D. (1983a); Uitvoering en controle van gelijkde wapening, *S&E-publikatie - Reparaties aan Betonconstructies*, Nr 5, Maart 1983, pp 84-96.
- Van Gemert, D. (1983b); Reparatie van doorbuigende en gescheurde betonconstructies met opgelijmde wapening, *PT Bouwtechniek*, 38, Nr 4, 1983, pp 25-28.
- Van Gemert, D and Maesschalck, R. (1983c); Structural repair of a reinforced concrete plate by epoxy bonded external reinforcement, *The International Journal of Cement Composites and Lightweight Concrete*, Volume 5, Number 4, November 1983, pp 247-255.
- Van Gemert, D, Vanden Bosch, M and Ladang, C (1986a); Design method for strengthening reinforced concrete beams and plates, *Report 32-ST-17*, Laboratorium Reyntjens, Jan 1986, p78.
- Van Gemert, D. and Van den Bosch, M. (1986b); Long-term performance of epoxy bonded steel-concrete joints, *RILEM International Symposium on adhesion between polymers and concrete*, Aix-en Provence, 1986, pp 518-527.
- Van Gemert, D, Norree, F and Ulix, E (1987); Stress analysis in epoxy bonded steel-concrete joints, *European Mechanics Colloquium 227 'Mechanical Behaviour of Adhesive Joints'*, France, Sept 1987,
- Van Gemert, D. (1990a); Berekening van gelijkde verbindingen, *De Constructeur*, nr 3, 1990, pp 56-63.
- Van Gemert, D. (1996); Design applications and durability of plate bonding technique, *International congress 'Concrete, In the Service of Mankind'*, Dundee, 24-28 June 1996, pp 559-569.
- Brosens, K., Van Gemert, D. (1997a); Anchoring Stresses between Concrete and Carbon Fibre Reinforced Laminates, *Proceedings IABSE Composite Construction - Conventional and Innovative*, 16-18 September 1997, Innsbruck, Austria.
- Brosens, K., Van Gemert, D. (1997b); Anchoring Stresses between Concrete and Carbon Fibre Reinforced Laminates, *FRPRS-3*, Japan, 1997.

5) Technischen Universität Carolo-Wilhelmina, Braunschweig, Germany

- Rostásy, F.S. and Ranisch, E.H. (1981); Verstärkung von Stahlbetonbauteilen durch angeklebte Bewehrung, *Betonwerk und Fertigteil-Technik*, Part I, Heft 1, 1981, pp 6-11, Part II, Heft 2, 1981, pp 82-86.
- Ranisch, E.-H. (1982); Zur Tragfähigkeit von Verklebungen zwischen Baustahl und Beton - Geklebte Bewehrung, *Dissertation*, Technische Universität Carolo-Wilhelmina, Braunschweig, 1982.
- Rostasy, F.S. and Ranisch, E-H (1984) *Strengthening of concrete structures with bonded fibre composites*, TU Braunschweig, Research Report.
- Ranisch, E.H. and Rostásy, F.S. (1986a); Bonded steel plates for the reduction of fatigue stresses of coupled tendons in multispan bridges, *RILEM International Symposium on adhesion between polymers and concrete*, Aix-en-Provence, 1986, pp 561-570.
- Rostásy, F.S. and Ranisch, E.H. (1986b); Koppelfugensanierung mit angeklebten Stahllaschen, *Bauingenieur*, 61, 1986, pp 305-311.

- Holzenkämpfer, P. (1989); Ingenieurmodell für das Verbundsystem Stahlbeton und Klebelasche. *Beiträge zum 22. Forschungskolloquium DAfStb*, TUBraunschweig 1989, pp 35-38.
- Holzenkämpfer, P. (1994); Ingenieurmodelle des Verbunds geklebter Bewehrung für Betonbauteile. *Dissertation*, Heft 108, Aug 1994, p 214.
- Hankers, Ch. (1995); Zum Verbundverhalten laschenverstärkter Betonbauteile unter nicht vorwiegend ruhender Beanspruchung. *Dissertation*, Heft ---, Nov 1995, p 202.
- Rostásy, F.S., Holzenkämpfer, P. and Hankers, Ch. (1996); Geklebte Bewehrung für die Verstärkung von Betonbauteilen. *Betonkalender 1996*, Teil II, pp 547-576.
- Rostásy, F.S., Neubauer, U. and Hankers, Ch. (1997); *Verstärkten von Betontragwerken mit geklebter äusserer Bewehrung aus Kohlenstoffaserverstärkten Kunststoffen*, Beton- und Stahlbetonbau, Heft 5, 1997

6) University of Sheffield, Sheffield, England

- Jones, R., Swamy, R.N., Bloxham, J. and Bouderalah, A. (1980); Composite behaviour of concrete beams with epoxy bonded external reinforcement, *International Journal of Cement Composites*, Vol 2, No 2, May 1980, pp 91-107.
- Swamy, R.N. and Jones, R. (1980); Technical Notes: Behaviour of plated RC beams subjected to cyclic loading during glue hardening, *International Journal of Cement Composites*, Vol 2, No 4, Nov 1980, pp 233-234.
- Jones, R., Swamy, R.N. and Ang, T.H. (1982); Under- and over-reinforced concrete beams with glued steel plates, *The International Journal of Cement Composites and Lightweight Concrete*, Volume 4, Number 1, February 1982, pp 19-32.
- Jones, R., Swamy, R.N. and Bloxham, J. (1986a); Crack control of reinforced concrete beams through epoxy-bonded steelplates, *RILEM International Symposium on adhesion between polymers and concrete*, Aix-en-Provence, Sept 1986, pp 542-555.
- Swamy, R.N., Jones, R. and Bloxham, J. (1987); Structural behaviour of reinforced concrete beams strengthened by epoxy-bonded steel plates, *The Structural Engineer*, Volume 65A, No 2, February 1987, pp 59-68.
- Jones, R., Swamy, R.N. and Charif, A. (1988); Plate separation and anchorage of reinforced concrete beams strengthened by epoxy-bonded steel plates, *The Structural Engineer*, Volume 66, No 5, March 1988, pp 85-94.
- Swamy, R.N., Jones, R. and Charif, A. (1989); The effect of external plate reinforcement on the strengthening of structurally damaged RC beams, *The structural Engineer*, Volume 67, No 3, February 1989, pp 45-56.
- Swamy, R.N. (1995a); Plate bonding - what can it do to your beams. *Construction Repair*, Vol 9, No 3, May-June 1995, pp 43-47
- Swamy, R.N. and Mukhopadhyaya, P. (1995b); Role and Effectiveness of non-metallic plates in strengthening and upgrading concrete structures. *Proceedings of the 2nd International Symposium on Non-metallic (FRP) Reinforcement for Concrete Structures*, August 1995, Ghent, pp 473-482.
- Swamy, R.N., Hobbs, B. and Roberts, M (1995c); Structural behaviour of externally bonded steel plated reinforced concrete beams after long term natural exposure. *The Structural Engineer*, Volume 73, No 16 August 1995, pp 255-261.
- Swamy, R.N., Jones, R and Charif, A (1996a); Contribution of externally bonded steel plate reinforcement to the shear resistance of reinforced concrete beams, ACI SP165
- Hobbs, B, Swamy, R.N. and Roberts, M (1996b); Corrosion performance of steel plated reinforced concrete beams after long term natural exposure. ACI SP-165

7) University of Wales, Cardiff, England

- Roberts, T.M. (1985); Finite difference analysis of composite beams with partial interaction, *Computers and Structures*, 21, No 3, 1985, pp 469-473.
- Roberts, T.M. (1988); Correspondence with reply on article by Jones, R., Swamy, R.N. and Charif, A.: Plate separation and anchorage of reinforced concrete beams strengthened by epoxy-bonded steel plates, *The Structural Engineer*, Volume 67, No 12, June 1988, pp 187-188.
- Roberts, T.M. and Haji-Kazemi, H. (1989a); Strengthening of under-reinforced concrete beams with mechanically attached steel plates, *The International Journal of Cement Composites and Lightweight Concrete*, Volume 11, Number 1, February 1989, pp 21-27.
- Roberts, T.M. and Haji-Kazemi, H. (1989b); Theoretical study of the behaviour of reinforced concrete beams strengthened by externally bonded steel plates, *Proc. Instn. Civ. Engrs*, Part 2, 87, March 1989, pp39-55.
- Roberts, T.M. (1989c); Approximate analysis of shear and normal stress concentrations in the adhesive layer of plated RC beams, *The Structural Engineer*, Volume 67, No 12, June 1989, pp 229-233.

8) University of Adelaide, Adelaide, Australia

- Oehlers, D.J. and Moran, J.P. (1989); Premature failure of externally plated reinforced concrete beams, *Journal of Structural Engineer*, Vol 116, No 4, April 1990, pp 978-995.
- Oehlers, D.J. (1990); Reinforced concrete beams with plates glued to their soffits, *Journal of Structural Engineer*, Vol 118, No 8, August 1992, pp 2023-2038.
- Oehlers, D.J. (1992); Discussion on Roberts and Haji-Kazemi, *Proc. Instn. Civ. Engrs*, Part 2, 87, Dec 1989, pp 651-663.
- Oehlers, D.J. (1997); Private Communications.

9) Luleå University of Technology, Luleå, Sweden

- Täljsten, B. and Elfgrén, L. (199-) *Externally bonded Reinforcement*, pp 1.130-1.134.
- Täljsten, B. (1989); *Strengthening of existing concrete structures with glued steel plates*, Analysis of concrete structures by fracture mechanics, Proceedings of the International RILEM Workshop, Abisko, Sweden, June 1989, edited by Elfgrén and Shah, Chapman and Hall, London, 1991, pp 208-219.
- Täljsten, B. (1994); Plate bonding, Strengthening of existing concrete structures with epoxy bonded plates of steel or fibre reinforced plastics. *PhD thesis Luleå University of Technology*, August 1994.
- Täljsten, B. (1995); Strengthening of structures using epoxy bonded steel- or fibre reinforced plastic plates. *IABSE Extending the Lifespan of Structures*, August 1995, San Francisco, pp 1173-1178.
- Täljsten, B. (1996); Strengthening of existing concrete structures by epoxy bonded plates of steel or fibre reinforced plastic plates, *International Congress Concrete, In the Service of Mankind*, Dundee, 24-28 June 1996, pp 623-632.
- Täljsten, B. (1997); Strengthening of Concrete Structure from Steel plates to Carbon Fibre Reinforced Plastic", *Proceedings FIP The Concrete Way to Development*, 9-12 March 1997, page 873-884, Johannesburg, South Africa.

10) King Fahd University of Petroleum & Minerals, Dhahran, Saudi Arabia

- Basunbul, I.A., Gubati, A.A., Al-Sulaimani, G.J. and Baluch, M.H. (1990); Repaired Reinforced Concrete Beams. *ACI Material Journal*, Vol 87, No 4, July-August 1990, pp 348-354.

- Sharif, A., Al-Sulaimani, G.J., Basunbul, I.A., Baluch, M.H. and Ghaleb, B.N. (1994a); Strengthening of initially loaded reinforced concrete beams using FRP plates. *ACI Structural Journal*, Vol 91, No 2, March-April 1994, pp 160-168.
- Al-Sulaimani, G.J., Sharif, A., Basunbul, I.A., Baluch, M.H. and Ghaleb, B.N. (1994b); Shear repair for reinforced concrete by fiberglass plate bonding, *ACI Structural Journal*, Vol 91, No 3, July-August 1994, pp 458-464.
- Ziraba, Y.N., Baluch, M.H., Basunbul, I.A., Sharif, A.M., Azad, A.K. and Al-Sulaimani, G.J. (1994c); Guidelines toward the design of reinforced concrete beams with external plates. *ACI Structural Journal*, Vol 91, No 6, Nov-Dec 1994, pp 639-646.
- Hussain, M., Sharif, A., basunbul, I.A., Baluch, M.H. and Al-Sulaimani, G.J. (1995a); Flexural behavior of precracked reinforced concrete beams strengthened externally by steel plates. *ACI Structural Journal*, Vol 92, No 1, Jan-Feb 1995, pp 14-22.
- Ziraba, Y.N., Baluch, M.H., Basunbul, I.A., Azad, A.K., Al-Sulaimani and G.J. Sharif, A.M. (1995b); Combined experimental-numerical approach to characterization of steel-glue-concrete interface. *Materials and Structures*, 28, 1995, pp 518-525.
- Sharif, A., Al-Sulaimani, G.J., Basunbul, I.A., Baluch, M.H. and Hussain, M. (1995c); Strengthening of shear-damaged RC beams by external bonding of steel plates. *Magazine of Concrete Research*, 47, No 173, Dec 1995, pp 329-334.
- Baluch, M.H., Ziraba, Y.N., Azad, A.K., Sharif, A.M., Al-Sulaimani, G.J. and Basunbul, I.A. (1995d); Shear strength of plated RC beams. *Magazine of Concrete Research*, 47, No 173, Dec 1995, pp 369-374.

11) Leopold Franzens Universität, Innsbruck, Austria

- Münger, F. Ammann, W. and Wicke, M. (1991) *Innovationen im Bereich der Geklebten Bewehrung*, Proceedings "Kleben Verbindet" February 1991, pp 185-190
- Wicke, M. and Fritsche, G. (1992) Dauerstandversuche an geklebten Bewehrung, Veruchsbericht, Technische Universität Innsbruck, Institut für Stahlbeton- und Massivbau, Bericht 13 / 1992.
- Pichler, D. (1993); *Die Wirkung von anpressdrücken auf die Verankerung von Klebelamellen*, Dissertation, Technische Universität Innsbruck, Innsbruck, Mai 1993.
- Pichler, D. , Wicke, M. (1993); *Verstärken von Betonbauteilen durch angeklebte Stahllamellen mit angepresster Endverankerung*, Beton- und Stahlbetonbau, Heft 10, pp261-265 and Heft11, pp 312-314, 1994.

12) University of Arizona, Tucson, USA

- Saadatmanesh, H. and Ehsani, M.R. (1990); Fiber composite plates can strengthen beams, *Concrete International*, March 1990, pp 65-71.
- Saadatmanesh, H. and Ehsani, M.R. (1991); RC beams strengthened with GFRP plates - I: Experimental Study, *Journal of Structural Engineering*, Vol 117, No 11, November 1991, pp 3417-3433.
- Wei An, Saadatmanesh, H. and Ehsani, M.R. (1991); RC beams strengthened with GFRP plates -II: Analysis and Parametric Study, *Journal of Structural Engineering*, Vol 117, No 11, November 1991, pp 3434-3451.
- Saadatmanesh, H. (1994); Fiber composites for new and existing structures, *ACI Structural Journal*, Vol 91, No 3, May-June 1994, pp 346-354.
- Saadatmanesh, H. (1995); *Wrapping with composite materials, Rilem Non-metallic (FRP) reinforcement for concrete structures*, editor L. Taerwe, 1995

13) Other publications on plate bonding technique

- Fleming, C.J. and King, G.E.M. (1967); The development of structural adhesives for three original uses in South Africa, *Materials and Structures*, No 37, 1967, pp 241-251.
- Lerchenthal, C.H. (1967); Bonded steel reinforcement for concrete slabs, *Materials and Structures*, No 37, 1967, pp 263-269.
- Kajfasz, S. (1967); Concrete beam with external reinforcement bonded by glueing, *RILEM International Symposium on adhesion between polymers and concrete*, Aix-en-Provence, 1986, pp 141-151.
- Et Al, (1974); Telefongebäude Füsslistrasse in Zürich - Umbau und Renovation, *Schweizerische Bauzeitung*, 92. Jahrgang, Heft 19, 9. Mai 1974, pp 457-474.
- Hugenschmidt, F. (1975); Epoxidharzkleber für Beton und Stahl, *VDI-Berichte*, Nr 225, 1975, pp 21-33.
- Tausky, R. (1977); Verstärkung von Tragkonstruktionen mit geklebter Armierung, *Technische Mitteilungen PTT*, Nr 2, 1977, pp 85-91.
- Hugenschmidt, F (1982); New experiences with epoxies for structural application, *International Journal of Adhesion and Adhesives*, Vol 2, No 2, 1982, pp 84-96.
- Ong, K.C.G. and Mansur, M.A. (1985); Punching shear of steel-concrete open sandwich slabs, *Magazine of Concrete research*, Vol 37, No 133, December 1985, pp 216-226.
- Vilnay, O. (1988); The analysis of reinforced concrete beams strengthened by epoxy bonded steel plates, *The International Journal of cement Composites and Lightweight Concrete*, Volume 10, Number 2, May 1988, pp 73-78.
- Standing Committee on Structural Safety of ISCE (1989)
- Ritchie, P.A., Thomas, A., Le-Wu Lu and Connelly, G.M. (1991); External reinforcement of concrete beams using fiber reinforced plastics, *ACI Structural Journal*, Vol 88, No 4, July/August 1991, pp 490-500.
- Ivány, G. (1989); Erhöhung der Biegetragfähigkeit von Stahlbetonbauteilen durch nachträgliche Ergänzung der Druckzone, *Bautechnik*, 66, H 7, 1989, pp 221-224.
- Midwinter, K. (1991); Floorstrengthening by steel plate bonding, *Construction Maintenance & Repair*, September/October 1991, pp 8-10.
- Price, A. and Moulds, R.J. (1991); Repair and strengthening of structures using plate bonding, *Construction & Building Materials*, Vol 5, No 4, December 1991, pp 189-192.
- Hutchinson, P.R. (1992); Strengthening structures with externally bonded reinforcement, *Construction & Building Materials*, Vol 6, No 1, March 1992, pp 43-46.
- Ramsay, B. (1993); Steel plate bonding for concrete bridge strengthening, *Construction Repair*, January-February 1993, pp 14-16.
- Swedish Codes; 47.33 (1995)
- Rutz, J. (1995); Mit Klebebewehrung verstärkte Stahlbetondecken im Brandfall, Schadenbegrenzung als Teil des vorbeugenden Brandschutzes, Kantons St.Gallen, 1995.
- Spanstaal (1996); private communications
- Beton-Kalender (1996); Geklebte Bewehrung für die Verstärkung von Betonbauteilen,
- Quantrill, R.J., Hollaway, L.C. and Thorne, A.M. (1996); Experimental and Analytical Investigation of FRP Strengthened Beam Response, Part I and Part II, *Magazine of Concrete Research*, Vol. 48, No. 177, pp 331-342 and pp 343-351.

14) Publications outside field of plate bonding technique

- Leonhardt, F. & Walther, R (1962); Versuche an Plattenbalken mit hoher Schubbeanspruchung, *Deutscher Ausschuss für Stahlbeton*, Heft 152, 1962.
- Kani, G.N.I. (1964); The riddle of shear failure and its solution, *ACI Journal*, Vol 61, No 4, April 1964, pp 441-465.

- Kani, G.N.I. (1966); Basic facts concerning shear failure, *ACI Journal*, Vol 63, No 6, June 1966, pp 675-692.
- Rafia, K. (1971); Empirische Formeln zur Berechnung der Schubtragfähigkeit von Stahlbetonbalken, Teil I, Einfeldrige Rechteckbalken ohne Schubbewehrung bei direkter Einleitung von Einzellasten, *Strasse, Brücke, Tunnel* 23, No 12, Dez. 1971, pp 311-320.
- Taylor, H.P.J. (1974); The fundamental behaviour of reinforced concrete beams in bending and shear, *ACI-SP-42*, Vol 1, 1974, pp 43-78.
- Leonhardt, F. (1977); Schub bei Stahlbeton und Spannbeton - Grundlagen der neueren Schubbemessung, *Beton - und Stahlbetonbau*, Vol 72, No 11, 1972, pp 270-277.
- Walraven, J.C. (1980); Aggregate Interlock, a theoretical and experimental analysis, *Dissertation*, Delft University of Technology, Oktober 1980.
- Petersson, P.E. (1981); Crack growth and development of fracture zones in plain concrete and similar materials, *Report TVBM-1006*, Div. Build. Mat, Lund University of Tech, 1981.
- Kotsovos, M.D. (1984); Behavior of Reinforced Concrete Beams with a Shear Span to Depth Ratio between 1.0 and 2.5, *ACI Journal*, Vol 81, No 3, May-June 1984, pp 279-286
- Hillerborg, A. (1985); The theoretical basis of a method to determine the fracture energy G_f of concrete, *Materials and Structures*, 18, pp 291-296.
- Rots, J.G., Nauta, P., Kusters, G.M.A. & Blaauwendraad, J. (1985); Smearred crack approach and fracture localization in concrete, *Heron*, Vol 30, No 1, 1985, pp1-45.
- Kotsovos, M.D. (1986); Behavior of Beams with Shear Span-to-Depth Ratio Greater than 2.0, *ACI Journal*, Vol 83, No 6, Nov.-Dec. 1986, pp 1026-1034.
- Rots, J.G. (1988); Computational Modeling of Concrete Fracture, *Dissertation*, Delft University of Technology, September 1988.
- Rußwurm, D. (1989); Spezielle Fragen beim Schweißen von Betonstählen. / Gleichmassdehnung von Betonstählen, Deutscher Ausschuss für Stahlbeton, Heft 397, 1989.
- CEB-FIP Modelcode (1990)
- Russo, G., Zingone, G. & Puleri, G. (1991); Flexure-Shear Interaction Model for Longitudinally Reinforced Beams, *ACI Structural Journal*, Vol 88, No 1, 1991, pp 60-68.
- Hordijk, D.A. (1991); Local Approach to Fatigue Concrete, *Dissertation*, Delft University of Technology, Oktober 1991.
- De Borst, R. (1991); Computational Methods in Non-Linear Solid Mechanics, Part I and Part II, *Report nr 25-2-90-5-04*, TU-Delft/TNO-IBBC, January 1991.
- Kim, W. & White, R.N. (1991); Initiation of Shear Cracking in Reinforced Concrete Beams with no Web Reinforcement, *ACI Structural Journal*, Vol 88, No 3, 1991, pp301-308.
- Reineck, K-H. (1991); Model for Structural Concrete Members without Transverse reinforcement, *Structural Concrete IABSE*, Stuttgart, 1991, pp 643-648.
- Eurocode 2 (1992) ENV 1992-1-1:1991.
- DIANA Manuals, Vol 0 - Introduction, Vol 1 - Linear Static Analysis, Vol 4 - Non-Linear Analysis, April 1993.
- Rots, J.G. (1993); The smeared crack model for localized Mode-I tensile fracture, *Numerical Models in Fracture Mechanics of Concrete*, Wittmann ed., Balkema, Rotterdam, 1993.
- Ozbolt, J. (1993); General microplane model for concrete, *Numerical Models in Fracture Mechanics of Concrete*, Wittmann ed., Balkema, Rotterdam, 1993.
- Jungwirth (1995); IABSE Symposium San Francisco, Extending the Lifespan of Structures, August 1995.
- CEB Bulletin 224 (1995); Model Uncertainties, Reports from CEB Task Group 1.2, 1995.
- Stroband, J. (1997); Shear Capacity of Reinforced Concrete Members, *Progress in Concrete Research*, Delft University of Technology, Concrete Structures, Vol 5, 1997.

LIST OF PUBLICATIONS

- Jansze, W., Walraven, J.C., Rots, J.G. (1995), "Lijm- en mortelvoegen tussen betonelementen met hoge sterkte", *Cement*, pagina 22-27, jaargang 47, no 2, februari 1995.
- Jansze, W. (1994), "Tragverhalten von polymermodifizierten Mörtel- und gefüllten Epoxidharzfugen unter Schub-Druckbeanspruchung", 29. Forschungskolloquium, Deutscher Ausschuss für Stahlbeton, pagina 21-30, 24-25 maart 1994, Delft, Nederland.
- Jansze, W., Den Uijl, J.A., Walraven, J.C. (1996), "Failure Behaviour of Joints between HSC Members, subjected to Shear- and Compressive Stresses", *Proceedings 4th International Symposium on Utilization of High-strength/High-performance Concrete*, 29-31 May 1996, page 1085-1093, Paris, France.
- Jansze, W., Den Uijl, J.A., Walraven, J.C. (1996), "Anchorage of Externally Bonded Steel Plates", *Proceedings Concrete, In the Service of Mankind, Repair, Rehabilitation and Protection*, 27-28 June 1996, page 591-598, Dundee, Scotland.
- Jansze, W., Den Uijl, J.A., Walraven, J.C. (1997), "Shear Capacity of Beams with Externally Bonded Steel Plates", *Proceedings FIP The Concrete Way to Development*, 9-12 March 1997, page 857-866, Johannesburg, South Africa.
- Jansze, W., Den Uijl, J.A., Walraven, J.C. (1997), "Beams Strengthened with Bonded-on Steel Plates; Simulations of Experiments on Anchorage and Shear", *Proceedings 2nd International Diana Conference on Finite Elements in Engineering and Science*, 4-6 June 1997, page 273-284, Amsterdam, The Netherlands.
- Jansze, W., Den Uijl, J.A., Walraven, J.C. (1997), "Beams with Bonded-on Steel Plates; Design for Shear", *Proceedings IABSE Composite Construction - Conventional and Innovative*, 16-18 September 1997, Innsbruck, Austria.
- Jansze, W., Den Uijl, J.A., Walraven, J.C. (1998), "Strengthening with Externally Bonded Steel Plates; Design for Beam Shear and Plate Anchorage", *Proceedings XIIIth FIP World Congress - Challenges for Concrete in the Next Millennium*, 23-29 May 1998, Amsterdam, The Netherlands.

NOTATIONS

Upper Case Symbols

A	shear span	[mm]
A_c	cross sectional area of concrete	[mm ²]
A_p	cross sectional area of plate	[mm ²]
A_s	cross sectional area of longitudinal reinforcement	[mm ²]
A_{sw}	cross sectional area of web reinforcement	[mm ²]
A_{bw}	cross sectional area of bolt	[mm ²]
B	bolt	-
C_m	modification factor	-
D_{11}	normal stiffness of interface element	[N/mm ³]
D_{22}	shear stiffness of interface element	[N/mm ³]
EI	flexural rigidity	[Nmm ²]
E_c	modules of elasticity of concrete	[N/mm ²]
E_e	modules of elasticity of epoxy	[N/mm ²]
E_p	modules of elasticity of plate	[N/mm ²]
E_s	modules of elasticity of steel bar	[N/mm ²]
F	load	[N]
F_r	force of first cracking	[N]
G	shear modulus of epoxy	[N/mm ²]
G_f	fracture energy	[N/mm ¹]
H	height of concrete member	[mm]
I	second moment of inertia ($1/12 bh^3$)	[mm ⁴]
I_p	second moment of inertia of plate ($1/12 b_p t_p^3$)	[mm ⁴]
K_n	normal stiffness factor of epoxy	[N/mm ²]
K_s	shear stiffness factor of epoxy	[N/mm ²]
L	unplated length; end plate to centre support	[mm]
M	moment	[Nmm]
M_o	unloading moment	[Nmm]
M_p	moment after strengthening	[Nmm]
M_{fl}	moment of maximum flexural capacity	[Nmm]
M_{vcu}	moment of maximum shear capacity	[Nmm]
N	maximum number of load cycles	[-]
N_{cum}	mean force of crushing of concrete compression zone	[N]
N_{sym}	mean force of yielding of longitudinal reinforcement	[N]
N_{psym}	mean force of yielding of plate	[N]
P	plate cross section	[mm ²]
V_{cu}	shear capacity of rc beam without web reinforcement	[N]
W	width of concrete member	[mm]

lower Case Symbols

a	shear span	[mm]
a_L	fictitious shear span	[mm]
b	width	[mm]
b_p	width of plate	[mm]
d_{max}	maximum diameter of a aggregate	[mm]
d	effective depth	[mm]
d_p	effective depth of plate	[mm]
d_s	effective depth of longitudinal reinforcement	[mm]
d_{sp}	weighed effective depth	[mm]
e	FEM element size	[mm]
f_{cm}	mean compressive cylinder strength of concrete	[N/mm ²]
$f_{cm,cube}$	mean compressive cube strength of concrete	[N/mm ²]
f_{ctm}	tensile strength of concrete	[N/mm ²]
$f_{ctm,ax}$	mean axial tensile strength of concrete	[N/mm ²]
$f_{ctm,sp}$	mean tensile splitting strength of concrete	[N/mm ²]
f_{sym}	mean yield strength of longitudinal reinforcement	[N/mm ²]
f_{pym}	mean yield strength of plate	[N/mm ²]
f_{ybd}	design yield strength of bolt	[N/mm ²]
f_{ywd}	design yield strength of web reinforcement	[N/mm ²]
g_f	volumic fracture energy	[N/mm ²]
h	height, width of smeared crack band	[mm]
h_{xu}	maximum concrete compression zone	[mm]
l_a	anchorage length	[mm]
l_{cr}	thickness of epoxy layer	[mm]
t_q	crack spacing	[mm]
t_p	thickness of plate	[mm]
w	crack width	[mm]
s	spacing of stirrups	[mm]
$s_{cr,m}$	average crack spacing	[mm]
s_p	bond slip of plate	[mm]
$w_{cr,m}$	average crack width	[mm]
x	location, height of concrete compression zone	[mm]
z_p	internal lever arm for plate	[mm]
z_s	internal lever arm for bars	[mm]

Greek Symbols

α	area factor = 0.75 according to Dutch codes	[-]
α_u	variable in Rafia's formulation on flexural shear	[mm]
β	distance factor = 0.338 according to Dutch Codes	[-]
β	shear retention factor	[-]

δ	deflection	[-]
ϵ_c	concrete strain	[-]
ϵ_{cu}	ultimate concrete strain	[-]
ϵ_c^{cr}	concrete crack strain	[-]
ϵ_m	average strain	[-]
ϵ_p	strain in plate	[-]
ϵ_{pym}	mean yield strain in plate	[-]
ϵ_s	strain in bar	[-]
ϵ_{sym}	mean yield strain in bar	[-]
ϵ_u	ultimate smeared crack strain	[-]
ϕ	angle of internal friction	[-]
ψ	angle of dilatation	[-]
γ	shear deformation	[-]
κ	plastic strain	[-]
η	strengthening ratio (A_p / A_s)	[-]
μ	friction of surface	[-]
ν	Poisson's ratio	[-]
ρ	reinforcement ratio	[-]
ρ_0	reinforcement percentage (=100 ρ)	[%]
$\rho_{p,0}$	plate reinforcement percentage	[%]
ρ_s	bar reinforcement ratio	[-]
$\rho_{s,0}$	bar reinforcement percentage	[%]
$\rho_{sp,0}$	bar and plate reinforcement percentage (= ($A_s + A_p$) / bd_{sp})	[%]
σ	stress	[N/mm ²]
σ_c'	concrete compressive stress	[N/mm ²]
σ_{max}	maximum normal anchorage stress	[N/mm ²]
σ_N	(σ_n) additional normal stress as a result of a bolt	[N/mm ²]
σ_1	principal maximum stress	[N/mm ²]
σ_2	principal minimum stress	[N/mm ²]
τ	shear stress	[N/mm ²]
τ_c	concrete shear stress	[N/mm ²]
τ_{cum}	mean maximum concrete shear stress	[N/mm ²]
τ_{exp}	experimental shear stress	[N/mm ²]
τ_{max}	maximum shear anchorage stress	[N/mm ²]
τ_{pm}	mean bond shear strength of plate	[N/mm ²]
τ_{sm}	mean bond shear strength of bar	[N/mm ²]
Δ	shear displacement	[mm]
\varnothing	diameter of bar	[mm]

A - LITERATURE DATA ON MAXIMUM SHEAR STRESS

no.	f_{cm}	d	b	a/d	ρ_o	τ_{exp}	τ_{Rafia}	τ_{CEB}	$\tau_{Rafia} / \tau_{exp}$	τ_{CEB} / τ_{exp}
	[MPa]	[mm]	[mm]	[-]	[%]	[MPa]	[MPa]	[MPa]	[-]	[-]
Mathey, Watstein, [1963]										
IIIa-17	29.24	403	203	3.78	2.54	1.08	1.10	1.19	1.02	1.11
IIIa-18	25.17	403	203	3.78	2.54	0.99	1.02	1.14	1.03	1.15
Va-19	23.52	403	203	3.78	0.93	0.77	0.71	0.79	0.92	1.03
Va-20	25.59	403	203	3.78	0.93	0.81	0.74	0.82	0.91	1.01
Vla-24	26.34	403	203	3.78	0.47	0.67	0.60	0.66	0.89	0.98
Vla-25	25.79	403	203	3.78	0.47	0.61	0.59	0.65	0.97	1.07
Leonhardt, Walter [1962]										
5	29.60	270	190	3	2.07	1.18	1.23	1.32	1.04	1.12
6	29.60	270	190	4	2.07	1.19	1.13	1.20	0.95	1.01
7-1	31.00	278	190	5	2.01	1.18	1.10	1.11	0.93	0.94
7-2	31.00	278	190	5	2.01	1.29	1.10	1.11	0.85	0.86
8-1	31.10	278	190	6	2.01	1.24	1.05	1.05	0.85	0.85
8-2	31.10	274	190	6	2.04	1.26	1.06	1.06	0.84	0.84
D1/1	35.76	70	50	3	1.71	2.07	1.78	1.91	0.86	0.92
D1/2	35.76	70	50	3	1.71	2.05	1.78	1.91	0.87	0.93
D2/1	35.92	140	100	3	1.66	1.51	1.48	1.54	0.98	1.02
D2/2	35.92	140	100	3	1.66	1.66	1.48	1.54	0.89	0.93
D3/1	37.12	210	150	3	1.62	1.47	1.35	1.39	0.92	0.95
D3/2	37.12	210	150	3	1.62	1.36	1.35	1.39	0.99	1.02
D4/1	35.42	280	200	3	1.67	1.32	1.24	1.29	0.94	0.98
D4/2	35.42	280	200	3	1.67	1.27	1.24	1.29	0.98	1.02
C1	39.25	150	100	3	1.33	1.44	1.42	1.45	0.98	1.01
C2	39.25	300	150	3	1.33	1.44	1.19	1.22	0.83	0.85
C3	39.25	450	200	3	1.33	1.13	1.08	1.12	0.95	0.99
C4	39.25	600	225	3	1.33	1.13	1.00	1.06	0.89	0.94
Kani [1967]										
40	26.41	140	152	5.35	2.59	1.51	1.29	1.33	0.85	0.88
43	28.00	137	151	5.92	2.73	1.39	1.33	1.35	0.95	0.97
47	24.76	132	151	5.12	2.85	1.41	1.32	1.39	0.94	0.98
48	24.76	133	151	5.09	2.81	1.34	1.31	1.38	0.98	1.03
52	24.83	138	152	3.93	2.69	1.37	1.34	1.47	0.98	1.07
55	25.10	135	150	3.02	2.89	1.61	1.50	1.66	0.93	1.03
56	27.20	137	153	3.46	2.67	1.33	1.43	1.58	1.07	1.19
57	26.41	139	153	5.39	2.6	1.49	1.29	1.33	0.87	0.90
58	27.24	138	152	3.44	2.68	1.37	1.43	1.58	1.04	1.16
81	27.52	274	153	5.94	2.76	1.21	1.11	1.13	0.92	0.93
83	27.45	271	156	3	2.73	1.54	1.30	1.41	0.84	0.92
84	27.45	271	151	4.01	2.83	1.35	1.21	1.30	0.90	0.96
91	27.45	269	154	6.05	2.71	1.23	1.10	1.12	0.90	0.91
93	30.28	273	155	6.46	2.66	1.27	1.13	1.12	0.89	0.88

no.	f_{cm}	d	b	a/d	ρ_0	τ_{exp}	τ_{Rafia}	τ_{CEB}	τ_R/τ_{exp}	τ_C/τ_{exp}
96	25.31	275	153	3.94	2.76	1.33	1.15	1.25	0.87	0.94
64	25.72	541	156	8.01	2.75	0.94	0.83	0.86	0.88	0.92
66	26.41	541	156	6.02	2.75	1.07	0.91	0.96	0.85	0.89
74	27.24	523	152	3.11	2.84	1.35	1.08	1.23	0.80	0.91
75	27.31	524	152	3.11	2.83	1.35	1.08	1.23	0.80	0.91
79	26.14	556	153	6.83	2.72	0.99	0.87	0.91	0.88	0.92
3043	26.97	1092	154	3	2.72	0.98	0.91	1.08	0.93	1.10
3044	29.52	1097	152	3.97	2.73	0.94	0.88	1.01	0.93	1.08
3045	28.28	1092	155	5	2.7	0.9	0.82	0.92	0.91	1.02
3046	26.69	1097	155	7	2.72	0.9	0.73	0.81	0.82	0.90
3047	26.69	1095	155	8	2.68	0.87	0.70	0.77	0.80	0.88
271	26.97	269	611	6.06	2.75	1.33	1.10	1.11	0.82	0.84
272	26.97	271	611	5.02	2.72	1.38	1.14	1.18	0.82	0.86
273	27.17	271	612	4.02	2.72	1.24	1.19	1.27	0.96	1.03
274	27.17	270	612	3.02	2.73	1.51	1.29	1.40	0.85	0.93
Bhal [1969]										
B1	24.23	297	240	3	1.29	1	0.93	1.03	0.93	1.03
B2	30.94	600	240	3	1.28	0.83	0.88	0.97	1.06	1.17
B3	28.73	900	240	3	1.28	0.76	0.76	0.88	1.01	1.16
B4	26.35	1200	240	3	1.28	0.63	0.68	0.82	1.08	1.30
B5	27.80	600	240	3	0.64	0.74	0.66	0.74	0.89	1.00
B6	25.84	600	240	3	0.6	0.79	0.62	0.71	0.79	0.90
B7	28.48	900	240	3	0.64	0.64	0.60	0.70	0.94	1.09
Aster, Koch [1974]										
2	27.50	250	1000	3.7	0.64	0.88	0.76	0.83	0.87	0.94
3	27.58	250	1000	3.7	0.91	0.9	0.86	0.93	0.95	1.03
11	28.00	500	1000	3.7	0.46	0.53	0.58	0.64	1.09	1.21
12	27.58	500	1000	3.7	0.65	0.66	0.65	0.72	0.98	1.09
16	28.33	750	1000	3.7	0.42	0.53	0.51	0.58	0.96	1.10
Mphonde, Frantz [1984]										
3-3b	20.77	298	152	3.6	3.36	1.42	1.11	1.27	0.78	0.89
3-3c	27.14	298	152	3.6	3.36	1.47	1.26	1.39	0.86	0.94
7-3a	37.68	298	152	3.6	3.36	1.81	1.49	1.55	0.82	0.85
7-3b	41.63	298	152	3.6	3.36	1.82	1.57	1.60	0.86	0.88
11-3a	74.94	298	152	3.6	3.36	1.97	2.10	1.95	1.07	0.99
11-3b	74.66	298	152	3.6	3.36	1.97	2.10	1.94	1.06	0.99
15-3a	81.36	298	152	3.6	3.36	2.06	2.19	2.00	1.06	0.97
15-3b	93.70	298	152	3.6	3.36	2.2	2.35	2.10	1.07	0.95
15-3c	91.86	298	152	3.6	3.36	2.15	2.33	2.08	1.08	0.97
Ahmad, Kahloo, Poveda [1986]										
A1	60.85	203	127	4	3.93	2.24	2.16	2.02	0.96	0.90
A2	60.85	203	127	3	3.93	2.67	2.35	2.23	0.88	0.83
A7	60.85	208	127	4	1.77	1.77	1.65	1.54	0.93	0.87
A8	60.85	208	127	3	1.77	1.85	1.79	1.70	0.97	0.92
B1	67	202	127	4	5.04	2	2.47	2.27	1.23	1.14
B2	67	202	127	3	5.04	2.69	2.68	2.50	1.00	0.93
B7	67	208	127	4	2.25	1.69	1.87	1.72	1.11	1.02
B8	67	208	127	3	2.25	1.77	2.03	1.90	1.15	1.07
C1	64.34	184	127	4	6.64	2.32	2.71	2.52	1.17	1.08
C2	64.34	184	127	3	6.64	3.23	2.94	2.77	0.91	0.86
C7	64.34	206	127	4	3.26	1.73	2.08	1.93	1.20	1.12

no.	f_{cm}	d	b	a/d	ρ_0	τ_{exp}	τ_{Rafia}	τ_{CEB}	τ_F/τ_{exp}	τ_C/τ_{exp}
C8	64.34	206	127	3	3.26	1.7	2.26	2.12	1.33	1.25
Bazant, Kazemi [1991]										
I-2.1	46.80	40.64	38.1	3	1.65	2.1	2.30	2.47	1.10	1.17
I-2.2	46.80	40.64	38.1	3	1.65	1.91	2.30	2.47	1.21	1.29
I-2.3	46.80	40.64	38.1	3	1.65	2	2.30	2.47	1.15	1.23
I-4.1	46.80	81.28	38.1	3	1.65	1.77	1.94	1.97	1.09	1.11
I-4.2	46.80	81.28	38.1	3	1.65	1.8	1.94	1.97	1.08	1.09
I-4.3	46.80	81.28	38.1	3	1.65	1.67	1.94	1.97	1.16	1.18
I-8.1	46.80	162.6	38.1	3	1.65	1.47	1.63	1.62	1.11	1.10
I-8.2	46.80	162.6	38.1	3	1.65	1.58	1.63	1.62	1.03	1.02
I-8.3	46.80	162.6	38.1	3	1.65	1.64	1.63	1.62	0.99	0.99
II-1.1	46.20	20.64	38.1	3	1.62	2.66	2.70	3.12	1.01	1.17
II-1.2	46.20	20.64	38.1	3	1.62	3.08	2.70	3.12	0.88	1.01
II-1.3	46.20	20.64	38.1	3	1.62	2.97	2.70	3.12	0.91	1.05
II-2.1	46.20	41.28	38.1	3	1.62	1.87	2.27	2.43	1.21	1.30
II-2.2	46.20	41.28	38.1	3	1.62	1.71	2.27	2.43	1.33	1.42
II-2.3	46.20	41.28	38.1	3	1.62	2.02	2.27	2.43	1.12	1.20
II-4.1	46.20	82.55	38.1	3	1.62	1.72	1.91	1.94	1.11	1.13
II-4.2	46.20	82.55	38.1	3	1.62	1.6	1.91	1.94	1.19	1.21
II-4.3	46.20	82.55	38.1	3	1.62	1.41	1.91	1.94	1.35	1.38
II-8.1	46.20	165.1	38.1	3	1.62	1.16	1.60	1.59	1.38	1.37
II-8.2	46.20	165.1	38.1	3	1.62	1.33	1.60	1.59	1.21	1.20
II-8.3	46.20	165.1	38.1	3	1.62	1.3	1.60	1.59	1.23	1.23
Bernhardt, Fynboe [1986]										
S9A	93.60	159	150	3.46	5.27	3.33	3.20	2.88	0.96	0.86
S9B	93.60	159	150	3.46	5.27	2.66	3.20	2.88	1.20	1.08
S9C	110.7	159	150	3.46	5.27	2.83	3.48	3.04	1.23	1.07
Walraven [1990]										
A1	27.40	125	200	3	0.83	1.19	1.06	1.15	0.89	0.97
A2	27.40	420	200	3	0.74	0.84	0.75	0.83	0.90	0.99
A3	27.80	720	200	3	0.79	0.7	0.68	0.77	0.97	1.10
Thorenfeldt, Drangshold [1990]										
B11	54.00	221	150	3	1.82	1.75	1.67	1.62	0.96	0.93
B13	54.00	207	150	4	3.23	2.27	1.90	1.81	0.84	0.80
B14	54.00	207	150	3	3.23	2.66	2.06	1.99	0.77	0.75
B21	77.78	221	150	3	1.82	2.05	2.01	1.83	0.98	0.89
B23	77.78	207	150	4	3.23	2.51	2.28	2.05	0.91	0.82
B24	77.78	207	150	3	3.23	2.66	2.47	2.25	0.93	0.85
B43	86.44	207	150	4	3.23	2.77	2.40	2.12	0.87	0.77
B44	86.44	207	150	3	3.23	3.45	2.61	2.33	0.76	0.68
B51	97.70	221	150	3	1.82	1.69	2.25	1.97	1.33	1.17
B53	97.70	207	150	4	3.23	2.47	2.55	2.21	1.03	0.89
B54	97.70	207	150	3	3.23	2.5	2.77	2.43	1.11	0.97
B61	77.70	442	300	3	1.82	1.36	1.69	1.57	1.24	1.15
B63	77.70	414	300	4	3.23	1.79	1.91	1.75	1.07	0.98
B64	77.70	414	300	3	3.23	2.26	2.08	1.92	0.92	0.85
Kim, Park, Lee [1993]										
CTL-1	52.09	270	300	3	1.9	1.54	1.59	1.55	1.03	1.01
CTL-2	52.09	270	300	3	1.9	1.56	1.59	1.55	1.02	0.99
P1.0-1	52.09	272	300	3	1.9	1.26	1.58	1.55	1.26	1.23
P1.0-2	52.09	272	300	3	1.9	1.22	1.58	1.55	1.30	1.27

no.	f_{cm}	d	b	a/d	ρ_0	τ_{exp}	τ_{Rafla}	τ_{CEB}	τ_R/τ_{exp}	τ_C/τ_{exp}
P3.4-1	52.09	267	300	3	3.4	1.72	1.93	1.89	1.12	1.10
P3.4-2	52.09	267	300	3	3.4	1.73	1.93	1.89	1.12	1.09
P4.6-1	52.09	255	300	3	4.6	2.07	2.16	2.11	1.04	1.02
P4.6-2	52.09	255	300	3	4.6	2.2	2.16	2.11	0.98	0.96
A4.5-1	52.09	270	300	4.5	1.9	1.45	1.43	1.35	0.99	0.93
A4.5-2	52.09	270	300	4.5	1.9	1.39	1.43	1.35	1.03	0.97
A6.0-1	52.09	270	300	6	1.9	1.29	1.35	1.23	1.05	0.95
A6.0-2	52.09	270	300	6	1.9	1.33	1.35	1.23	1.01	0.92
D142-1	52.09	142	300	3	1.9	1.7	1.86	1.82	1.10	1.07
D142-2	52.09	142	300	3	1.9	1.63	1.86	1.82	1.14	1.12
550-1	52.09	550	300	3	1.9	1.37	1.33	1.33	0.97	0.97
D550-2	52.09	550	300	3	1.9	1.3	1.33	1.33	1.02	1.03
D915-1	52.09	915	300	3	1.9	0.99	1.17	1.22	1.18	1.23
D915-2	52.09	915	300	3	1.9	1.21	1.17	1.22	0.97	1.01
Taylor [----]										
2A	25.50	222	-	4.1	0.9	0.92	0.83	0.90	0.91	0.98
2B	24.31	222	-	4.1	0.9	0.99	0.81	0.88	0.82	0.89
2C	24.06	222	-	4.1	1.19	1.18	0.89	0.97	0.75	0.82
2D	26.95	222	-	4.1	1.19	0.95	0.94	1.00	0.99	1.06
2E	26.69	222	-	4.1	1.49	1.08	1.01	1.08	0.93	1.00
2F	24.14	222	-	4.1	1.49	1.08	0.96	1.04	0.89	0.97
2G	23.72	222	-	4.1	1.49	0.98	0.95	1.04	0.97	1.06
2H	23.80	222	-	4.1	1.49	1.03	0.95	1.04	0.93	1.01
2I	26.18	222	-	4.1	1.8	1.1	1.06	1.14	0.97	1.04
2J	25.16	222	-	4.1	1.8	1.07	1.04	1.13	0.98	1.05
2K	22.36	222	-	4.1	2.33	1.1	1.07	1.18	0.97	1.07
2L	26.27	222	-	4.1	2.33	1.28	1.16	1.25	0.91	0.97
2M	26.18	222	-	4.1	2.33	1.28	1.16	1.24	0.91	0.97
2N	25.84	230	-	4	2.26	1.14	1.14	1.23	1.00	1.08
2P	22.95	230	-	4	2.26	1.19	1.07	1.18	0.90	0.99
3A	19.72	220	-	4.1	1.8	1.01	0.93	1.04	0.92	1.03
3B	18.70	220	-	4.1	1.87	1.12	0.91	1.04	0.82	0.93
3C	22.44	220	-	4.1	1.82	1.05	0.99	1.09	0.94	1.04
3D	27.97	220	-	4.1	1.8	1.1	1.10	1.17	1.00	1.06
3E	29.33	220	-	4.1	1.87	1.1	1.14	1.20	1.04	1.09
3F	26.78	220	-	4.1	1.82	1.18	1.08	1.16	0.92	0.98
3G	30.43	220	-	4.1	1.8	1.19	1.15	1.20	0.97	1.01
3H	31.28	220	-	4.1	1.87	1.33	1.18	1.23	0.89	0.92
3I	37.32	220	-	4.1	1.8	1.25	1.27	1.29	1.02	1.03
3K	35.28	220	-	4.1	1.87	1.3	1.25	1.28	0.97	0.98
no.	f_{cm}	d	b	a/d	ρ_0	τ_{exp}	τ_{Rafla}	τ_{CEB}	τ_R/τ_{exp}	τ_C/τ_{exp}
	[MPa]	[mm]	[mm]	[-]	[%]	[MPa]	[MPa]	[MPa]	[-]	[-]
									Σ	Σ
									0.986	1.013

TOTAL of 170 datapoints excluded Elzanaty, Nilson & Slate [1986]	Rafla CEB-FIP MC90	0.85 0.18
---	-----------------------	--------------

B - CONCRETE MATERIAL PROPERTIES

For all the test series the following normal strength concrete mixture was used:
Mixture nr. 106 - PCB 8 375 53, contents of 1000 litres:

<i>aggregate</i>	8-4 mm	30% [w/w]	522 kg
	4-2 mm	20% [w/w]	348 kg
	2-1 mm	15% [w/w]	261 kg
	1-0.5 mm	15% [w/w]	261 kg
	0.5-0.25 mm	13% [w/w]	226 kg
	0.25-0.125 mm	7% [w/w]	122 kg
<i>total aggregates</i>		740 kg	
<i>cement</i>		375 kg	
<i>water</i>		200 l	
<i>water/cement ratio = 0.53</i>			

For all the concrete mixtures standard tests on cubes measuring $150 \times 150 \times 150 \text{ mm}^3$ were carried out at a concrete age of 28 days with regard to the cube compressive strength $f_{\text{cm,cube}}$ and the tensile splitting strength $f_{\text{cm,sp}}$. Occasionally, the uniaxial compressive strength f_{cm} , Young's modulus E_c and Poisson's ratio ν were determined at various ages on prismatic specimens measuring $100 \times 100 \times 400 \text{ mm}^3$.

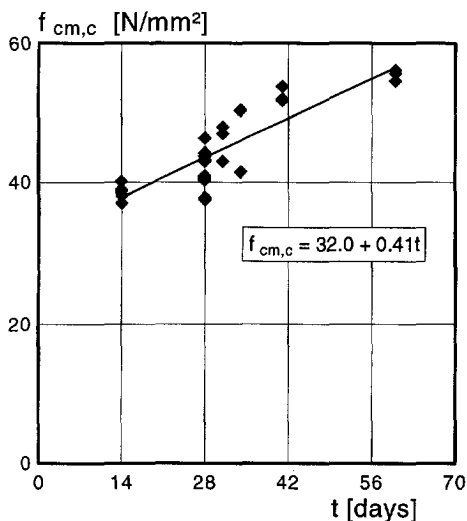


Fig. B.1 Cube compressive strength

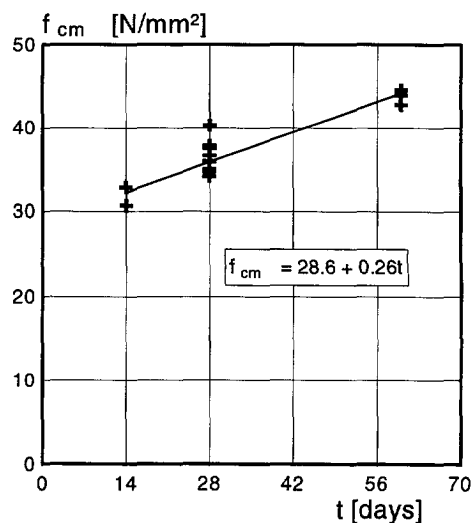


Fig. B.2 Uniaxial compressive strength

The material properties in relation to the hardening time are presented in B.1 - B.4 and Table B.1. In Table B.2 material properties of each test at an age of 28 days are listed. (The experiments were mostly carried out at a concrete age of 40-45 days).

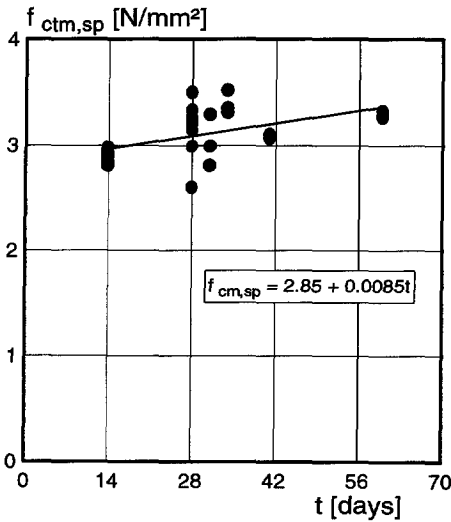


Fig. B.3 Tensile splitting strength

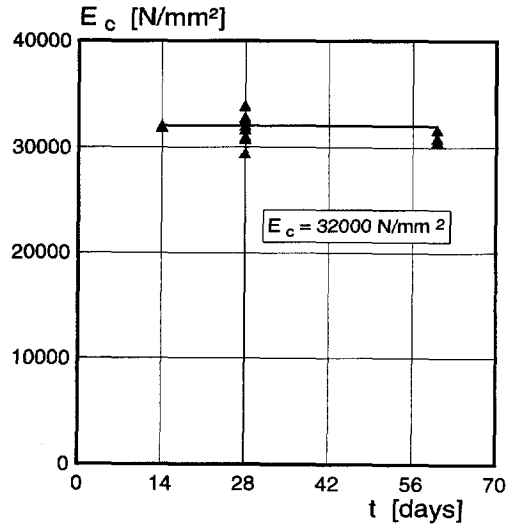


Fig. B.4 Young's modulus

Table B.1 Material properties in relation to concrete hardening time

SW3/SH3	$f_{cm,cube}$	$f_{cm,cube}$	$f_{cm,cube}$	X	S	$f_{ctm,sp}$	$f_{ctm,sp}$	$f_{ctm,sp}$	X	S
14 days	38.73	38.93	38.28	38.65	0.33	2.89	2.81	2.84	2.85	0.04
28 days	46.33	44.18	42.95	44.49	1.71	2.99	2.60	3.33	2.97	0.37
60 days	56.19	54.63	55.73	55.52	0.80	3.32	3.26	3.28	3.29	0.03
	f_{cm}	f_{cm}	f_{cm}	X	S	E_c	E_c	E_c	X	S
14 days	32.85	30.66	30.66	31.39	1.26	31860	31740	31740	31780	69
28 days	34.16	35.04	34.16	34.45	0.51	32650	32570	32370	32530	144
60 days	42.77	43.94	44.53	43.75	0.90	30400	30750	31540	30897	584

AB1/AB2	f_{cm}	f_{cm}	f_{cm}	X	S	E_c	E_c	E_c	X	S
28 days	37.52	37.81	40.29	38.54	1.52	31540	30830	33750	32040	1523

AL4/AL5	$f_{cm,cube}$	$f_{cm,cube}$	$f_{cm,cube}$	X	S	$f_{ctm,sp}$	$f_{ctm,sp}$	$f_{ctm,sp}$	X	S
41 days	53.79	51.97	51.78	52.51	1.11	3.06	3.10	3.09	3.08	0.02
136 days	57.10	60.02	58.13	58.42	1.48	4.07	3.56	4.05	3.89	0.29
	f_{cm}	f_{cm}	f_{cm}	X	S	E_c	E_c	E_c	X	S
136 days	45.69	47.15	48.61	47.15	1.46	31550	32530	33000	32360	740

AL1	$f_{cm,cube}$	$f_{cm,cube}$	$f_{cm,cube}$	X	S	$f_{ctm,sp}$	$f_{ctm,sp}$	$f_{ctm,sp}$	X	S
28 days	40.62	40.88	40.36	40.62	0.26	3.50	3.20	3.20	3.30	0.17
133 days	55.47	54.31	54.24	54.67	0.69	3.53	3.67	3.76	3.65	0.12
	f_{cm}	f_{cm}	f_{cm}	X	S	E_c	E_c	E_c	X	S
133 days	44.96	43.65	43.21	43.94	0.91	31410	30790	32630	31610	936

AR1	$f_{cm,cube}$	$f_{cm,cube}$	$f_{cm,cube}$	X	S	$f_{ctm,sp}$	$f_{ctm,sp}$	$f_{ctm,sp}$	X	S
34 days	50.35	50.41	41.46	47.41	5.15	3.31	3.35	3.52	3.39	0.11
129 days	58.13	58.65	61.77	59.52	1.97	3.91	3.73	3.93	3.86	0.11
	f_{cm}	f_{cm}	f_{cm}	X	S	E_c	E_c	E_c	X	S
130 days	48.18	46.86	48.18	47.74	0.76	33290	33070	33170	33177	110
AR2	$f_{cm,cube}$	$f_{cm,cube}$	$f_{cm,cube}$	X	S	$f_{ctm,sp}$	$f_{ctm,sp}$	$f_{ctm,sp}$	X	S
31 days	47.95	46.97	42.95	45.96	2.65	2.99	3.29	2.81	3.03	0.24
126 days	57.68	59.56	58.20	58.48	0.97	3.97	3.40	4.06	3.81	0.36
	f_{cm}	f_{cm}	f_{cm}	X	S	E_c	E_c	E_c	X	S
128 days	47.45	48.03	44.38	46.62	1.96	33240	32060	31150	32150	1048
AR4/AR5	$f_{cm,cube}$	$f_{cm,cube}$	$f_{cm,cube}$	X	S	$f_{ctm,sp}$	$f_{ctm,sp}$	$f_{ctm,sp}$	X	S
14 days	40.16	37.05	38.09	38.43	1.58	2.93	2.98	2.81	2.91	0.09
28 days	43.73	44.18	43.15	43.69	0.52	3.14	3.21	3.26	3.20	0.06
	f_{cm}	f_{cm}	f_{cm}	X	S	E_c	E_c	E_c	X	S
28 days	34.74	36.64	35.91	35.76	0.96	29260	31880	30630	30590	1310

Table B.2 Material properties of specimens at a concrete age of 28 days

NO	$f_{cm,cube}$	$f_{cm,cube}$	$f_{cm,cube}$	X	S	$f_{ctm,sp}$	$f_{ctm,sp}$	$f_{ctm,sp}$	X	S
A-B1	50.87	54.11	48.21	51.06	2.95	3.41	3.13	3.28	3.27	0.14
A-B2	50.87	54.11	48.21	51.06	2.95	3.41	3.13	3.28	3.27	0.14
A-B3	47.30	47.17	48.92	47.80	0.98	3.06	2.93	3.38	3.12	0.23
A-B4	45.68	45.29	48.47	46.48	1.73	3.03	3.09	3.05	3.06	0.03
A-B5	45.68	45.29	48.47	46.48	1.73	3.03	3.09	3.05	3.06	0.03
A-B6	48.40	49.76	48.79	48.98	0.70	2.86	3.36	3.51	3.24	0.34
A-B7	48.40	49.76	48.79	48.98	0.70	2.86	3.36	3.51	3.24	0.34
A-B8	47.30	47.17	48.92	47.80	0.98	3.06	2.93	3.38	3.12	0.23
A-B9	46.00	45.81	50.15	47.32	2.45	3.07	3.06	3.13	3.09	0.04
A-B10	46.00	45.81	50.15	47.32	2.45	3.07	3.06	3.13	3.09	0.04
				48.33	2.29				3.16	0.18
NO	$f_{cm,cube}$	$f_{cm,cube}$	$f_{cm,cube}$	X	S	$f_{ctm,sp}$	$f_{ctm,sp}$	$f_{ctm,sp}$	X	S
S-P1	50.22	48.66	49.76	49.55	0.80	3.03	3.46	3.12	3.20	0.23
S-P2	45.42	45.42	45.42	45.42	0.00	3.02	2.87	3.03	2.97	0.09
S-P3	45.42	45.42	45.42	45.42	0.00	3.02	2.87	3.03	2.97	0.09
S-P4	45.03	44.31	45.35	44.90	0.53	2.99	2.92	2.87	2.93	0.06
S-P5	45.03	44.31	45.35	44.90	0.53	2.99	2.92	2.87	2.93	0.06
S-P6	44.25	46.85	43.86	44.99	1.63	2.74	3.28	2.98	3.00	0.27
S-P7	43.47	45.48	47.30	45.42	1.92	2.90	2.78	2.85	2.84	0.06
S-P8	43.47	45.48	47.30	45.42	1.92	2.90	2.78	2.85	2.84	0.06
S-P9	50.22	48.66	49.76	49.55	0.80	3.03	3.46	3.12	3.20	0.23
S-P10	44.25	46.85	43.86	44.99	1.63	2.74	3.28	2.98	3.00	0.27
S-P11	42.30	43.86	42.82	42.99	0.79	2.88	3.08	2.90	2.95	0.11
S-P12	42.30	43.86	42.82	42.99	0.79	2.88	3.08	2.90	2.95	0.11
S-P13	44.38	44.12	44.90	44.47	0.40	2.99	2.84	2.82	2.88	0.09
S-13A	46.20	45.81	44.83	45.61	0.71	2.85	3.38	2.94	3.06	0.28

S-P14	38.35	39.90	37.18	38.48	1.36	3.04	3.04	3.15	3.08	0.06	26 days	
S-14A	38.35	39.90	37.18	38.48	1.36	3.04	3.04	3.15	3.08	0.06		
S-P15	44.38	44.12	44.90	44.47	0.40	2.99	2.84	2.82	2.88	0.09		
				44.59	2.97				2.99	0.17		
no	$f_{cm,cube}$	$f_{cm,cube}$	$f_{cm,cube}$	X	S	$f_{ctm,sp}$	$f_{ctm,sp}$	$f_{ctm,sp}$	X	S		
BM0	44.51	43.41	44.64	44.19	0.68	2.99	3.00	3.33	3.11	0.19		
BM1	42.95	42.76	42.69	42.80	0.13	2.96	2.91	2.99	2.95	0.04		
				43.49	0.88				3.03	0.15		
no	$f_{cm,cube}$	$f_{cm,cube}$	$f_{cm,cube}$	X	S	$f_{ctm,sp}$	$f_{ctm,sp}$	$f_{ctm,sp}$	X	S		
S-W1	43.28	43.93	40.68	42.63	1.72	3.01	3.18	3.01	3.07	0.10	22 days	
S-W2	45.22	45.35	47.43	46.00	1.24	3.26	2.92	2.95	3.04	0.19		
S-W3	46.33	44.18	42.95	44.49	1.71	2.99	2.60	3.33	2.97	0.37		
S-W4	43.41	44.85	42.43	43.56	1.22	2.91	3.11	2.98	3.00	0.10		
				44.17	1.82				3.02	0.19		
no	$f_{cm,cube}$	$f_{cm,cube}$	$f_{cm,cube}$	X	S	$f_{ctm,sp}$	$f_{ctm,sp}$	$f_{ctm,sp}$	X	S		
S-H1	43.28	43.93	40.68	42.63	1.72	3.01	3.18	3.01	3.07	0.10		
S-H2	45.22	45.35	47.43	46.00	1.24	3.26	2.92	2.95	3.04	0.19		
S-H3	46.33	44.18	42.95	44.49	1.71	2.99	2.60	3.33	2.97	0.37		
S-H4	-	-	-	-	-	-	-	-	-	-		
				44.37	2.00				3.03	0.22		
no	$f_{cm,cube}$	$f_{cm,cube}$	$f_{cm,cube}$	X	S	$f_{ctm,sp}$	$f_{ctm,sp}$	$f_{ctm,sp}$	X	S		
A-L1	40.62	40.88	40.36	40.62	0.26	3.50	3.20	3.20	3.30	0.17	41 days	
A-L2	45.16	43.80	44.44	44.47	0.68	3.09	3.10	3.18	3.12	0.05		
A-L3	43.60	41.72	43.54	42.95	1.07	2.84	2.90	2.64	2.79	0.14		
A-L4	53.79	51.97	51.78	52.51	1.11	3.06	3.10	3.09	3.08	0.02		
A-L5	53.79	51.97	51.78	52.51	1.11	3.06	3.10	3.09	3.08	0.02		
A-L6	43.60	41.72	43.54	42.95	1.07	2.84	2.90	2.64	2.79	0.14		
				46.00	4.94				3.03	0.21		
no	$f_{cm,cube}$	$f_{cm,cube}$	$f_{cm,cube}$	X	S	$f_{ctm,sp}$	$f_{ctm,sp}$	$f_{ctm,sp}$	X	S		
A-R1	50.35	50.41	41.46	47.41	5.15	3.31	3.35	3.52	3.39	0.11	34 days	
A-R2	47.95	46.97	42.95	45.96	2.65	2.99	3.29	2.81	3.03	0.24		
A-R3	44.25	44.31	44.83	44.46	0.32	3.05	2.88	3.17	3.03	0.15	31 days	
A-R4	48.79	44.83	45.42	46.35	2.14	2.95	3.16	3.03	3.05	0.11		
A-R5	48.79	44.83	45.42	46.35	2.14	2.95	3.16	3.03	3.05	0.11		
A-R6	44.25	44.31	44.83	44.46	0.32	3.05	2.88	3.17	3.03	0.15		
A-R7	42.76	44.25	43.86	43.62	0.77	3.06	2.78	2.57	2.80	0.25		
A-R8	42.76	44.25	43.86	43.62	0.77	3.06	2.78	2.57	2.80	0.25		
				45.28	2.38				3.02	0.23		

From the standard tests carried out at 28 days the mean value and standard deviation of the cube compressive strength and the tensile splitting strength are:

$$x(f_{cm,cube,28}) = 45.52 \text{ N/mm}^2$$

$$x(f_{ctm,sp,28}) = 3.03 \text{ N/mm}^2$$

$$s(f_{cm,cube,28}) = 2.59 \text{ N/mm}^2$$

$$s(f_{ctm,sp,28}) = 0.20 \text{ N/mm}^2$$

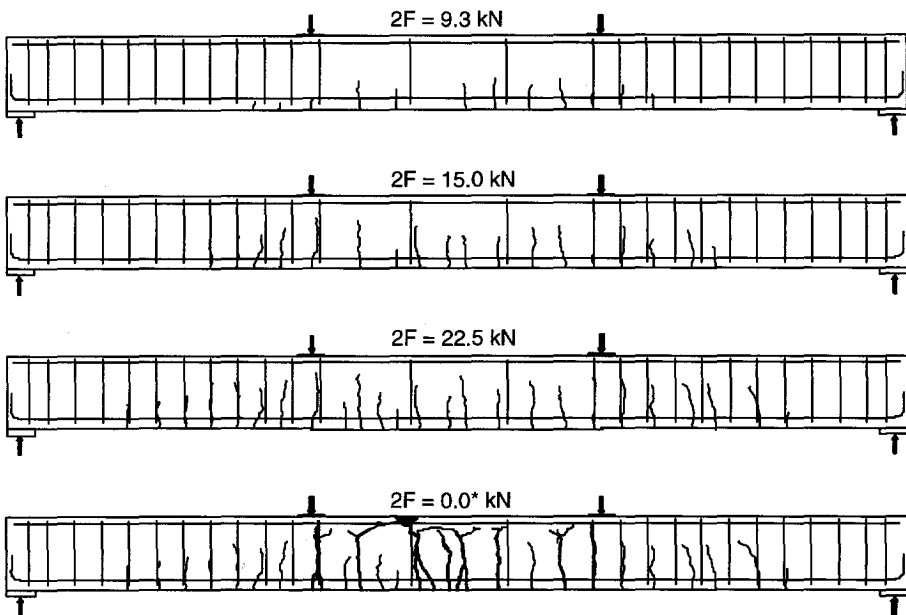
With regard to the uniaxial tensile strength derived from the tensile splitting strength, the conversion factor following from Eurocode 2, section 3.1.2.3 is used:

$$f_{ctm,ax} = 0.9 f_{ctm,sp}, \text{ hence } f_{ctm,ax} = 2.75 \text{ N/mm}^2$$

C - CRACK DEVELOPMENT AND LOAD-DEFLECTION DIAGRAM

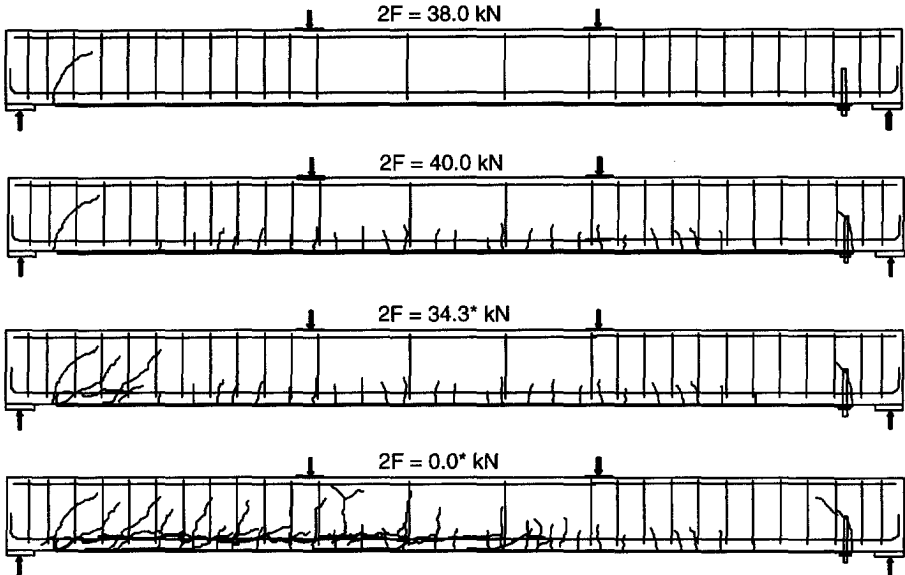
BM0 A800 W100 H200

$F_{max} = 24.1 \text{ kN} (=2F)$



BM1 P5×100 L100 A800 W100 H200

$$F_{\max} = 52.7 \text{ kN } (=2F)$$

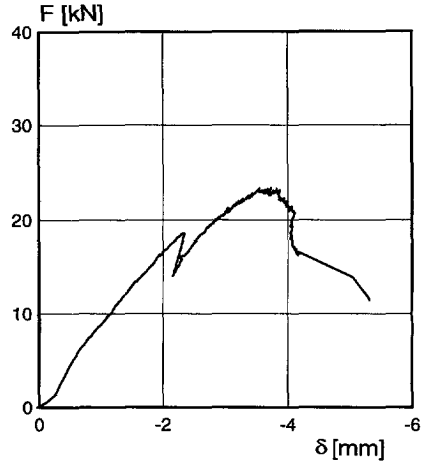
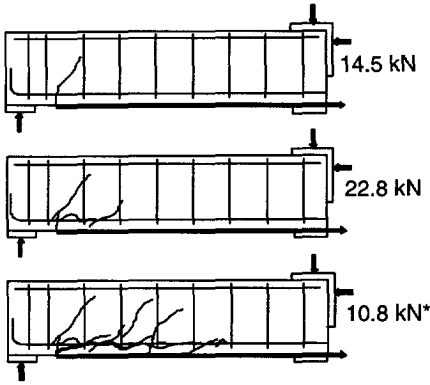


Remark 1: At the left side of the bonded-on plate measuring devices were placed for displacement control. Accordingly, at the right side of the bonded-on steel plate a bolt was installed to prevent plate separation at this side of the beam.

Remark 2: Due to an incorrect initial value for displacement control, the beam was very suddenly loaded up to a load level of 38 kN. As is sketched in the above crack pattern, a shear crack had developed at the plate ends. After resetting the control value, the beam was reloaded to a level of 40 kN at which the cracks were marked again on the beam. Then, the beam was loaded up to failure.

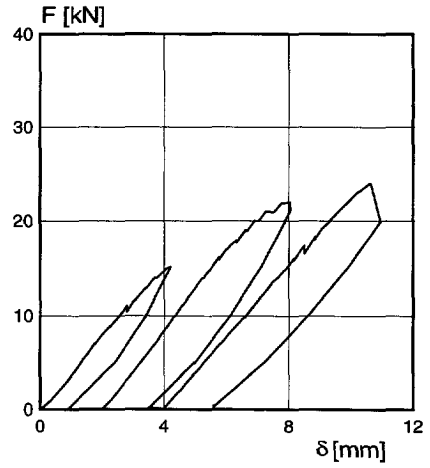
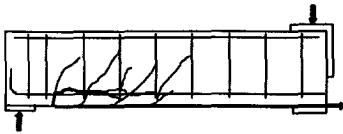
A-L1 P5×100 L100 W100 H200

$F_{max} = 23.4 \text{ kN}$



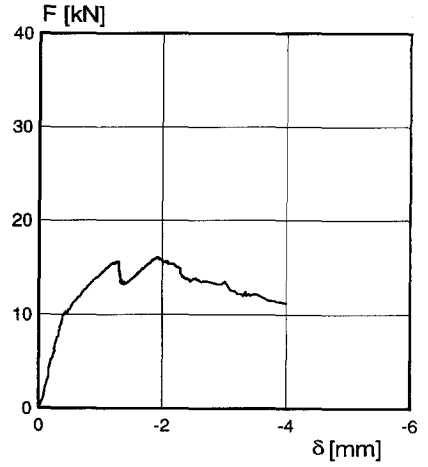
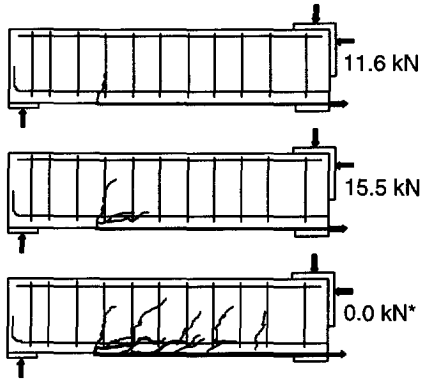
A-L2 P5×100 L100 W100 H200

$F_{max} = 23.9 \text{ kN}$



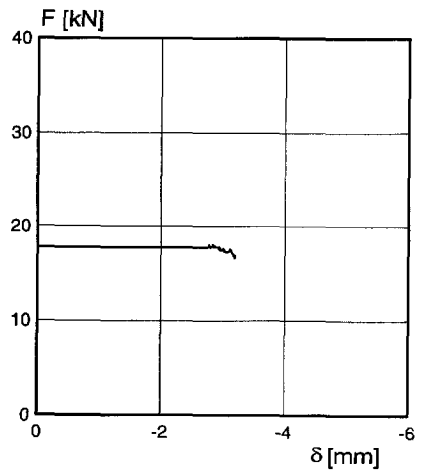
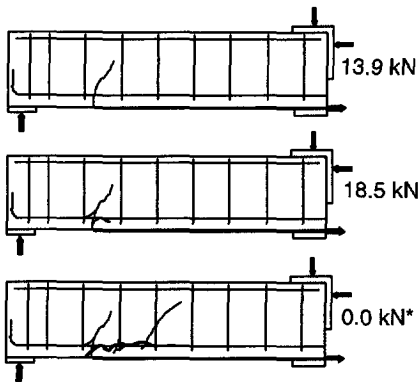
A-L3 P5×100 L200 W100 H200

$F_{max} = 16.1 \text{ kN}$



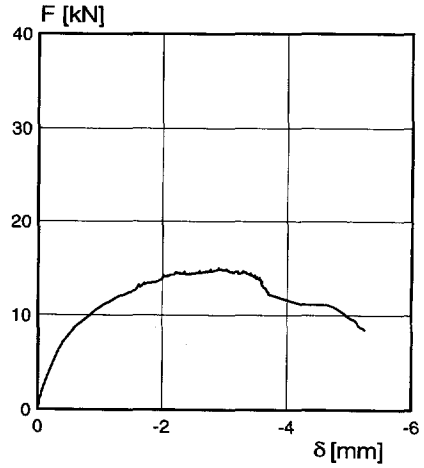
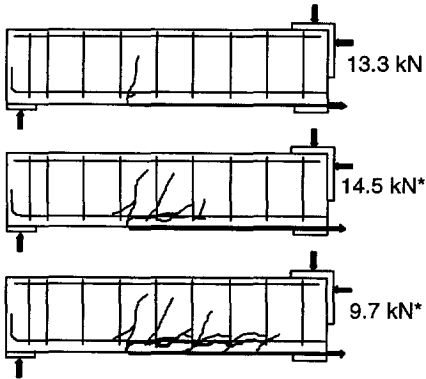
A-L4 P5×100 L200 W100 H200

$F_{max} = 18.9 \text{ kN}$



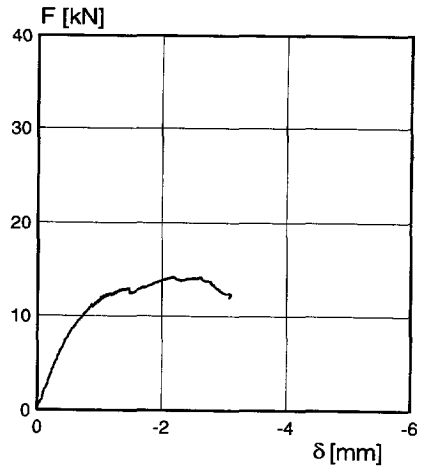
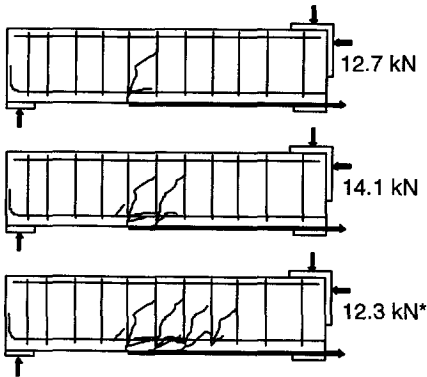
A-L5 P5×100 L300 W100 H200

$F_{max} = 14.5 \text{ kN}$



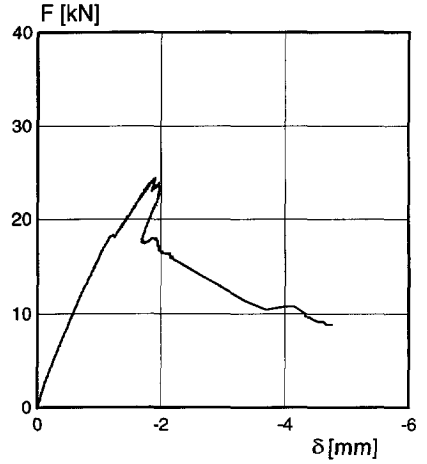
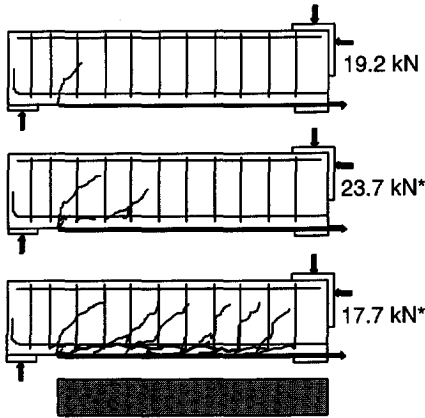
A-L6 P5×100 L300 W100 H200

$F_{max} = 14.3 \text{ kN}$



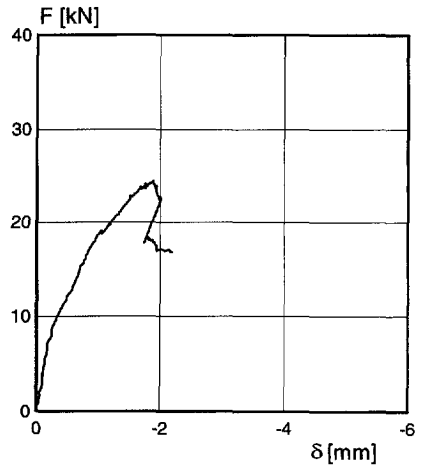
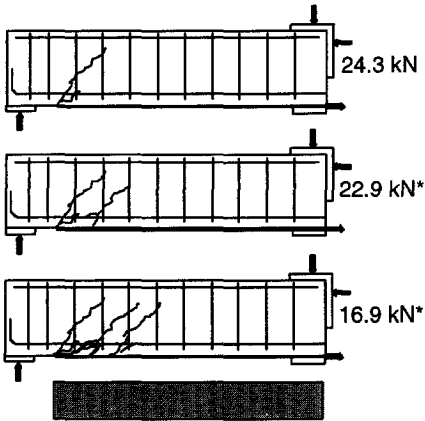
A-B1 P5×100L100 B-- W100H200

$F_{max} = 24.5 \text{ kN}$



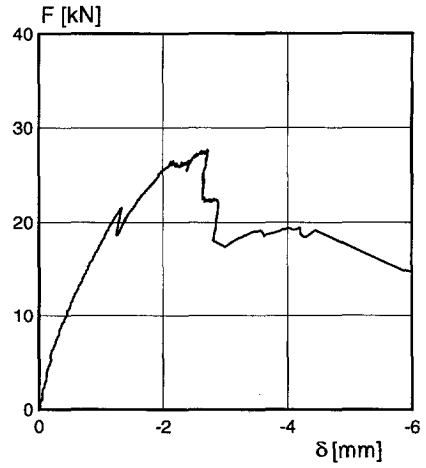
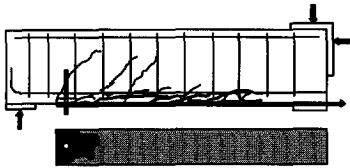
A-B2 P5×100 L100 B W100 H200

$F_{max} = 24.4 \text{ kN}$



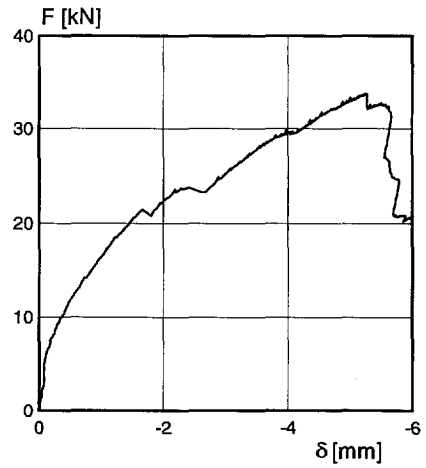
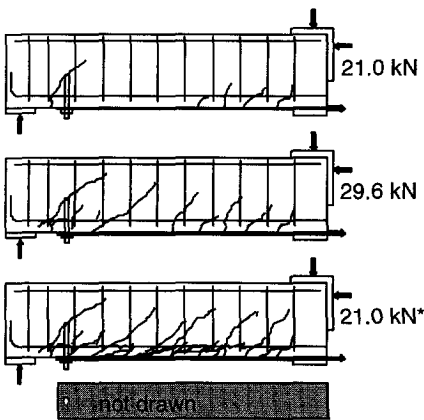
A-B3 P5×100 L100 B00 W100 H200

$F_{max} = 27.7 \text{ kN}$



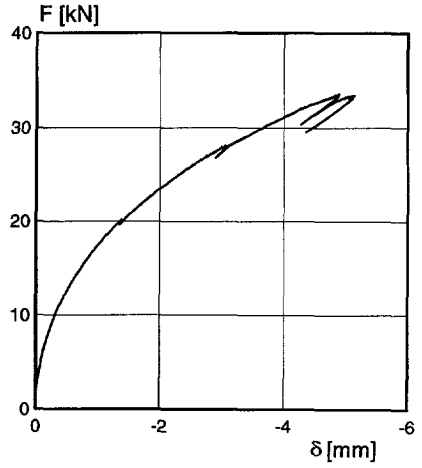
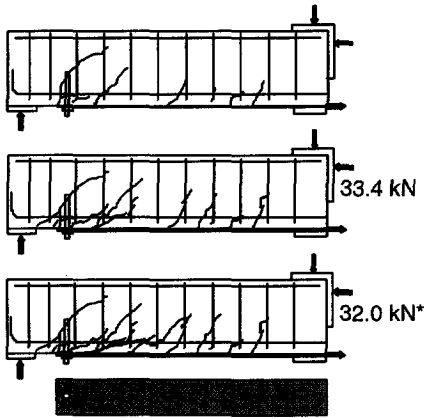
A-B4 P5×100 L100 B10 W100 H200

$F_{max} = 33.8 \text{ kN}$



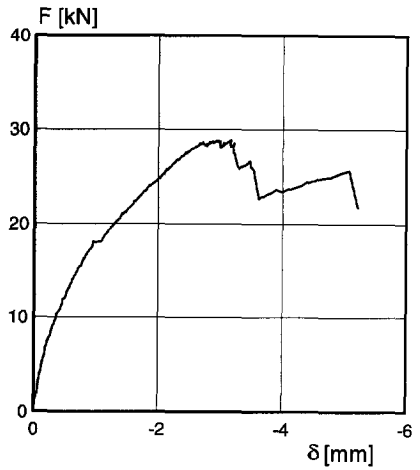
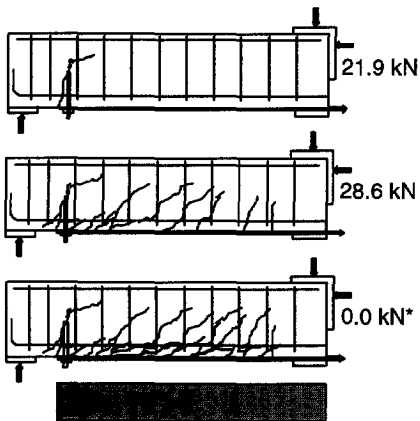
A-B5 P5×100 L100 B10 W100 H200

$F_{max} = 33.5 \text{ kN}$



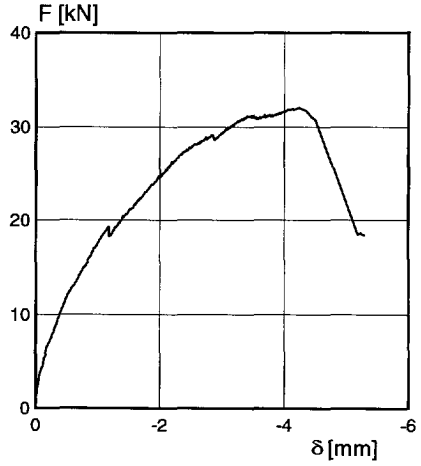
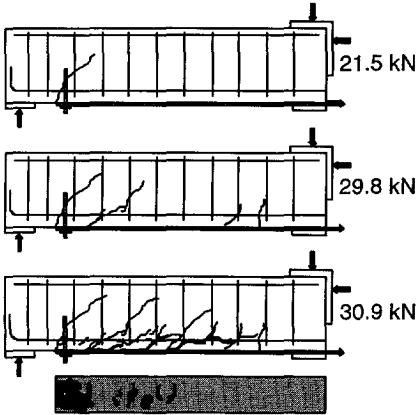
A-B6 P5×100 L100 B25? W100 H200

$F_{max} = 28.9 \text{ kN}$



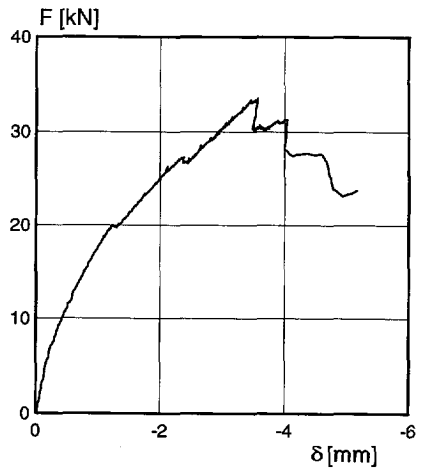
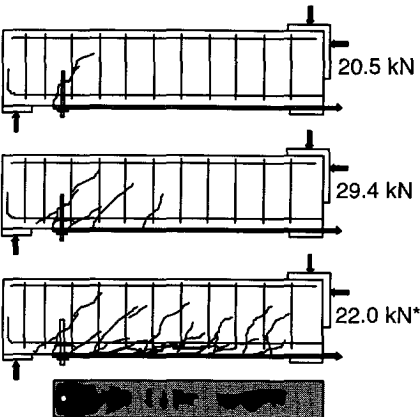
A-B7 P5×100 L100 B25 W100 H200

$F_{max} = 32.0 \text{ kN}$



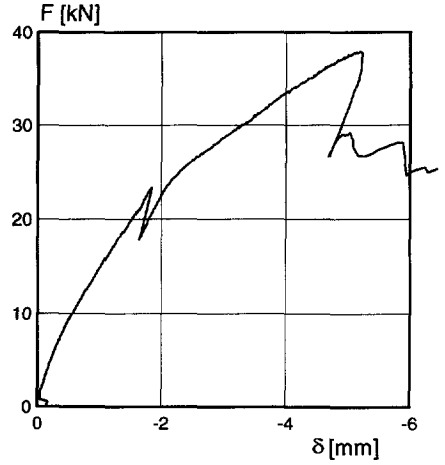
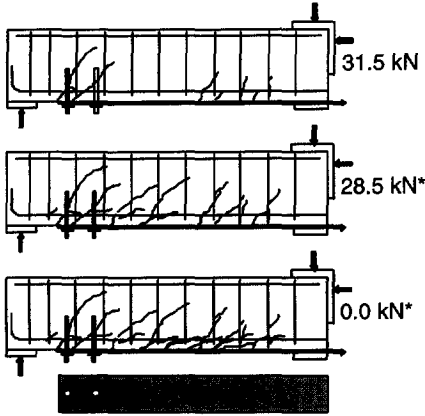
A-B8 P5×100 L100 B25 W100 H200

$F_{max} = 33.4 \text{ kN}$



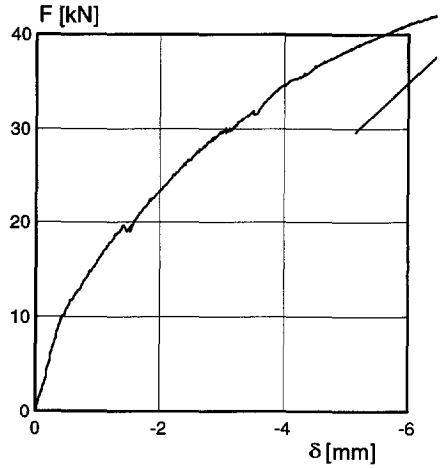
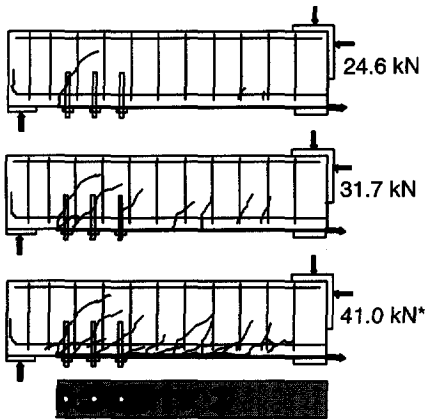
A-B9 P5×100 L100 B2×10 W100 H200

$F_{max} = 37.9 \text{ kN}$



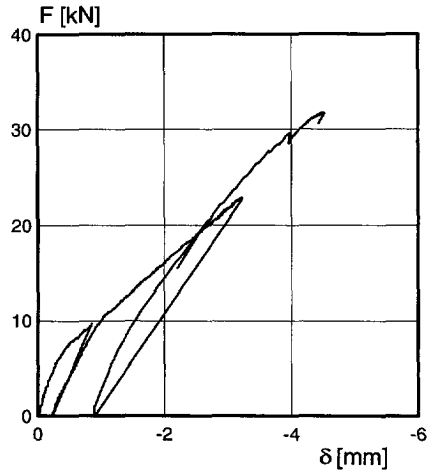
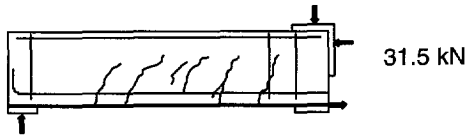
A-B10 P5×100 L100 B3×10 W100 H200

$F_{max} = 43.4 \text{ kN}$



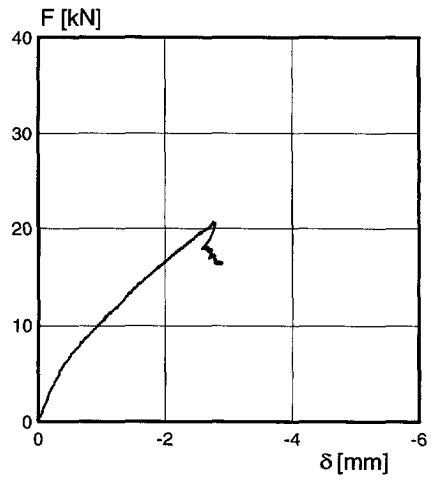
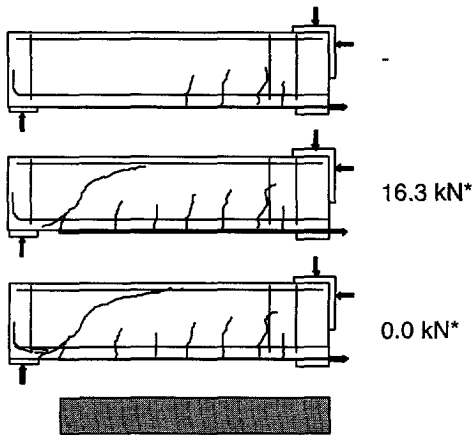
S-P1 P3×60 L000 W100 H200

$F_{max} = \pm 22.5 \text{ kN}$



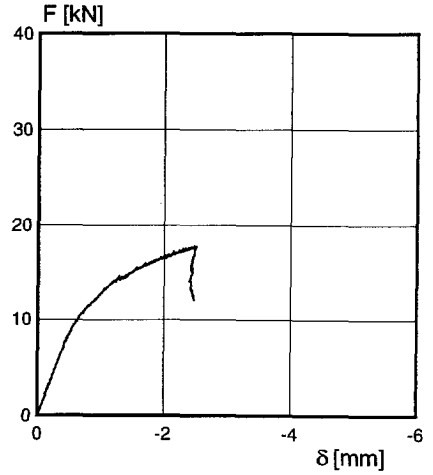
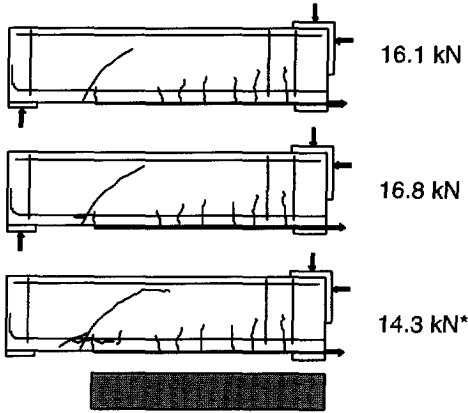
S-P2 P3×60 L100 W100 H200

$F_{max} = 20.6 \text{ kN}$



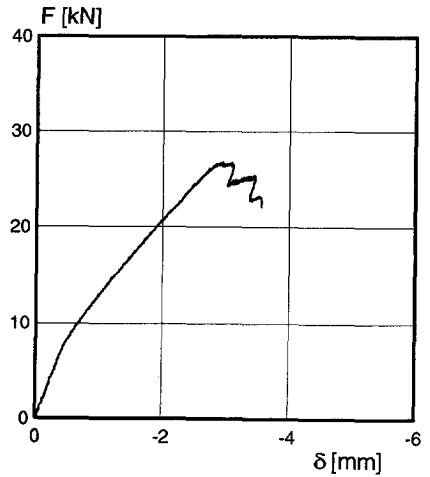
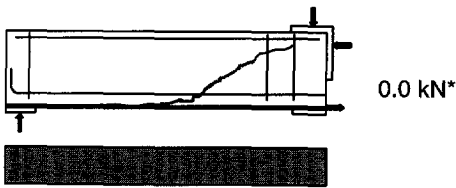
S-P3 P3×60 L200 W100 H200

$F_{max} = 17.8 \text{ kN}$



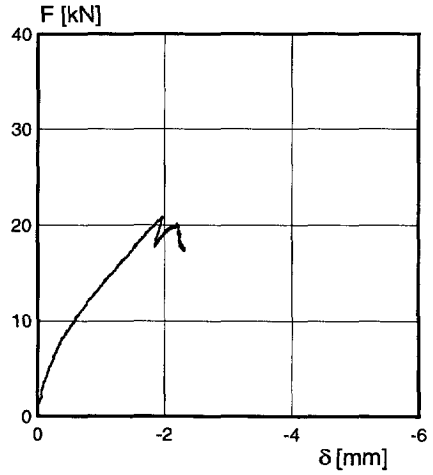
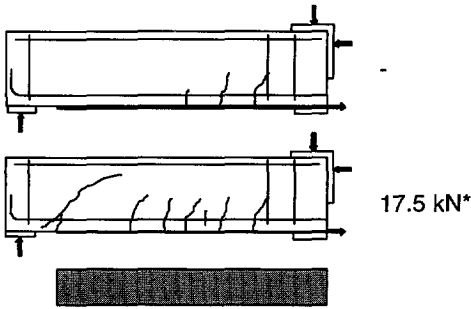
S-P4 P3×100 L000 W100 H200

$F_{max} = 26.7 \text{ kN}$



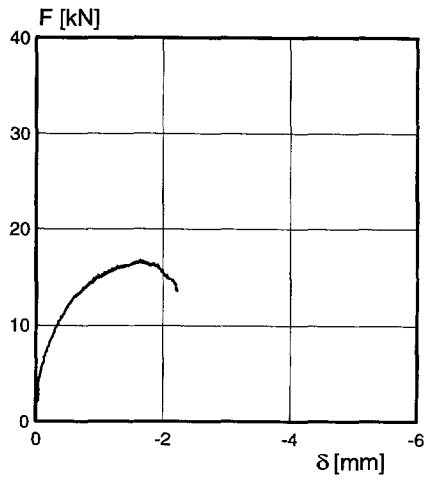
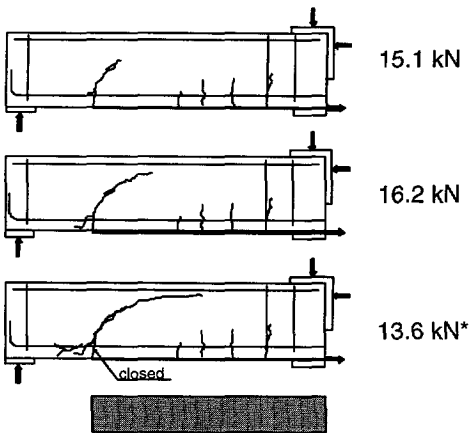
S-P5 P3×100 L100 W100 H200

$F_{max} = 20.9 \text{ kN}$



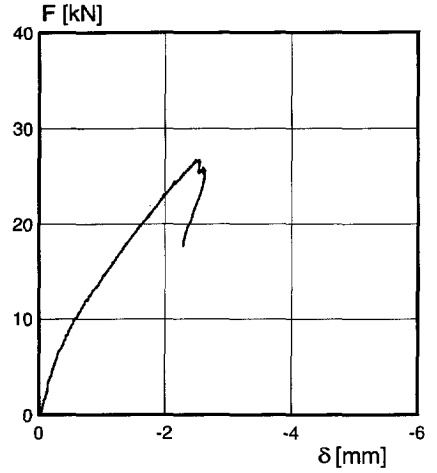
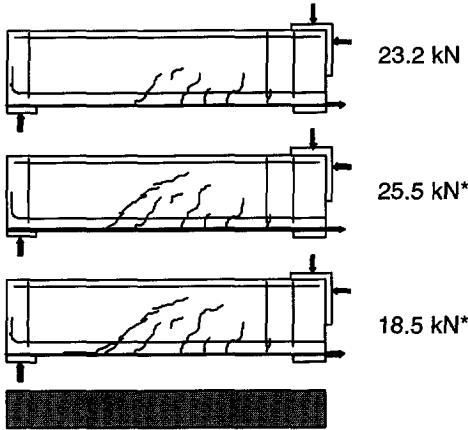
S-P6 P3×100 L200 W100 H200

$F_{max} = 16.7 \text{ kN}$



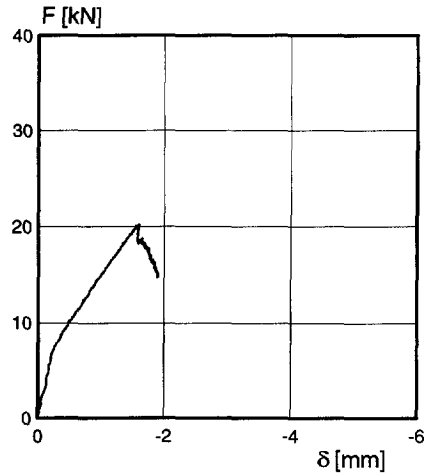
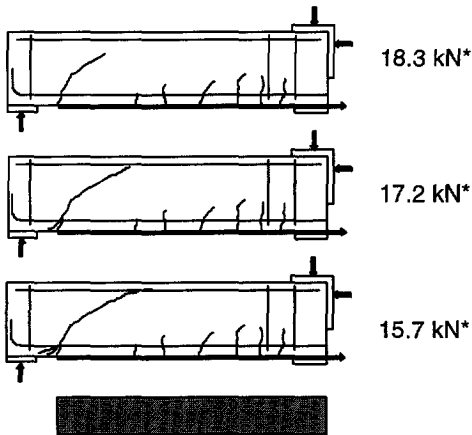
S-P7 P4×80 L000 W100 H200

$F_{max} = 26.7 \text{ kN}$



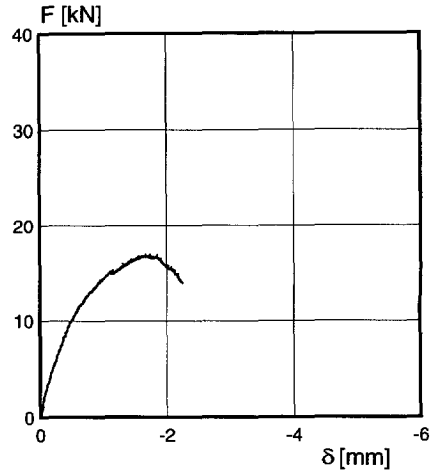
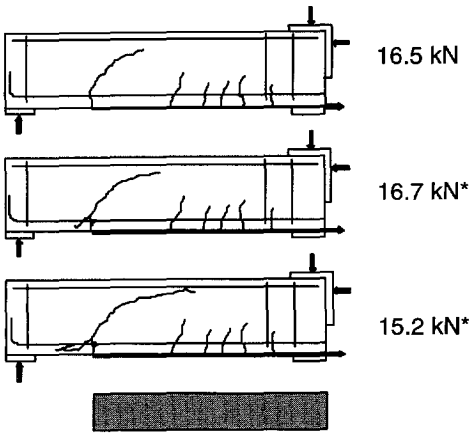
S-P8 P4×80 L100 W100 H200

$F_{max} = 20.2 \text{ kN}$



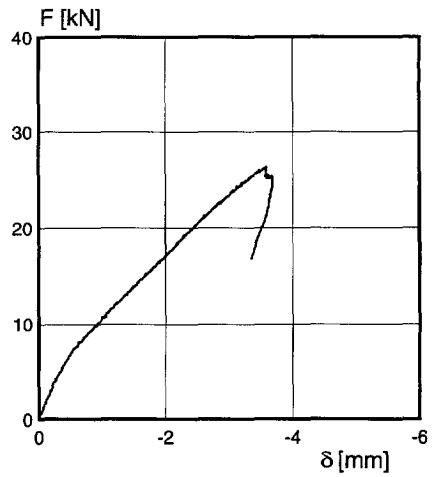
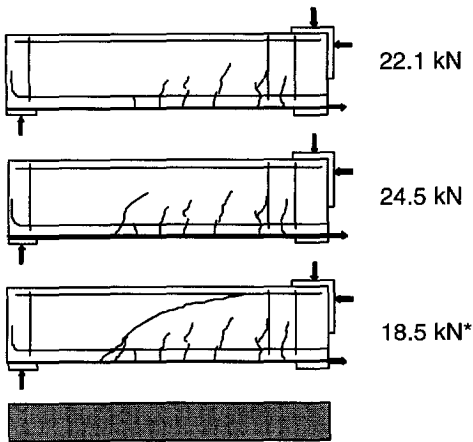
S-P9 P4×80 L200 W100 H200

$F_{max} = 16.9 \text{ kN}$



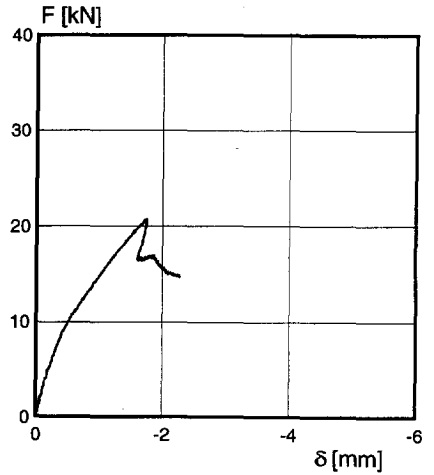
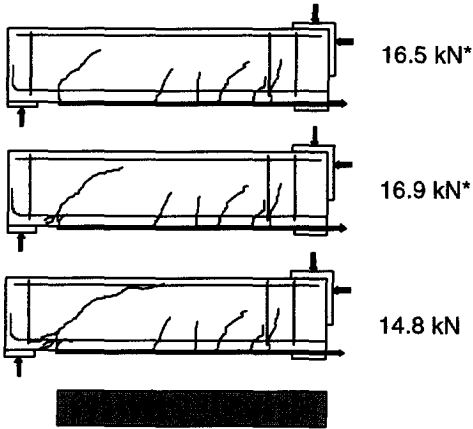
S-P10 P5×60 L000 W100 H200

$F_{max} = 26.3 \text{ kN}$



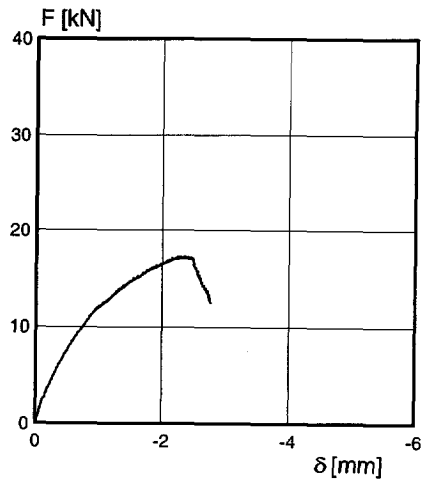
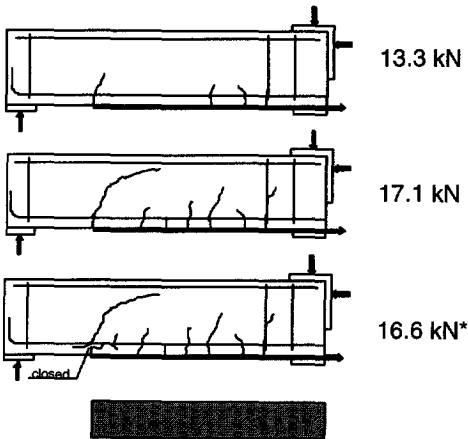
S-P11 P5×60 L100 W100 H200

$F_{max} = 20.7 \text{ kN}$



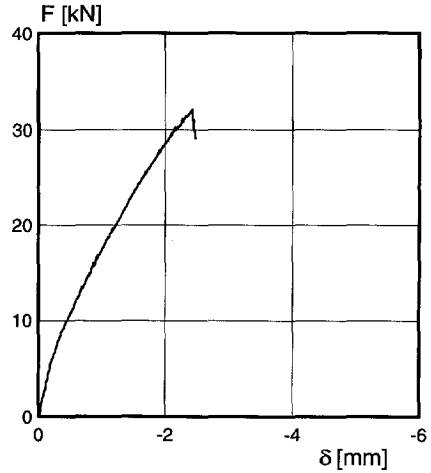
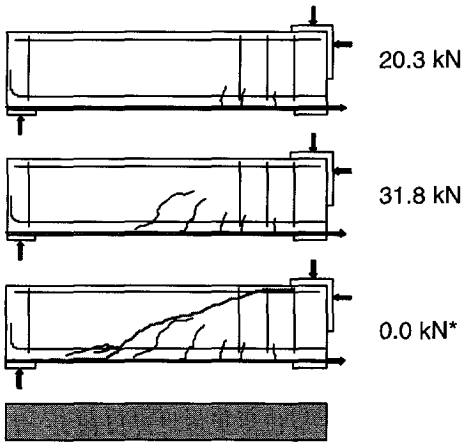
S-P12 P5×60 L200 W100 H200

$F_{max} = 20.6 \text{ kN}$



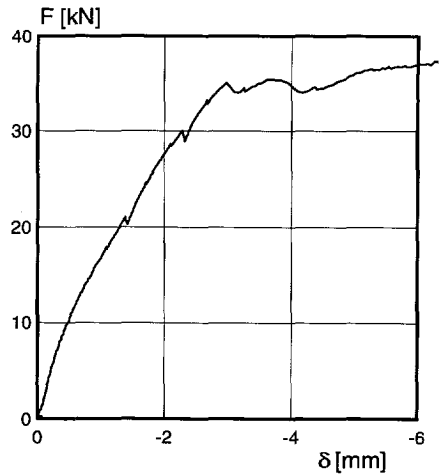
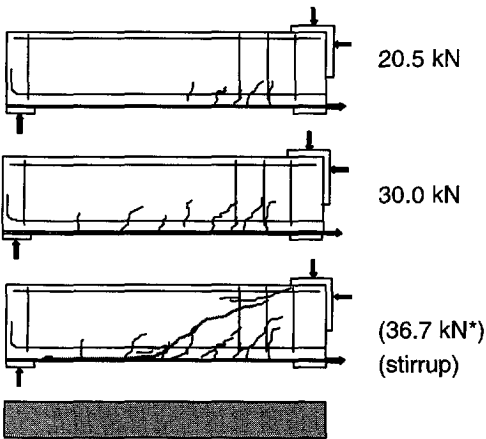
S-P13 P5×100 L000 W100 H200

$F_{max} = 32.1 \text{ kN}$



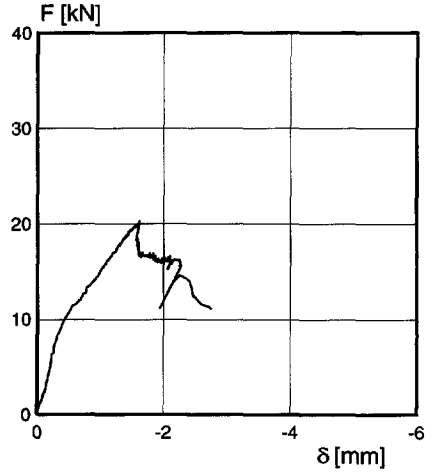
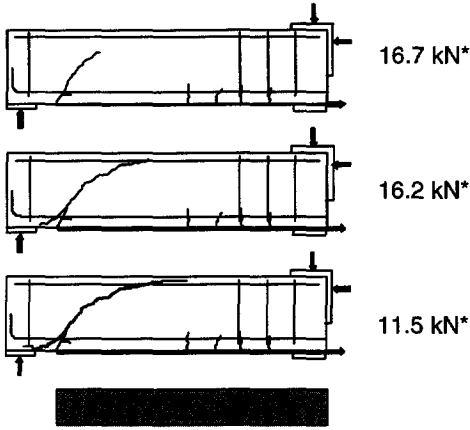
S-P13A P5×100 L000 W100 H200

$F_{max} = 35.3 \text{ kN}$



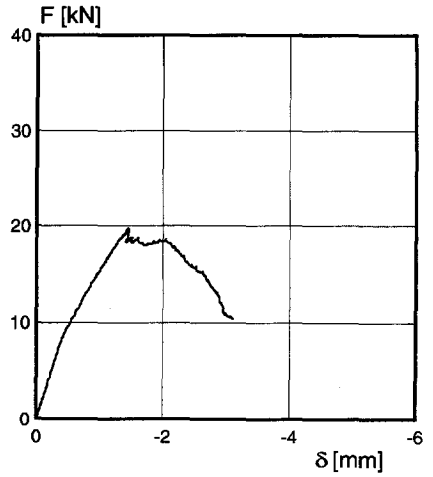
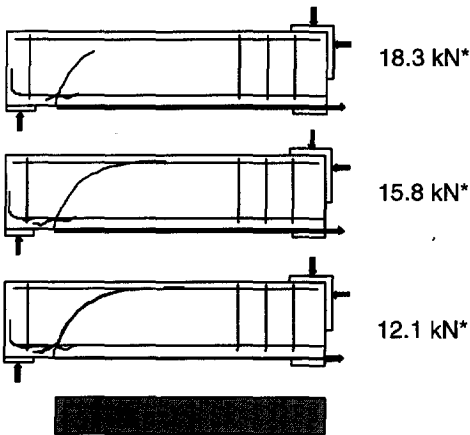
S-P14 P5×100 L100 W100 H200

$F_{max} = 20.1 \text{ kN}$



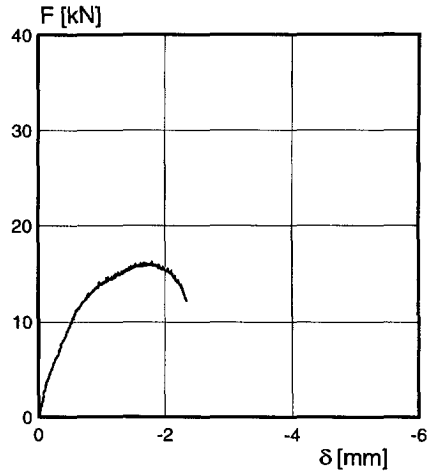
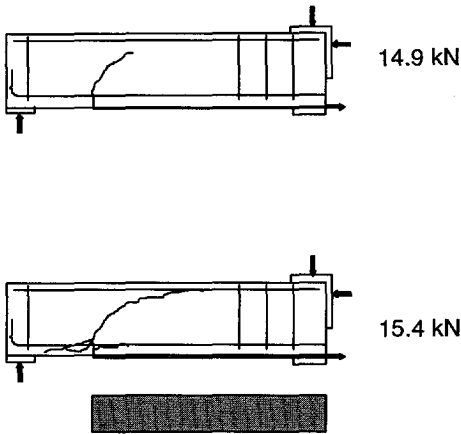
S-P14A P5×100 L100 W100 H200

$F_{max} = 19.6 \text{ kN}$

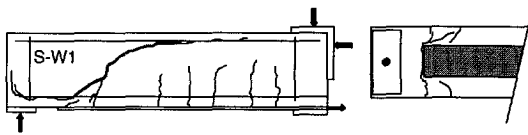


S-P15 P5×100 L200 W100 H200

$F_{max} = 16.1 \text{ kN}$

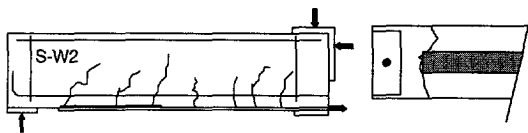


S-W1-W2-W3-W4



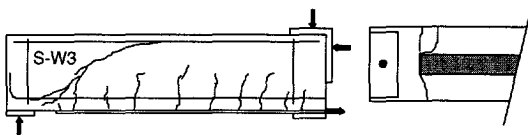
P4×80 L100 W200 H200

$F_{max} = 35.9 \text{ kN}$



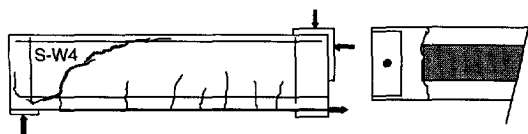
P3×100 L100 W200 H200

$F_{max} = 36.5 \text{ kN}$



P5×60 L100 W200 H200

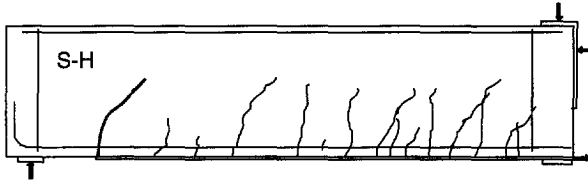
$F_{max} = 35.8 \text{ kN}$



P5×100 L100 W200 H200

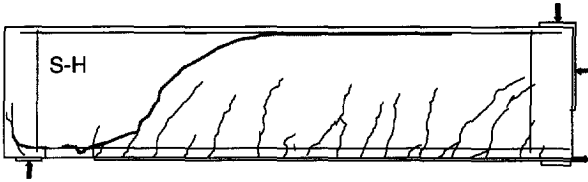
$F_{max} = 36.9 \text{ kN}$

S-H1-H2-H3-H4



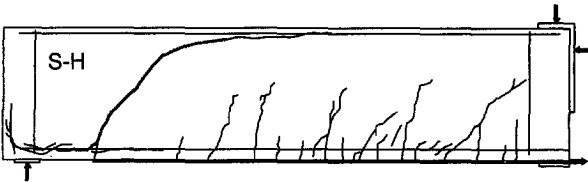
P4×80 L200 W100 H400

$F_{\max} = 38.1 \text{ kN}$



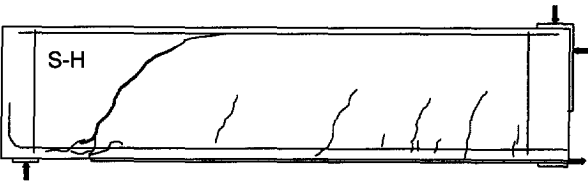
P3×100 L200 W100 H400

$F_{\max} = 40.6 \text{ kN}$



P5×60 L200 W100 H400

$F_{\max} = 40.3 \text{ kN}$



P5×100 L200 W100 H400

$F_{\max} = 34.4 \text{ kN}$

D - LITERATURE DATA ON MAXIMUM PEELING LOADS

reference	testnr	f_{test} [MPa]	b [mm]	h [mm]	d_s [mm]	a [mm]	a/d_s [-]
Jones et al [1982]	URB4	50.7	100	150	130	750	5.77
	URB5	50.7	100	150	130	750	5.77
Swamy et al [1987]	205	60	155	255	220	767	3.49
	206	60	155	255	220	767	3.49
	209	60	155	255	220	767	3.49
	210	60	155	255	220	767	3.49
	218	60	155	255	220	767	3.49
	219	60	155	255	220	767	3.49
Jones [1988]	F31	60	155	225	190	767	4.04
	F33	60	155	225	190	767	4.04
Swamy [1995]	123	95	155	255	220	767	3.49
	124	95	155	255	220	767	3.49
Hussain et al [1995]	FRB5	31	150	150	109	400	3.67
	FRB7	31	150	150	109	400	3.67
Basunbul et al [1990]	PB-A	37.7	150	150	109	400	3.67
	PB-B	37.7	150	150	109	400	3.67
	PB-C	37.7	150	150	109	400	3.67
MacDonald [1982]	3	38.4	150	250	210	1000	4.76
	6	38.4	150	250	210	1000	4.76
	7	38.4	150	250	210	1000	4.76
	13	38.4	150	250	210	1000	4.76
	16	38.4	150	250	210	1000	4.76
	19	38.4	150	250	210	1000	4.76
Holzenkamp [1989]	SB02	53	200	270	240	1250	5.21
Pichler [1993]	3	35	300	200	165	1050	6.36
Jansze [1997]	A-L1	43.94	100	200	170	800	4.71
	A-L2	46.5	100	200	170	800	4.71
	A-L3	41.6	100	200	170	800	4.71
	A-L4	47.15	100	200	170	800	4.71
	A-L5	47.15	100	200	170	800	4.71
	A-L6	41.6	100	200	170	800	4.71
	A-B1	42.2	100	200	170	800	4.71
	A-B2	42.2	100	200	170	800	4.71
	BM1	39.3	100	200	170	800	4.71
	Van Gemert [1980]	beam1	44.8	100	180	155	652.5
beam2		46.4	100	180	155	652.5	4.21
beam3		30	100	180	155	652.5	4.21
Taljsten [1994]	C8	37.3	120	150	115	370	3.22
	C9	34.6	120	150	115	370	3.22
	C10	37.3	120	150	115	370	3.22
	A3	25.8	200	300	260	1150	4.42
Ritchie et al [1991]	O	45	152.4	305	251	914	3.64

testnr	A_s [mm]	$\rho_{s,0}$ [%]	t_p [mm]	b_p [mm]	d_{sp} [mm]	$\rho_{sp,0}$ [%]	L [mm]	L/a [-]	V_{exp} [kN]	τ_{exp} [MPa]
URB4	157	1.21	5	80	147	3.78	50	0.0667	28.75	2.21
URB5	157	1.21	10	80	152	6.29	50	0.0667	26.55	2.04
205	943	2.77	6	125	237	4.60	50	0.065	106.5	3.12
206	943	2.77	3	125	231	3.68	50	0.065	110	3.23
209	943	2.77	6	125	237	4.60	50	0.065	110	3.23
210	943	2.77	6	125	237	4.60	50	0.065	107.5	3.15
218	943	2.77	6	125	237	4.60	50	0.065	97	2.84
219	943	2.77	6	125	237	4.60	50	0.065	110	3.23
F31	943	3.20	6	125	207	5.26	50	0.065	91	3.09
F33	943	3.20	6	125	207	5.26	50	0.065	95.5	3.24
123	943	2.77	1.5	125	226	3.22	50	0.065	147.5	4.33
124	943	2.77	3	125	231	3.68	50	0.065	145.6	4.27
FRB5	157	0.96	2	100	133	1.78	50	0.125	30	1.83
FRB7	157	0.96	3	100	138	2.21	50	0.125	29	1.77
PB-A	157	0.96	1.5	100	130	1.57	50	0.125	32.67	2.00
PB-B	157	0.96	1.5	100	130	1.57	50	0.125	32.72	2.00
PB-C	157	0.96	1.5	100	130	1.57	50	0.125	31.03	1.90
3	226	0.72	3.6	85	235	1.51	100	0.1	42	1.33
6	226	0.72	3.6	85	235	1.51	100	0.1	42	1.33
7	226	0.72	3.6	85	235	1.51	100	0.1	42	1.33
13	226	0.72	4.75	57	234	1.42	100	0.1	40	1.27
16	226	0.72	3.6	85	235	1.51	100	0.1	43	1.37
19	226	0.72	6	47	235	1.44	100	0.1	36	1.14
SB02	157	0.33	4	120	265	1.20	250	0.2	46	0.96
3	150.8	0.30	8	50	194	0.94	250	0.238	31.5	0.64
A-L1	100.5	0.59	5	100	198	3.03	100	0.125	23.4	1.38
A-L2	100.5	0.59	5	100	198	3.03	100	0.125	23.9	1.41
A-L3	100.5	0.59	5	100	198	3.03	200	0.25	16.1	0.95
A-L4	100.5	0.59	5	100	198	3.03	200	0.25	18.9	1.11
A-L5	100.5	0.59	5	100	198	3.03	300	0.375	14.5	0.85
A-L6	100.5	0.59	5	100	198	3.03	300	0.375	14.3	0.84
A-B1	100.5	0.59	5	100	198	3.03	100	0.125	24.5	1.44
A-B2	100.5	0.59	5	100	198	3.03	100	0.125	24.4	1.44
BM1	100.5	0.59	5	100	198	3.03	100	0.125	26.35	1.55
beam1	308	1.99	5	100	173	4.67	152.5	0.23	26.5	1.71
beam2	308	1.99	5	100	173	4.67	152.5	0.23	23	1.48
beam3	308	1.99	5	100	173	4.67	152.5	0.23	19	1.23
C8	100.5	0.73	3	100	143	2.33	50	0.135	26.4	1.91
C9	100.5	0.73	3	100	143	2.33	50	0.135	30.5	2.21
C10	100.5	0.73	3	65	140	1.76	50	0.135	24	1.74
A3	402	0.77	3	160	283	1.56	100	0.087	84.5	1.63
O	253	0.66	2.6	154	286	1.50	203	0.222	46.7	1.22

testnr	a_L [mm]	a_L/d [-]	V_{model} [kN]	V_{exp}/V_m [-]	τ_{model} [MPa]	b_p/t_p [-]	b_p/b_c [-]	x/d_{sp} [-]	S [-]	
URB4	180.69	1.39	26.66	1.08	2.05	16.00	0.80	0.49	2.13	P2x1.5
URB5	180.69	1.39	26.66	1.00	2.05	8.00	0.80	0.57	4.21	
205	162.14	0.74	104.97	1.01	3.08	20.83	0.81	0.52	0.66	
206	162.14	0.74	104.97	1.05	3.08	41.67	0.81	0.48	0.33	
209	162.14	0.74	104.97	1.05	3.08	20.83	0.81	0.52	0.66	
210	162.14	0.74	104.97	1.02	3.08	20.83	0.81	0.52	0.66	
218	162.14	0.74	104.97	0.92	3.08	20.83	0.81	0.52	0.66	
219	162.14	0.74	104.97	1.05	3.08	20.83	0.81	0.52	0.66	
F31	149.54	0.79	96.59	0.94	3.28	20.83	0.81	0.54	0.64	
F33	149.54	0.79	96.59	0.99	3.28	20.83	0.81	0.54	0.64	
123	162.14	0.74	122.33	1.21	3.59	83.33	0.81	0.47	0.17	2 mm
124	162.14	0.74	122.33	1.19	3.59	41.67	0.81	0.48	0.33	2P1.5
FRB5	184.33	1.69	25.96	1.16	1.59	50.00	0.67	0.40	0.86	
FRB7	184.33	1.69	25.96	1.12	1.59	33.33	0.67	0.42	1.30	
PB-A	184.33	1.69	27.71	1.18	1.69	66.67	0.67	0.39	0.64	
PB-B	184.33	1.69	27.71	1.18	1.69	66.67	0.67	0.39	0.64	
PB-C	184.33	1.69	27.71	1.12	1.69	66.67	0.67	0.39	0.64	
3	395.72	1.88	39.46	1.07	1.25	23.61	0.57	0.37	1.10	3P2x47
6	395.72	1.88	39.46	1.06	1.25	23.61	0.57	0.37	1.10	
7	395.72	1.88	39.46	1.06	1.25	23.61	0.57	0.37	1.10	
13	395.72	1.88	39.46	1.01	1.25	12.00	0.38	0.37	0.97	
16	395.72	1.88	39.46	1.09	1.25	23.61	0.57	0.37	1.10	
19	395.72	1.88	39.46	0.91	1.25	7.83	0.31	0.37	1.01	
SB02	1004.7	4.19	38.24	1.20	0.80	30.00	0.60	0.35	2.67	
3	932.28	5.65	33.34	0.94	0.67	6.25	0.17	0.34	2.10	
A-L1	395.65	2.33	20.54	1.14	1.21	20.00	1.00	0.45	4.12	
A-L2	395.65	2.33	20.93	1.14	1.23	20.00	1.00	0.45	4.12	
A-L3	665.40	3.91	16.96	0.95	1.00	20.00	1.00	0.45	4.12	
A-L4	665.40	3.91	17.68	1.07	1.04	20.00	1.00	0.45	4.12	
A-L5	901.88	5.31	15.98	0.91	0.94	20.00	1.00	0.45	4.12	
A-L6	901.88	5.31	15.33	0.93	0.90	20.00	1.00	0.45	4.12	
A-B1	395.65	2.33	20.26	1.21	1.19	20.00	1.00	0.45	4.12	
A-B2	395.65	2.33	20.26	1.20	1.19	20.00	1.00	0.45	4.12	
BM1	395.65	2.33	19.79	1.33	1.16	20.00	1.00	0.45	4.12	
beam1	378.00	2.44	28.47	0.93	1.84	20.00	1.00	0.52	1.35	
beam2	378.00	2.44	28.80	0.80	1.86	20.00	1.00	0.52	1.35	
beam3	378.00	2.44	24.91	0.76	1.61	20.00	1.00	0.52	1.35	
C8	201.59	1.75	20.68	1.28	1.50	33.33	0.83	0.42	2.19	
C9	201.59	1.75	20.17	1.51	1.46	33.33	0.83	0.42	2.19	
C10	201.59	1.75	20.68	1.16	1.50	21.67	0.54	0.39	1.41	
A3	408.98	1.57	59.02	1.43	1.13	53.33	0.80	0.38	1.01	
O	719.46	2.87	40.96	1.14	1.07	59.23	1.01	0.37	1.27	

X=108
s=15

reference	testnr	f_{test} [MPa]	b [mm]	h [mm]	d_s [mm]	a [mm]	a/d_s [-]
Sharif et al [1994]	P3	37.7	150	150	109	393	3.61
	P2	37.7	150	150	109	393	3.61
	P3B	37.7	150	150	109	393	3.61
	P2B	37.7	150	150	109	393	3.61
Quantrill et al [1996]	B2	42.4	100	100	85	300	3.53
	B4	42.4	100	100	85	300	3.53
	B6	42.4	100	100	85	300	3.53
	A1c	39.2	100	100	85	300	3.53
	A2b	39.2	100	100	85	300	3.53
	A2c	39.2	100	100	85	300	3.53
	A2e	39.2	100	100	85	300	3.53
	A2f	39.2	100	100	85	300	3.53
Ritchie et al [1991]	D	45	152.4	305	251	914	3.64
Saadatmanesh [1991]	C	35	205	455	400	1983	4.96
	D	35	205	455	400	1983	4.96
Deuring [1993]	BL02	37.6	300	250	210	660	3.14

testnr	A_s [mm ²]	$\rho_{s,0}$ [%]	t_p [mm]	b_p [mm]	d_{sp} [mm]	$\rho_{sp,0}$ [%]	L [mm]	L/a [-]	V_{exp} [kN]	τ_{exp} [MPa]
P3	157	0.96	3	80	135.60	1.95	75	0.19	33	2.02
P2	157	0.96	2	80	130.96	1.61	75	0.19	34	2.08
P3B	157	0.96	3	80	135.60	1.95	75	0.19	36.5	2.23
P2B	157	0.96	2	80	130.96	1.61	75	0.19	32.5	1.99
B2	85	1	1.2	80	94.07	1.92	20	0.07	17	2.00
B4	85	1	1.6	60	94.18	1.92	20	0.07	17.5	2.06
B6	85	1	1.2	80	94.07	1.92	20	0.07	20.4	2.40
A1c	85	1	1.2	80	94.07	1.92	20	0.07	22	2.59
A2b	85	1	1.2	80	94.07	1.92	20	0.07	18.4	2.16
A2c	85	1	1.2	80	94.07	1.92	20	0.07	18.7	2.20
A2e	85	1	1.2	80	94.07	1.92	20	0.07	20.1	2.36
A2f	85	1	1.2	80	94.07	1.92	20	0.07	19.8	2.33
A2g	85	1	1.2	80	94.07	1.92	150	0.50	15.8	1.86
D	253	0.66	4.76	151	293.81	2.17	203	0.22	59.6	1.56
C	253	0.31	6	152	446.58	1.27	155	0.08	92.5	1.13
D	1013	1.24	6	152	428.19	2.19	155	0.08	137.5	1.68
BL02	402	0.64	1	200	223.95	0.90	100	0.15	68.5	1.09

testnr	a_L [mm]	a_L/d [-]	V_{model} [kN]	V_{exp}/V_m [-]	τ_{model} [MPa]	b_p/t_p [-]	b_p/b_c [-]	x/d_{sp} [-]	S [-]	
P3	249.84	2.29	25.04	1.32	1.53	26.67	0.53	0.41	1.03	bolt bolt
P2	249.84	2.29	25.04	1.36	1.53	40.00	0.53	0.39	0.68	
P3B	249.84	2.29	25.04	1.46	1.53	26.67	0.53	0.41	1.03	
P2B	249.84	2.29	25.04	1.30	1.53	40.00	0.53	0.39	0.68	
B2	86.15	1.01	19.38	0.88	2.28	66.67	0.80	0.40	0.92	
B4	86.15	1.01	19.38	0.90	2.28	37.50	0.60	0.40	0.92	
B6	86.15	1.01	19.38	1.05	2.28	66.67	0.80	0.40	0.92	
A1c	86.15	1.01	18.88	1.17	2.22	66.67	0.80	0.40	0.92	
A2b	86.15	1.01	18.88	0.97	2.22	66.67	0.80	0.40	0.92	
A2c	86.15	1.01	18.88	0.99	2.22	66.67	0.80	0.40	0.92	
A2e	86.15	1.01	18.88	1.06	2.22	66.67	0.80	0.40	0.92	
A2f	86.15	1.01	18.88	1.05	2.22	66.67	0.80	0.40	0.92	
A2g	390.43	4.59	11.41	1.38	1.34	66.67		0.40	0.92	
D	719.46	2.87	40.96	1.46	1.07	31.72	0.99	0.41	2.28	
C	810.08	2.03	63.43	1.46	0.77	25.33	0.74	0.35	3.12	
D	555.56	1.39	114.15	1.20	1.39	25.33	0.74	0.41	0.78	
BL02	408.56	1.95	74.57	0.92	1.18	200.00	0.67	0.34	0.40	

x=117

s=21

CURRICULUM VITAE

Willem Jansze, geboren op 26 november 1966, te Voorhout

- 1979 - 1980 : MAVO, Dr. de Visserschool, Sassenheim
- 1980 - 1985 : VWO, Rijnland Lyceum, Sassenheim
- 1985 - 1986 : Militaire dienst, Luchtdoelartillerie, Den Helder
- 1986 - 1988 : Weg en Waterbouwkunde, Hogeschool Haarlem, Haarlem
- 1988 - maart 1993 : Civiele Techniek, Technische Universiteit Delft, Delft
Mechanica en Constructies, Betonconstructies
- april 1993 - mei 1997 : Technische Universiteit Delft, Stevin Laboratorium, Delft
Assistent in Opleiding, Betonconstructies
- vanaf mei 1997 : Van Hattum en Blankevoort /
Volker Stevin Construction Europe, Woerden
Afdeling Ontwerp en Engineering